UNIVERSITÀ
DEGLI STUDI
FIRENZE

DOTTORATO DI RICERCA IN

Area del Farmaco e Trattamenti Innovativi

Curriculum Farmacologia, Tossicologia e Trattamenti Innovativi

CICLO XXXII

COORDINATORE Prof.ssa Elisabetta Teodori
Settore Scientifico Disciplinare BIO/14

A study on different patterns of alteration of the neuron-glia interplay in experimental models of neurodegeneration

Dottorando
Dott. Ugolini Filippo

Tutore
Prof.ssa Maria Grazia Giovannini

Coordinatore
Prof.ssa Elisabetta Teodori

Anni 2016/2019

Index

Introduction

1.1 The main cells of the central nervous system

The main cells in the central nervous system are essentially of two types: neurons and glial cells. Neurons are excitable cells with the function of producing, transmitting and receiving nerve impulses (Rutecki, 1992), while glial cells mainly, but not only, are cells with function of structural support, nutrition, replacement and immune functions. Glial cells are a highly heterogeneous cell population that consist of astrocytes, microglia and oligodendrocytes, and contribute to regulation and control functions; recently it has also been re-evaluated their role in nerve impulse conduction.

1.1.1 Neurons

A neuron is an electrically excitable cell that processes and transmits information through electrical and chemical signals. These signals between neurons occur via synapses, which are specialized connections with other cells. Neurons can connect each other to form neural networks. Neurons are the main components of the brain and spinal cord of the central nervous system (CNS), and of the ganglia of the peripheral nervous system (PNS). There are several types of specialized neurons. Sensorial neurons respond to stimuli such as touch, sound or light and all other stimuli affecting the cells of the sensorial organs and then send signals to the spinal cord and brain. Motor neurons receive signals from the brain and spinal cord to cause muscle contractions and affect glandular secretions. Interneurons connect the neurons each other within the same region of the brain, or spinal cord in neural networks. A typical neuron consists of a cell body (soma), dendrites, and an axon. The term neurite is used to describe either a dendrite or an axon, particularly in its undifferentiated stage. Dendrites are thin structures that arise from the cell body, often extending for hundreds of micrometres and branching multiple times, giving rise to a complex "dendritic tree". An axon (also called nerve fibre when it is myelinated) is a special cellular extension (process) that arises from the cell body at a site called the axon hillock and travels for a distance, as far as one meter in humans or even more in other species. The axon terminal contains synapses, specialized structures where chemicals neurotransmitter are released to communicate with target neurons (Koester & Siegelbaum, 2000). Nerve fibres are often bundled into fascicles, and in the peripheral nervous system, bundles of fascicles make up nerves. The cell body of a neuron frequently gives rise to multiple dendrites, but never more than one axon, although the axon may branch hundreds of times before it terminates. In much of synapses, signals are sent from the axon of one

neuron to a dendrite of another. There are, however, many exceptions to these rules: for example, neurons can lack of dendrites, or haven't got an axon, and synapses can connect an axon to another axon or a dendrite to another dendrite. All neurons are electrically excitable, maintaining voltage gradients across their membranes by metabolically driven ion pumps, which combine with ion channels embedded in the membrane to generate intracellular-versus-extracellular concentration differences of ions such as Na^+, K^+, Cl^-, Ca^{2+}. Changes in membrane voltage can alter the function of voltage-dependent ion channels. If the voltage changes enough, an all-or-noneaction potential is generated, which travels rapidly along the cell axon, and activates synaptic connections with other cells when it arrives.

1.1.2 Astrocytes

Astrocytes (Astro from Greek astron = star and cyte from Greek "kyttaron" = cell), also known collectively as astroglia, are characteristic star-shaped glial cells of the brain and spinal cord. Astrocytes represent 40-50% of all glial cells. From the embryological point of view, they derive from the ectoderm of the neural tube. These cells consist of a cell body from which originate numerous processes. Immunohistochemical techniques based on the specific marker GFAP (Glial Fibrillary Acidic Protein) has allowed to define the morphology of these cells. Astrocytes are multifunctional cells that are indispensable for neuronal survival and function. They contribute to the formation and preservation of a secure blood-brain barrier (BBB), and their tight organization around the microvasculature provides anatomical evidence for the necessity of glucose to enter astrocytes on its way to neurons and other glial cells (Figure 1). Astrocytes are a reservoir of glycogen, which, depending on the degree of neuronal activity, is degraded to lactate that is delivered to neurons and oligodendrocytes as energy source (Tsacopoulos & Magistretti, 1996; Sanchez-Abarca et al., 2001; Brown et al., 2004).

Astrocytes have an orderly arrangement in the brain parenchyma with minimal overlap; each astrocyte covers a specific territory that interfaces with the blood vessels and includes hundreds of synapses (Bushong et al., 2004). The entire cell surface is covered by lamellar extensions and protrusions (Chao et al., 2002), processes with the same structural composition, endowed with motility, which confer to astrocytes the ability to have dynamic interactions with the surrounding synapses. Much of astrocytes also present "end feet", processes through which they contact the blood vessels and participate in the formation of the blood-brain barrier (Simard et al., 2003).

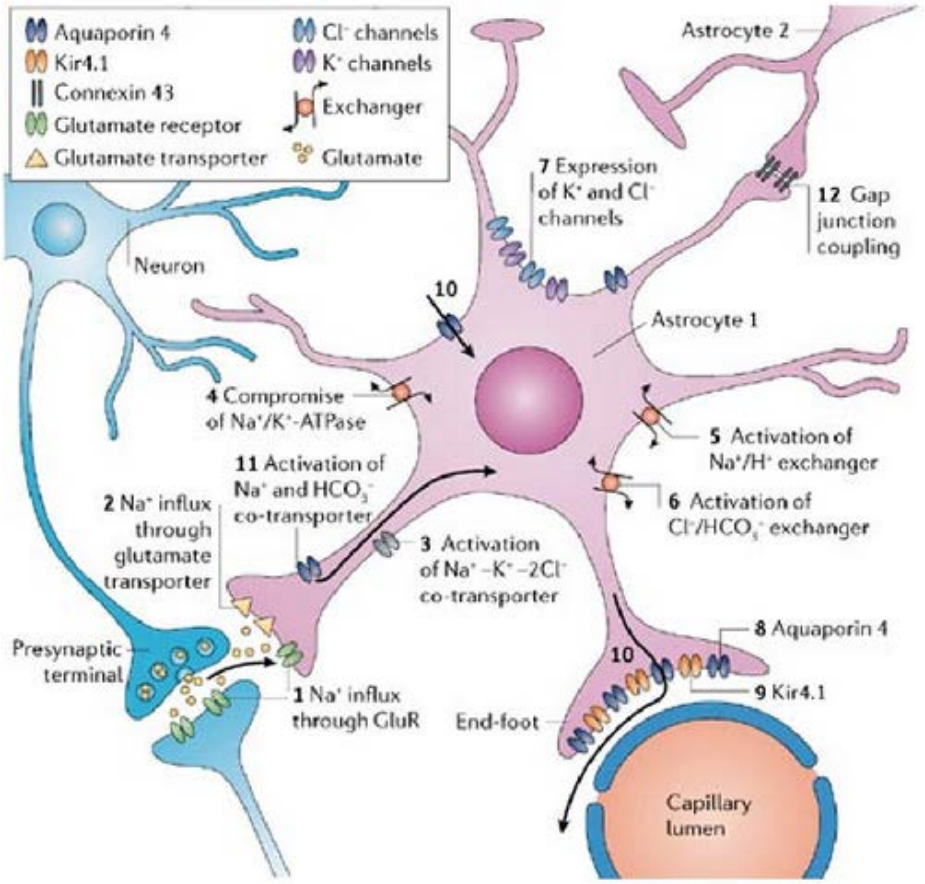

Figure 1. Astrocytes numerous functions that help maintaining CNS homeostasis (Seifert et al., 2006).

Until a few years ago it was thought that astrocytes had similar characteristics in different areas of the brain; however, recent studies have shown that it is a highly heterogeneous cell group (Grass et al., 2004; Matthias et al., 2003). Indeed, we can distinguish three types of astrocytes:

1- fibrous astrocytes, located in the white matter, characterized by the presence of thick fibrillar structures within the cell body, the gliofibrils, formed by the aggregation of thinner gliofilaments;

2- protoplasmic astrocytes, present in the grey matter, with less gliofilaments and bigger cell body than the previous one. Protoplasmic astrocytes, such as microglial cells, are capable of phagocytosis;

3- radial astrocytes, with an elongated shape, arranged perpendicularly to the axis of the ventricles; during the development of the nervous system they promote the migration of neural tube's cells toward their final location.

Functional studies on the hippocampus have also evidenced the presence of astrocyte populations with different types of voltage-gated channels (Steinhauser et al., 1992) and

different types of responses to the AMPA glutamate receptors (Zohu & Kimelberg, 2001).

Astrocytes are coupled via gap junctions, which are mainly formed by connexins 30 and 43 (Farahani et al., 2005). Gap junctions consist of clusters of closely packed hemichannels, which align between neighboring cells head-to-head to form channels. They provide direct cytoplasmic passage of ions and small molecules such as glucose metabolites, second messengers and neurotransmitters. Ca^{2+}-mediated intercellular signaling is a mechanism by which astrocytes communicate with each other and modulate the activity of adjacent cells, including neurons, oligodendrocytes and microglia (Scemes, 2006; Nedergaard, 1994; Nedergaard, 1995). The propagation of intercellular Ca^{2+} waves might work by enhanced release of ATP, which activates purinergic receptors on neighboring astrocytes (Cotrina, 1998; Nedergaard, 2003).

Astrocytes also interact with the blood vessels and with the synaptic terminals. The idea that astrocytes could connect blood vessels and neurons is due to Camillo Golgi back to the late XIXth century (Golgi, 1871). However, only recently we have highlighted the dynamic processes that complement these structural interactions, as the active dialogue between astrocytes and other brain elements. According to the new perspective, astrocytes are multipurpose cells involved in almost every process of the central nervous system, acting as local integration units and bridges between synaptic and non-synaptic communication (Volterra & Mendolesi, 2005).

It has become clear that astrocytes provide structural, metabolic and trophic support to nerve cells. More particularly, astrocytes:

- Ensure the maintenance of physiological concentrations of K^+, even during the intense firing activity of neurons, preventing depolarization and hyperexcitability (Karwoski, et al. 1989);
- Through specific transporters present on their membranes regulate and control the extracellular concentration of the neurotransmitters released into the synaptic cleft, such as GABA and glutamate (Coco et al., 1997; Dehnes et al., 1998);
- Have the capacity to synthetize glutamate and GABA precursors (Ransom et al., 2003);
- Provide lactate and other energy substrates to neurons (Tsacopoulos & Magistretti, 1996).

Over the last 20 years new experimental evidence has revolutionized the classical view of astrocytes as a simple passive support of neuronal cell function, demonstrating their

crucial role in synaptogenesis processes (Hama et al., 2004; Mauch et al., 2001) and neurogenesis (Garcia et al., 2004; Sanai et al., 2004). Recent studies have also demonstrated the role of astrocytes in the coupling of neuronal activity with cerebral blood flow (Gordon et al., 2008; Hirase, 2005). Studies conducted both *in vivo* and *in vitro* in the cortical region indicate that the synaptic release of glutamate activates metabotropic glutamate receptors on astrocytes. Stimulation of these receptors causes an increase in the levels of Ca^{2+} by astrocytic "end-feet" with the release of arachidonic acid and its metabolites, eventually leading to dilation of the arterioles (Takano et al., 2006). The discovery, which occurred in the '80s, that astrocytes express a wide range of neurotransmitter receptors, often similar to those in the surrounding synapses, signed a new era in the research on glial cells. It has been pointed out that these receptors can be activated by the release of neurotransmitters during synaptic activity and lead to increased Ca^{2+} in the cytoplasm of astrocytes. This event causes the release of chemical transmitters, the "gliotransmitters", such as glutamate, ATP, and D-serine, responsible for the intercellular communication between astrocytes and neurons (Araque et al., 1999). The released gliotransmitters can activate the neuronal receptors and modifying neuronal excitability and synaptic transmission (Fellin et al., 2004; Jourdain et al., 2007; Santello & Volterra, 2008; Schipke & Kettenmann, 2004). All these observations have led to formulate the new concept of "tripartite synapses", according to which astrocytes must be regarded as the third element of the signal integration unit (Araque et al., 1999; Volterra et al., 2014). Astrocytes can be excited, to take action in response to the neurotransmitter released at pre-synaptic neuron level and then to modify the neuron response at pre-synaptic and post-synaptic level. Furthermore, astrocytes are able to propagate this state of excitation to other astrocytes, at distance from the starting synapses.

1.1.3 Microglia

Microglia is composed by small cells located in both the white and grey matter and represents about 20% of glial cells. Microglia cell body is ovoid, with thin extensions and rich in lysosomes. The origin of microglia has been widely debated. It was thought that they descend from neuroectoderm or that they are myeloid mixed population. On the other hand, recent studies have shown that they are specialized cells, with capacity of self-renewal (Ajami et al., 2007; Ginhoux et al., 2013), which originate from bone marrow precursors in the mesoderm; and from here they migrate to the CNS, becoming

brain cells. For a long time, the central nervous system was considered isolated and inert from an immune point of view; given the low expression of MHC II molecules and the lack of lymphatic system it was thought that the blood-brain barrier isolated the brain from the peripheral immune system. The presence and activity of immune-competent cells, and the recent studies, aimed to understand the physiological role of microglia in the nervous tissue (Hanisch, 2013; Kettenmann et al., 2013; Tremblay et al., 2011), have allowed us to re-evaluate this hypothesis. It was also noted that lesions of the CNS cannot compromise the integrity of the barrier (Gay et al., 2007). Pio del Rio-Hortega conducted various research to qualify the microglia as the main immune intrinsic effector of the brain (Del Rio-Hortega, 1922). These cells can express on their surface a series of immune-molecules able to expose antigens to T lymphocytes; moreover, they are able to release mediators. The role of microglia is critical in the early stages of embryonic development in which excess neurons are produced; later, these neurons face programmed cell death and break up into small apoptotic bodies, removed by microglia (Pont-Lezica et al., 2011). Microglia change their morphology in relation to the development of the CNS and in particular pathological conditions.

We can identify four types of microglia:

1- amoeboid microglia: immature form that removes dying cells in the remodelling process of the foetal brain;

2- branched microglia at rest (or quiescent microglia): CNS adult form, characterized by long and branched apophyses and a small cell body;

3- non-phagocytic activated microglia: intermediate stage between the branching and the phagocytic form;

4- phagocytic microglia: mainly of amoeboid shape and large dimensions. It is situated in brain areas affected by necrosis or inflammation; it phagocytes foreign materials and exposes immune-molecules for the activation of T lymphocytes. Interacts also with astrocytes and neurons to re-establish quickly tissue homeostasis (Figure 2).

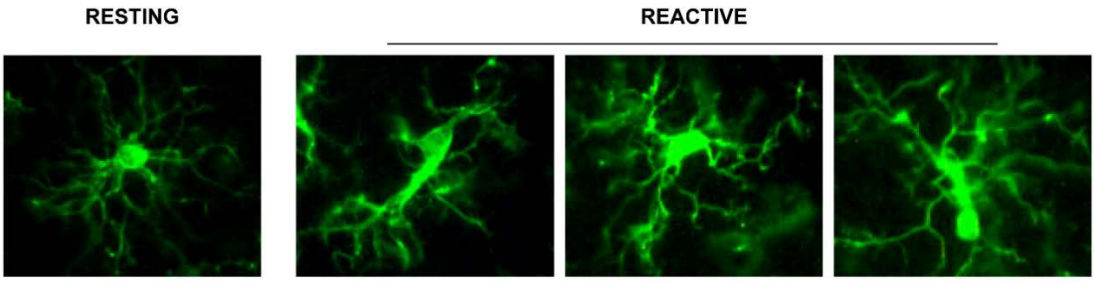

Figure 2. Representation of the different stages of microglia activation, marked with the anti IBA1 antibody (Cerbai et al., 2012).

Microglia is thus able to respond rapidly to physiological and pathological changes of the brain microenvironment, by processes of activation and modification of cell morphology, and through rapid monitoring movements of degeneration of neuronal cells. Actually, microglia cells in quiescence are in a status of alertness and patrolling to the extracellular environment variations (Kreutzberg, 1996). Activation of microglia is quick and leads to morphological, immunophenotypic and functional changes, a process which stimulates the migration of microglia to the part of the brain affected by tissue damage, as recently demonstrated by Morsch and collaborators in the spinal cord of zebrafish (Morsch et al., 2015), where it can phagocyte damaged cells or debris. The activated microglia, after having fulfilled its function of phagocytosis, is also able to regress rapidly to the quiescent form (Morsch et al., 2015). Several studies have shown that microglia can be activated more quickly compared to astrocytes. A 2007 study, conducted by induction of electrical stress in the hippocampus of rats, showed a rapid increase in the number of activated microglia, correlated with reduced expression of the neuronal glycoprotein CD200 (Frank et al., 2007). This glycoprotein is expressed on the neuronal surface and binds CD200 receptors expressed on the membrane of neutrophils, macrophages, monocytes, lymphocytes and microglia. It is supposed that the glycoprotein CD200 mediates an interplay between microglia and neurons. The glycoprotein-receptor interaction maintains microglia in a quiescent state; therefore, reduced expression of glycoprotein CD200 on the neuronal membrane (due, for example, to electric hippocampal stress) would promote the activation of microglia. The reduced expression of CD200 was evidenced also in animal models of inflammation and in the hippocampus of aged rats (Matsumoto et al., 2007; Lyons et al., 2007). It was highlighted also that there exists an astrocyte-microglia dialogue. Astrocytes release substances useful for the activation and proliferation of microglia, such as M-CSF (Macrophage Colony Stimulating Factors), and GM19 CSF (Granulocyte-Macrophage Colony Stimulating Factors) (Watkins et al., 2007). On the other hand, microglia communicate with astrocytes through the release of growth factors and cytokines, including IL-1, which regulates the proliferation of astrocytes (Streit et al., 1999). The rapid activation of microglia after damage has been associated with the rapid activation of NF-kB (Nuclear transcription Factor). This factor does not require "*de novo*" protein expression, but its active form must translocate from the cytoplasm to the nucleus, justifying the fast response of microglial cells to damage.

Inflammatory cytokines, such as IL-1 and IL-6, also act as activators of NF-kB and in this way, they recruit microglia (Gehrmann et al., 1995). The stimulation or inactivation process of microglia may be mediated by other factors produced by neurons, by pathogens or by immune cells. The interferon-γ and IL-4 are released by T cells and stimulate the expression of MHC II on microglia, accelerating the processes of proliferation. The mitogenic factors GM-CSF and M-CSF stimulate the proliferation and recruitment of microglia. LPS, expressed on the wall of Gram-negative bacteria, is an endotoxin, which behaves as an immunostimulant. Matrix metalproteinases (MMPs), membrane-zinc proteins, are released from apoptotic cells and stimulate microglial activation. On the contrary, TGF-β1 and IL-10 negatively modulate microglia, reducing the expression of MHC II. When microglia are activated, it rapidly expresses high levels of MHC II and several types of immunoglobulins family receptors, complement receptors, cytokines, chemokines (IFN-γ, IFN-β, IFN-α, IL-1, IL6, IL -10, IL-12) and receptors for mannose. Therefore, the cells acquire the ability to recognize and bind various antigens and present them to T lymphocytes (Rock et al., 2004). Microglia is involved in the repair of brain damage by removing the cause. The action of these cells is dichotomous. At first microglia intervenes in tissue repair, removal of apoptotic cellular debris and restore tissue homeostasis, playing the same role of macrophages in the peripheral organs. Later it acquires phagocytic activity and releases substances with potential cytotoxic action, such as reactive oxygen intermediates, NO, proteases, derivatives of arachidonic acid, excitatory amino acids, quinolinic acid and cytokines such as IL-1 and TNFα. These substances inhibit the proliferation of oligodendrocytes and the deposition of myelin (Merrill, 1991). This cytotoxic effect causes the expansion of inflammatory processes and appears to be responsible for the involvement of microglia in many neurodegenerative diseases such as Alzheimer's disease, Parkinson's disease, multiple sclerosis and dementia associated with HIV (Kim & Tong, 2006). Microglia then appears as a "double-edged sword" in the brain’s defence, and studies on the modulation of its activity may represent a future therapeutic target for the treatment of many diseases.

1.2 The hippocampus

The hippocampus is a major component of the brain of humans and other vertebrates (Amaral & Lavenex, 2007). Humans and other mammals have two hippocampi, one in each side of the brain (Anderson et al., 2007). The hippocampus, a structure located in

the temporal lobe, is a part of the limbic system, which consists of many different cerebral areas destined to spatial learning, emotion, correlated vegetative expressions and memory. It is located under the cerebral cortex (allocortical) and in primates in the medial temporal lobe. The functional significance of the limbic system, one of the most fascinating and mysterious encephalic areas, is not completely clear. Its anatomic location, halfway between the hypothalamus and cortical frontal lobe, allows the mediation between vegetative functions elaborated in the hypothalamus and the information derived from associative cortex, to produce and integrate emotions. It contains two main intercommunicating parts: the hippocampus proper (also called Ammon's horn, *Cornu Ammonis*) and the dentate gyrus. The hippocampus shows a typical structure that allows us to identify certain cell types such as the neurons of Stratum Pyramidalis, which are among the most sensitive to ischemia and display the characteristic neuropathological damages of Alzheimer's disease. Therefore, the rat or mouse hippocampus is a cerebral region that often is utilized in studies of neurodegenerative pathologies. Hippocampus neuroanatomy is an interesting trait: it is a subject of many studies due to its apparently simplified organization of its cellular layers, a well-defined structural organization, and its complex laminar distribution of afferent fibres (input). The hippocampus, including the dentate gyrus, shows a characteristic "C"-like elongated form, which makes it very similar to a sea horse, from which the name "hippocampus" derives (from the Greek "hippo" horse and "kampos" monster of the sea). One of the most important areas of the hippocampus resembles a ram's horn or *Cornu Ammonis* (CA) subdivided in the areas CA1, CA2, CA3, and CA4 (Amaral & Lavenex, 2007). Its main axis extends from the rostral region of septal nucleus, upper and dorsal segments of diencephalon, and reaches the temporal lobe in its ventral and caudal region. The hippocampus can be seen as a ridge of grey matter tissue, elevating from the floor of each lateral ventricle in the region of the inferior or temporal horn. This ridge can be seen also as an inward faged of the archicortex into the medial temporal lobe. The hippocampus can only be seen in dissections as it is concealed by the parahippocampal gyrus.

The term hippocampal formation is used to refer to the hippocampus proper and its related parts. However, there is no consensus on which parts are included. Sometimes the hippocampus is said to include the dentate gyrus and the subiculum (Amaral & Lavenex, 2007; Martin, 2003). Some references include the dentate gyrus and the subiculum in the hippocampal formation, and others include the

presubiculum, parasubiculum, and entorhinal cortex (EC). The neural layout and pathways within the hippocampal formation are very similar in all mammals.

In rodents, the hippocampus can be divided into two fundamental regions: a wide region that is populated by cells, which adjoin to dentate gyrus and a smaller one that follows it. Santiago Ramòn y Cajal named these two regions “lower” and “upper”, respectively. However, at present it is utilized the nomenclature introduced by Lorent de Nò, with CA2 and CA3 regions corresponding to lower region and CA1 corresponding to upper region. The other regions of hippocampal formation are dentate gyrus, subiculum, presubiculum and entorhinal cortex, which in rodents is divided in medial and lateral. Due to the presence of pyramidal neurons in large projections and interneurons of different and smaller dimensions, at organizational level the hippocampus resembles different cortical regions. Nevertheless, the mainly unidirectional transfer of information through intra-hippocampal circuits and the widespread three-dimensional organization of interconnections (intrinsic associational connections, IAC), make the hippocampal neuroanatomy unique (Figure 3).

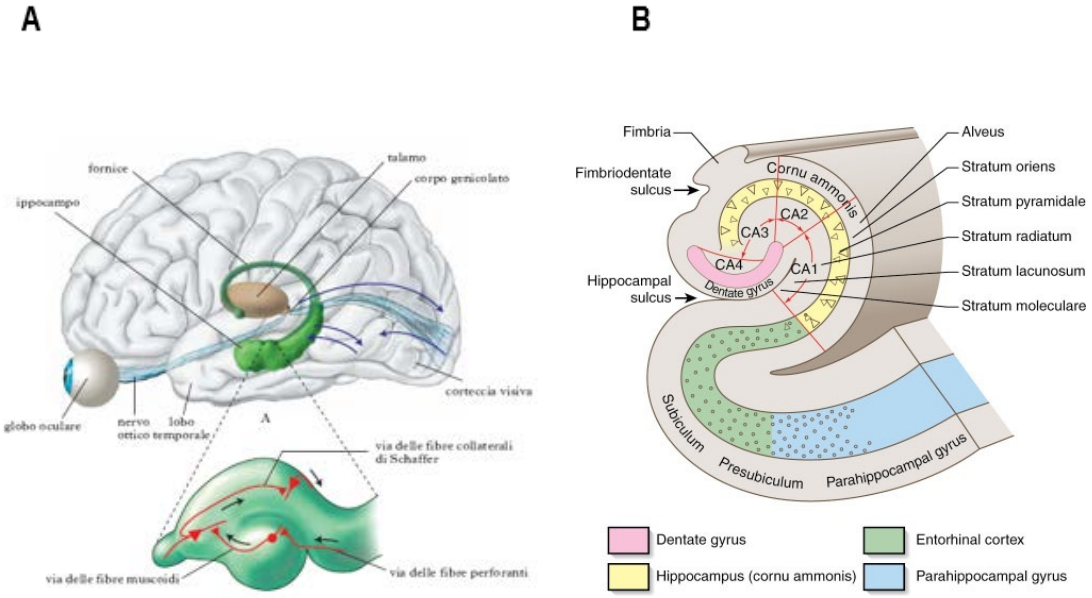

Figure 3: A. Hippocampal structure with its projections: note the unidirectional nature of the fiber pattern. B. The different regions of the hippocampus, with the input of the afferent fibers in the toothed wheel and the exit from the CA1 (Amaral & Lavenex, 2007).

The EC is considered the first entry passage into hippocampal structure: from its exterior layers cells originate axonical projections which reach the dentate gyrus (DG), forming the afferent paths of the structure called perforating fibres. This path is unidirectional because the dentate gyrus never projects towards EC. The granular cells of the dentate gyrus give rise to axonic projections, the musk fibres, which connect with

the pyramidal cells of CA3 region. Axons of CA3 cells form the Schaffer's collateral fibres, which represent the primary source of information to CA1, where subiculum excitation cells are present. From CA1 onwards the unidirectional and simple fibres organization becomes much more complex: indeed, the CA1 region project also towards EC, where arrive the cortical projections from the subiculum, connected to parasubiculum and presubiculum.

1.2.1 Principal subtypes of neurons of hippocampus

The principal neuronal cell type of the hippocampus is the pyramidal cell, which makes up most of the neurons in the pyramidal cell layer of CA1, CA2 and CA3. Pyramidal cells have basal dendrites that extend into the *stratum oriens* and an apical dendritic tree that extends into the *Stratum Radiatum* to the hippocampal fissure.

Pyramidal Cells of CA1

In contrast to the substantial heterogeneity of dendritic organization characteristic of CA3 pyramidal cells, investigators such as Norio Ishizuka and Dennis Turner and colleagues (Pyapali et al., 1998) demonstrated that the CA1 pyramidal cells show remarkable homogeneity of their dendritic trees. As well as being more homogeneous, they are also, on average, smaller than CA3 cells. The total dendritic length averages approximately 13.5 mm, and the average size of CA1 cell somata is about 193 μm^2 or 15 µm in diameter. Regardless of where a pyramidal cell is located in CA1, it has about the same total dendritic length and the same dendritic configuration. Some pyramidal cells have one apical dendrite, and others have two. Cells with two apical dendrites tend to have slightly greater total dendritic length in the apical direction. Neurons with a single apical dendrite, however, tend to have slightly larger basal dendritic trees; thus, overall, the dendritic tree in all CA1 neurons have about the same total length. This anatomical homogeneity, however, cannot reflect functional homogeneity because, as we shall see shortly, there are differences in the entorhinal cortex inputs received at different locations along the transverse axis of CA1.

Pyramidal Cells of CA3 and CA2

Ishizuka and colleagues (Ishizuka et al., 1995) demonstrated that the dendritic length and organization of CA3 pyramidal cells are quite variable. The smallest cells (with a soma size of about 300 μm^2 or 20 µm in diameter) are located in the limbs of the dentate gyrus and have a total dendritic length of 8 to 10 mm. The largest cells (with a

soma size of about 700 μm^2 or 30 μm in diameter), which are located distally in the field, have total dendritic lengths of 16 to 18 mm. The distribution of the dendritic trees of CA3 pyramidal cells also varies depending on where the cell body is located. Cells located in the limbs of the dentate gyrus, for example, have few or none of their dendrites extending into the *stratum lacunosum-moleculare*, and thus these cells receive little or no direct input from the entorhinal cortex. The cells, however, receive a larger number of mossy fiber terminals on their apical and basal dendritic trees and are thus under greater influence of the granule cells than distally located CA3 cells, which receive only apical mossy fiber input.

Dentate Granule Cell

The granule cell is the principal cell type of the dentate gyrus. This cell has an elliptical cell body with a width of approximately 10 μm and a height of 18 μm (Claiborne et al., 1990). Each cell is closely apposed to other granule cells, and in most cases, there is no glial sheath intervening between the cells. The granule cell has a characteristic cone-shaped tree of spiny dendrites with all the branches directed toward the superficial portion of the molecular layer; most of the distal tips of the dendritic tree end just at the hippocampal fissure or at the ventricular surface. The dendritic trees of granule cells located in the suprapyramidal blade tend, on average, to be larger than those of cells located in the infrapyramidal blade (3500 μm vs. 2800 μm). Desmond and colleagues (Desmond & Levy, 1985) provided estimates for the number of dendritic spines on the granule cell dendrites. They found that cells in the suprapyramidal blade have 1.6 spines/μm, whereas cells in the infrapyramidal blade have 1.3 spines/μm. With these numbers and the mean dendritic lengths given above, an estimate of the number of spines on the average suprapyramidal granule cell would be 5600 and for an infrapyramidal cell 3640. The total number of granule cells in one dentate gyrus of the rat is about $1.2*10^6$ (West et al., 1991; Rapp & Gallagher, 1996). The packing density and thickness of the granule cell layers varies somewhat along the septotemporal axis of the dentate gyrus (Gaarskjaer, 1978). The packing density of terminate exclusively on the initial segments of other axons. Interneurons have been distinguished also based on their inputs. Interneurons can be differentiated also from principal cells based on their electrophysiological characteristics. At least some interneurons have high rates of spontaneous activity and fire in relation to the theta rhythm. For this reason, interneurons are called often theta cells. A major challenge is to determine if different

classes of interneurons demonstrate distinct electrophysiological response profiles. Within the same subgranular region occupied by the cell bodies of the pyramidal basket cells are several other cell types with distinctly different soma shapes, as well as different dendritic and axonal configurations (Amaral, 1978). Some of these cells are multipolar with several a spiny dendrite entering the molecular and polymorphic layers, whereas others tend to be more fusiform shaped with a similar dendritic distribution. As Ribak and colleagues pointed out, many of these cells share fine structural characteristics such as infageded nuclei, extensive perikaryal cytoplasm with large Nissl bodies, and intranuclear rods. Moreover, it appears that all these cells give rise to axons that contribute to the basket plexus in the granule cell layer. Many of these neurons are immunoreactive for GABA. They form symmetrical synaptic contacts with the cell bodies, proximal dendrites, and occasionally axon initial segments of granule cells and therefore function as inhibitory interneurons. These cells are not neurochemically homogeneous, however, as subsets appear to colocalize distinct categories of other neuroactive substances.

Pyramidal Basket Cell

The most intensively studied interneuron is the pyramidal basket cell. These cells are generally located along the deep surface of the granule cell layer, have pyramidal shaped cell bodies (25 to 35 µm in diameter), and are wedged slightly into the granule cell layer. The basket portion of the name refers to the fact that the axon of these cells forms pericellular plexuses that surround and form synapses with the cell bodies of granule cells. Ramon y Cajal first described the pyramidal basket cells as having a single, principal aspiny apical dendrite directed into the molecular layer (where it divides into several aspiny branches) and several principal basal dendrites that ramify and extend into the polymorphic cell layer. Most of these cells contain biochemical markers for the inhibitory transmitter γ-aminobutyric acid (GABA) and are thus presumably inhibitory (Ribak et al., 1978; Ribak & Seress, 1983). The number of basket cells is not constant throughout the transverse or septotemporal extents of the dentate gyrus (Seress & Pokorny, 1981). At septal levels, the ratio of basket cells to granule cells is 1:100 in the supra-pyramidal blade and 1:180 in the infra-pyramidal blade. At temporal levels, the number is 1:150 for the supra pyramidal blade and 1:300 for the infrapyramidal blade. Despite the apparent cytoarchitectonic homogeneity of the

hippocampal fields, there are several differences (especially regarding neurochemical innervation) at different septotemporal levels of the hippocampal formation.

Mossy cell

The polymorphic layer harbors a variety of neuron types, but little is known about many of them (Amaral, 1978). The most common type, and certainly the most impressive, is the mossy cell. This cell type is probably what Ramon y Cajal referred to as the "stellate or triangular" cells located in his subzone of fusiform cells; and it is undoubtedly what Lorente de Nó referred to as "modified pyramids." The cell bodies of the mossy cells are large (25–35 μm) and are often triangular or multipolar in shape. Three or more thick dendrites originate from the cell body and extend for long distances in the polymorphic layer. Each principal dendrite bifurcates once or twice and generally gives rise to a few side branches. Although most of the daughter dendritic branches remain within the polymorphic layer, an occasional dendrite pierces the granule cell layer and enters the molecular layer. The mossy cell dendrites virtually never enter the adjacent CA3 field. The most distinctive feature of the mossy cell is that all its proximal dendrites are covered by large, complex spines evocatively called thorny excrescences. These spines are the distinctive sites of termination of the mossy fiber axons (i.e., axons of the dentate granule cells). Although thorny excrescences are also observed on the proximal dendrites of pyramidal cells in CA3, they are never as dense as the ones on the mossy cells. The distal dendrites of the mossy cell have typical pedunculate spines that appear to be less densely distributed than those on the distal dendrites of the pyramidal cells in the hippocampus. The mossy cells are immunoreactive for glutamate and give rise to axons that project to the inner third of the molecular layer of the ipsilateral and contralateral dentate gyrus, making asymmetrical terminations on the dendrites of granule cells. The mossy cells thus appear to be the major source of the excitatory associational/commissural projection to the dentate gyrus.

1.2.2 Morphology and role in cognitive and behavioural functions of CA1 and CA3 areas of hippocampus

A common organizational feature of connections between regions of the neocortex is that they are largely reciprocal (Felleman & Van Essen, 1991). If cortical region A projects to cortical region B, region B often sends a return projection back to region A. As first described by Ramón y Cajal (1893), this is clearly not the case for the connections that link the various parts of the hippocampal formation. The EC can, for

convenience, be considered the first step in the intrinsic hippocampal circuit, because much of the neocortical input reaching the hippocampal formation does so through the EC. Cells in the superficial layers of the EC give rise to axons that project, among other destinations, to the dentate gyrus. The projections from the EC to the dentate gyrus form part of the major hippocampal input pathway called the perforant path. Although the EC provides the major input to the dentate gyrus, the dentate gyrus does not project back to the EC. This pathway is therefore nonreciprocated, or unidirectional (Andersen et al., 2007).

The critical importance of CA1 neurons in learning and memory is seen in the profound memory loss exhibited by patients with lesions in this region, which has been complemented by numerous studies in animal models. Information from the EC reaches CA1 neurons along two excitatory pathways, one direct and one indirect. Together these inputs are termed the *perforant pathways* (Figure 4). The *direct pathway* has its origins in neurons of layer III of the EC. The axons of these neurons form synapses on the very distal apical dendrites of CA1 neurons (such perforant projections are also called the temporoammonic pathway). In the *indirect pathway* information from neurons of layer II of the EC reaches CA1 neurons through the *trisynaptic pathway*. In the initial leg of this pathway the axons of layer II neurons project through the *performant pathway* to the granule cells of the dentate gyrus. The granule cell axons project in the *mossy fiber pathway* to excite the pyramidal cells in the CA3 region of the hippocampus. Finally, the CA3 axons project through the *Schaffer collateral pathway* to make excitatory synapses on more proximal regions of CA1 pyramidal cell dendrites. The fact that CA1 pyramidal neurons receive cortical information through two pathways has led to the view that CA1 neurons compare information in the indirect circuit with sensory input from the direct pathway. Lesion studies indicate that both direct and indirect inputs to CA1 may be necessary for normal learning and memory. Lesions of the indirect Schaffer collateral pathway limit the ability of mice to perform a complex spatial learning and memory task, although some form of spatial learning remains intact. Lesions of the direct pathway to CA1 do not appear to alter initial formation of memory but inhibit the ability of an animal to store those initial memories as long-term memory, a process termed *consolidation*. Genetic inactivation of the direct path also interferes with episodic memory, in which an animal must learn about the temporal relation between two or more events (Kandel, 2001). The most important feature of the hippocampal CA3 is the presence of extensive interconnections between the main paths

of the side-fiber system (Amaral & Witter, 1989). Area CA3 receives inputs from many different converging pathways such as those derived from the performant path fibers from the medial and lateral EC, or the inputs of mossy fibers of dentate gyrus, returning an output in the form of new inputs through the side-recurring way (Amaral & Witter, 1989). Many researchers have reported that area CA3 projects to the nuclei of the medial and lateral septum and vertical limb of the diagonal band of Broca (Gaykema et al., 1991; Amaral & Witter, 1989; Risaged & Swanson, 1997).

The medial septum and vertical limb of the diagonal band of Broca, alternately, send cholinergic and GABAergic inputs to the hippocampus (Amaral & Witter, 1989; Giovannini et al., 1994). It has been demonstrated that the CA3 region is divided into three areas called CA3 a, CA3 b and CA3 c, as schematically shown in Figure 5 (Lorente de Nó, 1934; Li et al., 1994).

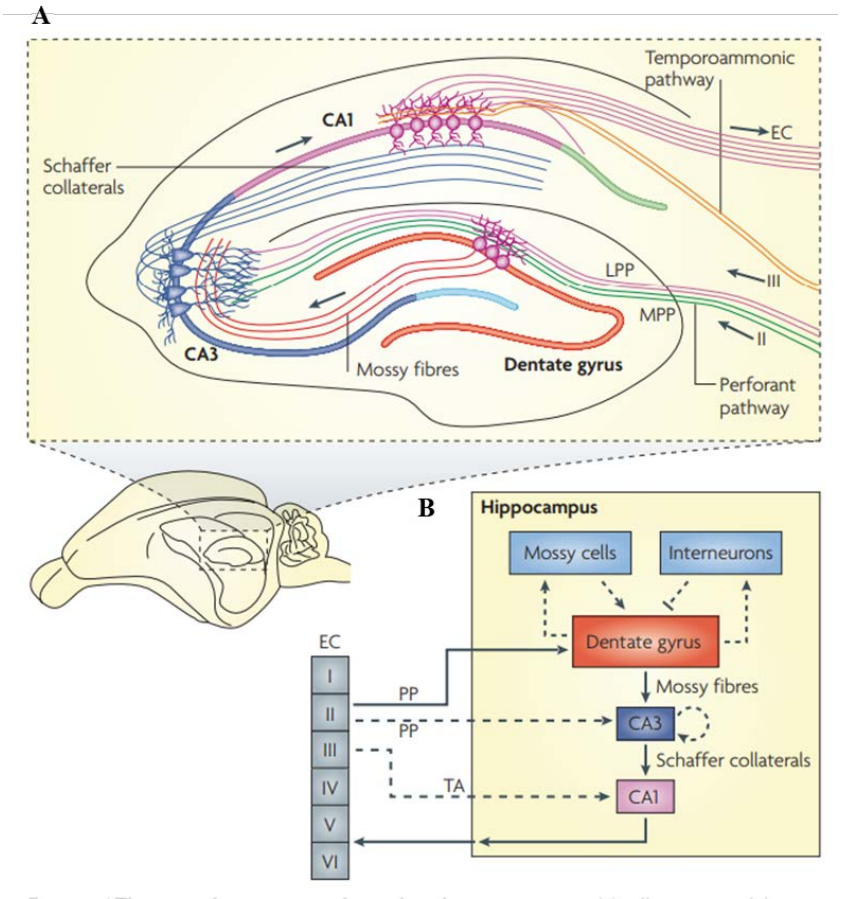

Figure 4: The neural circuitry in the rodent hippocampus. A. An illustration of the hippocampal circuitry. B. Diagram of the hippocampal neural network. The traditional excitatory trisynaptic pathway (entorhinal cortex (EC)–dentate gyrus–CA3–CA1–EC) is shown by solid arrows. The axons of layer II neurons in the entorhinal cortex project to the dentate gyrus through the perforant pathway (PP), including the lateral perforant pathway (LPP) and medial perforant pathway (MPP). The dentate gyrus sends projections to the pyramidal cells in CA3 through mossy fibres. CA3 pyramidal neurons relay the information to CA1 pyramidal neurons through Schaffer collaterals. CA1 pyramidal neurons send back-projections into deep-layer neurons of

the EC. CA3 also receives direct projections from EC layer II neurons through the PP. CA1 receives direct input from EC layer III neurons through the temporoammonic pathway (TA). The dentate granule cells also project to the mossy cells in the hilus and hilar interneurons, which send excitatory and inhibitory projections, respectively, back to the granule cells. (Deng et al., 2010).

Based on previous research (Li et al., 1994; Buckmaster & Schwartzkroin, 1994), it has been proposed that the mossy cells receive excitatory input from both granule cells of the dentate gyrus and from the pyramid cells of the CA3c area, which, alternately, through the axonal projections of the recurrent excitatory pathway activate many distal granule cells. Thus, the CA3c area might have a retrograde projection that can influence the granule cells of the dentate gyrus (Scharfman, 2007). Most of the integrated synaptic connections in all these different routes in area CA3 are modulated in their intensity (Marr, 1971; Treves & Rolls, 1994). These anatomical and physiological characteristics have inspired many theoretical models with the purpose of assign specific cognitive processes to the CA3 (Kesner et al., 2004; Rolls & Kesner, 2006).

From the behavioral point of view, the CA3a and CA3b areas of hippocampus play a fundamental role in both the encoding of new spatial information and in the formation of short-term memory with a duration from a few seconds to a few minutes. This can be observed easily in different behavioral tests: recognition of new objects, or test for the acquisition of short-term or working memory, or test focused on acquisition of spatial memory through audible and visual signals-clues. These tests have been developed to explore the processes that involve episodic memory and the interactions between the CA3a, CA3b and the dentate gyrus, through inputs arriving to CA3a,b from the mossy fibers. The CA3a,b area is also important for encoding spatial information which require multiple trials that also include the acquisition of arbitrary and relational associations. These tests tend to be non-episodic and can be mediated by arbitrary and joint operations. All these tests are designed to operate with an autoassociative function of the CA3 region.

The CA3 a,b area also plays a role in the sequential information processing in cooperation with the CA1 area, based on the output of Schaffer fibers that leave from CA3 and arrive to CA1 (Lorente de Nò, 1934). The CA3 a, b areas also support the recall of information arising from short-term memory based on the spatial patterns. Finally, the CA3a,b in cooperation with the dentate gyrus, plays an important role in the processing of environmental geometry.

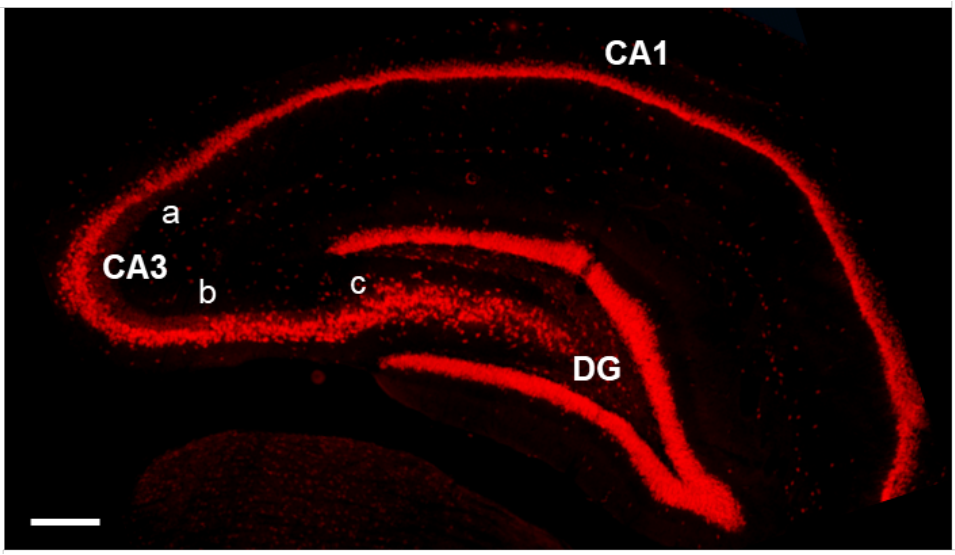

Figure 5. Representation of CA1, CA3 and DG areas of rat hippocampus with NeuN staining at the epi-fluorescent microscope. Evidence of the three regions a, b and c of the area CA3.

1.2.3 The hippocampus in neurodegenerative disease

The hippocampus is involved in many different disease processes, but only in rare instances is the hippocampus the only site of pathological damage. It is subject to the same pathologies that can affect other cortical areas, such as tumors, vascular malformations, and cortical dysgenesis; but in addition, the hippocampus is also notable for its vulnerability to damage as a consequence of ischemia/hypoxia, trauma, and hypoglycemia. There are also instances in which involvement of the hippocampal formation is critical to the manifestation of the disease; foremost among them are Alzheimer's disease and temporal lobe epilepsy, representing approximately 60% of all partial epilepsies. Damage to the hippocampus is also the central component of a variety of rare conditions, such as limbic encephalitis and dementia with isolated hippocampal sclerosis. In addition, involvement of the hippocampus is being increasingly recognized in schizophrenia, another common neuropsychiatric disorder. Acute encephalitis due to herpes simplex virus shows a predilection for limbic structures, and infection can result in selective damage to the hippocampus, amygdala, and associated structures, resulting in acute limbic encephalitis. Subacute limbic encephalitis has also been described in which the pathology more specifically affects the limbic system (Corsellis et al., 1968). The clinical presentation is characterized by behavioral and psychiatric problems (usually aggression and depression), disorientation, short-term memory deficits, hallucinations, seizures, and sleep disturbances (Corsellis et al., 1968; Gultekin et al., 2000). The pathological finding is aggregation of lymphocytes around blood vessels,

neuronal cell loss, and gliosis particularly affecting the hippocampus, dentate gyrus, amygdala, cingulate, and para-hippocampal structures. Limbic encephalitis can occur in response to certain cancers such as small-cell lung carcinomas, lymphomas, thymomas, and testicular tumors, as an immune-mediated syndrome. A similar syndrome has, however, been described in association with Wernicke's encephalopathy, systemic lupus erythematosus, and herpes simplex encephalitis. In these cases, there is a strong association with anti-neuronal antibodies directed against intracellular antigens, but the pathological role of these antibodies remains uncertain. Treatment of the underlying malignancy can alleviate the symptoms. Hippocampal sclerosis has been observed in a proportion of elderly patients presenting with cognitive impairment. In one study (Dickson et al., 1994), hippocampal sclerosis was observed in 26% of demented patients over the age of 80 years and in 16% of all patients aged over 80. In all cases there was neuronal loss and gliosis affecting CA1, the subiculum, and dentate granule cells, with additional neuronal loss in the entorhinal cortex in a proportion of cases. However, concomitant pathology, such as ischemic vascular damage or Alzheimer pathology, was noted in most of the cases in this study; "pure" hippocampal sclerosis is much rarer, affecting only 0.4% of patients with dementia (Ala et al., 2000). These rare instances of pure hippocampal sclerosis are not associated with any increase in risk factors for cerebrovascular disease, and in none of the cases was there a history of a hypoxic episode preceding the onset of cognitive impairment. The relation between hippocampal sclerosis, as a rare cause of dementia in the elderly, and mesial temporal sclerosis, as a substrate for epilepsy affecting a younger age group, remains undetermined. It is possible that the two diseases arise as a consequence of differing etiologies, with pure hippocampal sclerosis occurring as a consequence of a primary degenerative process rather than secondary to a systemic insult such as hypoxia or fever. Schizophrenia is thought to involve primarily the prefrontal cortex (Grossberg, 2000), but there is accumulating evidence for involvement of mesial temporal lobe structures in its pathophysiology. Neuropathological studies indicate that the loss of hippocampal volume correlates with a reduction in the size of hippocampal neurons rather than neuronal loss (Arnold et al., 1995). A reduction in neuronal density in certain hippocampal regions, with the CA2 interneurons particularly affected, is also observed in schizophrenia, as well as in manic depression (Benes et al., 1998). Loss of synaptic proteins in the hippocampus (Eastwood and Harrison, 1995) and abnormal MAP2

expression in subicular neuron dendrites also indicate abnormalities of connectivity in patients with schizophrenia (Cotter et al., 2000).

1.3 Astrocytes and microglia functional alterations in neurodegenerative processes

Until recently, neurons were considered the basic functional units of the central nervous system, while glia cells were believed to serve as only supportive elements. This concept is rapidly changing; it is becoming more and more evident that proper functioning of the neuron-microglia-astrocyte "triad" is fundamental for the functional organization of the brain (Barres, 2008; Allen & Barres, 2009) (Figure 6). Impaired interplay among neurons and glia may be responsible for derangements from normal brain aging to neurodegenerative processes (De Keyser et al., 2008; Sofroniew, 2009). Recruitment and activation of glial cells in a complex temporal pattern require well organized reciprocal communication between neurons and glia as well as among glial cells. Therefore, it is critical to better understand the interactions among neurons, astrocytes and microglia, the so-called triad, in physiological and during pathological processes.

Because of the plethora of roles in maintaining CNS functions and the many mechanisms controlling these functions, it is not surprising that alterations in astrocyte functionality is becoming recognised in an increasing number of diseases. Dysfunction of astrocytes is suspected to play a primary role in the pathogenesis of many brain disorders. Astrocyte swelling is a dramatic and very harmful component of any acute neurological injury, including stroke and brain trauma. Yet, it is not well understood why astrocytes are more likely to swell than neurons and how their swelling can be decreased. Neurological diseases, including dysmyelinating diseases and epilepsy, can result from mutations of astrocyte genes. Reactive gliosis (astrocytosis) also accompanies many neurological diseases. Although reactive astrocytosis clearly is beneficial in that it can encapsulate infections or traumatic tissue and help seal a damaged blood-brain barrier, there are many ways in which it has been found to be harmful. Glial scarring contributes substantially to the glial cues that inhibit severed CNS axons from regenerating (Silver, 2004).

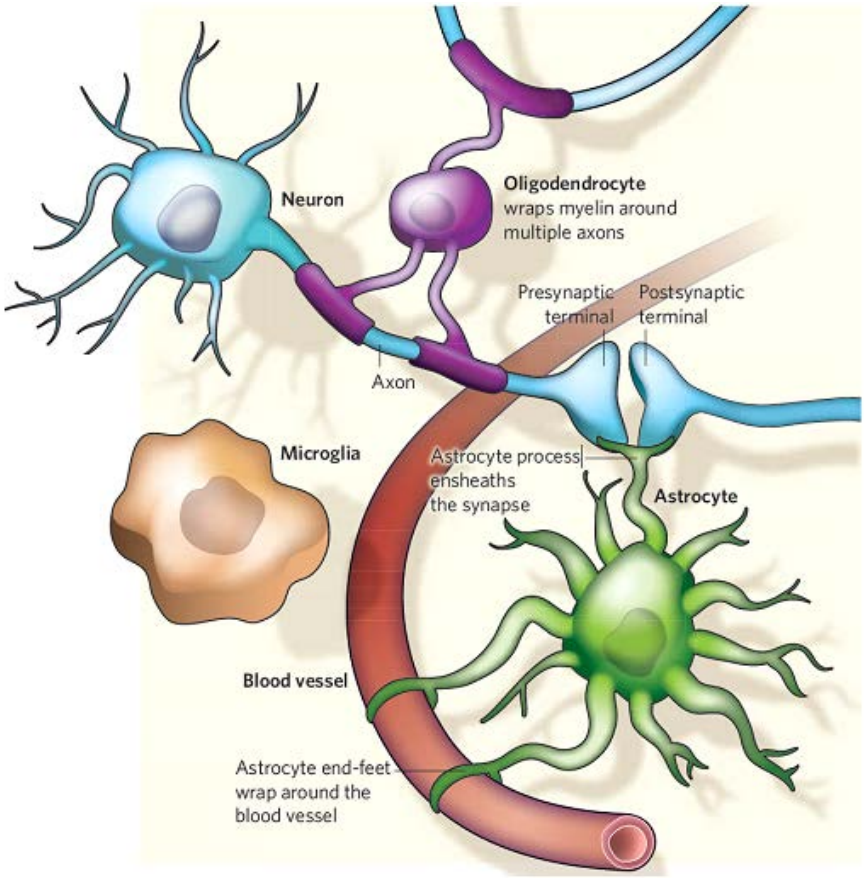

Figure 6. Glia–neuron interactions. Different types of glia interact with neurons and the surrounding blood vessels. Oligodendrocytes wrap myelin around axons to speed up neuronal transmission. Astrocytes extend processes that ensheath blood vessels and synapses. Microglia keep the brain under surveillance for damage or infection (Allen & Barres, 2009).

Reactive astrocytes upregulate synapse-inducing genes such as thrombospondins, which have the potential to help repair the brain (Liauw et al., 2008) but may also induce unwanted synapses that can cause epilepsy or neuropathic pain (Boroujerdi et al., 2008). In addition, recent studies have found that unhealthy astrocytes can release neurotoxic signals. For instance, mutant astrocytes carrying the SOD1 (G93A) allele release a toxic signal that rapidly kills wild-type motoneurons (Di Giorgio et al., 2007; Nagai et al., 2007; Lobsiger & Cleveland, 2007).

Emerging evidences provide a picture of growing complexity on the relationships between astrocytes, neurons, microglial cells and their function in the maintenance of the CNS in both physiological and non-physiological conditions. It has been demonstrated that in different neurodegenerative conditions astrocytes exhibit the morphological traits of clasmatodendrosis (Tomimoto et al., 1997). Clasmatodendrosis was described first by Alzheimer (quoted by Penfield, 1928) and named by Cajal (quoted by Duchen, 1992). It consists of modifications of astrocyte morphology such as

cytoplasmic vacuolization and swelling, beading and disintegration of distal cell projections (astrocyte projections, APJs), as well as modification of their functions with phagocytic removal of cytoplasmic debris (Tomimoto et al., 1997). Clasmatodendrosis has been described in the white matter of ischemic brains, in AD (Tomimoto et al., 1997) and in mixed Binswanger's/AD disease (Sahlas et al., 2002). Of note, clasmatodendrosis in astrocytes cultured *in vitro* has been demonstrated to be induced by mild acidosis, a microenvironmental condition commonly associated to aging (Ross et al., 2010), ischemia (Hulse et al., 2001) and amyloid fibrils deposition (Brewer, 1997; Hulse et al., 2001). The role of glia in neurological diseases is now the matter of much debate. Microgliosis and reactive astrocytosis generally occur at the same time, but it is not known whether there is a causal connection between the two and, should this be the case, in which direction. Astrocytes release signals such as CSF-1 and ATP that can signal to microglia, whereas microglia release signals such as TNFα that can signal to astrocytes. Nor is there agreement on whether lessening either type of gliosis might be helpful or harmful. The answer may depend on the type and stage of each disease process.

This is an emerging, understudied area of research that will undoubtedly remain fruitful for a long time, and it is likely to teach us much about normal and abnormal brain function.

1.4 Brain aging

Brain aging is characterized by decline of cognitive functions along with a variety of neurobiological changes. As the lifespan expectancy of Western population increases, age-related cognitive decline represents a major challenge for the scientific community. Franceschi and coworkers (Franceschi et al., 2007; Deleidi et al., 2015) introduced the term "inflammaging" which describes the progressive changes occurring in the aging brain, characterized by a low-grade chronic up-regulation of certain pro-inflammatory responses and neuroinflammation. Indeed, aging is considered a primary risk factor for Alzheimer's disease (AD), and the onset of low-grade pro-inflammatory conditions observed in senescence is regarded as a prodrome of AD (Giunta et al., 2008; Salminen et al., 2012; Baylis et al., 2013; Salvioli, et al., 2013). The association between inflammation, aging and neurodegeneration is based upon complex molecular and cellular changes that we are only just beginning to understand. For instance, it has been demonstrated that increase of pro-inflammatory molecules induces amyloid β (Aβ)-

deposition on neuron soma (Giunta et al., 2008; Blasko et al., 1999; Sastre et al., 2003; Mercatelli et al., 2015).

Emerging evidence indicates that inflammaging can modify the neuron-astrocyte-microglia interactions (Cerbai et al., 2012; Lana et al., 2014), and this mechanism may be involved not only in brain aging, but also in AD (Mercatelli et al., 2015). Astrocytes are known regulators of brain homeostasis (Wang and Bordey, 2008) and microglial phagocytosis (DeWitt et al., 1998; Yamanaka et al., 2007; Saijo and Glass, 2011; Cerbai et al., 2012; Lana et al., 2014). Both these cell types can recognize "danger signals", which include cellular debris produced from apoptotic or necrotic cells (Milligan & Watkins, 2009), and can clear damaged cells or cellular debris by phagocytosis (Cerbai et al., 2012; Lana et al., 2014). Functional alterations in senescent astrocytes are accompanied by remarkable morphological modifications: we recently demonstrated that senescent astrocytes in the CA1 hippocampal region exhibit morphological traits of clasmatodendrosis (Cerbai et al., 2012; Lana et al., 2014; Mercatelli et al., 2015).

1.5 Alzheimer's disease

In 1907, Alois Alzheimer (Alzheimer, 1907) described the case of a 51 year aged woman with dementia and prominent behavioural disturbances and gave a remarkable lecture (Alzheimer, 1907), in which he described for the first time a form of dementia that subsequently, at the suggestion of Emil Kraepelin, became known as Alzheimer's disease (AD). In his lecture, Alzheimer described the patient called Auguste D., who had shown progressive cognitive impairment, focal symptoms, hallucinations, delusions, and psychosocial incompetence.

Auguste Deter: *the case*

''She sits on the bed with a helpless expression.
What is your name?
Auguste.
Last name?
Auguste.
What is your husband's name?
Auguste, I think.
Your husband?
Ah, my husband. She looks as if she didn't understand the question.
Are you married?
To Auguste.
Mrs D?
Yes, yes, Auguste D.

How long have you been here? She seems to be trying to remember.
Three weeks.
What is this? I show her a pencil.
A pen.
A purse and key, diary, cigar are identified correctly.
At lunch she eats cauliflower and pork.
Asked what she is eating she answers spinach.''
Dr. Alois Alzheimer's notes: Nov 26, 1901.

At autopsy, the brain was found to be atrophic and microscopic examination with silver staining revealed widespread senile plaques and neurofibrillary tangles. Senile plaques were seen as dystrophic neuritic processes around a central core and neurofibrillary tangles as intensely staining intraneuronal perikaryal inclusions. It was only in 1910 that Emil Kraepelin, a famous German psychiatrist, gave a name to the dementia discovered by Alzheimer, naming it after him (Kraepelin & Ross Diefendorf, 1910). Alzheimer's disease (AD) is a cerebral degenerative disorder with gradual loss of memory, reasoning, orientation and judgment. The diagnosis of AD remains clinical unless histological confirmation is available at autopsy. Diagnostic criteria have been developed that allow a diagnosis of probable AD. Many classifications have been proposed based on age of onset, presence of a family history, presence of extrapyramidal features and focal cortical disease. One of the most widely considered distinctions is based on age of onset. Patients with an onset below the age of 65 are considered to have presenile dementia, in contrast to later onset cases of senile dementia of the Alzheimer type. Clinically, it has been suggested that early onset cases have a more severe disease with rapid progression, together with a predominance of language disturbances. A family history is also more readily apparent in young onset cases. A related group are patients with Trisomy 21 or Down's syndrome who develop Alzheimer histopathology and, in many instances, superimposed dementia in their third and fourth decade of life.

The clinical features of AD can be divided in two groups: cognitive and behavioural deficits. Cognitive deficits: the most prominent cognitive deficit in AD is memory impairment, and this is often the presenting feature. At the beginning of the disease, there appears a failure of STM but with the ongoing of the disease, LTM is also affected, and particularly the explicit, episodic or autobiographical memory, while the implicit memory is well conserved until the late stage of the disease. Language deficits and visuospatial deficits appear as the disease progresses. Early language preservation

may allow the patient to maintain a social façade that can mask the cognitive impairment. It is usually clear, however, that although speech may be fluent, it is rather empty of meaning or the patient may present with some difficulties finding words (*anomia*). Behavioural deficits: non-cognitive symptoms are common and about 40% have depression features, usually early in the disease. Delusion, hallucinations, and aggression are encountered commonly and can present considerable management problems for relatives and caretakers. AD patients also show anxiety and insomnia. The above features and the characteristic progression have been incorporated into clinical criteria (the NINCDS/ADRDA criteria), which provide levels of probability of diagnosis. It goes from *Possible* to *Definite* AD.

Possible AD: a dementia syndrome with atypical onset, presentation or progression and of an unknown etiology is present. No co-morbid diseases capable of producing dementia are believed to be at its origin.

Probable AD: dementia has been established by clinical and neuropsychological examination. In addition, cognitive impairments must be progressive and must be present in two or more areas of cognition. The onset of the deficits is between the age of 40 and 90 years and, finally, there must be an absence of other diseases capable of producing a dementia syndrome.

Definite AD: the patient meets the criteria for probable Alzheimer's disease and has histopathologic evidence of AD, demonstrated *via* biopsy or autopsy.

There are several risk factors for AD: age, family history, and lifestyle. Only 10% of AD cases are familial (FAD), start before 60 years of age, and are caused by autosomic dominant mutation on genes that codify for the protein precursor of amyloid (APP), and for the presenilin 1 and presenilin 2. These genes are localized in chromosomes 21, 14 and 1, respectively.

1.5.1 Neuropathology of Alzheimer's disease

Alzheimer's disease is characterized by atrophy in the cerebral cortex with loss of synapses and neurons, gliosis, and presence of intraneuronal accumulation of paired helical filaments in the form of neurofibrillary tangles (NFT), and senile plaques (Figure 7). NFT consist of aberrantly phosphorylated microtubule-associated protein (MAP) tau. Tau proteins represent a developmentally regulated family of proteins which *in vivo* are known to stabilize the microtubule network (Cleveland et al., 1977; Drubin & Kirschner, 1986). The hyperphosphorylation of MAP tau renders the protein insoluble,

which thus aggregates in filaments that precipitate (Hanger et al., 1991). Their presence signifies the failure of the neuron to maintain properly its cytoskeleton. Senile plaques are more complex; they consist of extracellular deposits of amyloid material and are associates with swollen, distorted neuronal processes called dystrophic neurites. The specificity of cerebral amyloid is provided by its major peptide component, β-amyloid (Aβ), a short 40-42 amino-acid fragment of the transmembrane protein, amyloid precursor protein (APP) (Figure 8). Plaques start as innocuous deposit of non-aggregated, putative non-neurotoxic Aβ (diffuse plaques). With time, they undergo an orderly sequential transformation into the mature senile neuritic plaques that are associated with the development of AD. The neuritic plaques are more diffuse in the cerebral cognitive areas like cortex, hippocampus and amygdala.

The amyloid is predominantly in the core of senile plaques, surrounded by abnormal neurites from degenerated neuronal cells and by glial cells: microglial cells in the centre of the plaque and astrocytes in the periphery (Selkoe, 1999). It is believed that activation of glial cells and production of cytokines, nitric oxygen (NO) and Reactive Oxygen Species (ROS) leads to plaque maturation (Sheng et al., 2000; Ramirez et al., 2008). Amyloid deposits are not homogeneous. They are made up of more than 90% of Aβ but they also contain α-1-antichimotrypsin (ACT), apolipoprotein E2 and E4 (apoE2 and apoE4), heparin sulphate proteoglycane (HSPG) and proteins of the complement (Selkoe, 1999).

1.5.2 Role of amyloid-β peptide in Alzheimer's disease

APP is a 105-130 kDa secretory protein and is involved in cell-cell or cell-matrix interaction. It may also be a component of the acute phase response and accumulates in astroglial cells in response to injury and is influenced by cytokines (Kushner, 1991;Trejo et al., 1994). In 1991 the gene for APP was localized in chromosome 21 by John Hardy, at St. Mary's Medical School, within the region that, when trisomic, is responsible for Down's syndrome (Hardy & Allsop, 1991). And indeed, there is a known association between Down's syndrome and AD (Patterson et al., 1988). The level of APP mRNA in the fetal brain with trisomy 21 is 50% higher than normal. By the fourth decade, all patients with Down's syndrome have pre-amyloid plaques containing APP-derived material. The APP gene is made of 19 exons and, after alternative splicing, different isoforms are obtained. The principal isoforms known are APP 695, APP 751 and APP 770. The APP 695 is the predominant isoform expressed in

the Central Nervous System, the other isoforms are expressed also in other tissues (Selkoe, 1994). Aβ is the product of an abnormal cleavage of APP operated by specific enzymes. It is delimitated by aa 672 and 712-715 of APP and part of it is localized in the transmembrane tract and the other part in the extracellular tract of APP. Two different processing pathways of the APP have been described: *non amyloidogenic* and *amyloidogenic*. Under physiological conditions, APP is converted to soluble β-amyloid precursor protein via the non-amyloidogenic pathway, since the hydrolysis is operated by α-secretases at the aa Lys687-Leu688, at the level of the transmembrane tract of β-amyloid. Currently, three different enzymes with α-secretase activity have been described: ADAM 9, ADAM 10 and ADAM 17. After cleavage, two different fragments are generated. One originates from the N-terminal tract of APP (sAPPβ) that is secreted in the extracellular space, and the other one, a fragment of 83 aa (C83), contains the C-terminal of APP (CTF, C-terminal fragment), that remains in the plasma membrane, and is hydrolyzed by γ-secretases to give a smaller fragment (p3) (Haass et al., 1993; Haass & Selkoe, 1993). The amyloidogenic pathway leads to the formation of Aβ. In this case the cleavage is operated by β-secretase at aa Met671-Asp672 with the release of sAPPβ in the extracellular space and the formation of a transmembrane fragment of 99 aa (C99), where the N-terminus correspond to the first aa of Aβ peptide. The enzyme responsible for the cleavage is BACE1 (β-site APP cleaving enzyme) that is a membrane protein (Vassar et al., 1999; Sinha & Lieberburg, 1999). The γ-secretase produces the other extremity of the Aβ by the hydrolysis of the aa near residue 712, producing the amyloid peptide and the short intracellular fragment AICD (APP intracellular domain) (Steiner, 2004; Comery et al., 2005). If the cleavage by γ-secretase is at the link 712-713 or 713-714, there is the formation of short Aβ (39-40 aa). The cleavage after the residue 714 leads to the formation of a longer Aβ peptide (42-43 aa) that is the major component of the neuritic plaques since it is more amyloidogenic than the shortest peptide, with a greater propensity to form amyloid fibrils.

The genetic bases of AD have been studied in patients with a family history. Four different mutated genes that are able to cause FAD have been identified and localized on chromosomes 21, 14, 1 and 19. There are different forms of FAD based on the age onset:

-Early onset (EOFAD) when pathology starts before age 65.

-Late onset (LOFAD) when the pathology starts after age 65.

This classification is important since different genes are involved in the EOFAD as compared to the LOFAD. Studying different families with EOFAD, researchers have found that a "missense" mutation at the exon 17 of the APP gene is the cause of the disease. The most common mutation is the substitution of an adenine with a guanine with the consequent conversion of the Valine 717 to Isoleucine. In other FAD forms, there is a mutation of Val to Gly or Phe. This kind of substitution makes the transmembrane domain of Aβ more hydrophobic, stabilizing the deposited form of the peptide.

Two Swedish families show a different double mutation (Mullan et al., 1992) with the substitution at the N-terminal of the Aβ of a Lys and a Met with an Asn and a Leu, respectively. This substitution facilitates the hydrolysis of APP operated by β-secretase.

The cleavage of APP can be operated also by a different family of proteases associated to apoptosis, the caspases. This cleavage leads to the formation of Aβ and correlates the cellular death with Aβ deposition. Gervais et al. (1999) have demonstrated that the cytoplasmatic domain of APP can be cleaved by caspase 3 with the consequent formation of Aβ (Gervais et al., 1999).

Studies have demonstrated that mutations at the genes for presenilin 1 and 2, localized on chromosome 14 and 1, respectively, enhance the probability of apoptosis of different types of cells.

In 1992 three different groups demonstrated independently that there is a linkage between the central region of the long arm of chromosome 14 and AD (Van Broeckhoven et al., 1992; St. George-Hyslop et al., 1992; Mullan et al., 1992). In 1995 the gene on this chromosome was cloned (PS-1). This gene seems to be responsible for 70% of the EOFAD. Families with PS-1 show the disease at early age (around 45 years of age).

In the same year, another gene similar to PS-1 was found on chromosome 1, and it was called PS-2. Seven families from Volga region and one family from North of Italy have mutations on this gene.

In 1994, Potter coined the term "pathological chaperones" (Potter et al., 1994), referring to apolipoprotein E (ApoE) and α_1-antichymotrypsin (αACT). *In vitro* ApoE and αACT act as catalysts, increasing amyloid filament formation by 10-20 faged (Ma et al., 1994). In an oxidant-dependent process, ApoE binds to Aβ in the region delimited by amino acids 12-18, the same region responsible for fibril formation.

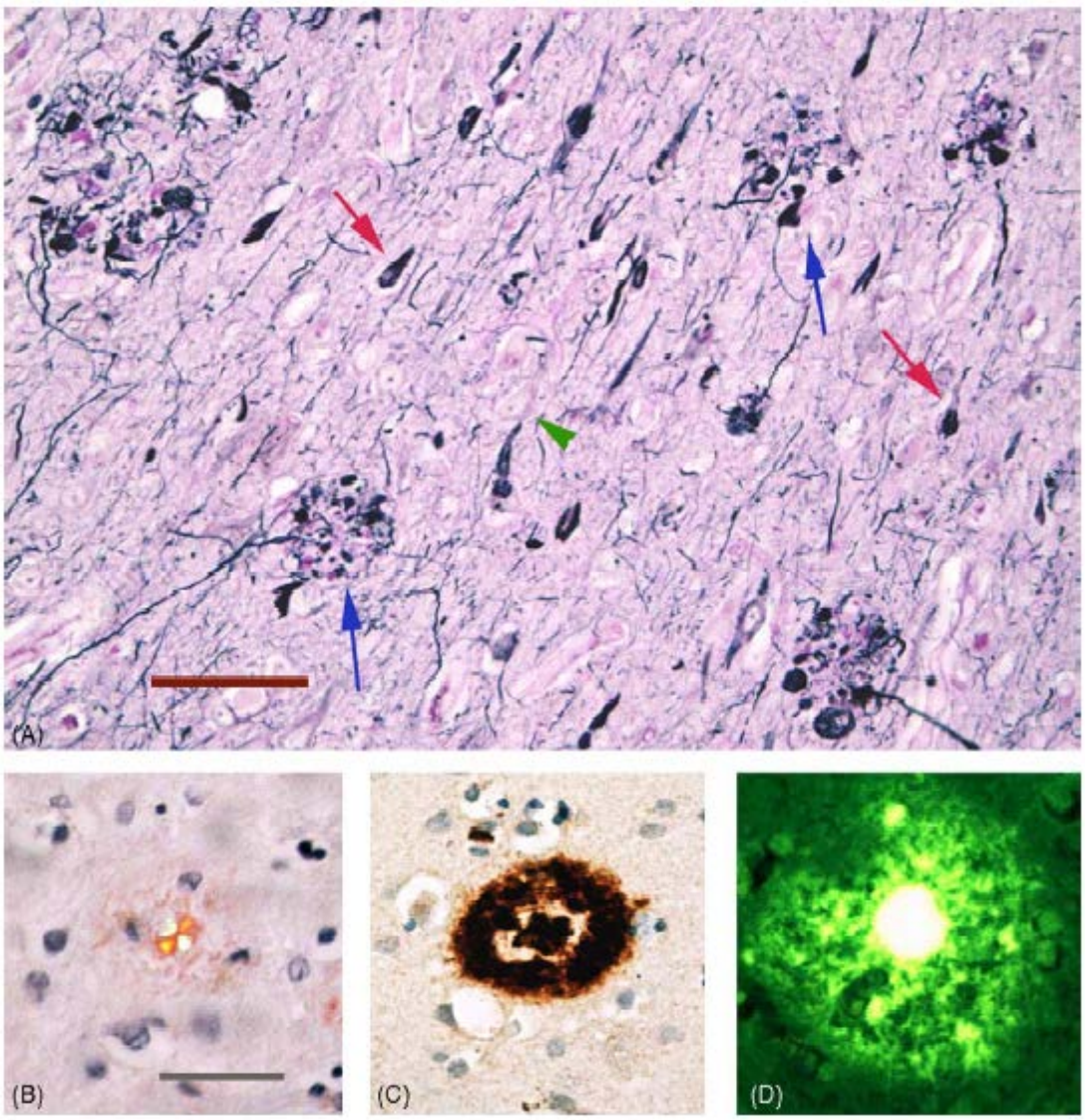

Figure 7. The canonical pathology of Alzheimer's disease. (A) senile plaques and neurofibrillary tangles in a hippocampal section stained with the Naoumenko-Feigen silver impregnation method and counterstained with periodic acid-Shiff (PAS). Two classical senile plaques are indicated by blue arrows, they consist of an extracellular core of amyloid (stained pink by PAS) encircled by black, distended neuronal processes (neurites). Note also the intracellular NFT (two are marked by red arrows); a pale normal appearing neuron is designed by a green arrowhead. Scale bar=100µm. (B) A neocortical senile plaque stained with Congo Red, the definitive stain for classically defined "amyloid" (regardless of the identity of the protein component); the photograph was taken with crossed polarizing filters, which produce a Maltese-cruciform pattern of green orange birefringence in compact, fibrillar amyloid deposits (the plaque core, center); Nissl counterstained. (C) A cortical senile plaque immunostained with antibody 10D5 to amino acids 3-7 of Aβ. Note the central core of β-amyloid, surrounded by a halo, and then an outer ring of Aβ, which is typical of many dense-cored plaques in AD; Nissl counterstained. (D) A cortical plaque stained with Thioflavin-T, a fluorescent dye that binds to generic amyloid. The core is intensely fluorescent, and the peripheral, more diffuse deposits also bind Thioflavin. Bar in B=50µm for B, C, D.

ApoE is a 34 kDa glycosylated protein, and is one of the major risk factors other than age for the development of AD. It is involved in synaptic repair, particularly in response

to tissue injury and it has an important role in the maintenance of neuronal structure and cholinergic function. In the brain, it is produced by microglial cells and astrocytes, but not by neurons. ApoE is a major component of lipoprotein and lipid complexes in the cerebrospinal fluid. In peripheral nerve regeneration, ApoE redistributes lipids to axons during neurite extension and Swann cells during remyelinization (Yankner et al., 1990). The ApoE gene is localized on chromosome 19 and exists in 3 allelic forms: ε2, ε3 and ε4 with frequencies of 8%, 78% and 14%, respectively. The ε4 allele increases the risk of developing late and sporadic AD by 5-15 faged. The prevalence of ApoE ε4 appears to vary by population according to the prevalence of AD; it is increased in the Finnish, Sudanese, Aborigines and decreased in the Chinese and Japanese (Harrington et al., 1994).

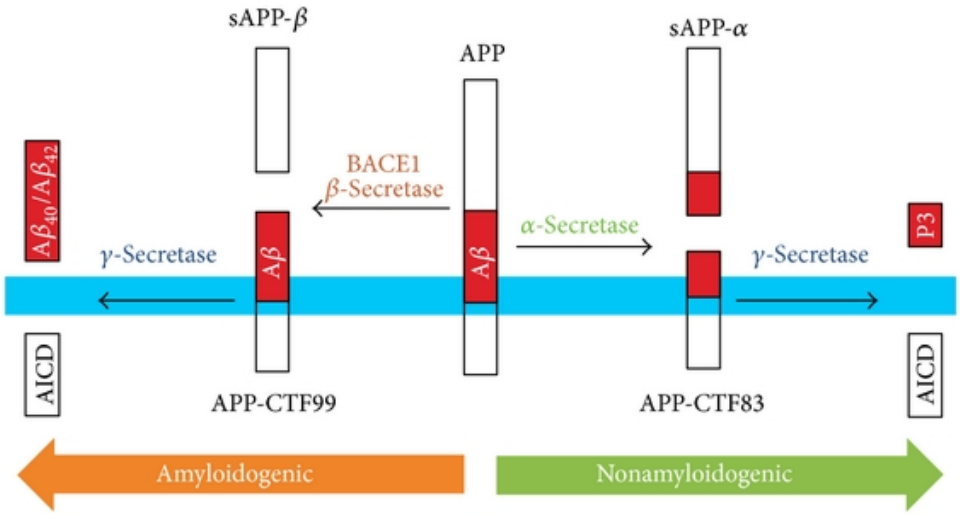

Figure 8. Schematic diagrams of the β-amyloid precursor protein (APP) and its principal metabolic derivatives (Pająk B et al., 2016).

In vitro ApoE ε4 binds more rapidly to Aβ than does ApoE ε3, forming a denser matrix of monofibrils. On the other hand, ApoE ε3 seems to bind to the protein tau. In contrast the ApoE ε2 allele has been associated with a reduced risk of AD and longevity (Rebeck et al., 1994). *In vitro* ApoE ε2 inhibits fibrillar aggregation. The familial forms of AD are correlated to mutations of the APP gene and other genes that alter the metabolism of this precursor, including the increased production of the Aβ (1-42) peptide that is the predominant form in the senile plaques. The crucial event for the pathogenesis of the disease is the amyloid-β peptide deposition. Studies on transgenic mice that present some of the AD alterations, have shown that the immunization with Aβ (1-42) interferes with the accumulation and deposition of Aβ and with the activation

of glial cells, leading to cognitive improvement (Schenk et al., 1999). The immunization of transgenic mice with Aβ before the onset of AD, prevents the formation of plaques and the activation of microglial cells and astrocytes. The *in vivo* injection of Aβ (1-40) in the cortex of a rat produces necrosis around the site of the injection, neuritic degeneration and neuronal loss (Scali et al., 1999).

Aβ binds also to metals like Cu^{2+}, Zn^{2+} and Fe^{2+}. In this case, the Aβ toxicity is induced by the production of H_2O_2 that induces the aggregation of the peptide.

1.5.3 Inflammation in Alzheimer's disease

The inflammatory response is primarily a host defence reaction. It serves to degrade and eliminate the foreign invader. Components of the inflammatory response play essential roles when phagocytic cells remove microorganisms, necrotic host tissue and undesired deposits of abnormal substances. However, prolonged inflammation often destroys the surrounding host tissue. Such a damage is particularly serious if it occurs in the brain, where regeneration and recovery take place only at a very limited degree. In neurodegenerative diseases, inflammation could be caused by several events: protein aggregates deposition, molecules associated to synapses or degenerated neurones. In AD, senile plaques and tangles could be the site of sustained inflammatory response. Several studies have demonstrated that Aβ deposits in the plaques are associated to numerous immune system proteins, complement proteins, cytokines, protease inhibitor, binding proteins (McGeer & McGeer, 1995; McGeer & McGeer, 1998). Activated microglia cells are associated to the neuritic plaques, producing cytokines and other neurotoxic components. The presence of molecules of immune system and of activated microglia associated to Aβ confirm the hypothesis that inflammation is the cause of neuronal degeneration in AD (Rogers et al., 2002). The activation of microglia associated with Aβ plaques in the AD brain is paralleled by similar processes in cells in culture. Exposure of microglia cultures from elderly AD and non-AD patients to Aβ (1-42) results in their activation. As in the AD brain, microglia cells increase their cell surface expression of MHCII (Rogers & Lue, 2001), a classic marker for the activation of scavenger cells. In addition microglia show a dose-dependent increase in thei secretion of the pro-inflammatory cytokines interleukin-1β (IL-1β), interleukin-6 (IL-6) and tumour necrosis factor-α (TNFα), the chemokines interleukin-8 (IL-8), macrophage inflammatory protein-1α (MIP-1α), and monocyte chemoattractant peptide-1 (MCP-1) (Lue et al., 2001). The mRNAs for all these proteins have been observed in AD

microglia. IL-1β is also increased after Aβ exposure to cultured AD microglia (Walker et al., 1995).

There are likely multiple mediators of microglia activation, chemotactic and phagocytic responses to Aβ. Evidence for complement mechanisms in microglia responses to Aβ has been reported. It seems that the peptide directly interacts with C1 complement factor that activates microglial cells (Eikelenboom et al., 1998). Activated microglia releases cytokines, proinflammatory proteins, complement proteins, reactive oxygen intermediates (Banati et al., 1993).

Inflammatory cytokines are a family of glycoproteins that amplify and sustain inflammatory and immune responses. They are not only released by activated microglia but also by astrocytes. Cytokines may interact directly or indirectly with neurons, influencing their survival. Cytokines, especially IL-1, enhance the production of prostaglandin E_2 (PGE_2) in human fibroblasts (Salvemini et al., 1993), stimulating cyclooxygenases enzyme (COX) activation. Recent studies have shown the importance of microglial IL-1 secretion in AD pathogenesis since IL-1 not only can promote neuronal injury, but can also perpetuate cycles of inflammation (Mrak & Griffinbc, 2001). IL-1 has been shown to increase APP production and subsequently increase Aβ, contributing to neuronal damage, and, simultaneously, to neuronal dystrophy (Buxbaum et al., 1992). Injection of aggregated Aβ into the NB of rats causes upregulation of IL-1β, COX-2, iNOS and phospho p38MAPK in the surrounding tissue, with microglial activation and cholinergic dysfunction (Giovannini et al., 2002).

Several epidemiologic studies suggested a beneficial effect of treatment with chronic nonsteroidal anti-inflammatory drugs (NSAIDs) (McGeer et al., 1996). NSAIDs are believed to act by inhibiting COX. Two distinct isoforms of COX have now been characterized, a constitutive form, COX-1, and an inducible form, COX-2. Studies have demonstrated that COX-2 may play a role in neurodegenerative mechanisms (Pasinetti & Aisen, 1998). A number of cross-sectional and longitudinal epidemiologic surveys also indicate that reported use of NSAID is associated with delayed onset and/or slowed cognitive decline in AD (Stewart et al., 1997; Halliday et al., 2000). However, these studies are not conclusive, and the results are controversial. Further examinations of traditional NSAIDs for the treatment of AD has been tempered by two considerations. First, NSAIDs are not the ideal class of anti-inflammatory agents to inhibit acute-phase response and complement activation, two mechanisms that contribute to

neurodegeneration in AD. Second, daily use of traditional NSAIDs is associated with adverse effects, particularly on the gastrointestinal (GI) tract of elderly subjects.

Some findings suggested that selective COX-2 inhibitors may have an advantage over nonselective NSAIDs as potential therapeutic agents in AD. Studies have shown that COX-2 isoform may have a central role in neurodegeneration, supporting clinical evaluation of selective COX-2 inhibitors as neuroprotective agents in AD (Pasinetti & Aisen, 1998; Tocco et al., 1997; Ho et al., 2001). Studies have demonstrated that COX-2 is up-regulated in response to excitotoxic lesions in animals and cell culture systems (Yamagata et al., 1993) Systemic administraion of kainic acid (KA) to rats induces excitotoxic neurodegeneration, which may be a model of AD. It has been demonstrated that excitotoxic lesions cause up-regulation of COX-2 expression coincident with the onset of apoptotic neuronal death. COX-2 expression has been shown to be up-regulated in AD brain compared with controls (Pasinetti & Aisen, 1998). Induction of COX-2 in AD may be stimulated by amyloid peptide, and may involve nuclear factor kappa b (NFkB) signalling (Pasinetti & Aisen, 1998). Evidence that COX-2 is involved in AD neurodegeneration may explain the apparent protective effect of NSAIDs. It has been demonstrated that COX-2 inhibitors protect neuronal cells from amyloid toxicity *in vitro* and promote neuronal survival in animal models of ischemic and excitotoxic neurodegeneration (Fagarasan & Efthimiopoulos, 1996; Graham et al., 1996). Epidemiologic evidence suggests a neuroprotective effect of non-selective NSAIDs from either COX-1 or COX-2 inhibition, or inhibition of both enzymes. Because COX-1 is constitutively expressed in the brain, it is plausible that COX-1 catalytic activity may also contribute to neurodegenerative mechanisms (Pasinetti & Aisen, 1998). Recent studies have demonstrated that ibuprofen therapy reduces inflammatory activity and amyloid deposition in transgenic mice (Lim et al., 2000).

Some trials (Lim et al., 2000) have been done using two different drugs: *Naproxene*, a non-selective NSAIDs, at low doses (220 mg) to minimize the risk of serious GI toxicity, to one group of patients, and *Rofecoxib*, a selective COX-2 inhibitor at standard doses, to a second group. A third group of patients was treated with placebo. It was a one year study and the results did not show any positive effect on memory, attention, speech and orientation of treated patients as compared to controls. An explanation for the negative results obtained could be the not sufficient doses of both drugs, or the short period of therapy. It has been demonstrated that a two year treatment with anti-inflammatory drugs is necessary to reduce AD risk (Ruitenberg et al., 2001).

A thorough review of the literature suggests conflicting opinions for the use of NSAIDs in AD. While observational and epidemiological studies have stressed on a beneficial role of NSAIDs in reducing the risk of AD or its progression, randomized clinical trials (RCTs) and meta-analyses thereof have failed to corroborate this significantly. No RCTs have been conducted to date in populations with APOE E4 genotype. For people with existing cognitive decline, as well as diagnosed AD, NSAIDs should not be administered, as no clinical evidence has been demonstrated regarding their benefit. The authors also recommend that further RCTs should be conducted over longer durations with larger samples to clarify the role of NSAIDs in the treatment of AD in selected population (Ali et al., 2019).

It has been shown that in AD brains there is a colocalization of hyperphosphorylated tau and phosphorylated p38MAPK in dystrophic neurons and neurites that are associated to activated microglia that over express IL-1 (Sheng et al., 2001).

Recent studies have demonstrated that there are different molecules involved in neuron-glia intercommunication, such as CD200 and HMGB1. CD200 is a membrane glycoprotein expressed by neurons that binds to a structurally similar receptor that is expressed by microglia. Their intercommunication hageds microglia in a quiescent state (Hoek et al., 2000; Lyons et al., 2007; Frank et al., 2007). HMGB1 is a non-histone DNA-binding protein that has a pro-inflammatory cytokine-like function that may influence the activation of microglia following injury or insult (Kim et al., 2006). HMGB1 levels are low in resting glia but are increased in the brains of patients with Alzheimer's disease (Takata et al., 2004). Extracellular HMGB1 has also been described as a mediator of lipopolysaccharide (LPS) toxicity (Ulloa & Messmer, 2006).

1.5.4 Animal models of Alzheimer's disease

Given the availability of methods for introducing genetic modifications, modeling in transgenic mice has been pursued vigorously, based on the amyloid hypothesis (Codita et al., 2006; McGowan et al., 2006). Transgenic mice overexpressing Aβ offer a powerful *in vivo* model to study the pathogenetic mechanisms related to Aβ neurodegeneration and allow to test possible therapeutic interventions. Among the many transgenic mouse strains developed (Hsiao et al., 1996), transgenic TgCRND8 mice (Chishti et al., 2001), expressing a double mutant form of human APP (K670/M671L and V717F), have been produced. Hemizygous TgCRND8 mice exhibit extensive cerebral amyloid deposition, cortical and hippocampal atrophy and memory impairment

by 3 months of age (Chishti et al., 2001). In 7-month aged TgCRND8 mice, extensive Aβ deposition in the cortex, hippocampus, thalamus and basal forebrain is accompanied by significant microglia and astrocyte activation, and by cholinergic dysfunction and cognitive impairment (Bellucci et al., 2006). This transgenic line is a good model of Aβ deposition, neurodegeneration and memory deficits, and can be useful to clarify the involvement of MAPK dysregulation in AD and in developing new therapeutic treatments.

Initially, before the discovery of FAD mutations, attempts were made to overexpress wildtype APP in transgenic mice by pronuclear injection. Although a variety of promoters was tried, none of these efforts produced anything that resembled an amyloid plaque or any other recognizable AD-type pathology. After the discovery of FAD mutations in APP, several groups turned their attention to making AD models based on the overexpression of transgenes containing FAD mutations (Elder et al., 2010). Games et al. (1995) reported the first successful application of this approach using a platelet derived growth factor-β (PDGF) promoter to drive a human APP transgene that contained a FAD associated mutation (V717F). The PDGF promoter was chosen because, despite its name, it was known to be highly expressed in the central nervous system and to drive strong expression of exogenous transgenes in neurons. In the line that was generated (termed PDAPP because of the PDGF promoter plus APP), 40 copies of the transgene integrated, and this resulted in approximately 18-faged elevation of APP RNA and approximately 10-faged elevation of human APP protein in comparison with endogenous mouse APP levels. Proportionate increases in human Aβ were found.

PDAPP mice exhibited age-dependent amyloid deposition in the brain along with thioflavin-S positive plaques, including compact plaques with dense cores that were highly reminiscent of those seen in human AD. Dystrophic neurites, reactive astrocytes, and activated microglia were all found near the plaques (Elder et al., 2010). The process was age-related, in that plaque deposition was minimal at 6 months of age but readily apparent by 9 months, increasing dramatically by 12 to 15 months (Reilly et al., 2003). PDAPP mice were subsequently shown to develop age related learning deficits (Chen et al., 2000) and synapse loss (Dodart et al., 2000).

Independently, Hsiao et al. (1996), taking a relatively similar approach, overexpressed a human APP transgene containing the Swedish FAD mutation (K670N/M671L). Expression was driven by a hamster prion [prion protein (PrP)] promoter that drives

expression widely in the nervous system. These mice, termed Tg2576 mice, expressed human APP at levels more than 5-faged above the levels of the endogenous mouse APP, and Aβ40 and Aβ42 levels increased with age. Like PDAPP mice, Tg2576 mice exhibited age-dependent amyloid deposition, which resulted in thioflavin-S–positive plaques similar to those found in AD, along with gliosis and dystrophic neurites. Plaque amyloid was first clearly seen by 11 to 13 months, eventually becoming widespread in cortical and limbic structures. Water maze learning, a test of spatial memory in mice, was normal in 3-month-aged animals but impaired in 9- to 10-month-aged mice. The Tg2576 mouse line is widely available and is the most widely studied transgenic AD model (Elder et al., 2010).

Subsequently, many other transgenic lines were developed with approaches similar to those used to develop PDAPP and Tg2576 mice (Codita et al., 2006; McGowan et al. 2006) typically relying on strong promoters to drive expression of APP transgenes containing single or multiple FAD mutations. Common features of the models have been the production of elevated levels of Aβ, amyloid plaques, dystrophic neurites, and gliosis. Behavioral deficits have been common (Games et al. 2006). Many additional neuropathological, electrophysiological, and neurochemical changes that model aspects of AD in humans have also been observed (Games et al. 2006).

Presenilin 1 (PS1) was found as part of a search for an early-onset FAD gene associated with a locus on chromosome 14 (Ertekin-Taner, 2007). Mutations in PS1 are the most commonly recognized causes of early onset FAD, and to date, more than 160 mutations in PS1 linked to FAD have been discovered. Mutations in a related gene on chromosome 1, now called presenilin 2 (PS2), were soon linked to FAD as well (Ertekin-Taner, 2007).

PS1 FAD mutant transgenic lines have been generated with many of the same promoters used to create APP mice, including PDGF (Duff et al., 1996) and PrP (Borchelt et al., 1996; Citron et al., 1997). A few PS2 FAD mutant lines also exist. In addition, several gene-targeted lines exist in which PS1 FAD mutations have been targeted to the endogenous mouse PS1 (Guo et al., 1999; Nakano et al., 1999). Presenilin FAD mutant mice consistently show elevations of Aβ42 with little, if any, effect on Aβ40. However, singly transgenic PS1 or PS2 mice do not develop plaques, although when crossed with plaque-forming APP lines, the presenilin FAD mutations cause earlier and more extensive plaque formation (Holcomb et al., 1998). Why singly transgenic PS1 and PS2 mice fail to develop plaque pathology is not entirely clear but

may be related to the generally lower levels of Aβ42 found in single presenilin transgenics versus APP-overexpressing lines as well as the lack of elevation of Aβ40 in presenilin transgenics. It may also be related to the differing aggregation properties of mouse Aβ versus human Aβ (Jankowsky et al., 2007). Although PS1/APP bigenic mice have been studied frequently, the parental presenilin lines have been less studied, likely because of their lack of a robust AD-like pathology. However, PS1 and PS2 FAD mutant lines show exaggerated hippocampal damage after kainite induced excitotoxicity, PS1 (Guo et al., 1999; Grilli et al. 2000; Schneider et al., 2001) and PS1 FAD mutants render animals more sensitive to trimethyltin-induced hippocampal damage (Kassed et al., 2003). Excessive neuronal loss in the EC cortex also occurs in mice harboring the delta E9 PS1 FAD mutation after lesioning of the perforant path (Lazarov et al., 2006). Increased protein oxidation and lipid peroxidation have also been reported in PS1 FAD mutant brain (Mohmmad Abdul et al., 2004; Schuessel et al., 2006). Several studies have documented impaired hippocampal neurogenesis in adult PS1 FAD mutant mice, (Chevallier et al., 2005; Wen et al., 2004) and, recently, an age-dependent impairment of spine morphology and synaptic plasticity in hippocampal CA1 neurons of a PS1 transgenic mouse model has been described (Auffret et al., 2009). Age-related neurodegenerative changes with neuronal loss have been reported in one PS1 FAD mutant line, (Chui et al., 1999) and age-related NFT-like inclusions have been described in a PS1 knock-in line (Tanemura et al., 2006).

Recently, a microvascular pathology that is highly reminiscent of the microvascular pathology found in AD has also been described (Gama Sosa et al., 2010). Thus, presenilin FAD mutant mice exhibit a phenotype. What is less clear is why they fail to exhibit the full range of AD related pathologies, given the potency of the mutations in humans (Elder et al., 2010).

1.6 Cerebral ischemia

The word ischemia derives from the Greek "*ισχαιμία*" ("Reduction of blood") and means the total lack of blood flow in an organ. Cerebral ischemic stroke represents a life-threatening neurological disorder, one of the main causes of death and long-term disability in surviving patients in Western Countries, with only very limited therapeutic options (Dirnagl, 2012).

Important risk factors for ischemic stroke include hypertension, high blood cholesterol, and diabetes. In addition, modifiable unhealthy lifestyle, such as tobacco smoke, high

alcohol consumption or lack of physical activity, considerably alter the predisposition to this pathological condition. Furthermore, age, gender, and other vascular risk factors are significant predictors of outcome of stroke severity, aetiology and efficacy of thrombolysis (Gibson et al., 2013). Furthermore, there are ischemic events defined cryptogenic (with no apparent cause) but normally at the bases of this condition, there are many diseases, such as obesity, solid and blood tumours but also myocardial infarction, anaemia and granuloma.

There are two main types of stroke:

1) *Ischaemic stroke* is caused by complete obstruction/occlusion of a cerebral vessel, which cuts off the blood supply to downstream brain parenkyma. Blocks can be caused by a blood clot or by fatty deposits and can occur in a brain artery or a small blood vessel deep inside the brain. Early after the obstruction, brain cells begin to die and the damage can have different effects, depending on the brain area affected.

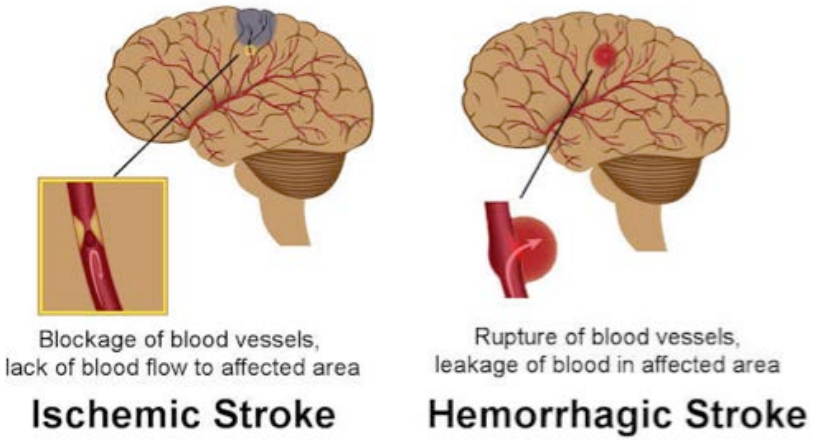

Figure 9. Etiopathological schematic picture of both types of ischemia: on the left, ischemic stroke, representing the obstruction of a blood vessel. On the right haemorrhagic stroke, commonly known as cerebral haemorrhage, here shown after the breakdown of a blood vessel (Dirnagl et al., 1999).

2) Haemorrhagic stroke is caused by a blood vessel that bursts within or on the surface of the brain. Haemorrhagic strokes are generally more severe and are associated with considerably higher risk of death within the first three months and after, when compared to ischaemic strokes. These are also referred to as subarachnoid haemorrhage (bleeding on the surface of the brain) or intracerebral haemorrhage (bleeding within the brain) (Figure 9).

Approximately 80% of strokes are ischemic in nature and result from thromboembolic occlusion of a major cerebral artery or its branches, which leads to loss of cerebral blood flow, a condition of hypoxia and glucose deprivation (oxygen-glucose deprivation: OGD) and subsequently tissue damage in the affected region (Gibson, 2013).

In 1970, cerebral ischemia was defined by WHO as "Neurological focal or global cerebrovascular injury syndrome persisting beyond 24 hours or leading to death within 24 hours" (24 hours were chosen arbitrarily to distinguish it from transient ischemic attack).

Thanks to this definition, we can presume that the nervous tissue subjected to ischemic damage, if reached in appropriate time, can recover neuronal activity. For this, therefore, rapidity of intervention is indispensable and, given the high risk of death and disability which ischemia implicates, this disease is considered a medical emergency for which immediate diagnosis is essential to formulate appropriate therapeutic interventions.

Ischemia could involve both large or small vessels but the symptomatology is almost always the same and consists of feeling oppression, asphyxiation, spasm, formication (paresthesia), dysarthria, hemiparesis, hemianopsia, migraine and aphasia (complex disorder of language and communication caused by damage to the language centres of the brain; people with aphasia may have difficulty speaking, reading, writing or understanding language).

The extent and location of the damage determines the severity of the stroke, which can range from minimal to catastrophic. Two major approaches have been developed to treat ischemic stroke: neuroprotection and reperfusion. The latter therapeutic strategy uses thrombolytic drugs or mechanical devices to recanalize occluded vessels. The only approved medical treatment for acute ischemic stroke is intravenous thrombolysis with recombinant tissue plasminogen activator (Adams et al., 2007). However, the therapeutic window of rtPA treatment is up to 4.5 hours after stroke, and consequently, rtPA is applicable as treatment in only up to 5% of all patients (Fonarow et al., 2011). Thus, there is an urgent need for other, more widely applicable, treatment options.

1.6.1 Epidemiology

Stroke is ranked as the second leading cause of death worldwide with an annual mortality rate of about 5.5 million. Stroke represents a huge public health burden, which

is set to rise over future decades because of demographic transitions of populations, particularly in the developing countries (Adogu et al., 2015).

According to data of the World Stroke Organization, 1 in 6 people worldwide will have a stroke in their lifetime, 15 million people worldwide suffer a stroke each year and 5.8 million people die from it. Current trends suggest that, without appropriate action, the number of annual deaths will climb to 6.7 million by 2015.

Stroke claims a life every 6 seconds. It is the second leading cause of death for people above the age of 60, the fifth leading cause in people aged 15 to 59, both males and females, and it affects children as well. Stroke is responsible for more deaths annually than AIDS, tuberculosis and malaria combined. In the United States, stroke is the third most common cause of death, exceeded only by cancer and coronary heart disease, and it claims a life every three minutes. Furthermore, stroke is also one of the leading causes of long-term disability worldwide.

1.6.2 Public health burden of stroke in the 21st Century

In both the developed and developing world, ischaemic stroke is currently the predominant stroke subtype. According to the current global burden of disease data on stroke, in 2013 there were almost 25.7 million stroke survivors, 6.5 million deaths, 113 million DALYs (disability-adjusted life years) due to stroke, and 10.3 million new strokes (Moran et al., 2013).

Thus, stroke is a disease of immense public health importance with serious economic and social consequences. In the past, stroke was considered a disease of the developed world. However, through the application of evidence-based control measures, the burden of stroke reduced drastically in many developed countries. In most western European countries, death from stroke declined by 30-50% from 1975 to around 2005 and this was most noticeable in countries like Iceland, Italy, Austria, and Germany (Lopez et al., 2006*).* The burden of stroke seems to be shifting to the developing world where, currently, there are 4.85 million stroke deaths and 91.4 million DALYs annually compared with 1.6 million deaths and 21.5 million DALYs in high-income countries (Moran et al., 2013). As shown in Figure 10, the burden of stroke is much higher in Eastern Europe, North Asia, Central Africa, and the South Pacific (Figure 10) (Johnston et al., 2009). In the next few decades, the burden of stroke in the developing world is likely to increase substantially, partly due to ongoing demographic changes, including

ageing of the population and health transitions in these countries (Moran et al., 2013; Amuna & Zotor, 2008).

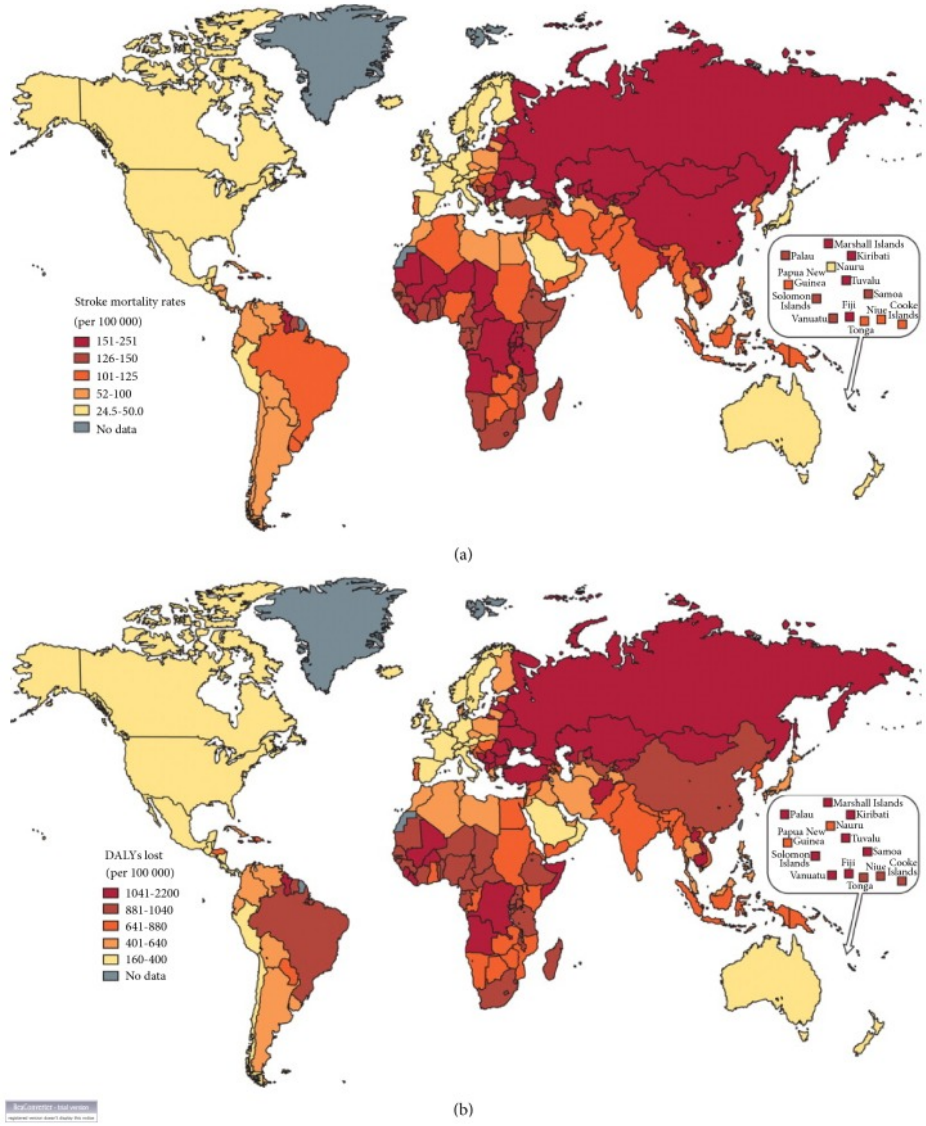

Figure 10. (a) Global distribution of stroke mortality rates. (b) Global distribution of DALY loss due to stroke.

1.6.3 Types of stroke

As already mentioned, generally cerebral stroke can be classified into two major categories, namely, ischaemic stroke and haemorrhagic stroke. Ischaemic stroke is caused by interruption of the blood supply to a part of the brain resulting in sudden loss of function, while haemorrhagic stroke is attributed to rupture of a blood vessel or an abnormal vascular structure. Approximately, ischaemic strokes account for about 80%

of stroke cases while haemorrhagic stroke accounts for 20% but the actual proportion of stroke type depends on the population (Bamford et al., 1991).

There are several subclassification schemes for ischaemic stroke and the Trial of ORG 10172 in Acute Stroke Treatment (TOAST) criteria is the most widely used.

Based on the TOAST criteria, ischaemic stroke can be grouped into five main pathological or etiological types (Table 1).

Table 1. Subclassification scheme of the ischaemic stroke (adapted from Adams et al.,1993).

Stroke type	**Causes**	**Percent**
Large artery thrombotic strokes	Atherosclerotic plaques in the large blood vessels of the brain lead to ischemia and infarction	20%
Small penetrating artery thrombotic stroke (Lacunar stroke)	One or more vessels in the brain are affected (microatheromatosis)	25%
Cardiogenic embolic stroke	Associated with cardiac dysrhythmias, valvular heart disease, and thrombi in the left ventricles	15%
Cryptogenic strokes	Cause is unknown	5-10%
Strokes associated with other causes	Such as illicit drug use	20-25%

There are two types of haemorrhagic stroke, including intracerebral haemorrhage and subarachnoid haemorrhage. Intracerebral haemorrhage is the most common type of non-traumatic intracranial haemorrhage; it accounts for 80% of haemorrhagic stroke and 10-15% of all strokes (Bradley et al., 1991). Intracerebral haemorrhage is mostly caused by uncontrolled hypertension leading to rupture of small vessels. The rupture leads to an avalanche type effect with breakage of nearby vessels resulting in haematoma expansion in up to 40% of cases. Subarachnoid haemorrhage is mainly due to saccular aneurysms though it is also associated with arteriovenous malformation, intracranial neoplasm, and some medications such as anticoagulants. About 65% of subarachnoid haemorrhage patients survive, but half remain disabled primarily due to severe cognitive deficit (Caplan et al., 2000; Bradley et al., 1991).

1.6.4 Traditional risk factors

The traditional risk factors of stroke can be classified into modifiable and unmodifiable risk factors.

The modifiable risk factors include hypertension, diabetes mellitus, high blood cholesterol, cardiovascular diseases, sedentary lifestyle, atrial fibrillation, smoking, and alcohol consumption.

The unmodifiable risk factors are relatively few and include factors such as age and gender (O'Donnell et al., 2010; Lopez et al., 2006*)*.

The total incidence of stroke is projected to rise substantially over the next 20 years, because of the rising age of the population. Age is the strongest determinant of stroke and the risk of stroke doubles every decade above age 55 (Caplan et al., 2000; Johnston et al., 2009).

1.6.5 Physiopathology

Cerebral ischemia triggers a series of haemodynamic, biochemical and behavioural disorders. Initially, due to the decrease in blood flow, neurological functions are affected. Subsequently, as a result of ischemia progress, the metabolic activity is suppressed in order to maintain the structural integrity of the cells (Hossmann, 1998).

The extension of the ischemic core is a time-dependent phenomenon. Cells die in the hours or days following a series of events named the ischemic cascade (Dirnagl et al., 1999) (Figure 11).

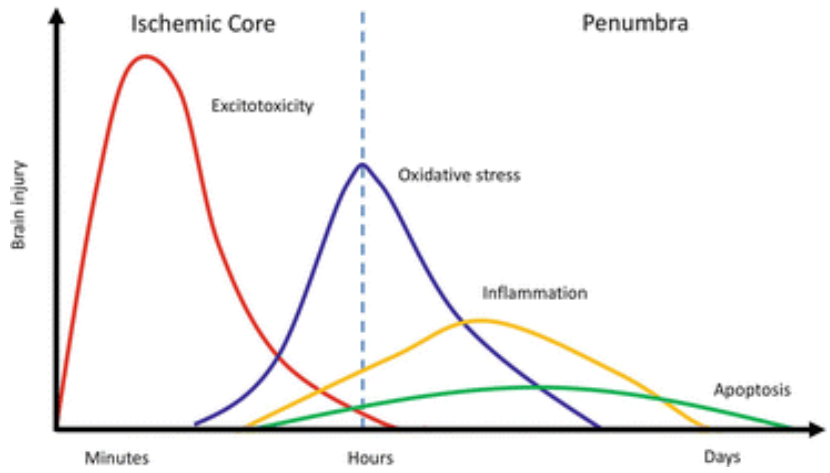

Figure 11. Spatiotemporal evolution of mechanism involved in cerebral ischemia (Velly, L., Boumaza, D., and Simeone, P. (2012). "Cerebral Ischemia: Pathophysiology, Diagnosis, and Management", in Metabolic Disorders and Critically III Patients, ed. C. Ichai (Verlage France, Paris: Springer) 301-325).

The ischemic process results from a sequence of physiopathologic effects which progress drastically through time and space, leading to cell death and consequently to the subsequent decline of brain damage. In sequence, these are excitotoxicity, peripheral depolarization, inflammation and cell death due to necrosis and apoptosis (Dirnagl et

al., 1999). Each of these physiopathological process occur at a define time in the ischemic phenomenon, some occurring after a few minutes and others after several hours or days (Doyle et al., 2008) (Figure 11).

The longer the cerebral blood flow (CBF) is disrupted, the more important is the extension of the ischemic core to the detriment of the penumbra zone, which requires to be reperfused as quickly as possible. In the ischemic core, where CBF is more severely limited, excitotoxicity and cellular death occur after a few minutes. On the periphery of the ischemic core, in the penumbra zone, when parallel blood flow can limit the effects of stroke, the degree of ischemia and the delay before reperfusion determine the individual outcome of each cell. In this zone, cellular death through apoptosis or inflammation occurs less quickly (Doyle et al., 2008). Shortly after the occlusion of the middle cerebral artery (MCA), penumbra is approximately the same size as the ischemic core. After 3 h, penumbra only represents 50% of the ischemic core and 6–8 h later almost all the penumbra zone disappears and is part of the irreversible damages in the ischemic core (Hata et al., 2000). Although the duration of ischemic period is a determinant element in the intensity of damages, reperfusion plays also an important role in damage distribution. During reperfusion, a consequent amount of oxygen reaches the brain, which is responsible for formation of free radicals (oxygen-activated species, ROS) and leads to additional oxidative stress.

Cells consume a substantial amount of oxygen and glucose, throughout catabolic processes to obtain the energy necessity for survival in the form of ATP. When the physiological concentration of oxygen and glucose decrease, such as during an ischemic insult, the cell necessarily looks for stock of energy since it cannot produce energy by itself and finds it in ATP. Given the disequilibrium between energy consumption and production, the cell is forced to initiate the anaerobic metabolism that causes ATP depletion, transformation to AMP and the consecutive extracellular accumulation of adenosine.

At intracellular level, ATP has essential functions, of which the operation of ATP-dependent pumps, such as the Na^+/K^+ pump, which allows the active transport of Na^+ and K^+ through the plasma membrane, is fundamental. The increase of ATP causes a block of the pump and consecutively a block of ions transport: thus, Na^+ accumulates in the intracellular side. This ionic distribution, strongly unbalanced, causes profound depolarization of the cell membrane, making the electrochemical potential more positive and causing the opening of other ion channels, such as the Ca^{2+} channel. Ca^{2+},

once inside the cell, contributes to the release of the neurotransmitters through the process of vesicle fusion, mediated by the protein of SNARE complex (Figure 12).

Thus, acute brain injury after stroke is caused primarily by the lack of oxygen and glucose. In such conditions, mammalian neurons rapidly depolarize, and excessive release of glutamate occurs, an amino acid and excitatory neurotransmitter, causing excitotoxic cell death, largely due to over-activation of glutamatergic N-methyl-d-aspartate (NMDA) receptors. NMDA receptors are highly permeable to Ca^{2+} and are responsible for intracellular Ca^{2+} increase that reaches neurotoxic levels which, by activating cell lipases, endonucleases, proteases and phosphatases, ultimately bring to acute excitotoxic cell death (Choi, 1992). Glutamate activates also AMPA, and Kainate postsynaptic receptors which further increase the intracellular concentrations of Na^{+}, K^{+} and Ca^{2+} further depolarizing the cell membrane (Figure 13).

In addition, the intracellular messenger activates a cascade of events (such as the synthesis of NO, characteristic of inflammation) which conduce to the onset of tissue damage (Beckman & Koppenol, 1996; Iadecola, 1997) and to the subsequent necrosis of the tissue (Dirnagl et al., 1999).

In addition, one of the early events occurring by an ischemic episode *in vivo* and during oxygen-glucose deprivation (OGD) *in vitro*, is the release of substantial amounts of adenosine (Latini et al., 1998; Melani et al., 1999).

Among the most remarkable events of ischemia are the activation of enzymes which break down the cytoskeleton protein (Furukawa et al., 1997), lipases, such as activation and consequently activation of cyclooxygenase (COX_2, involved in inflammation) and phospholipase A_2 (PLA_2). Activated PLA_2 by excess in Ca^{2+} during ischemic process leads to a disrupted phospholipidic metabolism with degraded glycerophospholipids and massive formation of free fatty acids (Zhang et al., 1995). Arachidonic acid is the principal free fatty acid produced during ischemia. It is then metabolized by cyclooxygenase (COX) to prostaglandin (PG), by the lipooxygenase to leukotriene (both pro-inflammatory lipidic mediators) but also to lysophospholipids (precursor of the platelet activating factor) and to superoxide anions responsible for free radical formation (Sapirstein & Bonventre, 2000). Oxidative stress is represented by the whole reactions using ROS, which are characterized by the presence of a very reactive unpaired electron (free radical).

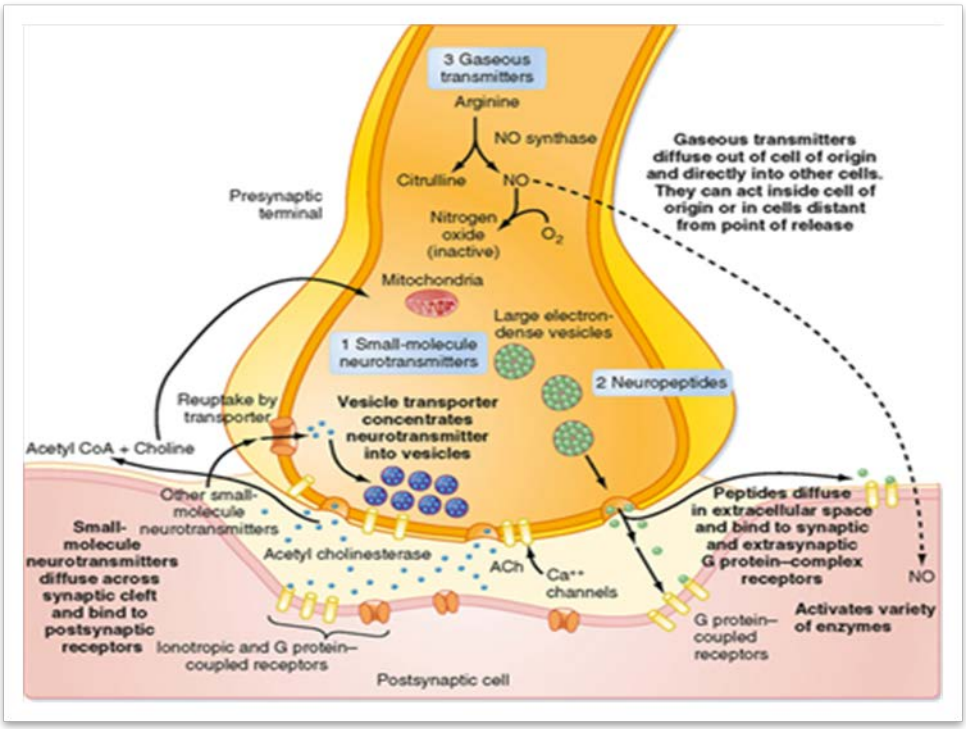

Figure 12. Schematic representation of a synapse. In the pre-synaptic and post-synaptic terminals are represented the main cell targets involved in the release and action of the neurotransmitter (Beckman & Koppenol, 1996; Iadecola, 1997; Dirnagl et al., 1999; Furukawa et al., 1997).

Cerebral ischemia and reperfusion are responsible for oxidative stress leading to free radicals production and to deleterious effects during pathogenesis. Free radicals produced during reperfusion are principally activated species of oxygen. The main ROS generated are: superoxide anion O2−·, hydroxyle radical (OH· the most reactive oxygen-free radicals), hydrogen peroxide (H2O2), nitric oxide, and peroxynitrite (ONOO·). These reactive species are controlled normally by protective reduction enzymes such as superoxide dismutase (SOD) or glutathiase peroxidase (GPx). However, in case of ischemia and reperfusion, excess in cytosolic Ca^{2+} and in mitochondria leads to accumulation of free radicals (Andreyev et al., 2005). Free radicals storaged in mitochondria will be able to react with oxygen when reperfusion occurs in order to produce superoxide ions ($O^{2-}\cdot$). Free radicals thus produced inhibit electron transport in mitochondria and intensify the free radicals formation by mitochondria. Metallic ions are also an important factor of free radicals formation (Iadecola, 1997). Fe^{2+} released during ischemia by transport proteins can convert hydrogen peroxide (H_2O_2) in hydroxyl radical (OH·). They can also induce a lipid peroxidation during reperfusion.

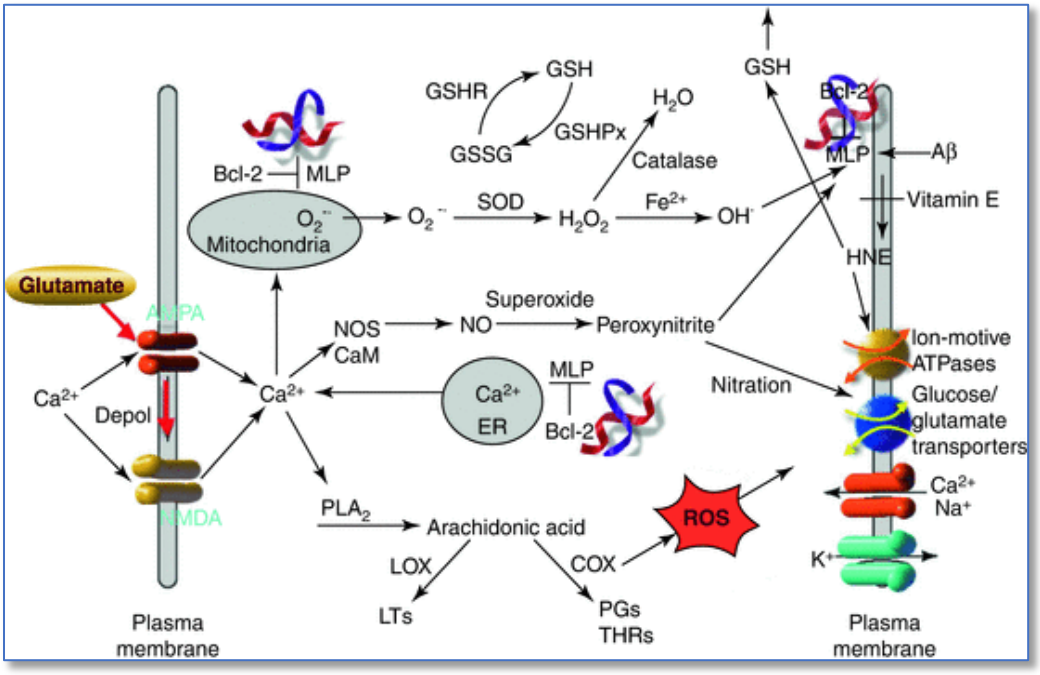

Figure 13. Involvement of excitotoxicity in neuronal death. In case of cerebral ischemia, increased glutamate concentration by exocytosis and/or decrease or inversion of its transport leads to an activation by AMPA and NDMA receptors, osmotic swelling, and a massive entry of calcium ions in neurons. (Velly et al. 2013).

In addition, Zn^{2+} stored in presynaptic vesicles of glutamatergic neurons and released in glutamate exocytosis induces a cellular death during ischemic phenomenon by producing free radicals via the activation of COX and PKC (Suh et al., 2000).

The resulting cerebral oedema is caused by the increase of intracellular ionic concentration, which hence recalls H_2O from outside. Furthermore, the energy-dependent glutamate transporters are blocked, and this contribute to the permanence of glutamate within inter-synaptic fissure and results in continuous receptors stimulation.

1.6.6 Ischemic core and penumbra

It is possible to identify two ischemic areas (Figure 14): the focal area which undergoes severe reduction of cerebral blood flow (CBF) and where neurons are continuously exposed to depolarization is defined the “ischemic core” (Hossmann, 1994). This causes rapid necrosis due to cytoskeleton destruction or to proteolysis.

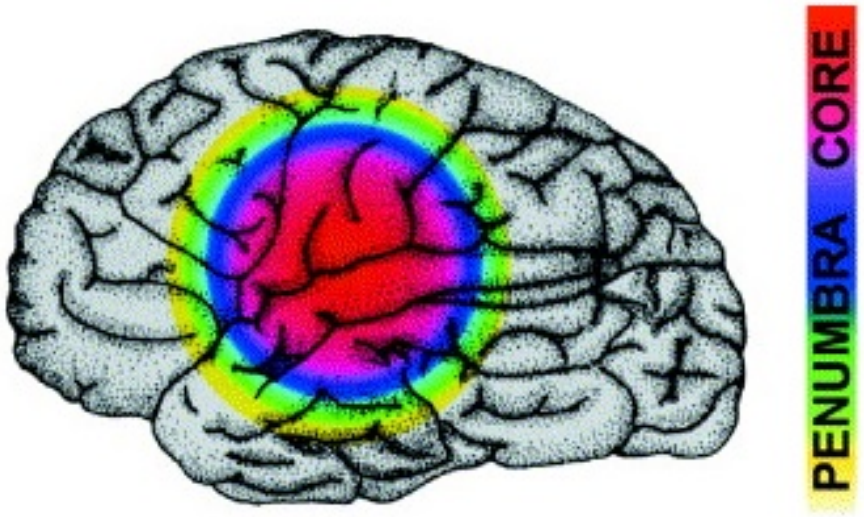

Figure 14. Ischemic *core* and *penumbra*: the red area on the figure marks the infarcted *core*, a brain region of low perfusion in which cells have lost their membrane potential. It is surrounded by a *penumbra* area, marked by the remaining colors, in which intermediate perfusion prevails and identified as the salvageble brain area. Figure modified from (Dirnagl et al., 1999).

The perifocal area, named ischemic penumbra or "penumbra", can maintain, in the first period after the ischemic attack, the physiologic metabolism of the tissue thanks to the perfusion of collateral anastomotic vessels (Astrup, 1981; Hossmann, 1994; Obrenovitch, 1995). Lacking a properly pharmacologic treatment or reperfusion, the ischemic penumbra may advance toward an infarcted condition caused by ischemia and apoptosis.

1.6.7 Perinfarctual depolarization

Penumbra is considered the portion of the tissue in which the ischemic damage causes cellular suffering which is potentially or partially reversible (Hossmann, 1994; Ginsberg, 2003). At this level repolarization, that occurs after the depolarization caused by high extracellular K^+, is possible. Therefore, a repetitive system of depolarization-repolarization is established which is observed until 6-8 hours since the onset of ischemic insult (Hossmann, 1996).

1.6.8 Anoxic depolarization

Neurons situated in the core are exposed constantly to anoxic depolarization (AD, a typical feature of ischemic insults) and gradually lose the ability of repolarization. AD is a spontaneous depolarization of the nervous tissue in response to the ischemic state, which propagates with a speed of 1-3 mm/sec. AD recalls another phenomenon, discovered in the '40s by Leão (1947), named spreading depression (SD). SD occurs

during normoxic conditions within the grey matter of the cerebral tissue after an excitatory stimulation, such as an epileptic condition.

Both AD and SD have similar features and occur as a quick and self-regenerating depolarization, of the all-or-none type, which originates from a focal area of the brain, the core, and then extends, gradually, to the surrounding space (Somjen, 2001).

Leão's discovery opened the way to many studies, both *in vivo* and *in vitro*, which have demonstrated with accuracy and reproducibility the occurrence of SD and AD in almost all the encephalic regions, with higher regularity within specific cerebral areas. The CA1 hippocampal area is considered the most susceptible area to this event (Somjen, 2001).

Positioning a stimulation electrode within the SR of CA1 and a recording electrode close to the dendrites of CA1 pyramidal neurons, it has been demonstrated that the high amplitude, long lasting depolarization, begins at the dendritic level before any other neural area: from the dendrites the depolarization then moves to the cell bodies (Herreras & Somjen, 1993).

This hyperexcitability, confirmed by studies conducted *in vivo* (Rosenblueth & Garcia, 1966), has been related to glutamate-induced excitotoxicity. Indeed, using antagonists of the NMDA receptors, voltage changes during the AD and SD phases are strongly reduced (Herreras & Somjen, 1993). The glutamatergic antagonists are known to be neuroprotective in experimental models (Calabresi et al., 2000; Lee et al., 1999).

Changes in ionic equilibrium during either AD or SD are reflected in morphological changes in the cell: evident cell swelling due to the elevated osmolarity and to the relative reduction of interstitial spaces occurs (Harreveld & Mendelson, 1959; Kow & Harreveld, 1972).

1.6.9 Inflammation process

The increase of intracellular Ca^{2+} concentration, the consequent mobilisation of second messengers, the production of free radicals and the state of hypoxia itself, trigger the activation of transcriptional factors, which increase gene expressions encoding for the inflammation factors involved in the activation of immune responses. Among these, we find PAF (platelet activating factor), TNFβ (tumour necrosis factor-β) and IL-1β (interleukin 1-β). At the same time, molecules of cells adhesion, such as P-selectin, D-selectin and ICAM-1 are expressed in high quantity on the vessel endothelium (Lindsberg et al., 1996; Zhang et al., 1998). The adhesion together with chemotactic

molecules lead to the invasion of the cerebral parenchyma by immune cells such as neutrophils, monocytes and macrophages.

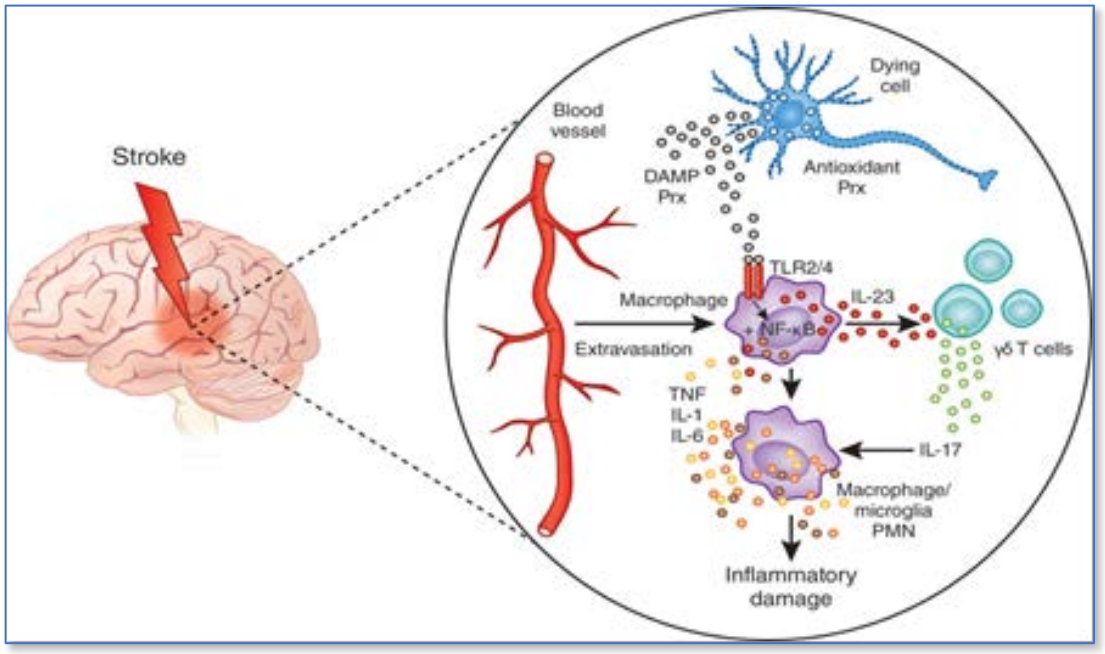

Figure 15. Schematic representation of the inflammation process in a blood vessel during cerebral stroke (Iadecola, 1997).

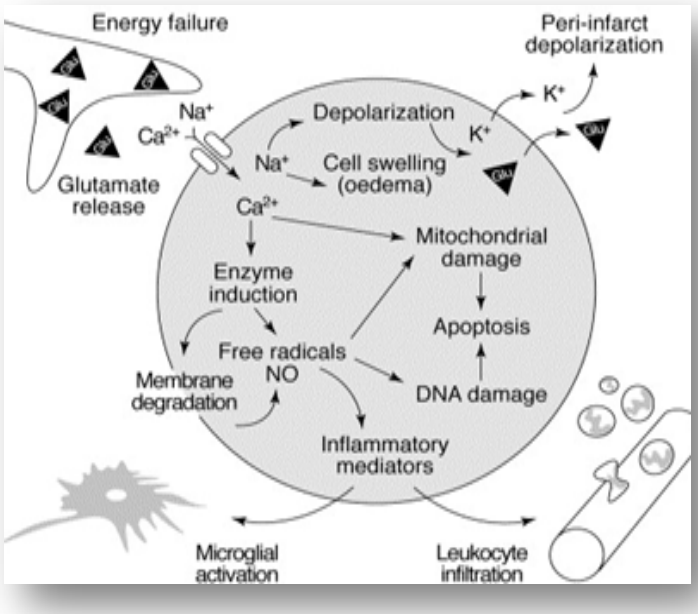

Figure 16. Representation of inflammation during a state of persistent hypoxia. Note the leukocyte infiltration during the inflammatory process (Iadecola, 1997).

The latter ones are the most represented cell type one week after the insult (Iadecola, 1997). Many studies demonstrate that post-ischemic inflammation plays a prevalent role in cellular damage (Feuerstein et al., 1998): indeed, the conspicuous presence of

neutrophils can cause over time microvascular blockade, which worsens the progression of the pathology (Del Zoppo et al., 1991).
Furthermore, the leukocyte abundance can recall inflammation mediators such as NO which causes toxicity, both directly, damaging neurons, and indirectly, recruiting other inflammation cells within the damage area (Figures 15, 16).

1.6.10 Necrosis and apoptosis

All these damaging effects cause loss of function and morphological modifications in neurons and over time become irreversible since, at mitochondrial and nuclear level, necrotic or apoptotic cellular processes initiate. Apart from the mechanism of cellular necrosis, which occurs early, the increase in intracellular Ca^{2+}, NO, free radicals, and inflammation mediators production are likely to induce the process of programmed cellular death called apoptosis (Nakka et al., 2008). A relevant difference between these two events is that necrosis reflects a real pathological state, recruiting inflammation mediators and causing expulsion of cytosolic material into the extracellular side. Apoptosis does not lead to inflammation but causes cellular phagocytosis without the start of inflammatory process. This makes it a protective and physiological cellular event. Necrotic processes are situated within areas where the damage is strong, such as the ischemic core, while apoptosis develops mostly where the damage is less intense such as in the penumbra area.
During ischemic conditions, genes encoding caspases become activated and their expression is highly increased (Dirnagl et al., 1999). Caspases are enzymes that belong to the family of proteases, more specifically of the aspartate-specific cysteine proteases (ASCPs) family, which in the absence of cellular alterations are situated within the cytosol in the form of zymogens. Among the twelve Caspases, only Caspase9 and Caspase3 seem to have a relevant role in apoptosis. At mitochondrial level, as cellular death initiates, the intrinsic apoptotic pathway is activated. The intrinsic pathway is distinguished from the extrinsic one that initiates from signals coming from the external environment (Figure 17).
CytochromeC (CytC) is released from mitochondria due to the activation of the mitochondrial intrinsic pathway, and once within the cytosol, CytC enters in contact with Caspase9 which, after its activation, in turn activates Caspase3. The release of CytC from mitochondria can also be actuated by a cytosolic protein, Bid, upon its proteolytic activation by Caspase8. Therefore, the activation of these Caspases can be

considered the link between the two pathways, intrinsic and extrinsic. Once Caspases are activated, they trigger a proteolytic cascade toward the nuclear lamina A and B, ICAD (Inhibitor of caspase-activated DNase), cytoskeleton actin and various other target proteins which, either directly or indirectly, lead to cellular death.

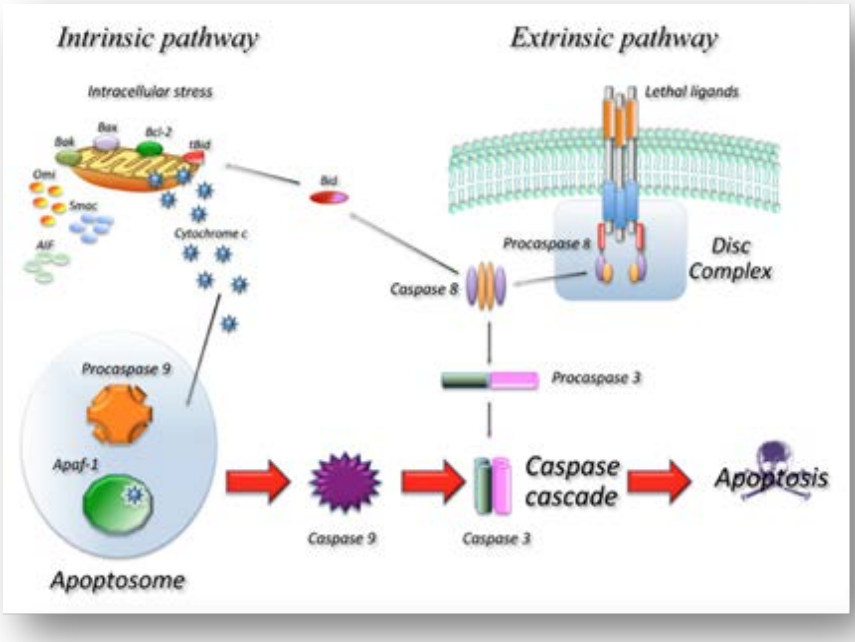

Figure 17. The activation of apoptotic, intrinsic and extrinsic pathways, with their caspases, respectively, 8 for the extrinsic pathway and 9 and 3 for the intrinsic (Dirnagl et al., 1999).

1.6.11 Cerebral oedema

Cerebral ischemia leads to dysfunction of membrane ionic pump that triggers complex mechanisms leading to cell swelling and cellular-related cerebral oedema: cytotoxic oedema. Ionic disruption triggers a passive osmotic flow of H_2O toward the cells. The rise in H_2O into cerebral tissue affects both grey and white matter, which leads macroscopically to an increase in volume. There exists also specific system of H_2O transport playing a role in the occurrence of cerebral oedema, aquaporines (AQP), and particularly AQP4 mostly found in central nervous system. The density of these channels is particularly high at the interface between brain and liquid spaces (blood, subarachnoid space, ventricles). AQP4 is expressed in astrocytes, endothelial cells, and ependymal cells. Neurons are free from AQP4. The role of cerebral AQP in pathology is yet not fully understood but these channels ease H_2O flow. In rodents, AQP4 expression varies following a cerebral ischemic damage or traumatic injury (Badaut et al., 2002); the level of AQP4 expression decreases the first moments after an ischemic

or traumatic damage and increases them (Unterberg et al., 2004). These results suggest that AQP4 contributes to oedematous process but the positive or negative role of AQP4 in oedema formation is not completely delucidated.

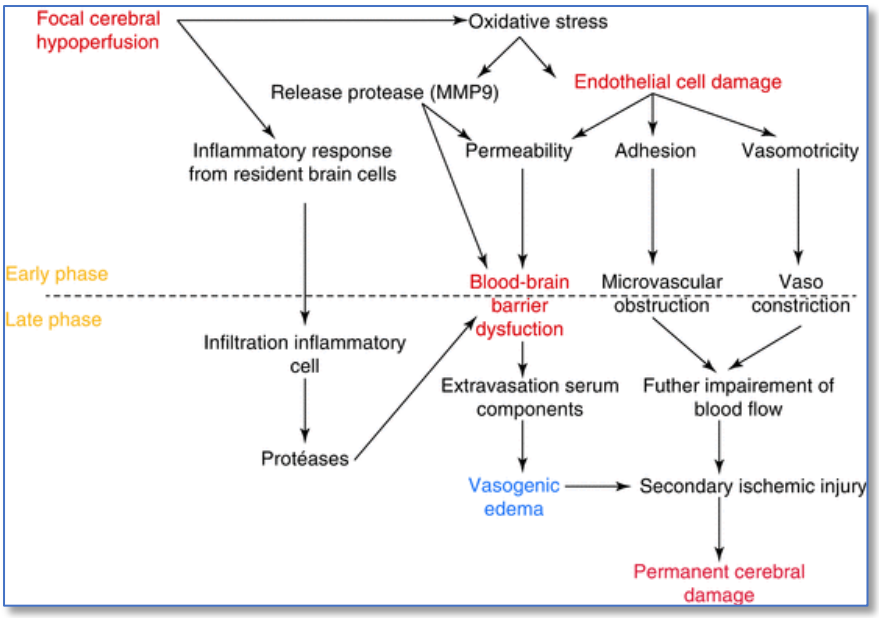

Figure 18. Alteration of the blood–brain barrier during cerebral ischemia (Velly et al. 2013).

In parallel, ischemia-reperfusion alters vessels and the blood–brain barrier, which leads to the formation of an oedema, whose origin is a capillary leak: the vasogenic oedema (Payen et al., 2003). When blood–brain barrier is disrupted, liquid, plasmatic proteins, and inflammatory cells enter in brain tissue. Most of the biological pathways leading to oedema are observed during ischemia: excessive release in glutamate, oxidative stress, and inflammatory cascade. Moreover, an increase in cerebral volume generates increased intracranial pressure and decreased cerebral perfusion pressure, which enhance the ischemic phenomenon.

Oedema grows to its maximal development the fourth day and declines during the second week. The “mass effect” is proportional to the volume of the infarction.

Finally, cytotoxic oedema, as vasogenic oedema can be worsened by reperfusion due to the intensification of oxidative stress and inflammatory response but also due to the brain–blood barrier disruption (Wang et al., 2014) (Figure 18).

1.6.12 Adenosine and its receptors

Adenosine is a purine nucleoside indispensable for DNA synthesis: it is formed by an adenine and ribose molecule joined through an N9-glicosidic bond, which, in the

nervous system, is continually formed both at intracellular and extracellular levels (Figure 19).

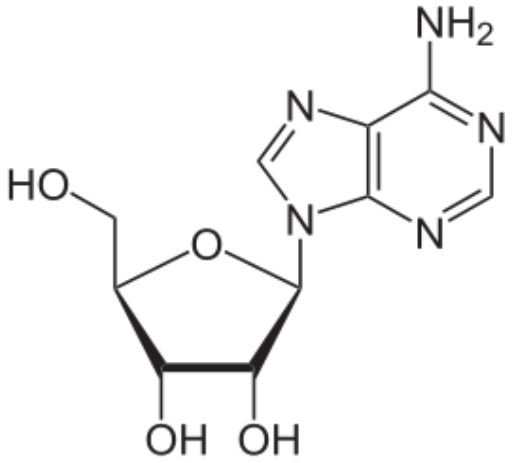

Figure 19. Adenosine structure. Its molecular formula is C10H13N5O4 (Ceruti et al., 2004).

Adenosine assumes an essential role also in biochemical processes and signal transduction, being correlated with molecules such as ATP, ADP and AMP. At central level, it carries out numerous actions: it acts as an endogenous anticonvulsant, influences control of motility, pain, learning and memory (Pedata et al., 2007). Moreover, adenosine has a crucial role in the modulation of emotional states, conditioning social interactions and aggressive behaviours. In physiologic conditions, extracellular adenosine inhibits synaptic transmission, and this makes adenosine a highly protective neuromodulator.

At the extracellular side, adenosine is produced from AMP (Adenosine monophosphate) which is dephosphorylated by the enzyme 5'-nucleotidase (5’-NT). Adenosine can also be formed through the breakdown of nucleotides, which are released into the extracellular space. The 5’-NT is inhibited by ATP and it has an elevated affinity for AMP: for this reason, when the cell is exposed to an intense metabolic activity with increased ATP consumption and consequent elevated production of AMP, the enzyme has very high enzymatic activity. Therefore, during low energetic support conditions as in epileptic attacks, hypoxia or ischemia, production of adenosine is significantly increased (Latini & Pedata, 2001).

Adenosine is a paramount chemical mediator, which can activate determined biologic responses and its action mainly occurs through purinergic receptors activation.

These receptors belong to the seven-transmembrane domain superfamily (Figure 20), structurally composed by 7 amphipathic α-helices (TM 1-7), which consist of a sequence of 20-25 hydrophobic amino acids.

The N-terminal portion is located at the extracellular level whereas the C-terminal exposes toward the intracellular side; all the 7 domains are strictly interconnected via 3 intracellular (IL 1-3) and 3 extracellular loops (EL 1-3) (Cristalli et al., 2008).

The seven transmembrane domain receptors are always associated, at the intracellular side, with specific transduction heterotrimeric protein, defined G protein, which are activated after the interaction between the receptor and substrate.

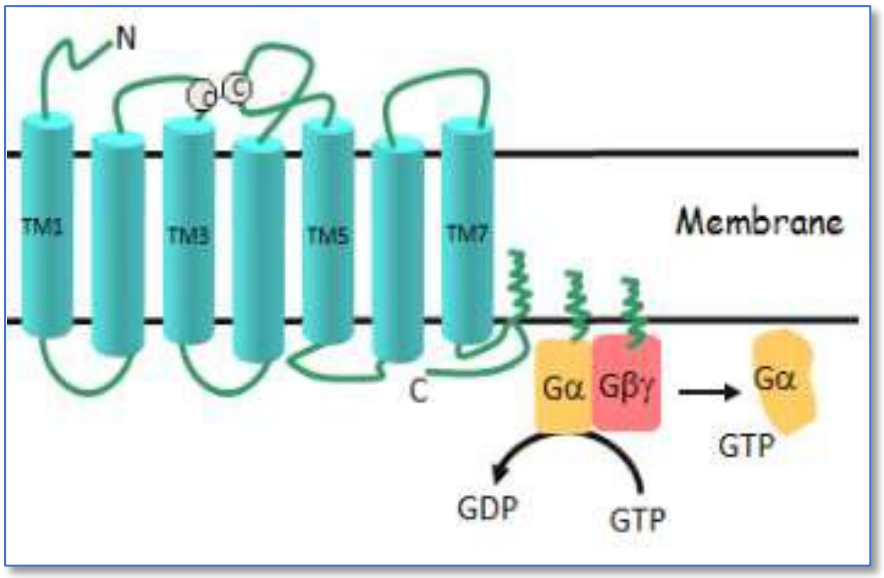

Figure 20. Adenosine seven transmembrane domain receptor (TM) coupled with a G-protein. The Gα, binding GTP, release itself and activates a biologic response (Cristalli et al., 2008).

The purine receptors have been classified in two classes by Burnstock in 1978, P1 and P2 (X, Y) receptors, the latter ones activated by ATP (Burnstock, 1978).

The P1 receptors, activated by adenosine, are present in different cell populations, starting from the nervous system to endothelial cells, the immune system, cardiac tissue and smooth muscle.

The P1 receptors family comprehends only two subtypes, A_1 and A_2, the latter subdivided by Daly and colleagues (Daly, 2001), in two subtypes, A and B, depending on their affinity for adenosine. Four P1 purine receptor subtypes (A_1, A_{2A}, A_{2B} and A_3) have been found so far, and each interacts with a specific G protein (Fredholm et al., 2001) (Table 2). The A_1 and A_3 receptors are coupled with an inhibitory G protein (G_i/G_o) which inhibits both the activation of adenylyl cyclase and PIP2 hydrolyses. A_2 receptors, subdivided in A_{2A} and A_{2B} subtypes, couple to stimulatory G proteins (G_s/G_q)

which activate adenylyl cyclase, thus increasing cAMP production, by AMP cyclization (Daly et al., 1983) (Figure 21).

Table 2. Representation of functions and distribution of purinergic receptors P1 (Fredholm et al., 2001).

Receptors subtypes	**G-protein**	**G-protein coupling effect**	**Adenosine affinity**	**Distribution**
A_1	$G_{i\ 1/2/3}$ G_o G_s	↓cAMP ↑PLC, IP_3/DAG ↑Arachidonico/PLA2 ↑PLD ↑cAMP	~100 nM	High levels in cortex, hippocampus, cerebellum. Intermediate levels in striatum and thalamus
A_{2A}	G_{olf} $G_{15/16}$	↑cAMP ↑IP_3	~20-300 nM	High levels in striatum, nucleus accumbens and olfactory tubercle. Low levels in cortex and hippocampus
A_{2B}	G_s $G_{q/11}$	↑ cAMP ↑ PLC, IP_3/DAG ↑PLD	~5-20 µM	Low level
A_3	$G_{i\ 2/3}$ $G_{q/11}$	↓ cAMP ↑ PLC, IP_3/DAG ↑ PLD	~25-290 nM	Widespread distribution. Higher levels in rat hippocampus and cerebellum

As is often the case for metabotropic receptors, the purine receptors are also pleiotropic, namely they can interact with more than one G protein class and consecutively can activate an ample array of signalling pathways (Cunha, 2005).

Furthermore, apart from the A_3 receptor, which shows intraspecies variations, the other receptor subtypes maintain high homology through molecular evolution (80-85%) (Sachdeva & Gupta, 2013; Haskó et al., 2007).

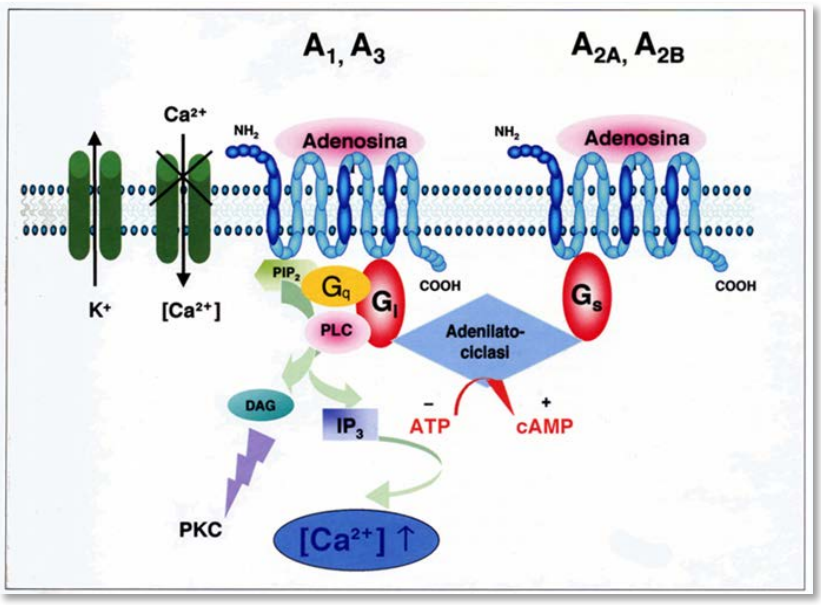

Figure 21. Adenosine receptors and signal transduction mechanisms. Adenosine receptors are G protein-coupled receptors. The A_1 and A_3 subtypes inhibit adenylate cyclase via Gi protein, while the A_{2A} and A_{2B} receptors mediate stimulation of the enzyme via Gs protein. In addition, A_1, A_3 and A_{2B} receptors can modulate, by Go protein or Gq, phospholipase activity, inducing the production of diacylglycerol (DAG) and inositol-triphosphate (IP_3) and an increase in Ca^{2+} release from intracellular deposits (Gessi & Borea, 2011).

A_1 receptors

The A_1 receptor is a monomeric glycoprotein of 35-36 kDa formed by 326 amino acids. It is highly conserved with an 87%-92% homology between different species (including humans), despite differences have been evidenced in the coupling with G proteins and specie-dependent tissue distribution. This receptor subtype is widely expressed in the central nervous system, with a comparable distribution in the pre- and post- synaptic neuronal membranes (Sachdeva & Gupta, 2013; Daly & Padgett, 1992).

An elevated level of expression can be found in the cerebral cortex, hippocampus, thalamus, spinal cord and in the adipose tissue, while lower receptor expression in lungs, ventricles and pancreas.

The A_1 receptors have an elevated affinity for adenosine (EC_{50} 3-30 nM) and they are metabotropic receptors coupled with a G_i/G_o protein, which inhibits the adenylyl cyclase activity, with consequent reduction of cAMP and inactivation of PKA.

On the contrary, the trigger of G_o protein leads to increase conductance of K^+ and Cl^- channels, which re-establish a rest electrochemical potential within the cells in which they are activated.

Many studies indicate that the A_1 receptors play a prominent inhibitory tone on synaptic transmission and that selective adenosine antagonists, acting on this receptor subtype,

have a protective role in ischemia (Pedata et al., 2016). Unfortunately, the development of A_1 receptor selective agonists as possible anti-ischemic drugs has been stalled by their sedative and cardiovascular side effects, including bradycardia and hypotension. Therefore, in order to identify putative targets for therapeutic intervention, the research on possible anti-ischemic drugs has focussed on the contribution of the other adenosine receptors.

A_{2A} receptors

A_{2A} receptors have high affinity for adenosine (EC_{50} 1-30 nM) (Sachdeva & Gupta, 2013). The A_{2A} receptor is a glycoprotein of approximately 45 kDa with an amino acid sequence highly conserved with a homology of 90% between different species (around 82.9% between human and rat).

A_{2A} receptors are coupled with stimulatory G protein (mainly G_s) and subsequently increase cAMP levels and PKA activation (Mulakayala et al., 2013; Chen et al., 2013).

This subtype is highly expressed at central level, even though its distribution is not uniform: it can be found primarily close to dopamine D_2 receptors, namely within striatum, in nucleus accumbens, in the olfactory tubercle and in the cerebellar cells of Purkinje (Lopes et al., 2004; Svenningsson et al., 1999). It can also be present at peripheral level on immune cells, on smooth muscle endothelial cells (Coney & Marshall, 1998; Ngai et al., 2001), in the heart, in the bladder and lungs. In accordance to what already observed for A_1, also A_{2A} receptors are expressed on the membrane of astrocytes (Li et al., 2001; Nishizaki et al., 2002), microglia (Fiebich et al., 1996) and oligodendrocytes (Melani et al., 2009).

Techniques such as *in situ* hybridization (Cunha et al., 1994; Dixon et al., 1996), receptor binding (Lopes et al., 2004), immunohistochemistry, and functional studies (Rebola et al., 2002; Rebola et al., 2003; Rosin et al., 1998) have evidenced that the receptor is present also on nerve endings of both hippocampus and cortex (Wan et al., 1990; Cunha et al., 1994; Johansson and Fredholm, 1995), at pre- and post- synaptical level (Rebola et al., 2005).

In the last few years, the antagonists of A_{2A} receptors have been shown to be efficacious neuroprotective agents, particularly for Parkinson’s disease and Huntington’s disease, representing a non-dopaminergic alternative to current therapies (Jacobson & Gao, 2006; Xu et al., 2005).

Moreover, the role of the adenosine A_{2A} receptor under ischemia has been largely investigated (Chen et al., 2007; Pedata et al., 2014). A_{2A} antagonists can be utilised as neuroprotective drugs in ischemia-induced cell death (Pedata et al., 2005; Melani et al., 2006) and can be used as anti-allergic agents, analgesic, positive ionotropic (Ledent et al., 1997) and for the treatment of alcoholism (Thorsell et al., 2007). A_{2A} receptors play a further important role in modulation of peripheral tissue inflammation (Carlsson et al., 2010). In 2003, Sitkovsky (Sitkovsky et al., 2003) demonstrated their anti-inflammatory effect in mice due to inhibition of tissue damage caused by the inflammatory phase.

Our research group highlighted that the activity of A_{2A} receptors blocks the Ik type of K^+ currents within the precursors of cultured oligodendrocytes, blocking their differentiation, without influences their proliferation (Coppi et al., 2013).

A_{2B} receptors

The A_{2B} receptor is a glycoprotein of approximately 36-37 kDa, coupled to Gs protein, that stimulates adenylate cyclase, intracellular Ca^{2+} mobilization (Mirabet et al., 1997) and activates PKC and PLC (Abbracchio et al., 1995; Feoktistov et al., 2011).

The A_{2B} receptors were identified and cloned for the first time by Rivkees and Reppert in rat hippocampus (Rivkees & Reppert., 1992) and by Pierce in human hippocampus (Pierce et al., 1992).

Among adenosine receptors, the A_{2B} receptor subtype is the least studied and still remains the most enigmatic, because of the relatively low potency of adenosine for this receptor (EC_{50} of 5-20 μM) (Beukers et al., 2000; Sachdeva & Gupta, 2013; Fredholm et al., 2011) and the very few selective ligands that have been described so far. Most of the present knowledge on A_{2B} receptors originates from their peripheral role on the control of cardiac myocyte contractility, intestinal tone, asthma, inflammation, cancer and diabetes (Feoktistov et al., 1999, 2002, 2004; Kolachala et al., 2008; Chandrasekera et al., 2010; Merighi et al., 2015; Allard et al., 2017). A_{2B} receptors play proinflammatory roles in human asthma, in chronic obstructive pulmonary disease (Yaar et al., 2005; Wang & Huxley, 2006; Yang et al., 2006) and murine colitis (Feoktistov et al., 1998; Kolachala et al., 2008; Csóka et al., 2007). In the central nervous system (CNS), adenosine A_{2B} receptors, although scarcely, are uniformly expressed (Dixon et al., 1996) including in the hippocampus (Perez-Buira et al., 2007), but their role or function, especially in ischemic/hypoxic conditions, is still to be clarified. The low affinity for adenosine makes them good therapeutic targets,

considering that their activation could be triggered mainly during pathologic conditions when adenosine levels exceeds μM concentrations.

A_{2B} receptors are coupled to stimulatory G protein, activating the cAMP signalling pathway (Murakami et al., 2000; Sitaraman et al., 2001; Lynge et al., 2003; Fang et al., 2007; Darashchonak et al., 2014); they have a molecular mass which is around 36 kDa (Feoktistov et al., 1999). The major signalling pathway of the A_{2B} receptor is cAMP, but also, by interaction with G_q, other important intracellular pathways, such as PLC (Gao et al., 1998; Linden et al., 1999; Panjehpour et al., 2005), and even MAPK and arachidonic acid (AA), probably through the action of the βγ dimer (Feoktistov et al., 1999; Jiménez et al., 1999; Schulte & Fredholm, 2003; Donoso et al., 2005).

Importantly, because of its low affinity for adenosine, we know that the A_{2B} receptor appears inactive during physiologic conditions. Indeed, its activation occurs during pathologic conditions influenced by environmental stimuli, such as inflammation, hypoxia, traumatic events and cellular damage (Xaus et al., 1999; Fredholm et al., 2001; Kolachala et al., 2005; Kong et al., 2006; Hart et al., 2009; Haskó et al., 2009). Furthermore, recent studies have evidenced a possible role of the A_{2B} receptor, probably through a receptor interaction, not known yet, with A_1 receptors (Gonçalves et al, 2015).

A_3 receptors

The A_3 receptor is a protein of approximately 39 kDa. The expression of A_3 adenosine receptor in the brain is generally lower than that of the other subtypes (Ji et al., 1994) and is highly species-dependent (Fredholm et al., 2000). The A_3 receptors are the last adenosine receptor category belonging to the P1 receptor family. Primarily they are expressed in the kidney, heart, lung, cerebral cortex and on immune cells (Livingston et al., 2004). These receptors show substantial pharmacological, functional and distribution differences among species.

Also, they have affinity for adenosine (with an EC_{50} of 300 nM) and, as the A_1 receptors, they are coupled to inhibitory G proteins (G_i), which inhibit adenylyl cyclase activation: when stimulated they cause, in certain cellular tissue, the activation of phospholipase C and B and the consequent release of intracellular Ca^{2+} (Sachdeva & Gupta, 2013).

In neuroprotection, the role of the A_3 receptors is contradictory, depending on the tissue in which they are expressed (Cheong et al., 2013): following cellular damage,

neuroprotection is induced by their sub-stimulation whereas cellular toxicity is induced by their stimulation (Yao et al., 1997).

A_3 receptors activation leads to the production of ROS and to mitochondrial depolarization, two events that are known to cause mitochondria destruction and the release of apoptotic proteins, which are soluble within the cytosol (Brady et al., 2004; Cao et al., 2011). Particularly, adenosine triggers the intrinsic apoptotic pathway, with involvement of the mitochondrion/caspase-9 pathway, whereas the extrinsic apoptotic pathway, with caspase-8 activation, is only triggered in case of low concentration of adenosine (Gonzàlez-Fernàndez et al., 2014).

1.6.13 Role of adenosine in cerebral ischemia

The increase of extracellular adenosine concentration during *in vivo* ischemia (Dux et al., 1990; Hagberg et al., 1987; Matsumoto et al., 1992; Melani et al., 1999; Phillis et al., 1994; 1996; Sciotti et al., 1992) is attributable to different reasons. Early after ischemia, the increase of adenosine is mainly due to extracellular released ATP (Melani et al., 2012) that is hydrolysed by ectonucleotidases (NTPDases 1, 2 and 3 that convert ATP o ADP and AMP) and ecto-5'-nucleotidase that converts AMP to adenosine (Zimmermann, 2000; Fausther et al., 2012). Thereafter adenosine *per se* is released mainly from cells likely through the action of ENT2 (Melani et al., 2012). Inhibition of adenosine-uptake processes due to down-regulation of CNT2 and 3 and of the ENT1 also contributes to the extracellular adenosine increase after stroke (Medina-Pulido et al., 2013).

Many authors have described the protective role of adenosine during cerebral ischemia. Indeed, it is largely known that agents that increase endogeneus adenosine, either inhibiting its metabolism (Wu et al., 1992) or preventing its reuptake (Dux et al., 1990), give protection against neuronal damage induced by hypoxic-ischemic insults in different experimental models both *in vivo* and *in vitro*.

At hippocampal level during a simil ischemic state obtained through oxygen and glucose deprivation, adenosine can reach a concentration of 30 µM, significantly higher than that recorded in normoxic conditions (50-200 nM) (Rudolphi et al., 1992; Dunwiddie and Diao, 1994; Latini & Pedata, 2001).

The extracellular adenosine concentrations reached after ischemia allow the stimulation of all adenosine receptor subtypes (A_1, A_{2A}, A_{2B} and A_3). Their broad distribution on neuronal, glial and inflammatory cells (Fiebich et al., 1996; Brodie et al., 1998;

Svenningsson et al., 1999; Hettinger et al., 2001; Yu et al., 2004), suggests that the role of adenosine in ischemia is the consequence of interplay among activation of different receptors, that changes depending on the time-related development of the pathological condition (Pedata et al., 2014).

During ischemia, adenosine has long been identified as a neuroprotectant endogenous agent (Cunha, 2001; Pedata et al., 2007; Fredholm et al., 2003; Ongini et al., 1997; Ribeiro et al., 2002; Schwarzschild et al., 2002). It was demonstrated that adenosine infusion into the ischemic striatum significantly ameliorates neurological outcome and reduces infarct volume after transient focal cerebral ischemia (Kitagawa et al., 2002). Protective effects are greatly attributed to A_1 receptor activation that reduces Ca^{2+} influx, lowering presynaptic release of excitatory neurotransmitters (Andiné, 1993; Corradetti et al., 1984; Dunwiddie & Diao, 1984; Zetterström & Fillenz, 1990; Pedata et al., 1993; Kitagawa et al., 2002; Zetterstrom & Fillenz, 1990), such as glutamate which exerts its excitotoxic effect mainly overstimulating NMDA receptors (Choi, 1990). In addition, by increasing the K^+ and Cl^- ion conductances (Takigawa & Alzheimer, 1999; 2002), adenosine stabilises the neuronal membrane potentials, thus reducing neuronal excitability (Choi, 1990). Nevertheless, the use of selective A_1 agonists is hampered by undesirable effects such as sedation, bradycardia, hypotension (White et al., 1996; Fredholm et al., 2005).

This is confirmed by the use of selective agonists of A_1 receptors both *in vivo* and *in vitro*. Their administration decreases both ischemic and excitotoxity neuronal damage. Indeed, *in vitro* it has been determined that either adenosine or A_1 receptors agonists can reduce the damage caused by an ischemic insult in both hippocampal and cortical cell cultures (Daval & Nicolas, 1994; Logan & Sweeney, 1997), as well as in cerebral slices (Dux et al., 1992; Mori et al., 1992; Newman et al., 1998). Local administration of an adenosine analogous, 2-chlorine-adenosine, or of a non-selective agonist of A_1 receptor, (-)-N6-(2-isopropyl-phenyl)-adenosine, attenuates the neuronal loss within the CA1 region of mouse hippocampus (Domenici et al., 1996).

Reduction of reactive oxygen species (ROS) production occurs in presence of A_1 receptors agonists, whereas when they are blocked an increase of ROS and cell death occurs in neuronal primary cultures (Milton et al., 2007). In *in vivo* animal models of cerebral ischemia, both systemic and intracerebroventricular administration of the A_1 receptors agonists, N6-cicloesyl adenosine (CHA) and N6-R-phenylisopropyl adenosine (R-PIA), improves the neurologic deficit and protects the CA1 hippocampal region

(Daval et al., 1989). Furthermore, systemic administration of an adenosine derivate substituted in N6-phenyl, ADAC, after cerebral ischemia, increases neuronal survival, preserves its morphology, maintains spatial memory and the learning ability in gerbils (Phillis & Goshgarian, 2001; Ling et al., 1999).

Through the stimulation of A_1 receptors, adenosine inhibits the release of all classic neurotransmitters: glutamate, acetylcholine, dopamine, norepinephrine and serotonin (Fredholm & Lindgren, 1988). Particularly, strong decrease of glutamate release from presynaptic ends has been detected in the hippocampus (Burke & Nadler, 1988; Corradetti et al., 1984), where the activation of A_1 receptors reduces neurotransmitters quanta released from the Schaffer's collateral commissural pathway (Lupica et al., 2001). Instead, the post-synaptic effect depends on direct hyperpolarization of the neurons through the K^+ channels activation (GIRK channels) on post-synaptic end (Takigawa & Alzheimer, 1999; 2002).

Although many data prove a neuroprotective effect of adenosine during ischemia through A_1 receptors, the clinical utility of A_1 selective agonists is hindered by their side effects both at central and peripheral level, such as sedation, bradycardia and hypotension (White et al., 1996).

On the contrary, the adenosine A_1 receptors antagonists increase synaptic transmission, impeding the synaptic potential recovery and shorten the appearance of the anoxic depolarization induced within the CA1 region of the hippocampus.

Theophylline, a non-specific A_1 receptor antagonist, increases cellular damage and mortality after ischemia in gerbil (Rudolphi et al., 1987). Similar deleterious effects are also observed after the acute administration of selective A_1antagonists, DPCPX (8-ciclo-pentyl-1,3-dipropyl xanthine) and 8-CPT (8-ciclopentyl theophylline) (Boissard et al., 1992).

Opposed effects against A_1-mediated synaptic inhibition are induced by the activation of A_{2A} receptors, which has been shown to mediate excitatory actions in the nervous system (Latini et al., 1996; Pedata et al., 1984; Sebastiao & Ribeiro, 1996; Spignoli et al., 1984). In physiological conditions, electrophysiological studies of synaptic functions on A_{2A} receptors have shown that they increase synaptic transmission. For instance, in hippocampal slices the stimulation of this receptor subtype results in acetylcholine release (Cunha et al., 1995; Spignoli et al., 1984). More recently, adenosine A_{2A} receptors emerged as an interesting target in ischemia. The application of

a selective A_{2A} agonist, CGS-21680, decreases the ability of A_1 receptor agonists to inhibit excitatory neurotransmission (Cunha et al., 1994; O'Kane & Stone, 1998).

The main problem of A_{2A} adenosine agonists lies in their cardiovascular effects, as the receptors present on smooth muscle cells and endothelial cells give rise to vasodilatory effect.

The less selective antagonists, CGS-15943 and CP-66713, both administered pre-ischemia, protect against ischemia-induced damage in the hippocampus and neocortex of gerbil (Phillis, 1995). Gao and Phillis (1994) were the first to demonstrate the reduction of ischemic damage in the gerbil following the administration of CGS-15943, a selective antagonist for this receptor subtype.

Subsequently, many studies confirmed this neuroprotective role in various animal models of ischemia: the selective A_{2A} receptor antagonist, SCH-58261, is efficacious in reducing brain damage in adult rats (Pugliese et al., 2009). This theory is also supported by experiments on genetically modified mice: KO mice for the A_{2A} receptor, subjected to cerebral ischemia, showed attenuation of brain damage and neurologic deficits (Pedata et al., 2016). The antagonist SCH-58261, acutely administered after hypoxia/ischemia to newborn mice, significantly reduces brain damage. SCH-58261, administered acutely 5 min after ischemia to adult mice, was found to be protective against brain damage up to 24 hours after the insult (Melani et al., 2003).

An additional mechanism through which A_{2A} receptor antagonism is protective may be the ability to increase extracellular GABA concentration during ischemia. The enhancement of GABA synaptic transmission induces neuroprotective effects in various experimental models of cerebral ischemia (Schwartz-Bloom & Sah, 2001).

In addition, CGS-21680 administered at the dose of 0.5 mg/Kg in awake mice decreases blood pressure and increases heart rate. The dose of 0.01 mg/Kg of CGS-21680 does not alter either mean blood pressure or heart rate (Melani et al., 2014). Adenosine acting on A_{2A} receptors at endothelial blood vessel levels acts as a vasodilating agent by regulating cerebral blood pressure. Consequently, A_{2A} receptor agonists may favour post-ischemic brain reperfusion. Many studies indicate that A_{2A} receptors located on blood cells are responsible for the protective effects of A_{2A} adenosine agonists following ischemia: these are expressed on both innate immune cells (microglia, macrophages, monocytes, mast cells, dendritic cells, neutrophils) and adaptive immune cells (lymphocytes) (Antonioli et al., 2014). In addition, the selective activation of A_{2A} receptors directly in blood cells inhibits pro-inflammatory response, reduces the

production of cell adhesion factors and reduces the activation of neutrophils, thus exerting anti-inflammatory and antioxidant effects (Sitkovsky et al., 2003).

Knowledge on A_{2B} receptors is very recent: given the scarcity of selective A_{2B} adenosine receptors ligands, there is little evidence on the role of these receptors in cerebral ischemia.

With an increase in the supply of KO mice for A_{2B} receptors, and the availability of selective ligands, the research is starting to shed light on their role in neurotransmission, both in rat (Dixon et al., 1996; Zhou et al., 2004) and human hippocampus (Perez-Buira et al., 2007).

In vitro studies have highlighted the increase in number and density of A_{2B} receptors on cells, which distinctly show astrocytes morphological characteristics, following ischemic preconditioning (Pedata et al., 2016).

Few studies have investigated A_{2B} receptors role in *in vivo* cerebral ischemia. In a recent paper, the selective antagonist MRS 1754 decreased ceramide production in astrocytes attenuating the inflammatory responses and neuronal damage after cerebral ischemia (Gu et al., 2013).

Some studies demonstrate that, after ischemia, the A_{2B} receptors present on cerebral cells are harmful for neurons, while those located on endothelial and blood immune cells hinder vascular adhesion signals and inflammation, induced by hypoxia (Koeppen et al., 2011). Indeed, pharmacological studies reveal that A_{2B} receptors, on neutrophils, contribute to decrease of their capability to adhere at endothelial cells and then transmigrate within the tissues parenchyma.

A further role of A_{2B} receptors in hypoxia/ischemia could be the developing of angiogenic response, since the activation of this receptors by adenosine allows endothelial cells proliferation, chemotaxis and the assembly of new blood vessels (Adair, 2005).

The role of A_3 receptors in ischemia is still poorly understood. Data in the literature are frequently conflicting, showing they sometimes carry out opposite actions in this pathology.

Intracerebroventicular pretreatment with the selective agonist CI-IB-MECA decreases the magnitude of infarctual area induced by an ischemic insult in wild-type but not in KO mice for A_3 receptors, revealing that protection induced by CI-IB-MECA is mediated by the activation of such receptors.

These data suggest that A_3 agonists can protect against neuronal damage induced by hypoxia/ischemia (Chen et al., 2013). More recent published data indicate an inhibitory role of A_3 receptors on synaptic transmission during short periods of OGD and suggest that, in those conditions, A_3 receptors, in synergy with A_1 receptors, have a role in decreasing synaptic transmission, confirming the neuroprotective effect mediated by A_1 receptors (Pedata et al., 2016).

Contrary to information just provided, it has been demonstrated that administration of A_3 selective antagonists such as MRS 1523 or LJ-1252 causes either increase or delay of anoxic depolarization appearance and prevention on synaptic damage caused by ischemia in rat hippocampal CA1 region due to (Pugliese et al., 2007; 2009).

Thus, A_3 activation results either protective or harmful following hypoxic/ischemic conditions. This appears to depend on various causes: OGD length which, if prolonged switches the protective A_3 receptors action in harmful (Pugliese et al., 2007); the sub or prolonged stimulation of A_3 receptors; the type and duration of administration of selective or non-selective drugs; the timing of administration with regard to the ischemic event. The contrasting information on A_3 receptors could be caused also by different experimental conditions utilized in different studies.

The effects of A_3 receptors can be mediated not only by neuronal receptors, but also by those located on glial cells. Some studies prove that A_3 receptors on astrocytes mediate neuroprotection, depending on the pharmacological concentration to which they are exposed (Di Iorio et al., 2002).

The results of all these studies raise the issue of A_3 receptors agonists/antagonists utility in the therapy of ischemia, especially concerning the administration timing. It can be supposed that, after ischemia, a prolonged treatment with A_3 agonists protects firstly through decrease of excitotoxicity mediated by glutamate and hereafter through the A_3 receptors desensitization, avoiding the prolonged harmful activation of A_3 receptors (Pedata et al., 2016).

1.6.14 Adenosine A_{2B} receptors in brain ischemia

Adenosine A_{2B} receptor is expressed at low levels uniformly throughout the CNS (Puffinbarger et al., 1995; Dixon et al., 1996; Fredholm et al., 2000) and has low affinity for adenosine. Their mRNA and protein expression levels increase on endothelial cells, neurons, and astrocytes to a greater extent than do those of the other three adenosine receptors (A_1, A_{2A}, and A_3) 24 hours after tMCAo in the rat (Li et al.,

2017). Thus, during conditions of hypoxia or ischemia when the extracellular adenosine levels rise, A_{2B} receptors might be extensively activated. Because of paucity of A_{2B} selective agonists and antagonists (Müller & Jacobson, 2011) few studies are published so far on the role of A_{2B} receptors in brain ischemia.

Few studies have investigated the role of A_{2B} receptors in brain ischemia *in vivo*. It was reported that the selective A_{2B} receptor antagonist, MRS 1754, reduced the ceramide production in astrocytes and attenuated inflammatory responses and neuronal damage after global cerebral ischemia induced by four-vessel occlusion in the rat (Gu et al., 2013). This effect was related to an early reduction of p38 MAPK activation. A_{2B} receptor plays a key role in the rapid activation of p38 MAPK and in the subsequent inflammatory process (Koscsó et al., 2012; Wei et al., 2013). Altogether, these experiments indicate that antagonism of A_{2B} receptors located on brain cells may be protective from the ischemic brain damage.

Besides brain cells, A_{2B} receptors are present on blood immune cells i.e. neutrophils, lymphocytes (Gessi et al., 2005; Eckle et al., 2008) where, in most cases, they are co-expressed with A_{2A} receptors. They are also expressed at low levels on platelets, where they are upregulated following injury and systemic inflammation *in vivo,* inducing an inhibition of platelet aggregation (Yang et al., 2010). Moreover, A_{2B} receptors are expressed on the surface of endothelial cells (Feoktistov et al., 2004) where they are up regulated by the hypoxia inducible factor (HIF-1α) (Eltzschig et al., 2004). In accordance, vascular permeability is increased significantly in organs of A_{2B} receptor KO mice subjected to ambient hypoxia. By contrast, hypoxia-induced vascular leak is not accentuated in A_1, A_{2A} or A_3 receptor KO mice, suggesting a specific role of A_{2B} receptor in endothelial cells (Eckle et al., 2007). Moreover, A_{2B} receptor KO mice exposed to hypoxia exhibit increased neutrophil infiltration into hypoxic tissues, revealing an inhibitory role for A_{2B} receptors in neutrophil transmigration *in vivo* (Eckle et al., 2007; 2008). Attenuation of hypoxia-associated increases in tissue neutrophil numbers appeared to depend largely on hematopoietic cell A_{2B} receptor signaling (Yang et al., 2006; Eckle et al., 2007). In agreement, A_{2B} receptor KO mice showed increased basal levels of TNFα and expression of adhesion molecules such as ICAM-1, P-selectin and E-selectin in lymphoid cells, resulting in increased leucocyte rolling and adhesion (Yang et al., 2006). Pharmacological studies indicate that A_{2B} receptors on neutrophils contribute to their decreased adhesion to endothelial cells and transmigration in tissue parenchyma (Eckle et al., 2007; Eltzschig et al., 2004).

Recent introduction of new pharmacological tools (Hinz et al., 2014) led to understand a role of A_{2B} receptors in ischemia. Intravenous treatment with the selective A_{2B} receptor agonist BAY 60-6583 (1 mg/kg), at the start of reperfusion after brain ischemia induced by transient Middle carotid Artery occlusion (tMCAo), reduced lesion volume, attenuated brain swelling and Blood Brain Barrier (BBB) disruption. In the presence of the thrombolythic drug tPA (administered after the ischemic stroke), BAY 60-6583 also mitigated sensorimotor deficits and reduced tPA-induced hemorrhages at 24 hours after ischemia (Li et al., 2017). The neurovascular protection afforded by BAY 60-6583 appears to derive from stimulation of the tissue inhibitor of matrix metalloproteinase-1 (TIMP-1) production, inhibition of tPA-induced matrix metalloprotease (MMP) activation, and prevention of tight junction protein degradation. In fact, overactivation of MMP leads to increased cerebrovascular permeability after ischemia-reperfusion injury (Mishiro et al., 2012). Thus, this study proposes that A_{2B} receptor agonists might be adjuvant to tPA and could be a promising strategy for decreasing the risk of hemorrhages during treatment for ischemic stroke (Li et al., 2017).

Altogether, these studies point toward a role of central A_{2B} receptors, in synergy with A_{2A} receptors, in promoting brain excitotoxicity, while A_{2B} receptors located on vascular endothelial cells would play a pivotal role in attenuating hypoxia-induced increases in vascular leak. Blood immune cells would be implicated in dampening vascular adhesion signals and hypoxia-induced inflammation (Koeppen et al., 2011).

To date there are no evidences in literature on the protective effects of A_{2B} receptor agonists at more distant times from ischemia when defined neuroinflammation develops. In our studies, object of the present thesis, we explored the protective effect of A_{2B} receptor agonist, BAY 60-6583, in a rat model of transient (1h) ischemia induced by MCAo, with a chronic treatment for 7 days, when a clear inflammatory response developed. Recent introduction of new pharmacological and genetic tools led to understand a role of A_{2B} receptors in the regulation of inflammation, immunity and tissue repair (Crespo et al., 2013; Feoktistov & Biaggioni, 2011; Hinz et al., 2014; Ortore & Martinelli, 2010). Besides brain cells, A_{2B} receptors are present on endothelial and blood immune cells and in most cases are coexpressed with A_{2A} receptors. A_{2B} receptor transcripts are found in neutrophils (Fredholm et al., 1996), lymphocytes (Gessi et al., 2005) and platelets (Amisten et al., 2008). Moreover, A_{2B} receptor are expressed on the surface of endothelial cells (Feoktistov et al., 2002) and regulate every aspect of endothelial inflammatory processes.

A further possible role of A_{2B} receptors in hypoxia|ischemia might be secondary to promotion of an angiogenic response because activation of A_{2B} receptors by adenosine increases endothelial cell proliferation, chemotaxis and capillary tube formation (Grant et al., 2001; Adair, 2005). Exposure of human umbilical vein endothelial cells to hypoxia increases expression of A_{2B} receptor which upon stimulation promotes the release of vascular endothelial growth factor (VEGF) (Feoktistov et al., 2004).

Aim of the Research

The aim of my research was to study the alterations of the interactions among neurons, astrocytes and microglia in different models of neurodegeneration and neuroinflammation in the hippocampus, a crucial cerebral region involved in short-term and long-term memory formation. In particular, I evaluated the morphological and functional changes induced by aging, neuroinflammation, Alzheimer's disease, and cerebral ischemia and characterized the molecular and cellular modifications of the interplay between neuron and glial cells, fundamental for the correct organization of the central nervous system.

My research project can be subdivided into different parts.

In the first part, I studied normal brain aging and LPS-induced neuroinflammation in the dentate gyrus, an important subregion of the hippocampus that represents the first link of the canonical trisynaptic pathway that conveys electrophysiological inputs from the enthorinal cortex to the hippocampus proper. The aim of this part of my research was to unravel whether similar or different pathophysiological mechanisms are at the basis of neurodegeneration caused by normal brain aging and acute inflammation. To this aim I investigated the qualitative, quantitative and functional alteration of neurons, astrocytes and microglia and the modification in their intermutual interaction in aged rats and adult rats with an acute cerebral inflammation induced by infusion of lipopolysaccharide (LPS) into the 4th ventricle.

Franceschi and coworkers in 2007 had introduced the term "inflammaging" which describes the progressive changes that occur in the aging brain, characterized by a low-grade chronic up-regulation of certain pro-inflammatory responses. Slowly evolving and regions specific series of changes induced by aging may differ from those caused by infusion of LPS and represent a complex interplay of glial and neuronal interactions. Thus, I studied not only the qualitative and quantitative alteration in neurons and glia but also the modifications of neuroinflammatory markers in the hippocampus of aged and LPS treated rats, a more aggressive form of brain inflammation.

In the second part of my thesis I focused my research on an animal model of Alzheimer's disease (AD). AD is a chronic neurodegenerative disease; the main clinical features of AD are cognitive and behavioural deficits. The most common early symptom is short-term memory loss, the difficulty to remember recent events, followed by problems of language, disorientation, mood swings, loss of motivation, not managing self-care, depression, hallucinations and aggression. At present, no therapy for AD is

available, except for cholinesterase inhibitors and memantine that act only on symptoms but not the etiopathology. Therefore, it is increasingly important to understand the pathogenetic mechanisms of AD to design drugs able to ensure a proper treatment.

In this part of my work, I investigated the new integrated view of neurodegenerative diseases as derangements of the interplay between neurons and glia. I analyzed quantitatively and qualitatively Aβ-plaques, neurons, astrocytes, total microglia and activated microglia, with particular insight on the interplay between neurons, astrocytes and microglia in the formation of triads. The modifications and alterations of neurons and glial cells within the Stratum Pyramidale (SP) and Stratum Radiatum (SR) of CA1 and CA3 of the hippocampus in TgCRND8 mice, an animal model of Aβ-deposition was also aimed at elucidating whether different pathophysiologic mechanisms neurodegeneration may exist in the different hippocampal structures of TgCRND8 mice. This research will help to understand the pathophysiological mechanisms of the disease and, possibly, to design and develop new drugs acting not only on neurons but also on glial cells to slow or counteract the progression of AD.

In the third part of the study, I focused on neurodegeneration induced by cerebral ischemia, exploiting an *in vivo* model of brain chronic hypoperfusion and an *in vitro* simil ischemic condition.

Cerebral hypoxia caused by chronic hypoperfusion is a condition in which there is insufficient blood flow to the brain to meet metabolic demands, leading to poor oxygen supply and thus to degeneration of brain tissue.

Brain chronic hypoperfusion was induced in the rat using the common carotid arteries occlusion method and immunohistochemical staining and analysis of neurons, astrocytes and microglia was performed on hippocampal slices from animal sacrified 3 months after bCCAo. In particular, I investigated the morphological and functional alterations of the neuron-astrocyte-microglia triad as a possible pathophysiological mechanism responsible for the neurodegeneration and inflammation that characterize these animal models of brain chronic hypoperfusion and the protective role of dipyridamole as an anti-inflammatory drug.

Finally, in the last part of my thesis I investigated the mechanisms of cerebral ischemia using the *in vitro* model of acute hippocampal slices under oxygen glucose deprivation (OGD). Ischemic damage results from a cascade of cellular and molecular events triggered by the lack of blood flow and subsequent reperfusion of the ischemic territory.

Neurons are more vulnerable than glia and vascular cells and, when exposed to hypoxia-ischemia, quickly become dysfunctional and die.

During ischemia, the extracellular concentration of adenosine significantly increases, as shown in both *in vivo* and *in vitro* cerebral ischemia models. In such conditions, adenosine reaches μmolar concentrations, which are sufficient to activate all its receptor subtypes: A_1, $A2_A$, A_{2B} e A_3. The neuroprotective role carried out by the activation of A1 receptors during ischemia is already well-know, whereas so far, the roles of the others receptor subtypes remain rather controversial.

Among the various adenosine receptor subtypes, the A_{2B} receptors is the most enigmatic due both to the limited number of selective ligands and to its low affinity for endogenous adenosine. Some studies have proved that during pathologic conditions such receptors are activated in brain and in glial cells. In the literature, there are no data concerning their involvement during cerebral ischemia.

I studied the role of A_{2B} receptors in hippocampal CA1 during ischemic-like condition obtained through OGD, an experimental condition that, although with some limits due to *in vitro* methodology, mimics the most frequent causes of cerebral ischemia such as vessel occlusion. For this aim, two selective antagonists for this receptor subtype were used in slices subjected to OGD and collected at various time after the end of OGD.

Extracellular registration of field Excitatory Post-Synaptic Potential (fEPSP), evoked by the electric stimulation of the CA1 region of rat hippocampus were combined with immunohistochemical analyses to evaluate the OGD-induced neuronal damage and glia alterations. In order to verify and quantify the time-course of the damage caused by OGD on neurons, astrocytes and microglial cells, double and triple labelling technique was performed, evaluating the results from both a qualitative and a quantitative point of view. Neurons, astrocytes, microglial cells and the possible reciprocal interactions among them were analysed in the CA1 region of the hippocampus on control slices and slices exposed to OGD in the absence and presence of A_{2B} receptor antagonists to evaluate their potential neuroprotective during the ischemic insult. Furthermore, using the immunohistochemical marker for CytochromeC, a typical marker of apoptosis late phases, I evaluated whether an increase of apoptosis occurred after OGD. Finally, we tested whether the activation of a cytoplasmic metabolic regulatory protein such as mTOR might be affected by OGD. Due to its involvement in the metabolism of cells and especially for its changes in expression patterns during ischemic conditions, mTOR merits a deep analysis.

Material and Methods

MODELS OF BRAIN AGING, NEUROINFLAMMATION AND ALZHEIMER'S DISEASE

Part I – Brain Aging and Inflammation

3.1 Animals

Male adult Wistar rats were used (3 and 22 months old Harlan, Milano, Italy). Rats were housed in cages with food and water *ad libitum*, in a temperature-controlled room (23±1°C, 12 h light–12 h dark cycle). Experiments were authorized by the IACUC of the University of Florence and by the Italian Ministry of Health (Italian Law on Animal Welfare, DL 116/92). According to the law, we did all efforts to fulfill the 3Rs requirements. The total number of rats used was: Adult rats, n=6; Aged rats, n=6; LPS-treated rats: n=7.

3.2 LPS treatment

Experiments on LPS-treated rats were performed in the Department of Psychology, The Ohio State University, Columbus, OH 43210, USA, (Hauss-Wegrzyniak et al., 1998; Cerbai et al., 2012; Lana et al., 2016) in accordance with the National Institute of Health Guide for the Care and Use of Laboratory Animals (NIH Publications No. 80-23) revised 1996; formal approval to conduct the experiments was obtained from the Institutional Animal Care and Use Committee (approval number 2008A0028). Male rats (3 months) aged were used. Briefly, LPS or artificial cerebrospinal fluid (aCSF, in mM: 140 NaCl; 3.0 KCl; 2.5 CaCl2; 1.0 MgCl2; 1.2 Na2HPO4, pH 7.4) was administered for 4 weeks to adult rats using an Alzet osmotic minipump containing 1.6 µg/ml LPS (Sigma; E. coli, serotype 055:B5, TCA extraction). The minipump was attached to a chronic indwelling cannula (Model 3280P, osmotic pump connect, 28 gauge, Plastics One, Inc., Roanoke, VA) that was positioned stereotaxically into the 4th ventricle (coordinates on the midline: -2.5 mm posterior to Lambda, 7 mm ventral to the dura). The animal was deeply anesthetized with isofurane for the duration of surgery. Post-operative care included a local antibiotic applied to the exposed skull and scalp (1% chloramphenicol), a long-acting topical anesthetic applied locally to the scalp (Bupivacaine), and 4 ml of sterile isotonic saline injected s.c. to prevent dehydration. During recovery, body weight and general behavior were monitored and at the end of the 4 weeks of LPS administration, rats were anestethized and perfused with paraformaldehyde (see below) to collect the brain for immunohistochemical analyses.

3.3 Fluorescent immunohistochemistry

Rats, deeply anesthetized with Zoletil, were perfused transcardially with ice-caged paraformaldehyde (500 ml of 4% solution in phosphate-buffered saline, PBS, pH 7.4). The brains were collected, postfixed for 4 h in 4% paraformaldehyde and then cryoprotected for 48-72 h in 18% sucrose/PBS solution. Coronal sections (40 µm) were cut with a cryostat, placed in 1 ml of anti-freeze solution and stored at -20 °C until use (Cerbai et al. 2012, Lana et al., 2016). Immunostaining was performed on coronal sections with the free-floating method (Giovannini, 2002; Lana et al., 2016).

The primary and secondary antibodies used for the immunohistochemical and Western Blot analyses are shown in Table 3.

Table 3: Antibodies used for immunohistochemistry and Western Blot.

Target	Antigen	Supplier	Catalog #	Antibody	Host	Usage	Conc
IMMNOHISTOCHEMISTRY							
Neurons	NeuN	Millipore	MAB377	Monoclonal	Ms	Primary	1:200
Neurons	NeuN	Millipore	MAB377X	Monoclonal conj	Ms	Primary	1:200
Neurons	MAP2	Chemicon	AB5622	Polyclonal	Rb	Primary	1:300
Astrocytes	GFAP	Dako	Z0334	Policlonal	Rb	Primary	1:500
Astrocytes (triple labelling IHC)	GFAP	Millipore	MAB3402X	Monoclonal	Ms	Primary	1:500
Astrocytes	S100 beta	Abcam	14849	Monoclonal	Ms	Primary	1:300
Total microglia	IBA1	Wako	016-20001	Policlonal	Rb	Primary	1:300
Activated microglia	OX6	BD	554926	Monoclonal	Ms	Primary	1:200
Cytocrome C	CytC	BD	556432	Monoclonal	Ms	Primary	1:200
CX3CL1	CX3CL1	Abcam	AB-25088	Polyclonal	Rb	Primary	1:400
Rabbit FC	Rabbit FC	Life Technologies	A21206	Polyclonal	Dn	Secondary Alexa Fluor 488	1:400
Mouse FC (triple labelling IHC)	Mouse FC	Life Technologies	A31570	Polyclonal	Dn	Secondary Alexa Fluor 555	1:400
Rabbit FC	Rabbit FC	Life Technologies	A31577	Polyclonal	Gt	Secondary Alexa Fluor 635	1:400
WESTERN BLOT							
CX3CL1	CX3CL1	Abcam	AB25088	Polyclonal	Rb	Primary	1:300
Actin	Actin	Sigma	A-2066	Polyclonal	Rb	Primary	1:10000

Day 1: primary antibodies

Selected brain sections containing the dorsal hippocampi were placed in multiwells with 1 ml of PBS-TX. Sections were rinsed 3 times for 5 min with 500 µl PBS-TX under slight agitation at room temperature (RT), blocked with 500 µl BB (10% Normal Goat Serum, 10% Normal Horse Serum, 0.05% NaN_3 in PBS-TX) for 1 h under agitation at RT, and washed 3 times as above. For single immunostaining, sections were incubated overnight (O/N) at 4°C under slight agitation with the primary antibody, dissolved in 250 µl of BB at the appropriate dilution (see Table 1). For double or triple immunostaining, sections were incubated O/N with a solution containing two or three primary antibodies, respectively, diluted in 250 µl of BB at the appropriate concentrations.

Day 2: secondary antibodies

Sections were washed 3 times as above and incubated for 2 h in the dark at RT under slight agitation with the appropriate secondary antibody diluted in 250 µl of BB. For double immunostaining, sections were incubated for 2 h in the dark at RT under slight agitation with a solution containing the appropriate fluorescent secondary antibodies diluted in 250 µl of BB. Sections were then washed as above. For triple immunostaining the sections were incubated for 2 h in the dark at RT under agitation with a fluorophore-conjugated primary antibody, diluted in 250 µl of BB (Table 1). Sections were thoroughly washed with PBS-TX and then with 1 ml of distilled H_2O in the dark, mounted on gelatinized microscopy slides, left to dry and covered in the dark with coverslips with a mounting medium (Vectashield, Hard set mounting medium with DAPI, Vector Laboratories, Burlingame, CA, USA) containing DAPI to counterstain nuclei. Slides were kept in the fridge until microscopy analysis.

Qualitative and quantitative analyses

Confocal scans were taken at 0.3 µm z-step, keeping constant all the parameters (pinhole, contrast and brightness), using a LEICA TCS SP8 confocal laser scanning microscope (Leica Microsystems CMS GmbH, Mannheim, Germany). Voxel size was $6.75x10^{-3}$ μm^3. Images were converted to green, red or blue using Image J (National Institute of Health). Qualitative analyses were performed on 3D renderings obtained using Image J 3D viewer from the stacks of confocal scans. All quantitative analyses, measures and image analysis were performed blind by two researchers with the ImageJ

program (freeware provided by National Institute of Health, http://rsb.info.nih.gov/ij) and the results were averaged.

For quantitative analysis images were acquired at 20x magnification with an Olympus BX63 microscope equipped with an Olympus DP 50 digital camera (Olympus, Milan, Italy). Analyses were carried out blind in the Dentate Gyrus of the hippocampus DG (see Figure 22 Region of Interest, ROI) (Lorente de No, 1934; Li et al., 1994) using Image J. Quantitative analyses were carried out separately in the following subregions *Granular Layer* (GL) and *Polymorphic Layer* (PL). Three coronal sections (spaced by 150 µm, starting at about -2.8 mm from bregma) containing the DG were analyzed.

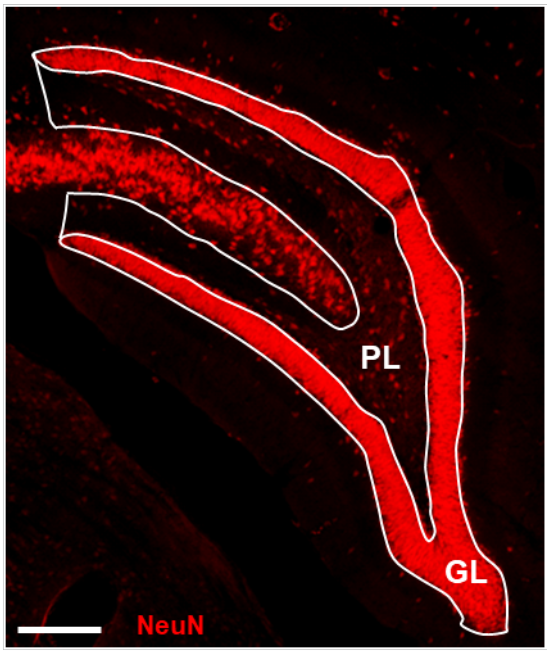

Figure 22. Representative image of the region of interest (ROI) for the analyses of DG. Fluorescent immunostaining of neurons with anti-NeuN antibody showing the DG subregions: Granular Layer (GL) and Polymorphic Layer (PL). Scale bar: 100 µm.

Quantitative analyses of NeuN+ neurons, $GFAP^+$ astrocytes, IBA1+ total microglia, $OX6^+$ activated microglia, CytC+ apoptotic neurons, neuron-astrocyte-microglia triads, were performed separately in GL and PL of the DG. Digitized images, acquired keeping all the parameters (contrast and brightness) constant using a 10x objective, were transformed into TIFF files and threshageded using ImageJ. Care was taken to maintain the same threshaged in all sections from the same experiment. The area above the set threshaged was calculated in pixels. Areas of GL and PL were calculated in mm^2 and the counts of immunopositive cells, or triads were expressed as number/mm^2. Quantitation of DG granular neurons was obtained counting the number of NeuN or MAP2 positive cells in GL. The length of principal astrocyte branches was measured

choosing randomly 4 principal branches (Figure 23) of three GFAP+ astrocytes per ROI and results were averaged. A "triad" was defined as a neuron in direct contact with astrocyte branches of surrounding astrocyte(s) and with a microglia cell (Cerbai et al., 2012; Lana et al., 2016). The reciprocal interplay of the neurons, astrocytes and microglia in the triads was highlighted digitally sub-slicing the triad as previously reported (Cerbai et al., 2012).

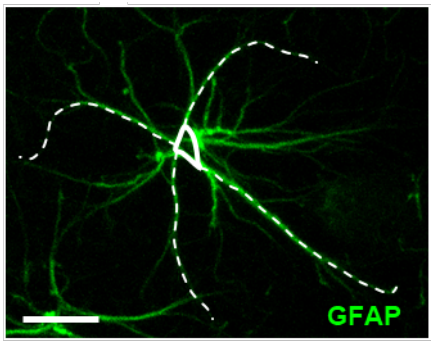

Figure 23. Schematic diagram showing the method used to measure the length of principal GFAP+ astrocytes branches. Scale bar: 10 μm.

A 3D rendering of the sub-slice was obtained using ImageJ 3D viewer. Control immunostaining was performed omitting the primary or secondary antibodies to verify the specificity of the immunostaining.

3.4 Western Blot

Western blot analysis of CX3CL1 was performed as previously described (Cerbai et al., 2012). Hippocampal slices (400 μm-thick), cut using a tissue chopper, were placed in an Eppendorff tube with 100 μl of ice-caged lysis buffer, and were homogenized on ice using a homogenizer directly in the Eppendorf tube (15 strokes, 1 stroke per second, on ice). Composition of the lysis buffer (in mM, unless otherwise indicated): 50 Tris-HCl, pH 7.5, 50 NaCl, 10 EGTA, 5 EDTA, 2 sodium pyrophosphate, 4 para-nitrophenylphosphate, 1 sodium orthovanadate, 1 phenylmethylsulfonyl fluoride (PMSF), 25 sodium fluoride, 2 DTT, 1 μM okadaic acid, 1 μM microcystin L-R, 20 μg/ml leupeptin, and 4 μg/ml aprotinin. After homogenization an additional 2.5 μl of PMSF was added to each tube, and protein determination was performed using Bio-Rad Protein Assay reagent (Bio-Rad, Hercules, CA). An appropriate volume of 6X Loading Buffer was added to the homogenates, samples were boiled for 5 min, immediately put on ice, loaded on a 10% SDS-PAGE gel (30 μg of proteins/well) and run using standard electrophoresis. The gels were transferred electrophoretically by the iBlot dry blotting system (Invitrogen) onto 0.2 mm nitrocellulose membrane, and incubated overnight at

4°C under slight agitation with the primary antibody against CX3CL1 (Table 1) dissolved in blocking solution. The day after, the blots were incubated for 1 hour with HRP-conjugated secondary antibody (1:4000 in blocking solution, Thermo Scientific, Waltham, MA, USA), were visualized with enhanced chemiluminescence (Immobilon Western, Millipore, Billerica, MA, USA), and resolved with ImageQuant 350 system (GE Healthcare, Buckinghamshire, UK). Densitometric band analysis was performed using the Image Quant TL software version 7.0 (GE Healthcare). For quantitative analysis, band density was normalized against βactin, run in the same gel.

Statistical analysis

Statistical analyses were performed using Graph Pad Prism (Graph Pad Software Inc., La Jolla, CA, USA). Unless otherwise stated, all statistical analyses were performed using ANOVA, followed by Newman-Keuls Multiple Comparison Test. Significativity was set at $P<0.05$.

3.5 Statistical analysis

Statistical comparisons were performed using Graph Pad Prism (Graph Pad Software Inc., La Jolla, CA, USA) by one way ANOVA followed by Newman-Keuls multiple comparison test (if more than two groups were compared) significance was set at $P<0.05$.

Part II - Brain Aging and Inflammation

3.6 Animals

Male Wistar rats (3 and 22 months old, Harlan, Milano, Italy) were used. Rats were housed in cages with food and water *ad libitum*, in a temperature-controlled room (23±1°C, 12 h light–12 h dark cycle). Experiments were authorized by the IACUC of the University of Florence and by the Italian Ministry of Health (Italian Law on Animal Welfare, DL 116/92). According to the law, we did all efforts to fulfill the 3Rs requirements. The total number of rats used was: Adult rats, n=6; Aged rats, n=6; LPS-treated rats: n=7.

3.7 LPS treatment

Experiments on LPS-treated rats were performed in the Department of Psychology, The Ohio State University, Columbus, OH 43210, USA, (38, 47, 48) in accordance with the National Institute of Health Guide for the Care and Use of Laboratory Animals (NIH

Publications No. 80-23) revised 1996; formal approval to conduct the experiments was obtained from the Institutional Animal Care and Use Committee (approval number 2008A0028). Male rats (3 months aged) were used. Briefly, LPS or artificial cerebrospinal fluid (aCSF, in mM: 140 NaCl; 3.0 KCl; 2.5 $CaCl_2$; 1.0 $MgCl_2$; 1.2 Na_2HPO_4, pH 7.4) was administered for 4 weeks to adult rats using an Alzet osmotic minipump containing 1.6 µg/ml LPS (Sigma; E. coli, serotype 055:B5, TCA extraction). The minipump was attached to a chronic indwelling cannula (Model 3280P, osmotic pump connect, 28 gauge, Plastics One, Inc., Roanoke, VA) that was positioned stereotaxically into the 4th ventricle (coordinates on the midline: -2.5 mm posterior to Lambda, 7 mm ventral to the dura). The animal was deeply anesthetized with isoflurane for the duration of surgery. Post-operative care included a local antibiotic applied to the exposed skull and scalp (1% chloramphenicol), a long-acting topical anesthetic applied locally to the scalp (Bupivacaine), and 4 ml of sterile isotonic saline injected s.c. to prevent dehydration. During recovery, body weight and general behavior were monitored till the end of the 4 weeks of LPS administration.

Rats of the three animal groups were deeply anesthetized with Zoletil and were perfused transcardially with 200 ml of ice-caged paraformaldehyde solution (4% paraformaldehyde in phosphate-buffered saline, PBS, pH 7.4); subsequently brains were collected for immunohistochemical analyses. After overnight post fixation and cryoprotection (18% sucrose/PBS), 40 µm-thick coronal sections were cut with a cryostat and stored at −20 °C in anti-freeze solution.

3.8 Fluorescent immunohistochemistry

Immunostaining was performed with the free-floating method (Giovannini, 2002; Lana et al., 2014), for details see Part I. The antibodies used are listed in Table 4.

3.9 Confocal imaging

3D confocal stacks (246x246 or 153x153 pixels, pixel size = 153 nm, z-step = 250 nm) were acquired with a 63x (NA 1.40) oil immersion objective on a LEICA TCS SP5 confocal laser scanning microscope (Leica Microsystems CMS GmbH, Mannheim, Germany). Background subtract, and brightness/contrast filtering were applied equally to all parts of each figure by using Fiji software (https://fiji.sc). Three dimensional renderings of fluorescence volumes were obtained by using OsiriX software (www.osirix-viewer.com/). Immunofluorescence signals in each image were visualized

by case specifically assigned color look-up tables (LUTs) in order to emphasize different structures and interactions.

Integrin-β1 is known to be expressed by both microglia and astrocytes (Chen et al., 2017; Barcia et al., 2012). Immunofluorescence of microglial integrin-β1 was isolated by subtracting inverted binary masks of microglia from the integrin-β1 confocal stack.

Table 4: Antibodies used for immunohistochemistry.

Target	Antigen	Supplier	Catalog #	Antibody	Host	Usage	Conc
IMMNOHISTOCHEMISTRY							
Neurons	NeuN	Millipore	MAB377	Monoclonal	Ms	Primary	1:200
Astrocytes	GFAP	Dako	Z0334	Policlonal	Rb	Primary	1:500
Astrocytes (triple labelling IHC)	GFAP	Millipore	MAB3402 X	Monoclonal	Ms	Primary	1:500
Total microglia	IBA1	Wako	016-20001	Policlonal	Rb	Primary	1:300
β1-integrin	β1-integrin	Millipore	Mab2079z	Monoclonal	Ms	Primary	1:100
Rabbit FC	Rabbit FC	Life Technologies	A21206	Polyclonal	Dn	Secondary Alexa Fluor 488	1:400
Mouse FC (triple labelling IHC)	Mouse FC	Life Technologies	A31570	Polyclonal	Dn	Secondary Alexa Fluor 555	1:400
Rabbit FC	Rabbit FC	Life Technologies	A31577	Polyclonal	Gt	Secondary Alexa Fluor 635	1:400

3.10 Quantitative Analyses

Quantitative analyses on immunofluorescence density, and all 3D-particle analyses were performed by using Fiji software. All immunofluorescence analyses were performed in the CA1 region of six coronal hippocampus sections per animal. Ten randomly selected Optical Volumes (153x153x40µm) containing 5-7 microglia cells were analyzed in each section. The parameter "n" reported in all statistical analyses indicates the number of animals analyzed in each animal group. All values are reported as average ± SE.

3.11 Statistical analysis

Statistical comparisons were performed using Graph Pad Prism (Graph Pad Software Inc., La Jolla, CA, USA) by one way ANOVA followed by Newman-Keuls multiple comparison test (if more than two groups were compared) significance was set at $P<0.05$.

Part III – Alzheimer's disease

3.12 TgCRND8 mice

The TgCRND8 (Tg) mice express two mutated human APP genes implicated in AD (Swedish, KM670/672NL and Indiana, V717F) under the regulation of Syrian hamster prion promoter gene (Chishti et al., 2001). The mice were maintained on a hybrid (C57)/(C57/CH3) background by crossing transgenic heterozygous TgCRND8 males with wild-type (WT) female mice.

The main feature of this model is the very rapid development of amyloid deposition in the brain. Mice display amyloid plaques in the cortex and hippocampus already at three months of age (Chishti et al., 2001) since the two mutations involve both the β and γ secretase APP cleavage sites. These neuropathologic manifestations are accompanied by impaired acquisition and learning deficits (Chishti et al., 2001; Bellucci et al., 2006). The transgenic mice were generated and supplied by Dr. P. St George Hyslop (Center for Research in Neurodegenerative Diseases, Toronto, Canada), and the colony was bred in our animal house facility (Ce.S.A.L., Centro Stabulazione Animali da Laboratorio), University of Florence. All animal experiments were performed according to the Italian Law on Animal Welfare (DL 26/2014), approved by the Institutional Animal Care and Use Committee of the University of Florence and by the Italian Ministry of Health. All efforts were made to minimize animal sufferings and to use only the number of animals necessary to produce reliable scientific data. Two groups of transgenic mice were used: 3 months (n=6, equally divided for sex) and 6 months aged (n=6, equally divided for sex). WT mice of 3 and 6 months of age (n = 6, equally divided for sex and age were used); since no significant differences were ever observed in any of the parameters investigated, the data from the two groups were averaged and used as controls.

At the appropriate ages (3 and 6 months), mice were deeply anesthetized with Zoletil (80 mg/kg i.p.) and were perfused transcardially with 200 ml of ice-caged paraformaldehyde solution (4% paraformaldehyde in phosphate-buffered saline, PBS, pH 7.4). After overnight post fixation and cryoprotection (18% sucrose/PBS), 40 μm-thick coronal sections were cut with a cryostat and stored at −20 °C in anti-freeze solution until immunohistochemistry.

3.13 Fluorescent immunohistochemistry

Immunostaining was performed with the free-floating method (Giovannini, 2002; Lana et al., 2014), for details see Part I. The following antibodies were used:

Table 5: Antibodies used for immunohistochemistry.

Target	Antigen	Supplier	Catalog #	Antibody	Host	Usage	Conc
IMMNOHISTOCHEMISTRY							
β amyloid 1-42	Aβ 1-42	Cell Signaling	8243P	Polyclonal	Rb	Primary	1:150
β amyloid 1-16	Aβ 1-16	Covance	SIG-39320	Monoclonal	Ms	Primary	1:400
Neurons	NeuN	Millipore	MAB377	Monoclonal	Ms	Primary	1:200
Neurons	NeuN	Millipore	MAB377X	Monoclonal conj	Ms	Primary	1:200
Astrocytes	GFAP	Dako	Z0334	Policlonal	Rb	Primary	1:500
Astrocytes (triple labelling IHC)	GFAP	Millipore	MAB3402X	Monoclonal	Ms	Primary	1:500
Total microglia	IBA1	Wako	016-20001	Policlonal	Rb	Primary	1:300
Reactive microglia	CD68	Abcam	AB-955	Monoclonal	Ms	Primary	1:100
Cytocrome C	CytC	BD	556432	Monoclonal	Ms	Primary	1:200
TNFα	TNFα	Thermo-Fisher	PA-19810	Polyclonal	Rb	Primary	1:500
Inducible Nitric Oxide Sintase	iNOS	Thermo-Fisher	PA3-030A	Polyclonal	Rb	Primary	1:150
Interleukin-1β	IL-1β	Abcam	Ab-9722	Polyclonal	Rb	Primary	1:100
Rabbit FC	Rabbit FC	Life Technologies	A21206	Polyclonal	Dn	Secondary Alexa Fluor 488	1:400
Mouse FC (triple labelling IHC)	Mouse FC	Life Technologies	A31570	Polyclonal	Dn	Secondary Alexa Fluor 555	1:400
Rabbit FC	Rabbit FC	Life Technologies	A31577	Polyclonal	Gt	Secondary Alexa Fluor 635	1:400

3.14 Microscopy techniques and quantitative analysis

Epifluorescence and confocal microscopy acquisitions were performed in the Regions Of Interest (ROIs, SP and SR of CA1 and CA3 dorsal hippocampus, separately) to acquire immunofluorescence signals. The ROIs were the proximal region for CA1 as defined by Masurkar (2018) and area CA3 as defined by Lorente de Nó (1934), Li et al. (1994) and Amaral and Lavenex (2007).

The epifluorescence microscopy images were obtained with an Olympus BX63 microscope equipped with a Metal Halide Lamp (Prior Scientific Instruments Ltd, Cambridge, UK) and a digital camera Olympus XM 10 (Olympus, Milan, Italy).

The confocal microscopy images were obtained with a LEICA TCS SP5 confocal laser scanning microscope (Leica Microsystems CMS GmbH, Mannheim, Germany. The parameters of acquisition were maintained constant: frame dimension 1240x1240 points, frequency of acquisition 200Hz.

Two experimenters performed all quantitative analyses blind, and data were averaged. All evaluations of cell density were made on z projections of 10 consecutive confocal scans (total thickness 15 µm). Cells were counted, and the area of analysis was measured. Cells were expressed as density (number/mm^2).

We performed the following quantitative analyses using ImageJ software (National Institute of Health, http://rsb.info.nih.gov/ij) separately in the SP and SR of CA1 and CA3.

Density of cells (neurons, astrocytes, microglial cells, TNFα, iNOS and IL1β positive cells) was calculated as cells/mm^2 in SP and SR of CA1 and CA3, on confocal z projections of 5 scans (total 7.5 µm inside the section).

Aβ load was calculated as total plaque density in SP or SR of CA1 and CA3 (plaques/mm^2). Plaques were further subdivided by size into Small (S, below 2500 $µm^3$), Medium (M, between 2500 and 7000 $µm^3$), and large (L, over 7000 $µm^3$) and counted in SP or SR of CA1 and CA3.

For the evaluation of the volume of pyramidal neurons, we considered the neuron as a spheroid. We measured the x and y axes of five neurons chosen randomly in three different confocal planes equally spaced in the depth of the sections (total 30 cells/animal in CA1 and CA3, separately). The volumes of the cells were calculated, and data were averaged.

For the evaluation of the thickness of CA1 and CA3 SP layers, the cell layer was measured at three fixed, equidistant locations taken in three different confocal planes equally spaced in the depth of the sections (total 9 measures in CA1 and CA3, separately), and data were averaged.

For the evaluation of the density of apoptotic neurons in CA1 and CA3 SP, every neuron (identified by NeuN immunostaining) with a diffuse and intense CytC cytoplasmatic immunostaining was considered "apoptotic" (Suen et al., 2008).

For the evaluation of the length of astrocytes branches, the length of three principal branches of five astrocytes randomly chosen was measured in three different confocal planes, equally spaced in the depth of the sections (total 30 cells/animal in CA1 and CA3, separately), and data were averaged.

For the evaluation of the expression of GFAP and TNFα immunofluorescence, the following protocol was used: a z-projection of 10 consecutive confocal z-scansions was done (total thickness 15 µm). Selecting an appropriate threshaged of intensity of GFAP and TNFα immunofluorescence, z-projection was converted in a black and white image using Image J (care was taken to maintain a fixed threshaged value among sections). Black and white pixels are points of fluorescence intensity above or under the selected threshaged, respectively. The ratio between the number of black pixels and the area of analysis (mm^2) in each section was calculated, taken as quantitative expression of GFAP and TNFα immunofluorescence, and reported on graphs.

For the evaluation of the volume of reactive microglia, we considered the body of CD68+ microglia as a spheroid. We measured the x and y axes of 30 reactive microglia cells/animal chosen randomly in a z-projection of 10 consecutive confocal z-scans (total thickness 15 µm). The volumes of the cells were calculated, and data were averaged. Spatial orientation of IBA1+ microglia towards plaques was calculated counting the microglial cells with soma contacting the surface of Large plaque plus those with their soma located within 10 µm around Large plaques, as percent of total microglia cells in the ROIs.

For the evaluation of the density of the neuron-astrocyte-microglia triads, we defined "triads" any cluster of cells in which a neuron is in direct contact with a microglial cell (undergoing phagocytosis) and one (or more than one) astrocytes take contact with the neuronal body with their branches, frequently forming a scar around it. The evaluation was made on a z projection of 10 consecutive confocal z scans (total thickness 15 µm).

3.15 Statistical analysis

Statistical comparisons were performed using Graph Pad Prism (Graph Pad Software Inc., La Jolla, CA, USA) by Student's t test, one way ANOVA followed by Newman-Keuls multiple comparison test (if more than two groups were compared), two-way ANOVA and three-way ANOVA followed by Bonferroni post test, or linear regression analysis, as appropriate. Significance was set at $P<0.05$.

IN VIVO AND *IN VITRO* MODELS OF BRAIN ISCHEMIA

Part IV – In vivo model of ischemia

3.16 Animals

Male adult Wistar rats (3 months old, Harlan, Milano, Italy) were used. The animals were housed in cages with *ad libitum* food and water and were maintained on a 12 h light–12 h dark cycle in a temperature-controlled room (23±1°C). Experiments were approved by the IACUC of the University of Florence and performed according to the Italian Law on Animal Welfare (DL 116/92, Italian Directive on the protection of animals used for scientific purposes). All efforts were made to minimize animal sufferings and to use only the number of animals necessary to produce reliable scientific data.

3.17 Surgery

Bilateral common carotid artery occlusion (two-vessel occlusion, 2VO) was carried out in rats (Sarti et al., 2002a, b; Farkas et al., 2007) according to the scheme represented in Figure 1A, according to the method previously published (Lana et al., 2014). Briefly, rats were anesthesed with halothane and the ***right*** common carotid artery was occluded, (day -7, Figure 1A), as follows. After exposure, the common carotid artery was exposed and firmly ligated with a silk suture. After one week (day 0, Figure 24), the ***left*** common carotid artery was occluded using the same procedure. Diaminocillin (1,200,000 U in 8 ml saline, 1 ml/day i.m.) was administered after each procedure. Sham rats underwent the same surgical procedures, but the arteries were not occluded. Animals were randomly allocated in 3 experimental groups: sham-operated rats (sham, n=15), 2VO-operated rats treated with vehicle (2VO-vehicle, n=15), and 2VO-operated rats treated with dipyridamole (2VO-dipyridamole, n=15) from day 0 to day 7. We did not include the sham-dipyridamole-treated animals group in the project because we wanted to verify the effect of the drug in 2VO treated rats. Ninety days after surgery, anesthetized rats were perfused transcardially with 500 ml of ice-caged paraformaldehyde (4% in phosphate-buffered saline, PBS, pH 7.4). After overnight postfixation and cryoprotection (18% sucrose/PBS) 40 µm thick coronal sections were cut with a cryostat and stored at -20 °C in anti-freeze solution until immunohistochemistry.

3.18 Drug administration

Dipyridamole (Persantin, Boehringer Ingelheim, 5 mg/mL) or vehicle were administered into the jugular vein (10 µL/h per 7 days) using a miniosmotic pump (Model 2001, Alzet, Cupertino, CA, USA) according to Lana et al. (2014). The pumps were implanted subcutaneously in the thoraco-lumbar region immediately after the left common carotid artery occlusion and removed after 7 days (Figure 24).

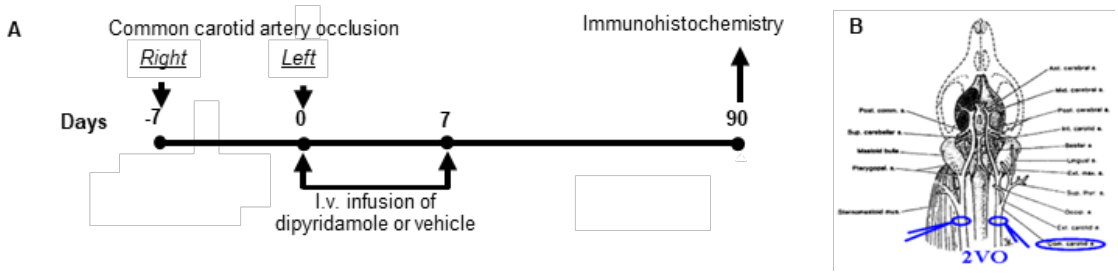

Figure 24. A: Experimental scheme that shows the time course of brain common carotid artery occlusion (two-vessel occlusion, 2VO), dipyridamole infusion and hippocampal samples collection. B: Schematic representation of the rat brain blood vessels, and the site of two-vessel occlusion.

Each animal received about 4 mg/kg/day of dipyridamole which gave an estimated dipyridamole plasma concentration of 2–2.5 µM plasma concentration over the entire week, close to the therapeutic concentration (1.6 µ g/mL) reached after extended-release dipyridamole administered to ischemic stroke patients (Serebruany et al., 2009).

3.19 Fluorescent immunohistochemistry

Immunostaining was performed with the free-floating method (Giovannini, 2002; Lana et al., 2014), for details see Part I. The antibodies used are listed in Table 6.

Table 6: Antibodies used for immunohistochemistry.

Target	Antigen	Supplier	Catalog #	Antibody	Host	Usage	Conc
IMMNOHISTOCHEMISTRY							
Neurons	NeuN	Millipore	MAB377	Monoclonal	Ms	Primary	1:200
Neurons	NeuN	Millipore	MAB377X	Monoclonal conj	Ms	Primary	1:200
CA3 Interneurons	Calretinin	Millipore	AB-5054	Policlonal	Rb	Primary	1:200
Dendrites	Neurofilament	Cell Signaling Technology	2838	Monoclonal	Ms	Primary	1:100
Astrocytes	GFAP	Dako	Z0334	Policlonal	Rb	Primary	1:500
Astrocytes (triple labelling IHC)	GFAP	Millipore	MAB3402X	Monoclonal	Ms	Primary	1:500

Target	Antigen	Supplier	Catalog #	Antibody	Host	Usage	Conc
Total microglia	IBA1	Wako	016-20001	Policlonal	Rb	Primary	1:300
Cytocrome C	CytC	BD	556432	Monoclonal	Ms	Primary	1:200
TNFα	TNFα	Thermo-Fisher	PA-19810	Polyclonal	Rb	Primary	1:500
Rabbit FC	Rabbit FC	Life Technologies	A21206	Polyclonal	Dn	Secondary Alexa Fluor 488	1:400
Mouse FC (triple labelling IHC)	Mouse FC	Life Technologies	A31570	Polyclonal	Dn	Secondary Alexa Fluor 555	1:400
Rabbit FC	Rabbit FC	Life Technologies	A31577	Polyclonal	Gt	Secondary Alexa Fluor 635	1:400

3.20 Methodological considerations

All confocal qualitative double or triple immunostaining analyses were performed in 2VO-vehicle, 2VO-dipyridamole and sham rats. All analyses were performed in Area CA3 of the hippocampus (Lorente de No, 1934; Li et al., 1994), defined Region of Interest (ROI, Figure 1B), further subdivided into the subregions stratum pyramidale (SP), Stratum Lucidum (SL), and Stratum Radiatum (SR) as shown in Figure 1B1 (Amaral & Lavenex, 2007; Lana et al., 2016). Quantification analyses were performed in SP, SL and SR (Figure 25) by two researchers blind to the experimental conditions and results were averaged.

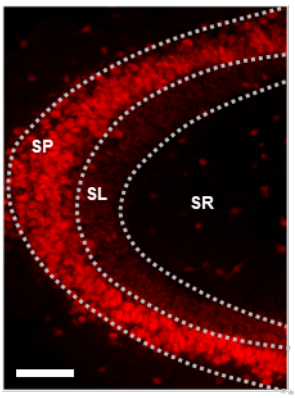

Figure 25. Representative image of CA3 using the immunostaining of neurons with anti-NeuN antibody showing the regions of interest (ROIs): Stratum Pyramidale (SP), Stratum Lucidum (SL) and Stratum Radiatum (SR). Scale bar: 100 µm.

Three coronal sections (spaced by 150 µm, starting at about -2.8 mm from bregma) containing the ROI were immunostained. Since differences were never found between the two hippocampi (Sarti et al., 2002b; Lana et al., 2014) the regions of interest (ROI) of both CA3 areas, containing SP, SL and SR were used. Areas of SP, SL and SR were

measured in mm^2. Astrocytes, microglia, ectopic neurons, neuronal debris and the neurons-astrocytes-microglia triads in CA3 SL and SR, and apoptotic neurons in CA3 SP were consistently counted in the same area in all sections and were expressed as cells/mm^2. CA3 pyramidal neurons were quantified counting NeuN+ cells in SP. Neuronal debris, defined as NeuN+ fragments with dimensions between 2.5 µm and 6.5 µm, were counted in the central z-scans (15 µm total thickness) of confocal microscopy images to make sure that we were not capturing ends of whole cells. The length of principal astrocyte branches was measured using Image J. Two independent experimenters measured 4 principal branches of three astrocytes chosen randomly in the ROIs, and results were averaged. The length of TNFα+ dendrites (3 dendrites chosen randomly in 4 quadrants of a 20x image taken in CA3 SR) was measured using Image J by two independent experimenters and results were averaged. Since IBA1 labels not only microglia, but also monocytes and macrophages, care was taken to avoid the quantification of IBA1+ cells located inside blood vessels. A "triad" was defined as a neuron in direct contact with a microglia cell and astrocyte branches deriving from surrounding astrocyte(s) (Cerbai et al., 2012; Lana et al., 2016). To visualize the ''top-down view'' and the ''bottom-up view'' of the triad, the 3D rendering was digitally rotated by 180°. The reciprocal interaction of the three cells in the triad was visualized by stacking few consecutive confocal z-scans acquired in the depth of the neuronal cell body and digitally ''sub-slicing'' the neuron. The 3D rendering image was obtained using ImageJ 3D viewer. Control immunostaining, to verify the specificity of the antibodies, was performed omitting the primary or secondary antibodies.

3.21 Statistical analysis

Statistical comparisons were performed using Graph Pad Prism (Graph Pad Software Inc., La Jolla, CA, USA) by one way ANOVA followed by Newman-Keuls Multiple Comparison Test, two way ANOVA followed by Bonferroni multiple comparison test, or two tailed Student's t test, as appropriate. Significance was set at $P<0.05$.

Part V - In vitro model of ischemia

3.22 Animals

All animal experiments were performed according to the Italian Law on Animal Welfare (DL 26/2014), approved by the Institutional Animal Care and Use Committee of the University of Florence and by the Italian Ministry of Health. All efforts were made to minimize animal sufferings and to use only the number of animals necessary to produce reliable scientific data. Male Wistar rats (Envigo, Italy, 150–200 g body weight) were used. Experiments were carried out on acute rat hippocampal slices, prepared as previously described (Pugliese et al., 2006, 2009).

3.23 Preparation of slices

Animals were killed with a guillotine under anesthesia with isoflurane (Baxter, Rome, Italy) and hippocampi were rapidly removed and placed in ice-caged oxygenated (95% O_2-5% CO_2) artificial cerebrospinal fluid (aCSF) of the following composition (mM): NaCl 124, KCl 3.33, KH_2PO_4 1.25, $MgSO_4$ 1.4, $CaCl_2$ 2.5, $NaHCO_3$ 25 and D-glucose 10. Slices (400 μm nominal thickness) were cut using a McIlwain tissue chopper (Mickle Laboratory Engineering, Co. Ltd., Gomshall, UK) and kept in oxygenated aCSF for at least 1 h at room temperature. A single slice was then placed on a nylon mesh, completely submerged in a small chamber (0.8 ml) and superfused with oxygenated aCSF (31-32°C) at a constant flow rate of 1.5 ml/min. The treated solutions reached the preparation in 60 s and this delay was taken into account in our calculations.

3.24 Extracellular recordings

Test pulses (80 μs, 0.066 Hz) were delivered through a bipolar nichrome electrode positioned in the Stratum Radiatum of the CA1 region of the hippocampus to stimulate the Schaffer collateral-commissural pathway (Figure 26). Evoked potentials were extracellularly recorded with glass microelectrodes (2-10 MΩ, Harvard Apparatus LTD, UK) filled with 150 mM NaCl. The recording electrode was placed at the dendritic level of the CA1 region to record field excitatory postsynaptic potentials (fEPSPs) (Figure 26).

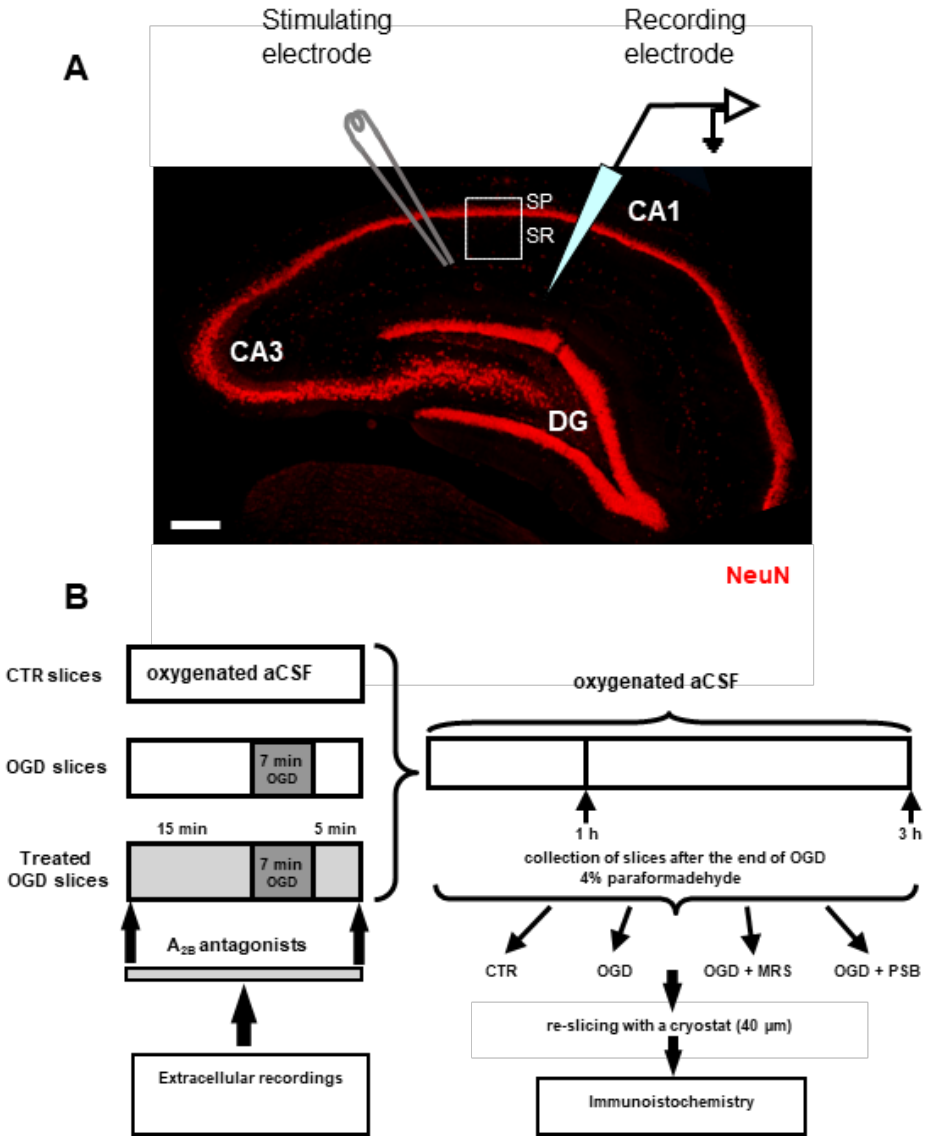

Figure 26. Experimental methods. **A**: Microphotography of a hippocampal slice showing the three subregions, the localization of the stimulating and recording electrodes and the region of interest in CA1 (ROI, framed area) used for the immunohistochemical analyses. SP: stratum pyramidale; SR: stratum radiatum. Scale bar: 200 µm. **B**: Schematic representation of the experimental method for *in vitro* OGD and collection of the slices.

Responses were amplified (200×, BM 622, Mangoni, Pisa, Italy), digitized (sample rate, 33.33 kHz), and stored for later analysis with LTP (version 2.30D) program (Anderson and Collingridge, 2001). The amplitude of fEPSP was measured as the difference between the negative peak following the afferent fiber volley and the baseline value preceding the stimulus artefact. In some experiments both the amplitude and the initial slope of fEPSP were quantified, but since no appreciable difference between these two parameters was observed under control conditions, in the presence of drugs or during *in vitro* ischemia, only the measure of the amplitude was expressed in the figures. When a

stable baseline of evoked responses was reached, fEPSP amplitudes were routinely measured and expressed as the percentage of the mean value recorded 5 min before the application of any treatment (in particular pre-OGD). Stimulus-response curves were obtained by gradual increase in stimulus strength at the beginning of each experiment. The test stimulus strength was then adjusted to produce a response whose amplitude was 40% of the maximum and was kept constant throughout the experiment. Simultaneously, with fEPSP amplitude, AD was recorded as negative extracellular direct current (d.c.) shifts induced by OGD. The d.c. potential is an extracellular recording considered to provide an index of the polarization of cells surrounding the tip of the glass electrode (Farkas et al., 2008). AD latency, expressed in min, was calculated from the beginning of OGD; AD amplitude, expressed in mV, was calculated at the maximal negativity peak. In the text and bar graphs, AD amplitude values were expressed as positive values. The terms “irreversible synaptic failure” or “irreversible loss of synaptic transmission” used in the present work refer to the maximal time window of cell viability in our experimental model (acutely isolated hippocampal slice preparation) which, according to our previous results is 24 h (Pugliese et al., 2009).

3.25 Drugs

Two selective adenosine A_{2B} receptors antagonists, N-(4-Cyanophenyl)-2-[4-(2,3,6,7-tetrahydro-2,6-dioxo-1,3-dipropyl-1H-purin-8-yl)phenoxy]-acetamide) (*MRS1754)* and 8-[4-[4-(4-Chlorophenzyl) piperazide-1-sulfonyl) phenyl]]-1-propylxanthine (*PSB603)* were used. D-2-amino-5-phosphonovalerate, a selective NMDA receptor antagonist was used. All these compounds were purchased from Tocris (Bristol, UK). The A_1 receptor antagonist DPCPX (8-cyclopentyl-1,3-dipropylxanthine) was purchased from SIGMA Aldrich (https://www.sigmaaldrich.com).

All drugs were dissolved in dimethyl sulphoxide (DMSO). Stock solutions, of 1000–10,000 times the desired final concentration, were stored at -20 C. The final concentration of DMSO (0.05% and 0.1% in aCSF) used in our experiments did not affect either fEPSP amplitude or the depression of synaptic potentials induced by OGD (data not shown).

3.26 Application of OGD and adenosine A_{2B} receptor antagonists

The experimental method is shown in Figure 1B. Conditions of OGD were obtained by superfusing the slice with aCSF without glucose and gassed with nitroen (95% N_2-5% CO_2) (Pedata et al., 1993). This causes a drop in pO_2 in the recording chamber from

~500 mmHg (normoxia) to a range of 35-75 mmHg (after 7 min OGD) (Pugliese et al., 2007, 2009). At the end of the ischemic period, the slice was again superfused with normal, glucose-containing, oxygenated aCSF. The terms 'OGD slices' or 'treated OGD slices' refer to hippocampal slices in which OGD was applied in the absence or in the presence of A_{2B} receptor antagonists, respectively. Control slices were not subjected to OGD or treatment with A2B receptor antagonists but were incubated in oxygenated aCSF for identical time intervals. All the selective adenosine A_{2B} receptors antagonists were applied 15 min before, during and 5 min after OGD. In a typical experimental day, first a control slice was subjected to 7 min of OGD. If the recovery of fEPSP amplitude after 60 min of reperfusion with glucose containing and normally oxygenated aCSF was ≤15% of the pre-OGD value, and AD developed into 7 min OGD, a second slice from the same rat was subjected to an OGD insult in the presence of the A_{2B} receptor antagonist under investigation. To confirm the result obtained in the treated group, a third slice was taken from the same rat and another 7 min OGD was performed under control conditions to verify that no difference between slices was caused by the time gap between the experiments. In some slices the OGD period was prolonged to 30 min and the A_{2B} receptor antagonists were applied 15 min before and during OGD application. After the extracellular recordings, slices were maintained in separate chambers for 1 or 3 hours from the end of OGD in oxygenated aCSF at room temperature (RT). At the end, slices were harvested and fixed overnight at 4°C in 4% paraformaldehyde in PBS, cryopreserved in 18% sucrose for 48 h, and resliced as written below.

3.27 Treatment of hippocampal slices with glutamate in vitro

Experiments were carried out on acute hippocampal slices, prepared from male Wistar rats as described above. The A_{2B} receptor antagonists were dissolved in DMSO to obtain a stock solution suitable for a 1:2000 dilution. Slices, maintained oxygenated throughout the procedure, were incubated according to the following scheme:

1) Control slices were incubated for 1 h in aCSF and then for 25 min in aCSF with DMSO (1:2000; 0.05%);

2) Glutamate (GLU) treated slices were incubated 1 h in aCSF and then for 10 min with 100 µM glutamate in aCSF;

3) MRS+GLU treated slices were incubated for 1 h in aCSF, then for 15 min with 500 nM MRS1754 and for further 10 min with 500 nM MRS1754 plus 100 µM glutamate, in aCSF;

4) PSB+GLU treated slices were incubated for 1 h in aCSF, then for 15 min with 50 nM PSB603, and for further 15 min with 50 nM PSB603 plus 100 µM glutamate in aCSF;

After the incubation with glutamate and A_{2B} receptor antagonists, slices were further incubated for 3 h in aCSF, and then harvested and fixed overnight at 4°C in 4% paraformaldehyde in PBS, cryopreserved in 18% sucrose for 48 h, and resliced as written below.

3.28 Fluorescent immunohistochemistry

One hour or 3 h after OGD, or after the incubation with glutamate and A_{2B} receptor antagonists, the 400 µm thick slices fixed in paraformaldehyde were placed on an agar support (6% agar in normal saline), included in an embedding matrix and re-sliced with a cryostat to obtain 40 µm thick slices. The more superficial sections were eliminated, while those obtained from the inner part of the slice were collected and stored in vials with 1 ml of antifreezing solution at -20°C until immunohistochemical analyses. From the 400 µm thick slices on average only a maximum of 2-3 complete 40 µm thick slices were obtained, which were then randomly allocated to the fluorescent immunohistochemical staining groups. Immunostaining was performed with the free-floating method (Giovannini, 2002; Lana et al., 2014), for details see Part I. The following antibodies were used:

Table 7: Antibodies used for immunohistochemistry

Target	**Antigen**	**Supplier**	**Catalog #**	**Antibody**	**Host**	**Usage**	**Conc**
IMMNOHISTOCHEMISTRY							
Neurons	NeuN	Millipore	MAB377	Monoclonal	Ms	Primary	1:200
Neurons	NeuN	Millipore	MAB377X	Monoclonal conj	Ms	Primary	1:200
Astrocytes	GFAP	Dako	Z0334	Policlonal	Rb	Primary	1:500
Cytocrome C	CytC	BD	556432	Monoclonal	Ms	Primary	1:200
Activated m-TOR	P-mTOR	Abcam	AB-51044	Polyclonal	Rb	Primary	1:100
Rabbit FC	Rabbit FC	Life Technologies	A21206	Polyclonal	Dn	Secondary Alexa Fluor 488	1:400
Mouse FC (triple labelling IHC)	Mouse FC	Life Technologies	A31570	Polyclonal	Dn	Secondary Alexa Fluor 555	1:400
Rabbit FC	Rabbit FC	Life Technologies	A31577	Polyclonal	Gt	Secondary Alexa Fluor 635	1:400

Epifluorescence microscopy: sections were observed under an Olympus BX63 microscope equipped with an Olympus DP 50 digital camera (Olympus, Milan, Italy). For quantitative analysis images were acquired at 20x magnification with the digital camera.

Confocal microscopy: scans were taken at 0.3 μm z-step, keeping constant all the parameters (pinhole, contrast and brightness), using a LEICA TCS SP5 confocal laser scanning microscope (Leica Microsystems CMS GmbH, Mannheim, Germany). Images were converted to green, or red using Image J (freeware provided by National Institute of Health, (http://rsb.info.nih.gov/ij). The region of interest (ROI) in CA1, containing SP and SR was consistently analyzed in all slices, as shown in Figure 1A (Lana et al., 2014). Quantitative analyses of NeuN+ neurons, HDN neurons, LDN neurons, GFAP+ astrocytes, CytC+ apoptotic neurons and phospho-mTOR+ cell bodies and dendrites were performed blind by two experimenters and results were averaged. Areas were expresses as mm^2. Digitized images were transformed into TIFF files and threshageded using ImageJ. Care was taken to maintain the same threshaged in all sections within the same experiment. In CA1 pyramidal layer, the area labeled above the set threshaged with NeuN or phospho-mTOR was calculated in pixels and expressed as NeuN+ pixels/mm^2 or phospho-mTOR+ pixels/mm^2. HDN neurons, LDN neurons, CytochromeC-positive (CytC+) apoptotic neurons in CA1 SPand $GFAP^+$ astrocytes in CA1 SR were counted and were expressed as number of cells/mm^2. In order to evaluate mTOR activation in basal dendrites the length of phospho-$mTOR^+$ dendrites was measured at 3 fixed locations, equal in all slices and evenly distributed throughout the CA1 SR ROI, and results were averaged.

3.29 Statistical analysis

Statistical significance was evaluated by Student's paired or unpaired *t* tests. Analysis of variance (one-way ANOVA), followed by Newman-Keuls multiple comparison *post hoc* test was used, as appropriate. *P*-values from both Student's paired and unpaired *t* tests are two-tailed. Data were analyzed using software package GraphPad Prism (version 7.0; GraphPad Software, San Diego, CA, USA). All numerical data are expressed as the mean±standard error of the mean (SEM). A value of $P<0.05$ was considered significant.

.

Results

MODELS OF BRAIN AGING, NEUROINFLAMMATION AND ALZHEIMER'S DISEASE

Part I – Brain Aging and Inflammation

4.1 Analysis of neurons in the Dentate Gyrus of Adult, Aged, and LPS-treated rats

To evaluate whether aging or acute inflammation induced by LPS might cause loss of neurons in the dentate gyrus, neurons were immunostained with anti NeuN or MAP2 antibody, and counted separately in the granular layer (GL) and polymorphic layer (PL), as shown in the representative images in Figure 27A-C and 27G-I.

Using the anti NeuN antibody (Figure 27), we found a significant decrease of neurons in GL and PL of aged rats in comparison to adult rats while no effect was found in LPS rats. Statistical analysis showed that in DG of aged rats, neurons decreased by 13% in GL (*P<0.05 aged vs adult, $F_{(2;13)}$=3.874), and by 20% in PL (*P<0.05 aged vs adult, $F_{(2;12)}$=4.212) in comparison to adult rats (Figure 27D-E).

Using anti the anti MAP2 antibody (Figure 27G-I), we confirmed that granular neurons significantly decreased in GL of aged rats (-23% in comparison to adult rats; *P<0.05 aged vs adult, $F_{(2;12)}$=6.483), but not in GL of LPS-treated rats (n.s., Figure 27F).

To define whether the decrease of granular neurons in the dentate gyrus of aged rats might be caused by apoptosis, DG sections were immunostained for CytC, one of the late markers of apoptosis (Suen et al., 2008). CytC is currently being utilized as a marker of apoptosis since it has been demonstrated that, following complete release from the mitochondria at late stages of apoptosis, CytC becomes diffusely and highly visible in the cell cytoplasm (Suen et al., 2008). Figure 27J-L show the immunolabelling of CytC in GL of an adult (J), an aged (K) and an LPS-treated rat (L). The arrows show neurons with increased cytoplasmic immonostaining for CytC.

Quantitative analysis of CytC+ neurons in GL is shown in Figure 27M. Statistical analysis demonstrated that CytC+ neurons were significantly more numerous in GL of aged (+300%) and of LPS treated rats (+108%) than in adult rats (***P<0.001 aged vs adult; *P<0.05 LPS vs adult; $F_{(2;9)}$=40.04).

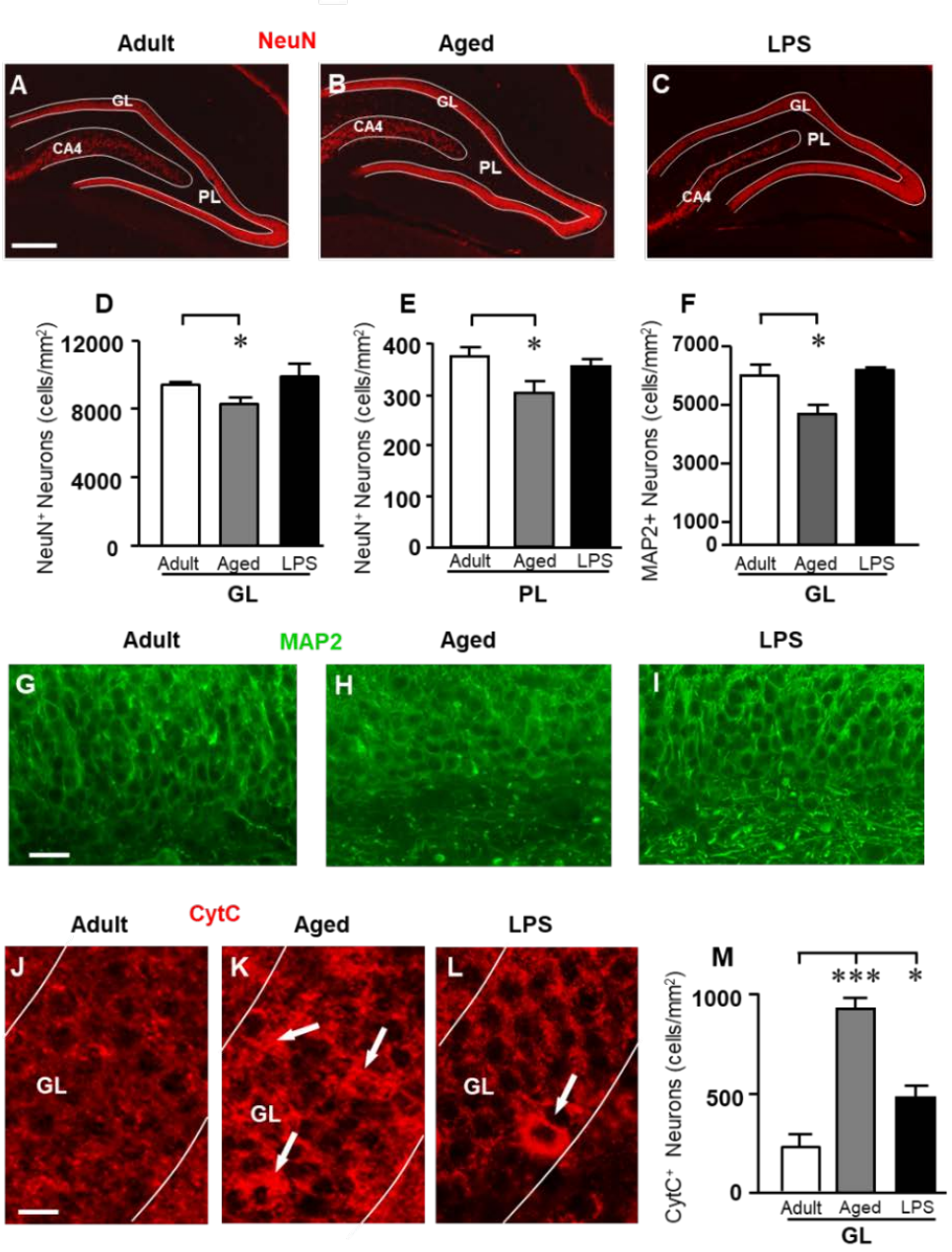

Figure 27. Analysis of neurons in GL and PL of adult, aged and LPS-treated rats. **A-C:** Representative photomicrographs of NeuN immunostaining of neurons (red) in DG of an adult (A), an aged (B) and an LPS-treated rat (C). Scale bar: 200 μm. **D-E:** Quantitative analysis of neurons/mm^2 in Dentate Gyrus GL (D) and PL (E) of adult (n=6), aged (n=5) and LPS-treated rats (n=6). Neurons were significantly less numerous in GL and PL of aged rats. **F:** Quantitative analysis of MAP2 neurons/mm^2 in DG GL of adult (n=6), aged (n=5), and LPS-treated rats (n=4). MAP2+ granular neurons were significantly less numerous in GL of aged rats. **G-I:** Representative photomicrographs of MAP2 immunostaining (green) in the GL of an adult (G), an aged (H) and an LPS-treated rat (I). Scale bar: 25 μm. **J-L:** Representative photomicrographs of CytC immunostaining (red) in the GL of an adult (J), an aged (K) and an LPS-treated rat (L). The arrows in K and L point to apoptotic neurons in GL. Scale bar: 10 μm. **M:** Quantitative analysis of apoptotic neurons/mm^2 in GL of adult (n=4), aged (n=4), and LPS-treated rats (n=4). Apoptotic granular neurons were significantly more numerous in GL of aged and LPS-treated rats. Data reported in all graph bars are expressed as mean±SEM.

4.2 Analysis of astrocytes in the Dentate Gyrus of Adult, Aged, and LPS-treated rats

As shown in the representative images of Figure 28, astrocytes were immunolabelled with anti GFAP antibody (Figure 28A-C1) and anti S100 antibody (Figure 28F-H1), and counted separately in GP and PL of adult, aged and LPS-treated rats. Quantitative analysis of the density of GFAP+ astrocytes, reported in Figure 28D, showed that astrocytes decreased in both GL and PL of aged and LPS-treated rats.

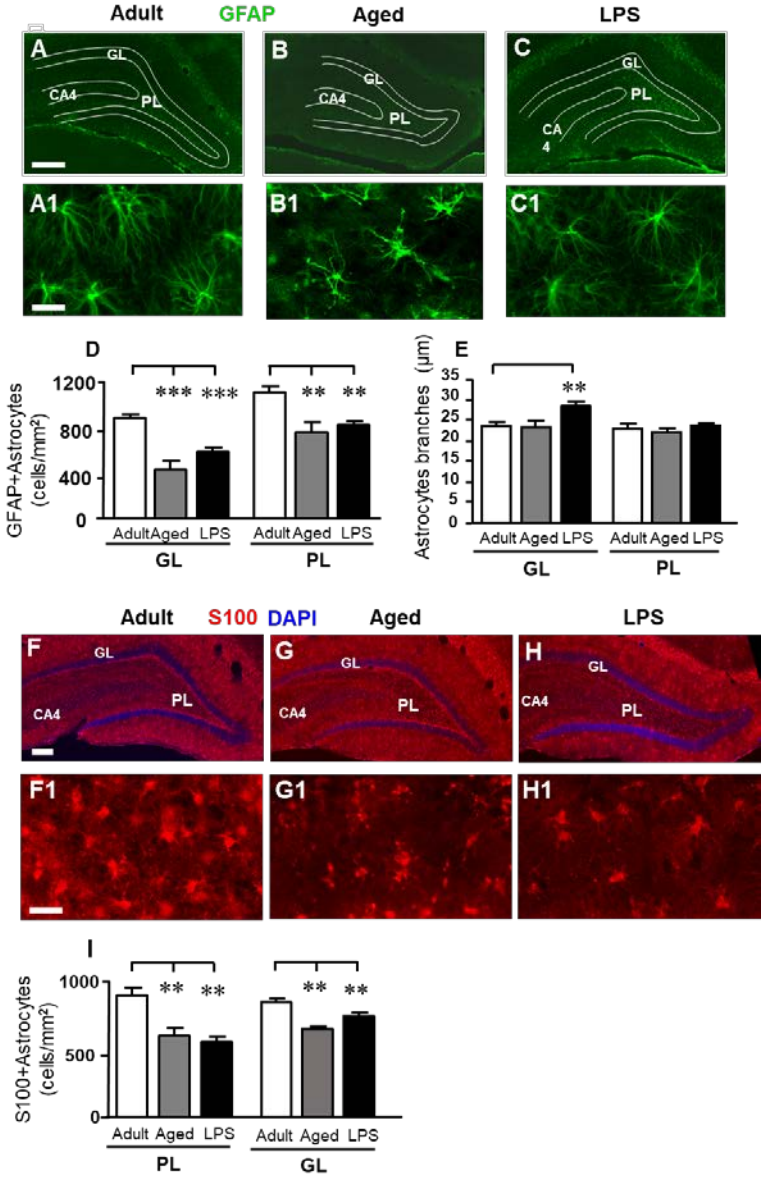

Figure 28. Characterization and quantitative analysis of astrocytes in GL and PL of adult, aged and LPS-treated rats. **A-C:** Representative photomicrographs showing immunoreactivity of GFAP (green) in DG of an adult (A), an aged (B) and an LPS-treated rat (C). Scale bar: 150 µm. **A1-C1:** Magnification of GFAP+ astrocytes in the PL of an adult (A1), an aged (B1) and an LPS-treated rat (C1). Scale bar: 25 µm. **D:** quantitative analysis of GFAP+ astrocytes/mm^2 in hippocampal GL and PL of adult (n=5), aged (n=4) and LPS-treated rats (n=6). GFAP+ astrocytes were significantly less numerous in GL and PL of aged and LPS-treated rats. **E:**

Length of principal astrocyte branches in GL and PL of adult (n=5), aged (n=5), and LPS-treated rats (n=7). GFAP+ astrocytes branches were significantly longer in GL of LPS-treated rats. **F-H:** Representative photomicrographs showing immunoreactivity of S100 (red) in DG of an adult (F), an aged (G) and an LPS-treated rat (H). Nuclei were counterstained with DAPI (blue). Scale bar: 100 μm. **F1-H1:** Magnification of S100+ astrocytes in the PL of an adult (F1), an aged (G1) and an LPS-treated rat (H1). Scale bar: 50 μm. **I:** quantitative analysis of S100-positive astrocytes/mm^2 in hippocampal GL and PL of adult (n=6), aged (n=5) and LPS-treated rats (n=5). S100+ astrocytes were significantly less numerous in GL and PL of aged and LPS-treated rats. Data reported in all graph bars are expressed as mean±SEM.

Statistical analysis demonstrated that GFAP+ astrocytes were significantly less numerous in GL of aged rats (-50%, ***P<0.001 aged vs adult rats, $F_{(2;16)}$=19.67) and in GL of LPS-treated rats (-33%, **P<0.01 LPS vs adult rats, $F_{(2;16)}$=10.43) in comparison to adult rats, respectively (Figure 28D). Similarly, GFAP+ astrocytes were less numerous in PL of aged rats (-31%, **P<0.01 aged vs adult rats, $F_{(2;16)}$=10.43), and in PL of LPS treated rats (-25%, **P<0.01 LPS vs adult rats, $F_{(2;16)}$=10.43) in comparison to adult rats, respectively (Figure 28D). Similar results were obtained immunostaining astrocytes with a different marker, protein S100. The density of S100+ astrocytes was significantly lower in GL of aged (-33%) and of LPS-treated (-39%) rats (*P<0.05 aged vs adult rats, and **P<0.01 LPs vs adult rats; $F_{(2;13)}$=10.04). The significant decrease of S100+ astrocytes was also evident in PL of aged (-26%) and of LPS treated (-14%) rats (***P<0.01 aged vs adult rats, **P<0.01 LPS vs adult rats, $F_{(2;13)}$=18.28) (Figure 28I). Higher magnification GFAP+ astrocytes in PL (Figure 28A1-C1), show that in aged rats the principal branches of astrocytes appeared shorter and twisted, as compared to those of adult and LPS-treated rats. We measured the length of GFAP+ astrocytes branches (see methods, Figure 28C) and the results are shown in Figure 28E. In the GL of LPS-treated rats, the length of astrocytes principal branches was significantly longer (+21%) than in adult rats (**P<0.01 LPS vs adult rats, $F_{(2;16)}$=6.814, Figure 28E). On the contrary, in PL the length of astrocytes branches did not differ significantly among the three experimental groups (Figure 28E). Figure 29A-C shows the confocal 3D rendering of astrocyte branches extending through the GL of an adult (A), an aged (B) and an LPS-treated rat (C). Each image, obtained stacking 17 consecutive confocal z-scans (0.3 μm each, total thickness 5.1 μm) confirms that in LPS-treated rats astrocyte branches were significantly longer than in aged and adult rats.We calculated the ratio between NeuN+ neurons and GFAP+ astrocytes both in GL and PL of adult, aged and LPS-treated rats to verify whether the decrease of GFAP+ astrocytes, paralleled by a decrease of neurons, might mask a possible astrocytosis. The results obtained presented in Figure 29D-E demonstrate that in GL of aged and LPS-treated rats the ratios NeuN+

neurons/GFAP+ astrocytes were significantly higher than in adult rats (+95% and +56%, respectively), and were both statistically significant (*P<0.05 aged vs adult rats, and LPS vs adult rats, $F_{(2;13)}$=4.24). In PL, the ratios NeuN+ neurons/GFAP+ astrocytes were not significantly different in the 3 experimental groups ($F_{(2;14)}$=1.434, n.s.; one-way ANOVA). These data further demonstrate that no astrocytosis was present in GL and PL of aged and LPS-treated rats.

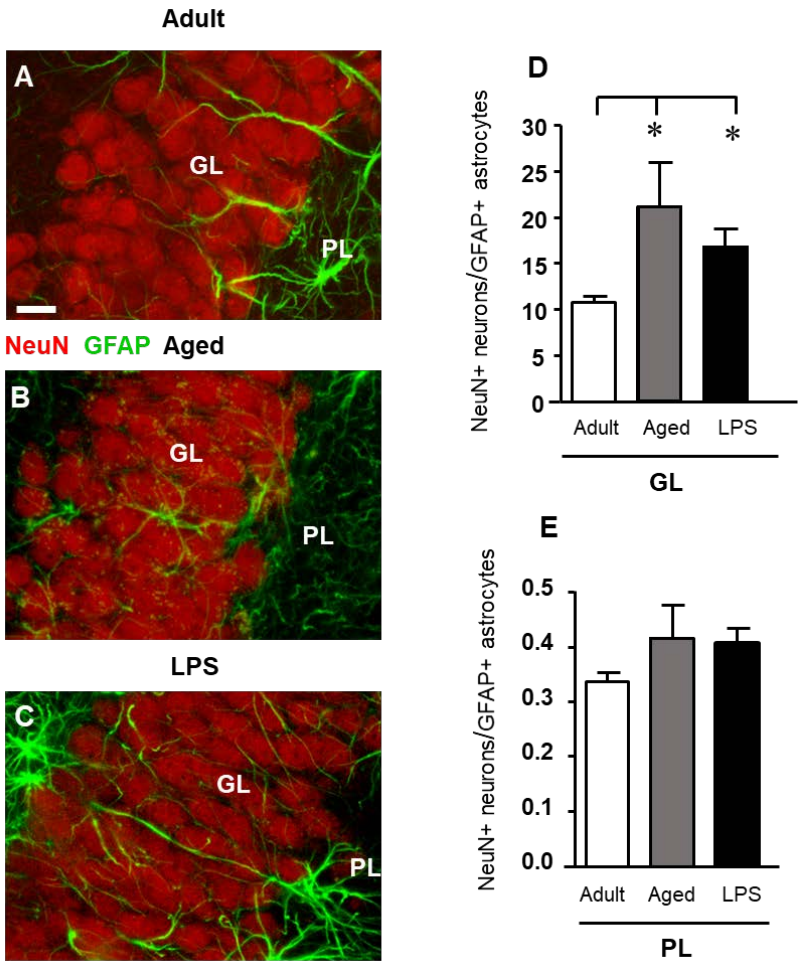

Figure 29. Confocal microscopy 3D renderings of double immunostaining of neurons (NeuN, red), and astrocytes (GFAP, green) in the GL of an adult (A), an aged (B) and of an LPS-treated rat (C). Scale bar:10 µm. **D-E:** Ratios between NeuN+ neurons and GFAP+ astrocytes in GL (D) and PL (E) of adult (n=6), aged (n=5), and LPS-treated (n=6) rats. The ratios NeuN+ neurons/GFAP+ astrocytes increased in GL of aged and LPS-treated rats. Data reported in all graph bars are expressed as mean±SEM.

4.3 Quantification of Total and Activated Microglia in the Dentate Gyrus of Adult, Aged, and LPS-treated rats

Total microglia were identified using the fluorescent immunostaining for IBA1, as shown by the representative images of Figure 30A-C1 (left panels).

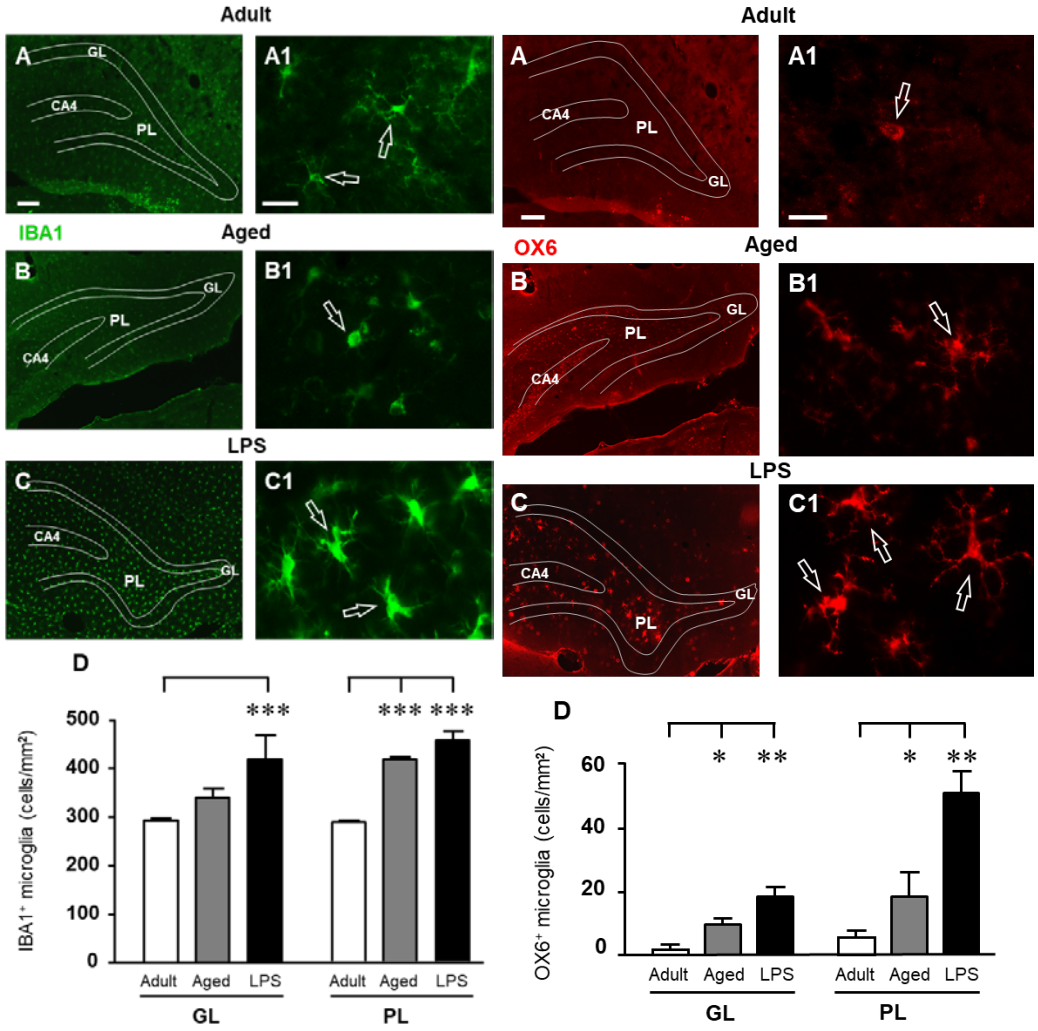

Figure 30. Left panels: Analysis of total microglia in GL and PL of adult, aged and LPS-treated rats. **A-C:** Representative photomicrographs of IBA1 immunostaining of total microglia (green) in DG of an adult (A), an aged (B), and an LPS-treated rat (C). Scale bar: 100 µm. **A1-C1:** Magnification of total microglia in the PL of an adult (A1), an aged (B1), and an LPS-treated rat (C1). Scale bar: 15 µm. **D:** quantitative analysis of IBA1+ microglia/mm^2 in hippocampal GL and PL of adult (n=5), aged (n=5) and LPS-treated rats (n=5). Microglia were significantly more numerous in GL of LPS-treated rats and in PL of aged and LPS-treated rats. Data reported in all graph bars are expressed as mean±SEM.
Right panels: Analysis of OX6+, activated microglia in GL and PL of adult, aged and LPS-treated rats. **A-C:** Representative photomicrographs of OX6 immunostaining of activated microglia (red) in DG of an adult (A), an aged (B) and an LPS-treated rat (C). Scale bar: 100 µm. **A1-C1:** Magnification of activated microglia in PL of an adult (A1), an aged (B1) and an LPS-treated rat (C1). Scale bar: 15 µm. **D:** quantitative analysis of activated microglia/mm^2 in hippocampal GL and PL of adult (n=3), aged (n=5) and LPS-treated rats (n=4). Activated microglia cells were significantly more numerous in GL and PL of aged and LPS-treated rats. Data reported in all graph bars are expressed as mean±SEM.

Quantitative analysis of IBA1+ cells revealed that the density of total microglia significantly increased by 42% in comparison to adult rats in the GL of LPS-treated rats (***P<0.001 LPS vs adult rats, $F_{(2;14)}$=4,22), while the increase found in GL of aged rats (+16% vs adult rats) was not statistically significant. Furthermore, total microglia

significantly increased both in the PL of aged (+44%, ***P<0.001 aged vs adult rats, $F_{(2;14)}$=56.33) and of LPS-treated rats (+58%, ***P<0.001 LPS vs adult rats, $F(_{2;14})$=56.33), in comparison to adult rats (Figure 30D, left panels).

IBA1 immunostained microglia in the DG of aged and LPS-treated rats (Figure 30B1-C1, left panels) had morphological features typical of activated microglia. Indeed, immunostaining with OX-6, a marker of activated microglia, shown in Figure 30A-C1(right panels), indicated that numerous OX6+, activated microglia cells were found in the GL and PL of aged and LPS-treated rats. Magnifications of OX6+, activated, microglia are shown in Figure 30A1-C1 (right panels). Quantitative analysis demonstrated that activated microglia significantly increased both in GL and PL of aged and LPS-treated rats in comparison to adult rats (Figure 30D, right panels). Activated microglia increased by 489% in GL of aged rats (*P<0.05 aged vs adult rats, $F_{(2,11)}$=11.20) and by 2160% in GL of LPS-treated rats (**P<0.01 LPS vs adult rats, $F_{(2,11)}$=11.20). Activated microglia increased by 235% in PL of aged rats (*P<0.05 aged vs adult rats, $F_{(2,9)}$=13.83) and by 829% in PL of LPS-treated rats (**P<0.01 LPS vs adult rats, $F_{(2,9)}$=13.83), in comparison to adult rats (Figure 30D, right panels).

4.4 Quantification of neuron-astrocyte-microglia triads in the PL of the Dentate Gyrus of Adult, Aged, and LPS-treated rats

Triple immunostaining for neurons, GFAP+ astrocytes and microglia was performed in the DG of adult, aged and LPS-treated rats. Representative 3D renderings of triple immunostaining of astrocytes, neurons and microglia (Figure 31) with anti NeuN antibody (red, Figure 31A1-C1), anti GFAP antibody (green, Figure 31 A2-C2), and with anti IBA1 antibody for microglia (blue, Figure 31A3-C3) in the PL of an adult (Figure 31 A-A3), an aged (Figure 31B-B3), and of an LPS-treated rat (Figure 31C-C3) clearly shows that many neuron-astrocytes-microglia triads were found in the PL of aged and of LPS-treated rats (Figure 31B and C, merge). The 3D rendering in Figure 31A (stack of 53 consecutive confocal z-scans, 0.3 µm each, total thickness 15.9 µm), shows that in the PL of an adult rat astrocytes and microglia surrounded a neuron but did not form a triad. The microglia cell had morphological characteristics of a resting microglia, with a small cell body and long, thin branches (Figure 31A3, open arrow). The 3D rendering in Figure 3B (stack of 53 consecutive confocal z-scans, 0.3 µm each, total thickness 15.9 µm) shows that in the PL of an aged rat a damaged neuron was

surrounded by 2 different GFAP+ astrocytes that sent their branches to form a micro scar around the neuron.

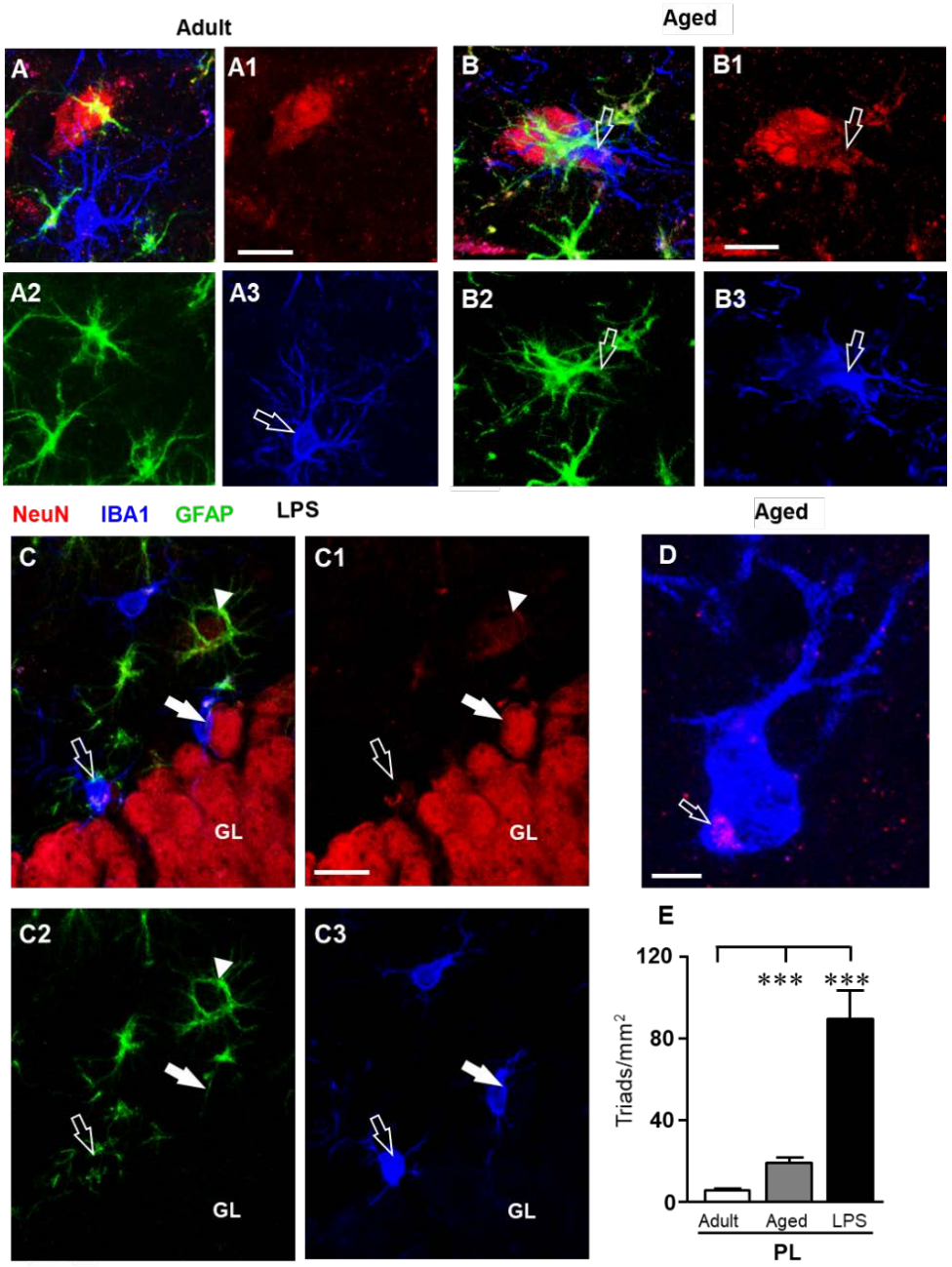

Figure 31. Quantification and characterization of the neuron-astrocyte-microglia triads in PL of adult, aged and LPS-treated rats. **A-A3, B-B3, C-C3:** Confocal microscopy 3D renderings of triple immunostaining of neurons (NeuN, red), astrocytes (GFAP, green) and microglia (IBA1, blue) in the PL of an adult (A-A3), an aged (B-B3), and of an LPS-treated rat (C-C3). **A-A3:** The images show neuron, astrocytes and microglia in the PL of an adult rat, not forming a triad. Scale bar: 10 µm. **B-B3**: The arrows indicates neurons (B1) showing signs of degeneration with surrounding GFAP+ astrocytes (B2) and a microglial cell in reactive, phagocytic state (B3), forming a triad (A). Scale bar: 5 µm. **C-C3**: The open arrow in C1 indicates a neuron showing signs of degeneration with surrounding GFAP+ astrocytes and microglial cells in reactive, phagocytic state (C3) involved in the triad formation (C). Scale bar: 15 µm. **D:** Representative photomicrograph of an activated microglia cell (IBA1, blue) engulfing a neuronal debris (NeuN,

red, open arrow) in PL of an aged rat. Scale bar: 2 μm. **E:** Quantitative analysis of neuron-astrocyte-microglia triads/mm^2 in DG PL of adult (n=6), aged (n=5) and LPS-treated rats (n=4). Triads were significantly more numerous in PL of aged and LPS-treated rats. Data reported in all graph bars are expressed as mean±SEM.

A microglial cell (Figure 31B3) with phenotypical characteristics of reactive microglia, such as an enlarged cell body and short cellular processes (Miller and Streit, 2007), was in close proximity to the damaged neuron and was phagocytosing the cytoplasm, as shown by the pink color inside the microglia cytoplasm (Figure 31B, open arrow). The 3D rendering in Figure 31C (stack of 14 consecutive confocal z-scans, 0.3 μm each, total thickness 4.2 μm), shows that two damaged neurons, very close to the GL, formed triads with astrocytes and activated microglia cells which were engulfing the damaged neurons (Figure 31C, open arrow and white arrow). It is evident that both granular neurons were close but slightly detached from the GL. The open arrow indicates a neuron that has almost completely been phagocytized by the microglia cell, while the white arrow indicates a neuron that is starting to be attacked by the microglia cell. The arrowhead in Figure 31C shows an astrocyte forming a microscar around a degenerating neuron. Figure 31D, (stack of 6 consecutive confocal z-scans, 0.3 μm each, total thickness 1.8 μm), taken in the PL of an aged rat shows the magnification of a digital subslice (starting at about 4 μm inside the cell) of an amoeboid-shaped activated microglia that is phagocytosing a neuron (pink colour, open arrow). Quantitative analysis of neuron-astrocytes-microglia triads in the PL of adult, aged and LPS-treated rats showed that the triads increased by 170% in aged rats (***P<0.001 aged vs adult rats, $F_{(2,14)}$=43.37), and by 887% in LPS-treated rats (***P<0.001 LPS vs adult rats, $F_{(2,14)}$=43.37) in comparison to adult rats (Figure 31E).

4.5 Increased Fractalkin (CX3CL1) Expression in DG of Adult, Aged, and LPS-treated rats

Quantitative WB analysis of CX3CL1 in homogenates of whole hippocampus of adult, aged, and LPS treated rats are shown in Figure 32. In accordance with previous data (Cerbai et al., 2012), here we demonstrated that levels of CX3CL1 were significantly higher in aged (+80%), and in LPS-treated rats (+90%) hippocampus than in adult rat hippocampus ($F_{(2,12)}$=5.365; P<.005; **P<0.05 vs adult rats, Figure 32A). Double labelling immunofluorescent analysis of CX3CL1 (Figure 32C2-E2, green) and activated microglia (Figure 32B, C1-E1, red) showed that immunostaining of CX3CL1 colocalized in the cell body (open arrows) and in the branches (arrows) of activated

microglia cells in the PL of aged and LPS-treated rats (Figure 32C-8E), but not of adult rats (Figure 32B).

Colocalization of CX3CL1 with neurons or astrocytes was never found in the DG of any of the three experimental groups (data not shown).

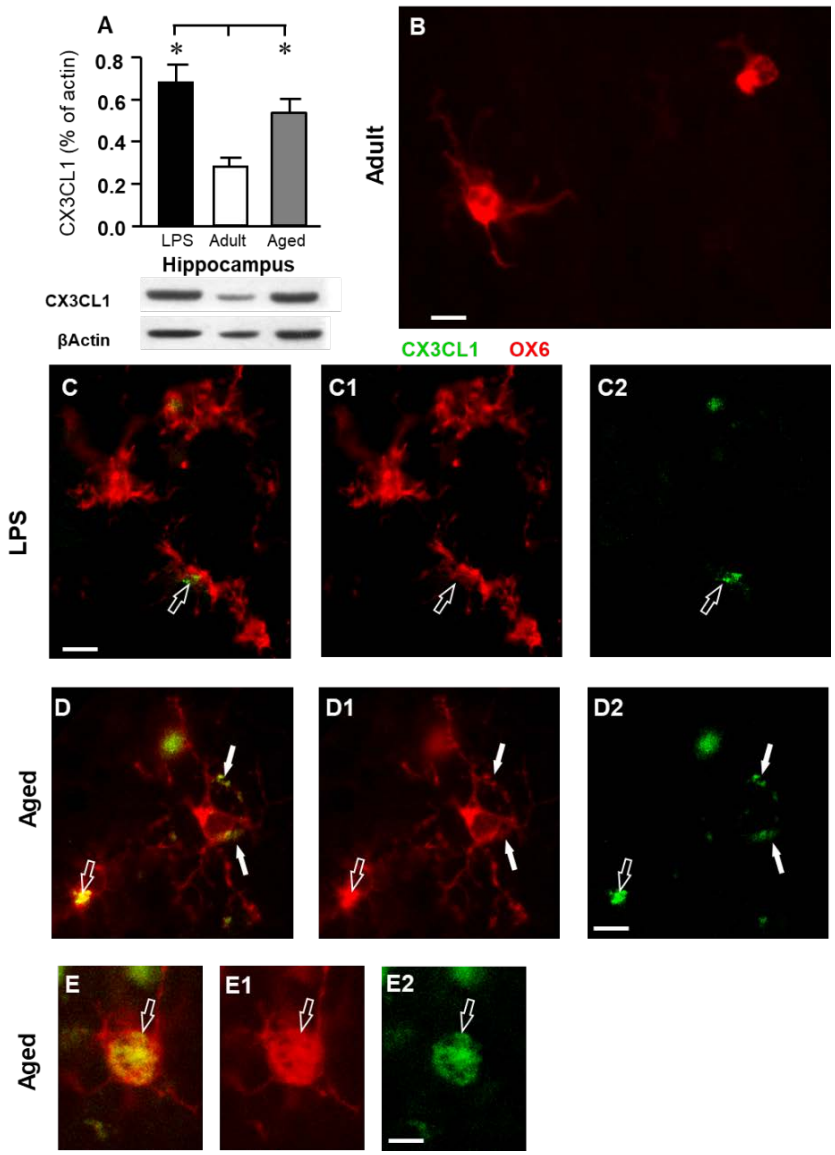

Figure 32. Analysis of CX3CL1 expression in the hippocampus of adult, aged, and LPS-treated rats. **A:** Quantitative Western Blot analysis of CX3CL1 in whole hippocampus homogenates of adult (n =6), aged (n = 4), and LPS-treated (n = 4) rats. Each column in the graph represents the level of CX3CL1 normalized to β-actin run in the same gel, expressed as mean±SEM (*P<0.05 vs adult rats). Typical Western Blots of CX3CL1 and actin run in the same gel are shown below. **B-D2**: Fluorescent immunohistochemistry of CX3CL1 (C2-D2, green), of OX6+ microglia (C1-D1, red), and the merge of CX3CL1 and OX6 (B, C, D) in the PL of an adult (B), an LPS-treated rat (C) and of an aged rat (D). B, Scale bar: 5 µm; C-C2, D-D2, Scale bar: 10 µm. These images show that CX3CL1 colocalized with microglia cells (arrows) in aged and LPS-treated rats. **E-E2**: Representative photomicrographs demonstrating that CX3CL1 (E2, green) is expressed in the cytoplasm of an activated microglial cell (E1, OX6, red) in the PL of an aged rat. E is the merge of the two previous images. Scale bar: 5 mµ.

Part II – Brain Aging and Inflammation

4.6 Analysis of microglia reactivity in the CA1 hippocampal region of control, LPS, and aged rats

In order to define some of the features of microglia dysregulation in aged CNS, microglial reactivity was compared by confocal microscopy in the CA1 hippocampus of control, LPS and aged rats (Figure 33A-C). Cytoskeleton remodeling was monitored using immunostaining for IBA1, a microglial marker of Ca^{2+} dependent actin polymerization. In LPS rats IBA1 expression appeared higher than in controls, as it is possible to appreciate qualitatively in the 3D Z-projections of confocal stacks (Figure 33A, B). This data was confirmed by quantitative analysis of immunofluorescence (Figure 33D, whole columns). Conversely, in aged rats IBA1 immunofluorescence was significantly lower than in LPS rats and was not differ from control rats (Figure 33C, D whole columns). An in-depth evaluation of IBA1 immunofluorescence distribution showed that the differences observed among the three experimental groups were characterized by a high degree of complexity. In microglial cell bodies, no significant difference in IBA1 immunofluorescence was found between aged and LPS rats, whereas its value was considerably lower in young rats (Figure 33D, light grey columns). These data indicated that a remarkable cytoskeletal rearrangement occurred in cell body of aged microglia cells rather than in their branches. It is possible appreciate qualitatively that rich branching was present in microglia of control and LPS rats (Figure 33A, B). On the other hand, the mean volume of IBA1+ branch tree was significantly higher in LPS than in control rats (Figure 33E). In LPS rats, microglia cell arborizations showed a more complex branching pattern in comparison to control rats (Figure 33A inset a1 and B insets b1, arrowheads). In aged rats (Figure 33C) microglial cells were characterized by an extremely poor arborization: qualitative evaluation of cell morphology suggested a decrease in the number of microglia cells branches (Figure 33C, insets c1), confirmed by a significantly lower volume of the branches (Figure 33E). Accordingly, sprouting of branches was rare (Figure 33C insets c1, arrowheads).

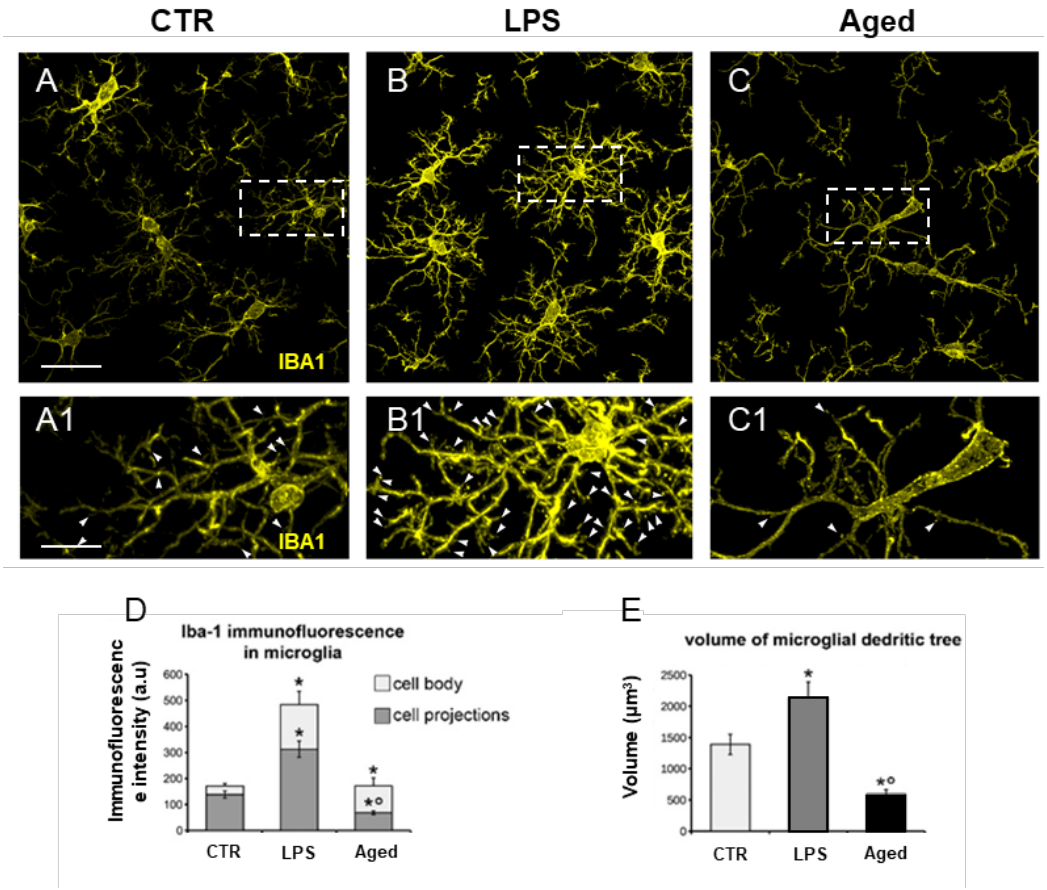

Figure 33. A-C: Confocal images of the CA1 hippocampus of control (**A**), LPS (**B**) and aged (**C**) rats immunostained for IBA1 (yellow). **A1-C1:** Magnifications of framed areas in A, B and C, small arrowheads indicate sites of branch sprouting. **D:** Quantitative analysis of IBA1 immunofluorescence on microglia cells bodies (light grey) and branches (dark gray; one way ANOVA $F_{(2\text{-}12)} = 6.2$, * $p < 0.05$ *vs* control, ° $p < 0.05$ *vs* LPS, n = 5 for each animal group). **E:** Evaluation of the microglia cells projections volume in the different animal groups (one way ANOVA $F_{(2\text{-}12)} = 14.6$, * $p < 0.05$ *vs* control, ° $p < 0.01$ *vs* LPS, n = 5 for each animal group).

4.7 Characterization of neuronophagia in CA1 hippocampus

Interactions between microglia cells and neurons were analyzed in order to correlate the above data with possible variations of neuron debris clearance in LPS and aged rats. Microglia positioned in close contact with neurons (Figures 34A-B, 34A1-B1), showed morphological characteristics of phagocytic cells. The percentage of microglia involved in phagocytic activity was significantly higher in LPS than in control rats (Figures 34A, B; D). These data confirmed the significant role of microglia in the removal of injured neurons in neuroinflammation. In aged rats, quantitative analyses revealed that the number of neuronophagic microglia was higher in the CA1 hippocampus than in control rats, but significantly lower than in LPS-treated rats (Figure 34D). Therefore, microglial efficiency in removing damaged neurons from the nervous tissue resulted lower in aged rats than in the other two animal groups. These results suggest that age-related chronic

processes of neuroinflammation might imply defective microglial targeting and phagocytosis of damaged neurons.

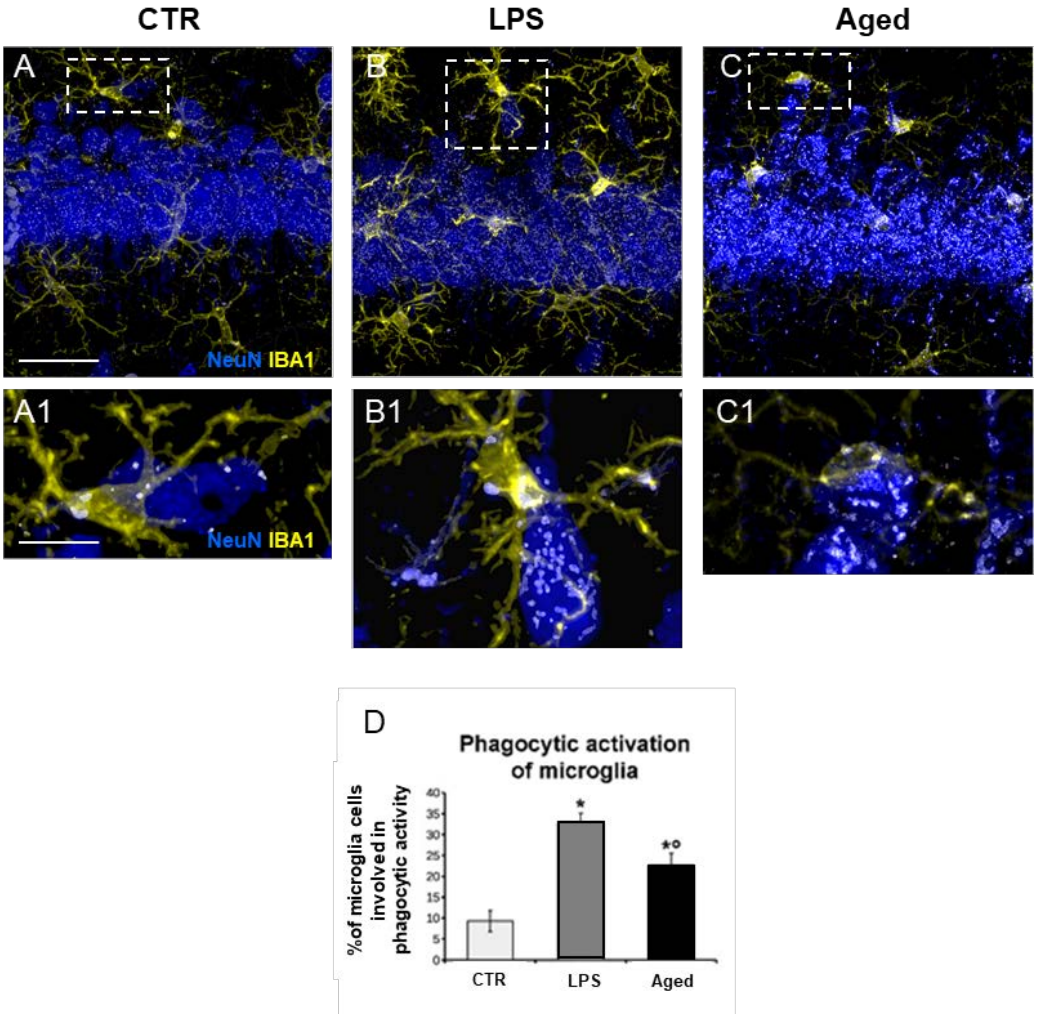

Figure 34. A-C: Confocal images of the CA1 hippocampus of control (**A**), LPS(**B**) and aged (**C**) rats immunostained for IBA1 (yellow) and NeuN (blue), arrows point to phagocytic event. **A1-C1**) Magnifications of framed areas in A, B and C. Percentage of microglia involved in phagocytic activity out of the total number of microglia (one way ANOVA $F_{(2\text{-}15)} = 23.8$, *p < 0.01 *vs* control, °p < 0.05 *vs* LPS, n = 6 for each animal group).

4.8 Evaluation of astrocyte-microglia interactions

Astrocyte-microglia interactions were analyzed in the three animal groups by confocal analysis on hippocampal sections immunostained to reveal IBA1 and GFAP (Figures 35A-C). Confocal images showed that astrocytes projections, in control and LPS rats, formed a continuous meshwork extending throughout the CA1 hippocampus (Figure 35A, B). Both in control and LPS rats, microglia appeared in contact with astrocytes projections (Figure 35A1-B1). In CA1 hippocampus of aged rats, astrocytes branches were often smaller and with distal fragmentation, a typical sign of clasmatodendrosis, thus causing disruption of astrocytic meshwork (Figure 35C1-C2). Generally, microglia

were localized within the intact astrocytes meshwork and, in those areas, their projections were normally branched (Figure 35C1). Conversely, we found fewer microglia within the disrupted astrocytes meshwork showing a typical amoeboid morphology (Figure 35C2). These data suggested that in aged rat hippocampus the branching of microglia was dependent on astrocyte meshwork integrity.

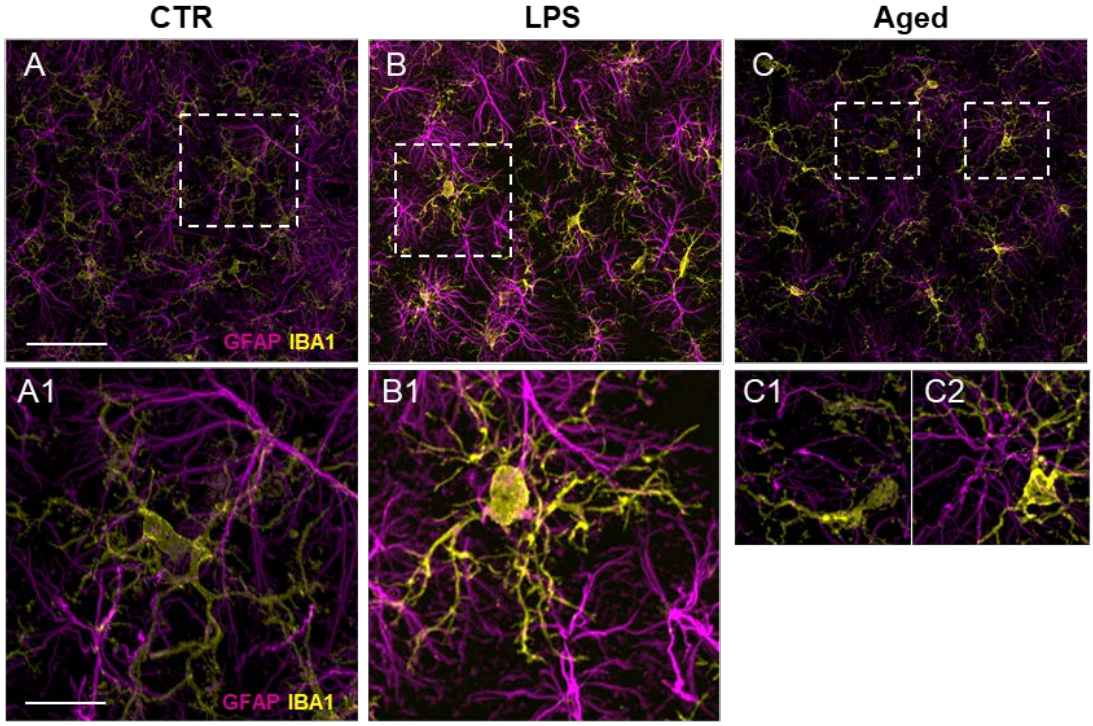

Figure 35. A-C: Confocal images of control (**A**), LPS (**B**), and aged (**C**) rats immunostained to reveal GFAP^{+} astrocyte meshwork (magenta) and IBA1 in microglia (yellow). Areas of astrocyte meshwork disruption are detectable in aged rats. **A1-C2:** Mgnifications of framed areas showing representative microglia in control (**A1**), LPS (**B1**) and aged rats (**C1-C2**) within the astrocyte meshwork.

4.9 Evaluation of integrin-β1 role in astrocyte-microglia interaction

Sections of hippocampus from the three animal groups were triple immunostained to reveal GFAP for astrocytes, IBA1 for microglia, and integrin-β1. Immunofluorescence of integrin-β1 in microglia is shown by the red dots (Figure 36A-C) scattered mainly on the branches and on the cell body (Figure 36A- C). These data suggested the involvement of integrin-β1 in microglia-astrocyte contacts. Quantitative analysis of the of immunofluorescence revealed that integrin-β1 expression was higher in LPS than in control rats (Figure 36D). Microglia of aged rats showed lower integrin-β1 immunofluorescence than the other groups, as shown qualitatively by the confocal images (Figure 36C) and quantitatively (Figure 36D). Notably, these quantitative data appeared mainly related to damaged microglia population. Ramified microglia were

contiguous to healthy astrocytes (Figure 36C1, C1^{I}) and showed high levels of integrin-β1 immunofluorenbscence (Figure 36C1).

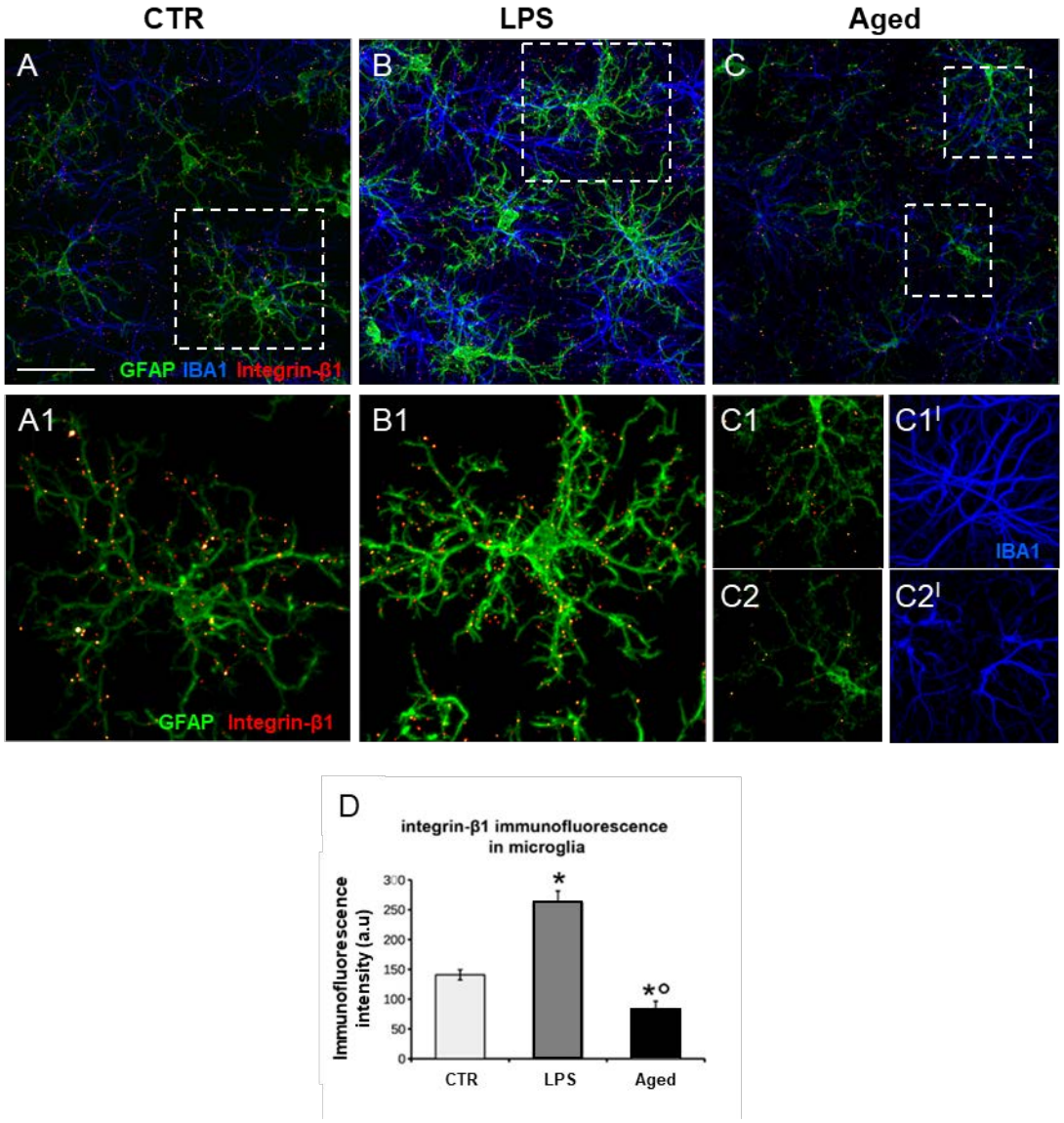

Figure 36. A-C: Z-projections of confocal stacks showing IBA1 (green), GFAP (blue) and integrin-β1 (red hot) immunofluorescence in the CA1 hippocampus of control (**A**), LPS (**B**) and aged (**C**) rats. **A1-C2'**) Mgnifications of framed areas selected in A, B and C showing integrin-β1 immunofluorescence in representative microglia cells from control, LPS and aged rats. respectively; GFAP immunofluorescence was omitted to emphasize the localization of integrin-β1 on microglia (**A1, B1, C1-C2**). **D:** Integrin-β1 immunofluorescence (one way ANOVA $F_{(2,12)} = 40.9$, * $p < 0.05$ *vs* control, °$p < 0.01$ *vs* LPS, n = 5 for each animal group).

Conversely, amoeboid microglia (Figure 36C2) were close to dystrophic astrocytes (Figure 36C2, C2^{I}) and exhibited low integrin-β1 immunofluorescence (Figure 36C2). These data provided evidence that low expression of integrin-β1 in aged rats microglia, could be correlated with the disruption of the astrocytes projections meshwork and a defective microglia-astroglia interaction.

Part III - Alzheimer's disease

4.10 Quantitative analysis of Aβ plaques deposition in CA1 and CA3 hippocampus of TgCRND8 mice and evaluation of glial response

We visualized the plaques by immunohistochemistry using an anti Aβ1-42 antibody (green) in hippocampal sections of TgCRND8 at 3 (Tg 3M) and 6 months of age (Tg 6M). No plaques were ever found in CA1 and CA3 hippocampus of WT mice. Images of fluorescent immunostaining were taken in CA1 (Figure 37A-B) and CA3 hippocampal regions (Figure 37E-F) with confocal microscopy and the quantitative analysis of the density of Aβ (plaques/mm^2) was performed separately in Str. Pyramidalis (SP) and Str. Radiatum (SR).

The panels in Figure 37A-B and Figure 37E-F show the images of plaques (green) in CA1 SP and SR and CA3 SP and SR, respectively. Quantitative analysis showed that in CA1 SP (65.8 ± 19.2 plaques/mm^2) and SR (247.9 ± 101 plaques/mm^2) of Tg 6M the density of Aβ plaques was significantly higher than in SP (1.0 ± 0.4 plaques/mm^2) and SR (10.1 ± 7.8 plaques/mm^2) of Tg 3M, respectively. The statistical analysis was performed by Student's t test in CA1 SP ($P < 0.05$, Tg 6M vs Tg 3M; Tg 3M: n=4; Tg 6M: n=4) and in CA1 SR ($P < 0.05$. Tg 6M vs Tg 3M; Tg 3M: n=4; Tg 6M: n=4).

Quantitative analysis showed that in CA3 SP (62.4 ± 28.3 plaques/mm^2) and SR (134.5 ± 46.8 plaques/mm^2) of Tg 6M the density of Aβ plaques was significantly higher than in SP (0.5 ± 0.25 plaques/mm^2) and SR (0.5 ± 0.25 plaques/mm^2) of Tg 3M. The statistical analysis was performed by Student's t test in CA2 SP ($P < 0.05$, Tg 6M vs Tg 3M; Tg 3M: n=4; Tg 6M: n=4) and in CA3 SR (Student's t test: $^*P < 0.05$. Tg 6M vs Tg 3M; Tg 3M: n=4; Tg 6M: n=5).

The plaques were then further characterized and quantified subdividing them by size into small (S, less than 2500 μm^3), medium (M, between 2500 and 7000 μm^3), and large (L, more than 7000 μm^3) in SP or SR of CA1 and CA3, as shown in Figure 37C-D, G-H. Two way ANOVA statistical analysis on Aβ plaques in CA1 SP of Tg 3M and Tg 6M revealed a significant main effect for experimental group ($F(1,18)=7.156$, $P<0.05$), no significant effect for plaque size ($F(2,18)=1.084$, $P>0.05$), and Interaction ($F(2,18)=1.084$, $P>0.05$). Bonferroni post test showed that small plaques (S) in CA1 SP of Tg 6M were significantly more numerous than in Tg 3M ($^*P<0.05$ Tg 6M S vs Tg 3M S). Two way ANOVA statistical analysis on Aβ plaques in CA1 SR of Tg 3M and Tg 6M revealed a significant main effect for experimental group ($F(1,18)=45.69$,

P<0.001), no significant effect for plaque size (F(2,18)=0.003925, P>0.05), and Interaction (F(2,18)=0.1647, P>0.05). Bonferroni post test showed that small (S), medium (M) and large plaques (L) in CA1 SR of Tg 6M were significantly more numerous than in Tg 3M (**P<0.01 Tg 6M S, M, L vs Tg 3M S, M, L). Two way ANOVA statistical analysis on Aβ plaques in CA3 SP of Tg 3M and Tg 6M revealed a significant main effect for experimental group (F(1,18)=10.04, P>0.01), plaque size (F(2,18)=6.774, P>0.01), and Interaction (F(2,18)=6.774, P>0.01). Bonferroni post test showed that small plaques (S) in CA3 SP of Tg 6M were significantly more numerous than in Tg 3M (***P<0.01 Tg 6M S vs Tg 3M S). Two way ANOVA statistical analysis on Aβ plaques quantification in CA3 SR of Tg 3M and Tg 6M revealed a significant main effect for experimental group (F(1,18)=13.36, P<0.01), plaque size (F(2,18)=3.965, P<0.05), and Interaction (F(2,18)=3.965, P<0.05). Bonferroni post test showed that small plaques (S) in CA3 SR of Tg 6M were significantly more numerous than in Tg 3M (**P<0.01 Tg 6M S vs Tg 3M S).

Statistical analysis with three way ANOVA with Plaque Size, ROI and Age as the three variables was performed between CA1 SP and CA3 SP of Tg 3M and Tg 6M. Results showed a significant main effect for Age (F(1,47)=18.01, P<0.001), for Size (F(2,47)=7.77, P<0.01), and for Interaction AgexSize (F(2,47)=7.77, P<0.01). Bonferroni post test showed that Small plaques (S) in CA3 SP of Tg 6M on average were significantly more numerous than in CA1 SP of Tg 6M mice (P<0.05), while Medium (M) and Large (L) plaques were not significantly different.

Statistical analysis with three way ANOVA with Plaque Size, ROI and Age as the three variables was performed between CA1 SR and CA3 SR of Tg 3M and Tg 6M. Results showed a significant main effect for ROI (F(1,47)=13.16, P<0.01), Age (F(1,47)=77.49, P<0.001), for Interaction AgexROI (F(1,47)=9.02, P<0.01), and for Interaction AgexSize (F(2,47)=3.63, P<0.05). Bonferroni post test showed that Medium plaques (M) and Large plaques (L) in CA1 SR of Tg 6M were on average significantly more numerous than in CA3 SR of Tg 6M mice (P<0.05), while Small plaques were not significantly different.

We performed triple immunostaining of astrocytes with GFAP (green), of microglia with IBA1 (red), and of plaques using an Aβ1-16 antibody (blue) in area CA1 of a TgCRND8 mouse at 6 months of age. The confocal image of the triple immunostaining in Figure 37I shows that Aβ plaques (Figure 37I3, asterisks) were surrounded and infiltrated by many hypertrophic astrocytes (Figure 37I1, arrows) and microglia cells

(Figure 37I2, open arrows). Astrocytes and microglia located more distantly from the plaques were in a less reactive state.

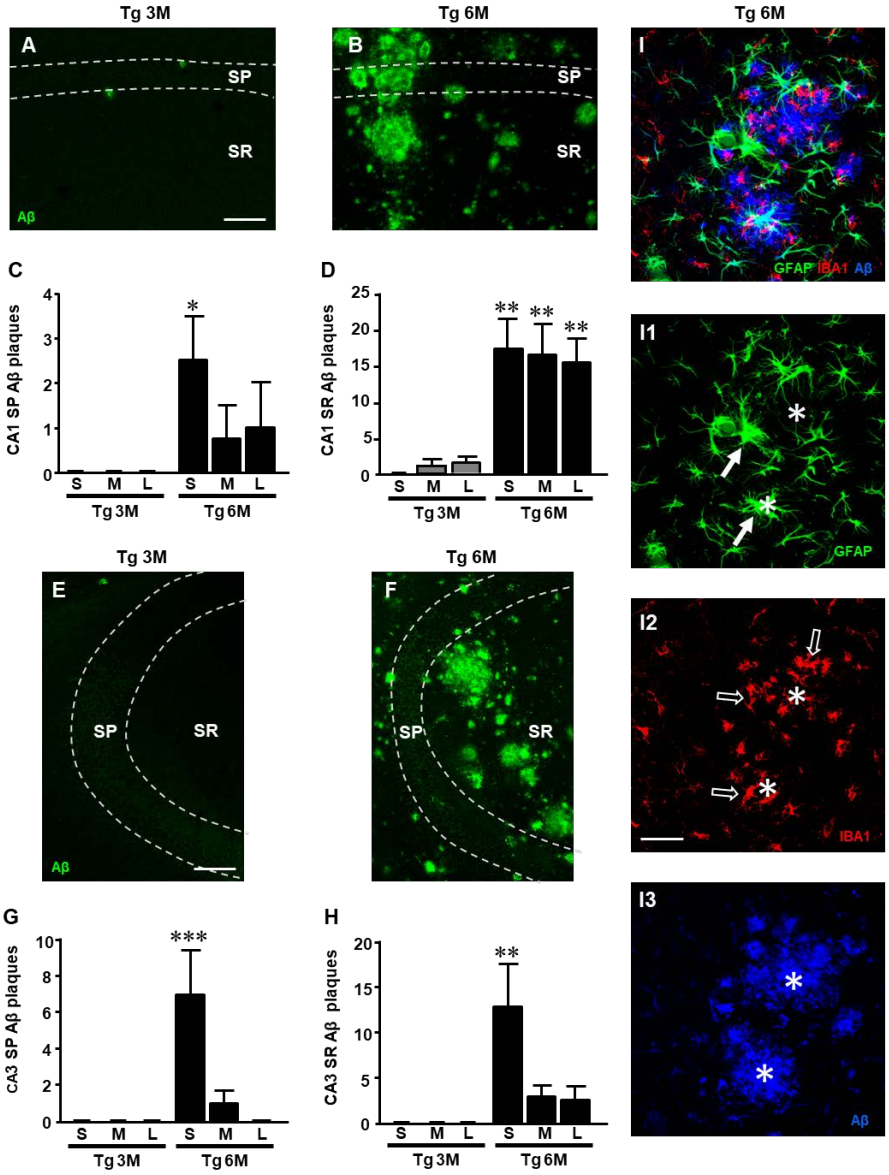

Figure 37. Analysis of Aβ1-42 plaques in CA1 and CA3 of Tg 3M and Tg 6M mice, and their subdivision by size into Small (S), Medium (M) and Large (L). **A-B:** Representative confocal photomicrographs of Aβ1-42 immunostaining in plaques (green) in CA1 of a Tg 3M (A) and a Tg 6M (B) mouse. Scale bar: 100µm. **C-D:** Quantitative analysis of S, M and L plaques CA1 SP (C) and SR (D) of Tg 3M and Tg 6M. S plaques were significantly more numerous in CA1 SP of Tg 6M, while in CA1 SR of Tg 6M mice S, M, and L plaques were significantly more numerous than in Tg 3M mice. **E-F:** Representative confocal photomicrographs of Aβ1-42 immunostaining in plaques (green) in CA3 of a Tg 3M (E) and a Tg 6M (F) mouse. Scale bar: 100µm. **G-H:** Quantitative analysis of S, M and L plaques CA3 SP (G) and SR (H) of Tg 3M and Tg 6M. S plaques were significantly more numerous in CA3 SP and CA3 SR of Tg 6M than in Tg 3M mice. **I-I3:** Representative confocal photomicrographs of triple immunostaining of astrocytes (I1, green), microglia (I2, red) and Aβ plaques (I3, blue) in CA1 of a Tg 6M (B) mouse. The merge is shown in Figure 1I. Scale bar: 40µm Data reported in all graph bars are expressed as mean±SEM.

4.11 Characterization of astrocytes in CA1 and CA3 hippocampus of TgCRND8 mice

For qualitative and quantitative analyses, astrocytes were visualized by immunohistochemistry with anti GFAP antibody (green) in hippocampal sections of TgCRND8 at 3 (Tg 3M) and 6 months of age (Tg 6M), and of WT control mice. Images of fluorescent immunostaining were taken in CA1 (Figure 38A-C) and CA3 hippocampal regions (Figure 38G-I) with confocal microscopy, separately. Figure 38A1-C1 show the magnification of the framed areas in the SR of WT (A), Tg 3M (B) and Tg 6M (C) mice. We performed separately in CA1 and CA3 SP and SR the qualitative and quantitative analyses to characterize the astrocytes.

The graphs in Figure 38D-F show the results of the quantitative analyses of astrocytes in CA1 SP (Figure 38D) and SR (Figure 38E, F). We found that the density of astrocytes significantly increased in SP of Tg mice both at 3 (+43%) and 6 months (+65%) of age in comparison to WT mice (Figure 38D). (One-way ANOVA: $F(2,14)=10.69$, $P=0.0015$; Newman-Keuls post-test: **$P<0.01$ Tg 3M vs WT, Tg 6M vs WT; WT: n=5; Tg 3M: n=6; Tg 6M: n=6). Nevertheless, in CA1 SR we found no statistically significant difference of astrocytes density among the three experimental groups (WT: 873.0±3.74, Tg 3M: 912.9±41.53, Tg 6M: 860.1±36.24; One-way ANOVA: $F(2,14)=0.615$, $P=0.5543$).

Qualitative analysis (Figure 38A1-C1) showed that, in CA1 SR of Tg 3M and Tg 6M, astrocytes, although not more numerous than in WT mice, had a different morphology from those present in the SR of WT mice. We thus performed further analyses on immunofluorescence intensity of GFAP and on the length of primary astrocyte branches to compare the morphology of astrocytes among the three experimental groups. We found that GFAP immunofluorescence significantly increased in CA1 SR of Tg 3M in comparison to WT mice, (+33%), reaching a plateau in CA1 SR of Tg 6M (+32%) (Figure 38E). (One-way ANOVA: $F(2,11)=19.26$, $P=0.0003$; Newman-Keuls post-test: ***$P<0.001$ Tg 3M vs WT, Tg 6M vs WT; WT: n=4; Tg 3M: n=6; Tg 6M: n=4). In addition, in CA1 SR the primary branches of Tg 6M astrocytes were significantly longer (+24%) than those of WT mice (Figure 38F) (One-way ANOVA: $F(2,13)=3.622$, $P=0.0562$; Newman-Keuls post-test: *$P<0.05$ Tg 6M vs WT; WT: n=4; Tg 3M: n=6; Tg 6M: n=4). Also, in CA1 SR the primary branches of Tg 3M (+17%) and Tg 6M (+32%) astrocytes were both significantly longer than those of WT mice (Figure 38F)

(One-way ANOVA: $F(2,12)=9.819$, $P=0.003$; Newman-Keuls post-test: *$P<0.05$ Tg 3M vs WT; **$P<0.01$ Tg 6M vs WT; WT: n=5; Tg 3M: n=6; Tg 6M: n=4).

On the contrary, no statistically significant differences were detected in the density of astrocytes in SP CA3 of transgenic mice at both 3 (+8% vs WT) and 6 months (+ 5% vs WT) of age (Figure 38J) (One-way ANOVA: $F(2,14)=0.089$, $P=0.09150$, n.s.; WT: n=5; Tg 3M: n=6; Tg 6M: n=6). In addition, the expression of GFAP protein increased slightly but not significantly in astrocytes of CA3 SR at both 3 (+13% vs WT) and 6 months (+ 8% vs WT) of age (Figure 38K) (One-way ANOVA: $F(2,9)=0.570$, $P=0.5843$, n.s.; WT: n=5; Tg 3M: n=4; Tg 6M: n=3).

In CA3 SR, we found no statistically significant difference of astrocytes density among the three experimental groups (WT: 1308.0±68.30, Tg 3M: 901.8±106.2, Tg 6M: 1023.0±198.8; One-way ANOVA: $F(2,15)=1.675$, $P=0.2205$, n.s.). The length of astrocyte branches in CA3 SR of transgenic mice was not statistically different from WT mice at both 3 (-3%) and 6 months (-5%) of age (Figure 38L) (One-way ANOVA: $F(2,12)=0.2175$, $P=0.8076$, n.s..; WT: n=5; Tg 3M: n=6; Tg 6M: n=4).

We compared the results obtained in CA1 (Cerbai et al., 2012) to those obtained in CA3 by two-way ANOVA with ROIs and experimental groups as the two variables. The statistical analysis on SP astrocytes density revealed that in WT animals there was no significant difference between CA1 and CA3 SP while a significant increase was found in CA1 SP of Tg 3M and Tg 6M. Indeed, we found a significant main effect for ROIs (ROI, $F(1,28)=55.69$, $P<0.001$), experimental groups ($F(2,28)=6.626$, $P<0.01$), and a significant Interaction ($F(2,28)=5.077$, $P<0.05$). Bonferroni post test showed that astrocytes density in CA1 SP of Tg 3M ($P<0.001$ vs CA3 SP) and Tg 6M ($P<0.001$ vs CA3 SP) was significantly higher than in CA3 SP.

The statistical analysis on GFAP immunofluorescence revealed that in WT animals there was no significant difference between CA1 and CA3 SR while a significant increase was found in CA1 SR of Tg 3M and Tg 6M. Indeed, we found a significant main effect for ROIs (ROI, $F(1,20)=29.66$, $P<0.001$), experimental groups ($F(2,20)=7.654$, $P<0.01$), while the Interaction was not significant ($F(2,20)=2.437$, n.s.). Bonferroni post test showed that GFAP immunofluorescence in CA1 SR of Tg 3M ($P<0.01$ vs CA3 SR) and Tg 6M ($P<0.01$ vs CA3 SR) was significantly higher than in CA3 SR.

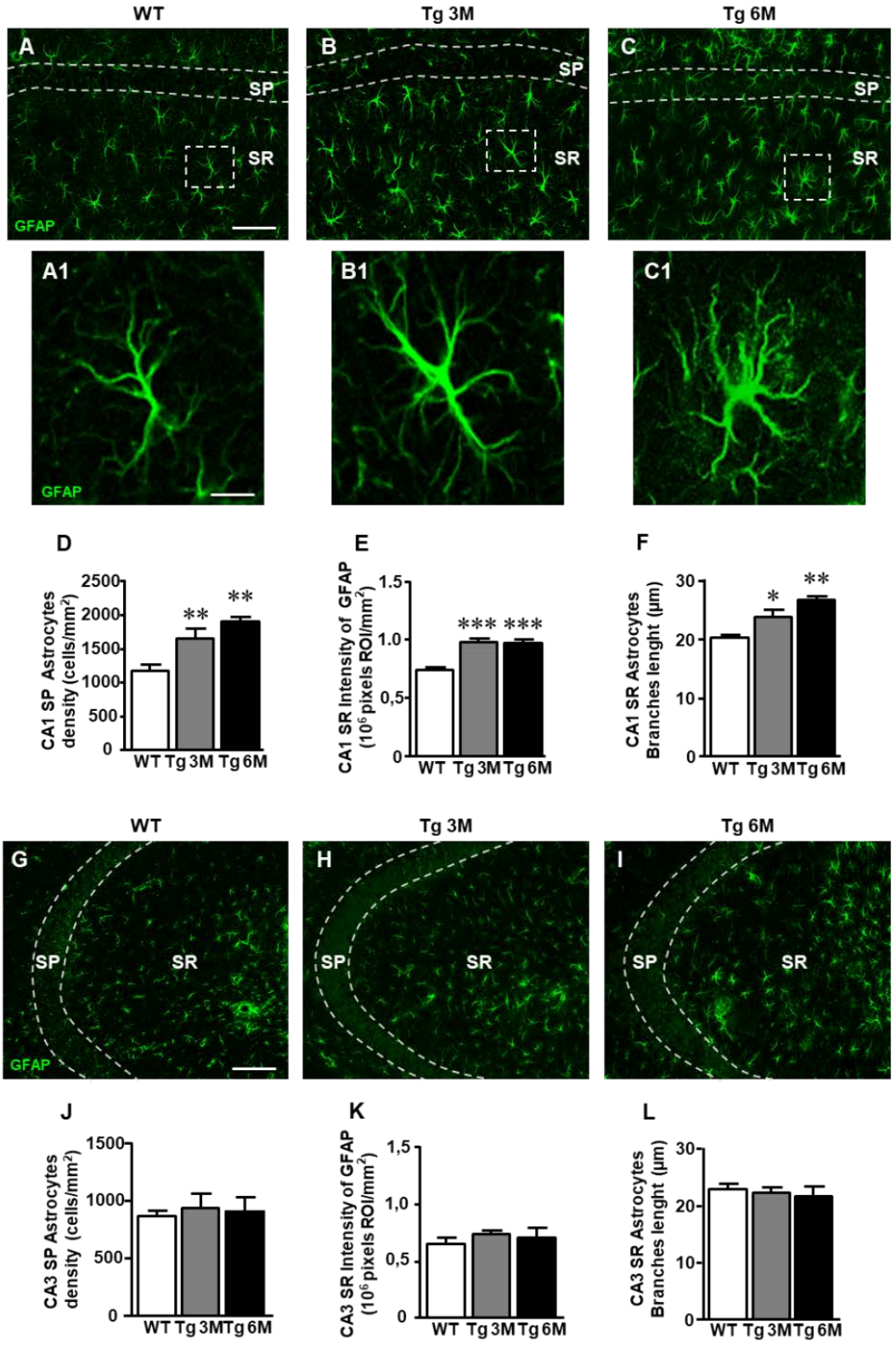

Figure 38. Analysis of total microglia in CA1 and CA3 of WT, Tg 3M and Tg 6M. **A-C:** Representative confocal photomicrographs of IBA1 immunostaining of microglia (green) in CA1 of a WT (A), a Tg 3M (B), and a Tg 6M (C). Scale bar: 100 µm. Panels A1, B1 and C1 shows the magnification of microglial cells framed in Panels A, B and C. Scale bar: 20 µm. **D-E:** Quantitative analysis of microglia/mm^2 in CA1 SP (D) and SR (E) of WT, Tg 3M and Tg 6M. Microglia cells are significantly more numerous in CA1 SR of Tg 6M mice vs WT and Tg 3M. **F-H:** Representative confocal photomicrographs of IBA1 immunostaining of microglia

(green) in CA3 of a WT (F), a Tg 3M (G), and a Tg 6M (H). Scale bar: 100 μm. **I-J:** Quantitative analysis of microglia/mm^2 in CA3 SP (I) and SR (J) of WT, Tg 3M and Tg 6M. Microglia cells are significantly more numerous in SP and SR of Tg 6M mice vs WT and Tg 3M. **K**: Representative confocal image of microglia cells (green) spatially oriented towards a Large Aβ1-42 plaque (blue). The dotted line represents the area used for the quantitative analysis of spatially oriented microglia. Scale bar: 20 μm. **L-M:** Quantitative analysis of spatially oriented microglia in CA1 SR (L) and CA3 SR (M), represented as microglia located on or within 10 μm around Large plaques (area enclosed in the dotted line in Figure 38K) expressed as percent of total microglia. In both CA1 and CA3 SR of Tg 6M mice the percent of microglia spatially oriented towards Large plaques was significantly higher than in Tg 3M. Data reported in all graph bars are expressed as mean±SEM.

The statistical analysis on the length of primary astrocytes branches revealed that in WT and Tg 3M animals there was no significant difference between CA1 and CA3 SR while a significant increase was found in CA1 SR of Tg 6M. Indeed, we found a significant main effect for Interaction ($F(2,24)=6.044$, $P<0.01$). Bonferroni post test showed that the length of primary astrocytes branches in CA1 SR of Tg 6M was significantly higher than in CA3 SR ($P<0.05$).

4.12 Quantitative analysis of total and reactive microglia in CA1 and CA3 hippocampus of TgCRND8 mice

To perform the quantitative analysis of total microglia on hippocampal sections of TgCRND8 (Tg 3M, Tg 6M) and control mice (WT), we immunolabelled microglia with anti IBA1 antibody. Images of fluorescent immunostaining were taken in CA1 (Figure 39A-C) and CA3 hippocampal regions (Figure 39F-H) with confocal microscopy. Figure 39A1-C1 show the magnification of the framed areas in the SR of WT (A), Tg 3M (B) and Tg 6M (C) mice. The quantitative analyses of total microglia were performed in CA1 and CA3 SP and SR, separately.

The graphs in Figure 39D-E show the results of the quantitative analyses of the density of IBA1+ microglia in CA1 SP and CA1 SR. In CA1 SP of Tg 6M we found a slight (+35%), although not statistically significant, increase of the density of IBA1+ microglia in comparison to WT mice (Figure 39D) (One-way ANOVA: $F(2,14)=1.252$, $P=0.3161$, n. s.; WT: n=6; Tg 3M: n=5; Tg 6M: n=6). However, the density of IBA1+ microglia in CA1 SR of Tg 6M significantly increased both in comparison to WT and to Tg 3M (+72% vs WT; +43% vs Tg 3M; Figure 39E). (One-way ANOVA: $F(2,13)=11.23$, $P=0.0015$; Newman-Keuls post-test: $^{**}P<0.01$ Tg 6M vs WT, $^{\#\#}P<0.01$ Tg 6M vs Tg 3M; WT: n=6; Tg 3M: n=5; Tg 6M: n=5).

In CA3 SP of Tg 6M mice, we found a statistically significant increase of the density of IBA1+ microglia in comparison both to WT and Tg 3M mice (+46% vs WT; +43% vs

Tg 3M; Figure 39I). (One-way ANOVA: F(2,13)=6.217, P=0.0127; Newman-Keuls post-test: *P<0.05 Tg 6M vs WT, #P<0.05 Tg 6M vs Tg 3M; WT: n=6; Tg 3M: n=5; Tg 6M: n=5). IBA1+ microglia density increased also in CA3 SR of Tg 6M and the effect was statistically significant from both WT and Tg 3M mice. (+48% vs WT; +51% vs Tg 3M; Figure 39J) (One-way ANOVA: F(2,13)=5.570, P=0.0179; Newman-Keuls post-test: *P<0.05 Tg 6M vs WT, #P<0.05 Tg 6M vs Tg 3M; WT: n=6; Tg 3M: n=5; Tg 6M: n=5).

Two-way ANOVA analysis demonstrated that IBA1+ microglia density was not significantly different in CA1 SP and SR in comparison to CA3 SP and SR of all groups examined.

We studied the spatial orientation of IBA1+ microglia towards Large plaques calculating the percent microglia cells located on or within 10 µm around Large plaques in CA1 and CA3 SR (see dotted line in Figure 39K which shows a Large plaque in blue and microglia cells in green). Quantitative analysis showed that in CA1 and CA3 SR of TG 6M mice a highly significant percent of microglia was oriented towards Large plaques in comparison to TG 3M (**P<0.01, Tg 6M vs Tg 3M, Student's t test, Figure 39L-M). Two-way ANOVA analysis demonstrated that the orientation of IBA1+ microglia towards Large plaques was not significantly different in CA1 SR in comparison to CA3 SR in all groups examined.

To visualize reactive microglia, we performed the immunolabelling with anti CD68 antibody, a marker of reactive microglia cells, on hippocampal sections of TgCRND8 (Tg 3M, Tg 6M) and control mice (WT). Images of fluorescent immunostaining were taken in CA1 (Fig 4A-C) and CA3 hippocampal regions (Fig 4G-I) with confocal microscopy and the quantitative analysis of the density of reactive microglia was performed in CA1 and CA3 SP and SR, separately. Figs. 6A1-C1 show the magnification of the framed areas in the SR of WT (A), Tg 3M (B) and Tg 6M (C) mice.

The graphs in Figure 40D-E show the results of the quantitative analyses of reactive microglia in CA1 SP and CA1 SR, respectively. In CA1 SP of Tg 3M and Tg 6M the density of reactive microglia increased (+82% and + 347% vs WT, respectively) although not significantly, in comparison to WT mice (Figure 40D) (One-way ANOVA: F(2,14)=1.395, P=0.2802, n. s.; WT: n=6; Tg 3M: n=5; Tg 6M: n=6). On the contrary, in CA1 SR of Tg 6M we found a highly significant increase of the density of microglia

in comparison both to WT and Tg 3M mice (+902% vs WT; +636 vs Tg 3M; Figure 40E).

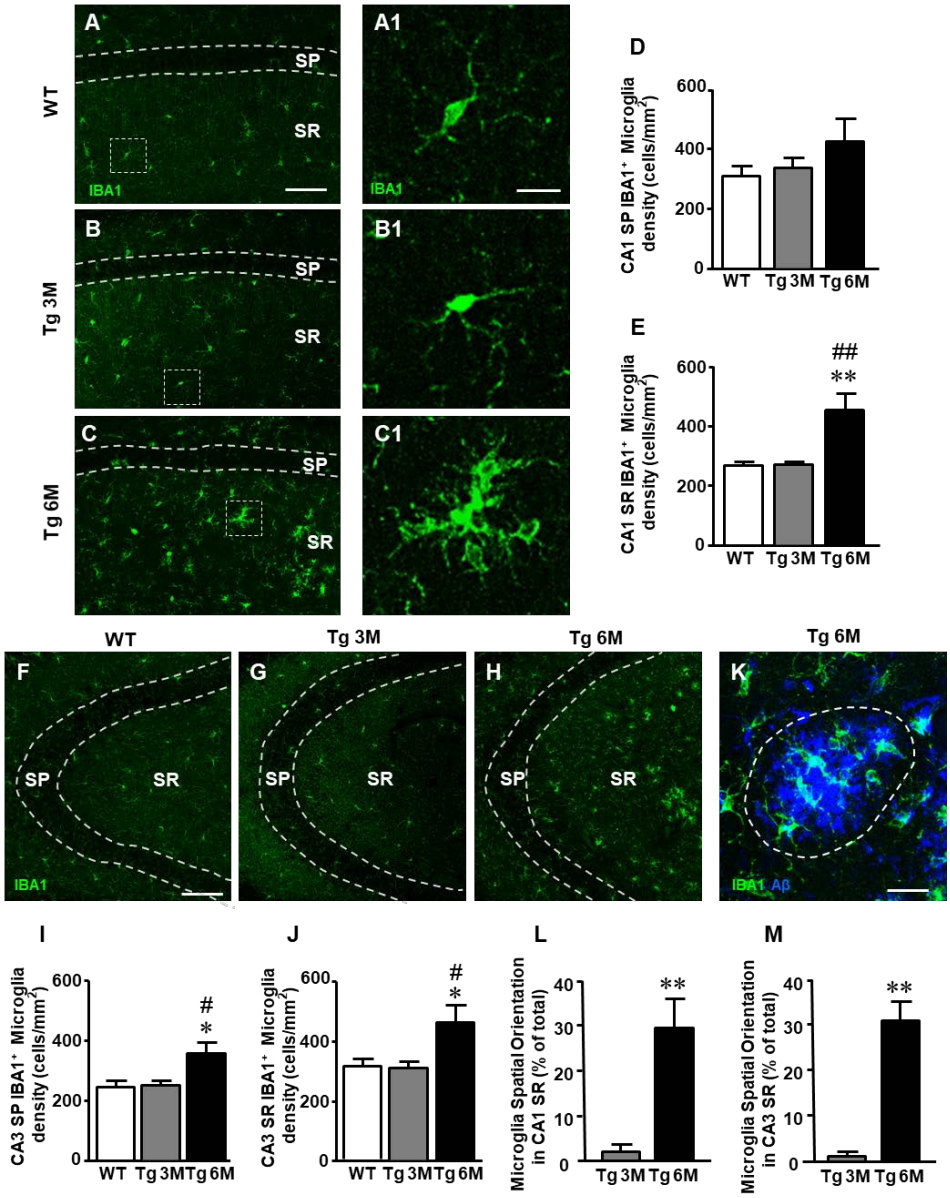

Figure 39. Analysis of total microglia in CA1 and CA3 of WT, Tg 3M and Tg 6M. **A-C:** Representative confocal photomicrographs of IBA1 immunostaining of microglia (green) in CA1 of a WT (A), a Tg 3M (B), and a Tg 6M (C). Scale bar: 100 μm. Panels A1, B1 and C1 shows the magnification of microglial cells framed in Panels A, B and C. Scale bar: 20 μm. **D-E:** Quantitative analysis of microglia/mm^2 in CA1 SP (D) and SR (E) of WT, Tg 3M and Tg 6M. Microglia cells are significantly more numerous in CA1 SR of Tg 6M mice vs WT and Tg 3M. **F-H:** Representative confocal photomicrographs of IBA1 immunostaining of microglia (green) in CA3 of a WT (F), a Tg 3M (G), and a Tg 6M (H). Scale bar: 100 μm. **I-J:** Quantitative analysis of microglia/mm^2 in CA3 SP (I) and SR (J) of WT, Tg 3M and Tg 6M. Microglia cells are significantly more numerous in SP and SR of Tg 6M mice vs WT and Tg 3M. **K**: Representative confocal image of microglia cells (green) spatially oriented towards a Large Aβ1-42 plaque (blue). The dotted line represents the area used for the quantitative analysis of spatially oriented microglia. Scale bar: 20 μm. **L-M:** Quantitative analysis of spatially oriented microglia in CA1 SR (L) and CA3 SR (M), represented as microglia located on or within 10 μm around Large plaques (area enclosed in the dotted line in Figure K)

expressed as percent of total microglia. In both CA1 and CA3 SR of Tg 6M mice the percent of microglia spatially oriented towards Large plaques was significantly higher than in Tg 3M. Data reported in all graph bars are expressed as mean±SEM.

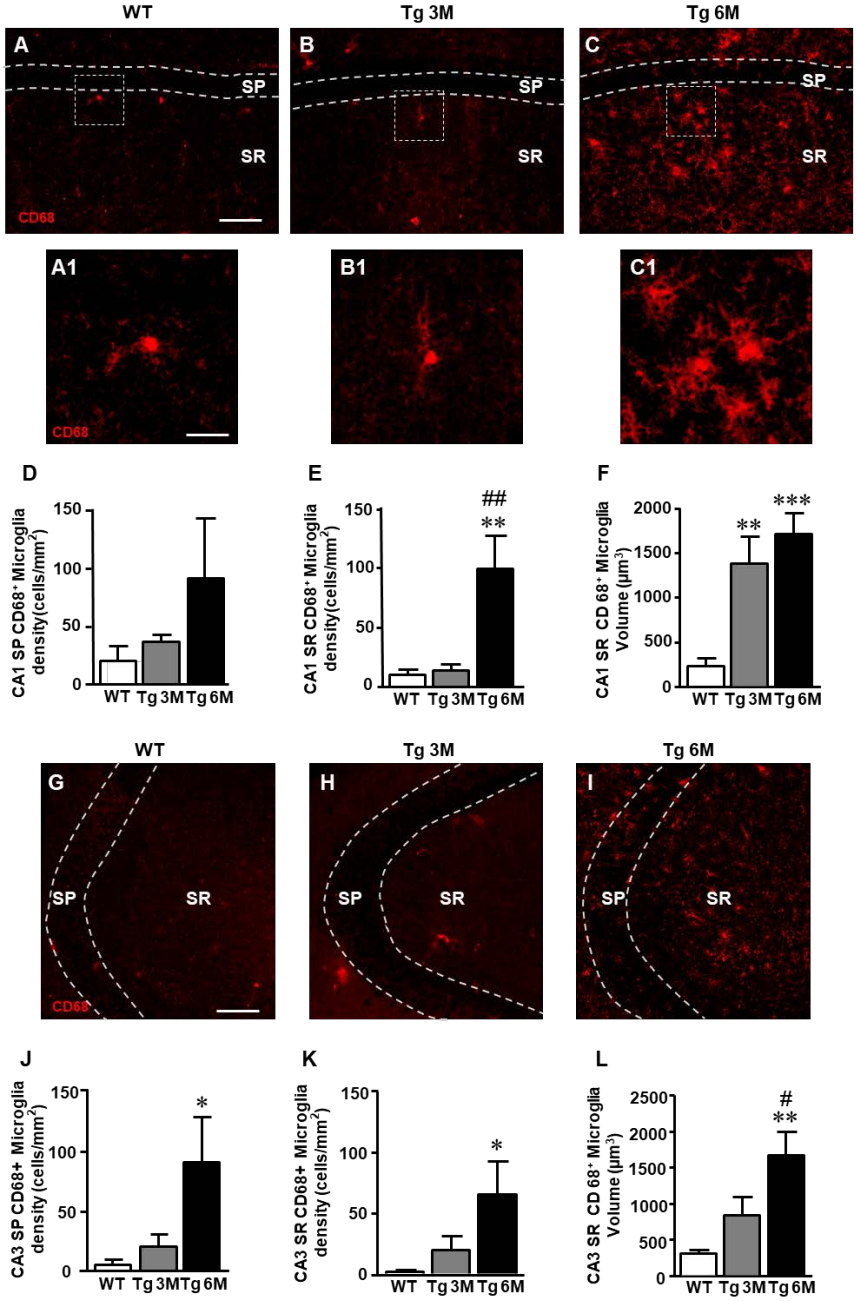

Figure 40. Analysis of reactive microglia in CA1 and CA3 of WT, Tg 3M and Tg 6M. **A-C:** Representative confocal photomicrographs of CD68 immunostaining of reactive microglia (red) in CA1 of a WT (A), a Tg 3M (B), and a Tg 6M (C). Scale bar: 100 µm. Panels A1, B1 and C1 shows the magnification of reactive microglial cells framed in Panels A, B and C. Scale bar: 20 µm. **D-E:** Quantitative analysis of reactive microglia/mm^2 in CA1 SP (D) and CA1 SR (E) of WT, Tg 3M and Tg 6M. Microglia cells are significantly more numerous in CA1 SR of Tg 6M mice vs WT and Tg 3M. **F:** Measure of reactive microglia cells volume in CA1 SR (F) of WT, Tg 3M and Tg 6M. Reactive microglia cells volume was significantly increase in Tg 6M and Tg 3M vs WT. **G-I:** Representative confocal photomicrographs of CD68 immunostaining of reactive microglia (red) in CA3 of a WT (G), a Tg 3M (H), and a Tg 6M (I). Scale bar: 100 µm. **J-K:** Quantitative analysis of microglia/mm^2 in CA3 SP (J) and SR (K) of WT, Tg 3M and Tg 6M. Microglia cells are significantly more numerous in SP and SR of Tg 6M mice vs WT. **L:**

Measure of reactive microglia cells volume in CA3 SR (L) of WT, Tg 3M and Tg 6M. Reactive microglia cells volume was significantly increase in Tg 6M vs WT. Data reported in all graph bars are expressed as mean±SEM.

(One-way ANOVA: $F(2,13)=10.77$, $P=0.0017$; Newman-Keuls post-test: **P<0.01 Tg 6M vs WT, ##P<0.01 Tg 6M vs Tg 3M; WT: n=6; Tg 3M: n=5; Tg 6M: n=5). We evaluated the volume of reactive microglia in CA1 SR, and we found a statistically significant increase of the average volume of $CD68^+$ microglia in CA1 SR both at 3 (+487% vs WT) and 6 months (+626% vs WT) of age, in comparison to WT mice (Figure 40F). (One-way ANOVA: $F(2,14)=13.84$, $P=0.0005$; Newman-Keuls post-test: **P<0.01 Tg 3M vs WT, ***P<0.001 Tg 6M vs WT; WT: n=6; Tg 3M: n=5; Tg 6M: n=6).

Results obtained in CA3 (Figure 40J-L) are in accordance with those in CA1. In CA3 SP we found a statistically significant increase of the density of reactive microglia in Tg 6M in comparison to WT and Tg 3M mice. (+1448% vs WT; +339% vs Tg 3M; Figure 40J) (One-way ANOVA: $F(2,14)=4.002$, $P=0.0422$; Newman-Keuls post-test: *P<0.05 Tg 6M vs WT; WT: n=6; Tg 3M: n=5; Tg 6M: n=6). In addition, in CA3 SR of Tg 6M mice reactive microglia significantly increased in comparison to WT (+3395%) (Figure 40K) (One-way ANOVA: $F(2,13)=4.244$, $P=0.0381$; Newman-Keuls post-test: *P<0.05 Tg 6M vs WT; WT: n=6; Tg 3M: n=5; Tg 6M: n=5). The evaluation of the volume of reactive microglia in CA3 SR showed that there was a statistically significant increase of the average volume of $CD68^+$ microglia in CA3 SR at 6 months (434% vs WT) of age, in comparison to WT mice (Figure 40L). (One-way ANOVA: $F(2,14)=8.350$, $P=0.0041$; Newman-Keuls post-test: **P<0.01 Tg 6M vs WT, #P<0.05 Tg 6M vs Tg 3M; WT: n=6; Tg 3M: n=5; Tg 6M: n=6).

Two-way ANOVA analysis demonstrated that the $CD68^+$ microglia density was not significantly different in CA1 SP and SR in comparison to CA3 SP and SR of all groups examined.

4.13 Analysis of inflammatory mediators in CA1 and CA3 hippocampus of TgCRND8 mice

To verify whether different expression of inflammatory mediators might be present in CA1 and CA3, we first performed immunofluorescence staining with anti TNFα antibody on hippocampal sections of TgCRND8 (Tg 3M, Tg 6M) and control mice (WT). Neurons were counterstained with anti NeuN antibody. Images of fluorescent immunostaining were taken in CA1 (Figure 41A-C) and CA3 hippocampal regions

(Figure 41F-H) with confocal microscopy and the quantitative analysis of the density of TNFα+ cells was performed in CA1 and CA3 SR, separately.

In CA1 of transgenic mice, TNFα immunostaining increased and was localized mainly in astrocyte-like cells evenly scattered throughout the SR. To identify unequivocally the type of TNFα+ cells, we performed a double staining immunohistochemistry with anti TNFα and anti GFAP antibodies. In CA1 SR of transgenic mice, we found a near complete colocalization of TNFα in GFAP+ astrocytes. Figure 41D-D2 show a group of TNFα+ astrocytes in the CA1 SR of a Tg 6M mouse. It is evident that all GFAP+ astrocytes (D1, red) express TNFα (D2, green), as evidenced by the yellow-orange colour in Figure 41D. The graph in Figure 41E shows the results of the quantitative analysis of TNFα+ cells in CA1 SR. We found a significant increase of density of TNFα+ cells in CA1 SR in Tg 6M (+410% vs WT) in comparison to WT (One-way ANOVA: $F(2,13)=8.712$, $P=0.0040$; Newman-Keuls post-test: $^{**}P<0.01$ Tg 6M vs WT, $^{\#}P<0.05$ Tg 6M vs Tg 3M; WT: n=6; Tg 3M: n=6; Tg 6M: n=5). In Tg 3M we found a slight, not significant increase of TNFα+ cells in comparison to WT (+187% vs WT).

In CA3 SR of transgenic mice, TNFα immunostaining increased. The double staining immunohistochemistry with anti TNFα (Figure 41I2, green), and anti GFAP antibodies (Figure 41I1, red) revealed that in CA3 SR of transgenic mice all GFAP+ astrocytes expressed TNFα, as evidenced by the yellow-orange colour in Figure 41I. TNFα+ astrocytes were quantified in CA3. The results showed that the density of TNFα+ astrocytes significantly increased in CA3 SR of Tg 6M in comparison to WT and to Tg 3M (+1646% vs WT; +393% vs Tg 3M) (Figure 41J). (One-way ANOVA: $F(2,12)=4.454$, $P=0.0358$; Newman-Keuls post-test: $^{*}P<0.05$ Tg 6M vs WT, $^{\#}P<0.05$ Tg 6M vs Tg 3M; WT: n=6; Tg 3M: n=6; Tg 6M: n=3). In CA3 SR, other structures, mainly located towards the DG were also positive for TNFα (Figure 41I2).

We compared the results obtained in CA1 to those obtained in CA3 by two-way ANOVA with ROIs and experimental groups as the two variables.

The statistical analysis on the density of TNFα+ cells revealed that in WT animals there was no significant difference between CA1 and CA3 SR while a significant increase was found in CA1 SR of Tg 3M and Tg 6M. Indeed, we found a significant main effect for ROIs (ROI, $F(1,25)=16.04$, $P<0.001$), experimental groups ($F(2,25)=13.94$, $P<0.001$), but no significant Interaction ($F(2,25)=1.326$, n.s.). Bonferroni post test showed that astrocytes density in CA1 SR of Tg 3M ($P<0.05$ vs CA3 SR) and Tg 6M ($P<0.05$ vs CA3 SP) was significantly higher than in CA3 SR.

Immunofluorescence staining with anti iNOS antibody (Figure 41 K, K2, green) was performed on hippocampal sections of TgCRND8 (Tg 3M, Tg 6M) and control mice (WT). Astrocytes were counterstained with anti GFAP antibody (Figure 41 K, K1, red) and neurons with anti NeuN antibody (not shown). Images of fluorescent immunostaining were taken in CA1 (Figure 41K-K2) and CA3 (not shown) hippocampal regions with confocal microscopy and the quantitative analysis of the density of iNOS+ cells was performed in CA1 and CA3 SR, separately.

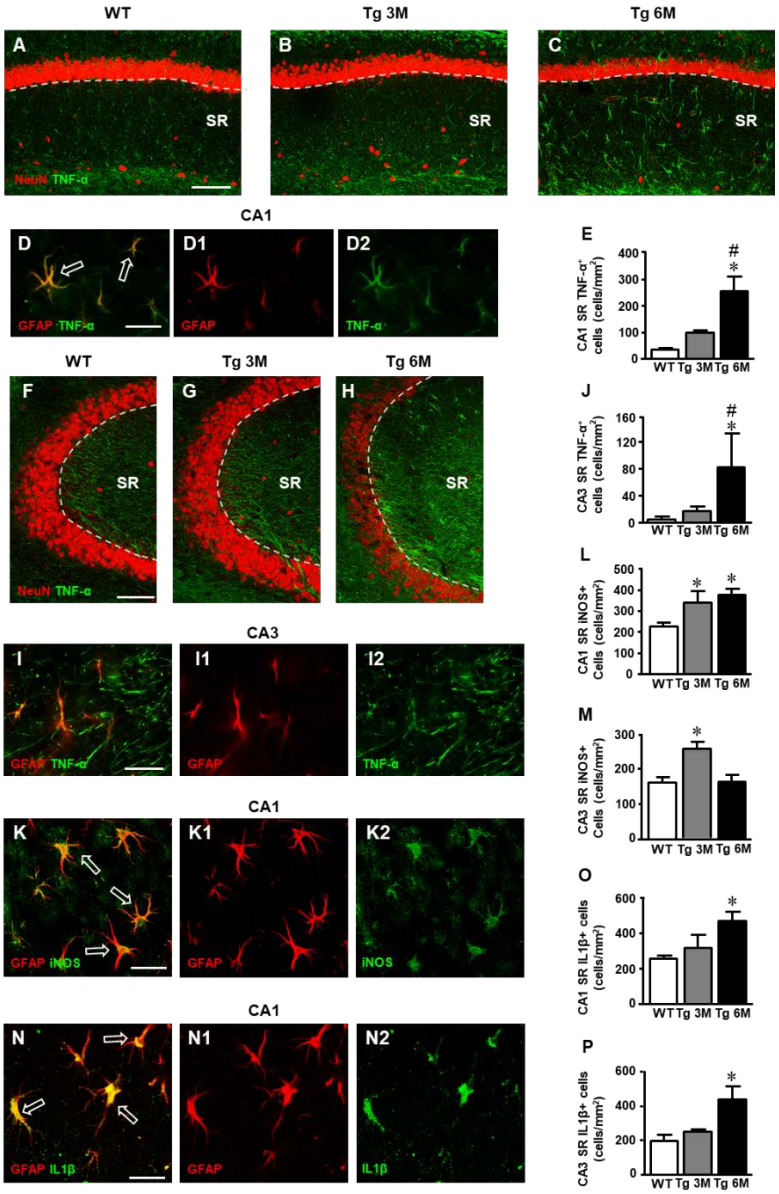

Figure 41. Analysis of TNFα cellular expression in CA1 and CA3 of WT, Tg 3M and Tg6M. **A-C:** Representative confocal photomicrographs of TNFα immunostaining (green) and NeuN immunostaining of neurons (red) in CA1 of a WT (A), a Tg 3M (B) and a Tg 6M (C). Scale bar: 100 µm. **D-D2:** Double staining immunohistochemistry with anti TNFα (green) and anti GFAP (red) antibodies. In CA1 SR we obtained a near complete colocalization of TNFα on astrocytes (GFAP+ cells). Scale bar: 25 µm. **E:** Quantitative analysis of $TNF\alpha^{+}$ cells/mm^2 in CA1 SR. TNFα+ cells were significantly more numerous in SR of Tg 6M vs WT mice. **F-H:**

Representative confocal photomicrographs of TNFα immunostaining (green) and NeuN immunostaining of neurons (red) in CA3 of a WT (H), a Tg 3M (I) and a Tg 6M (J). Scale bar: 100 μm. **I-I2:** Double staining immunohistochemistry with anti TNFα (green) and anti GFAP (red) antibodies in CA3 SR of Tg 6M mice. We found partial colocalization of TNFα in astrocytes. Scale bar: 25 μm. **J:** Quantitative analysis of $TNF\alpha^+$ cells/mm^2 in CA3 SR. $TNF\alpha^+$ cells were significantly more numerous in SR of Tg 6M vs WT mice. **K-K2**: Double staining immunohistochemistry with anti iNOS (green) and anti GFAP (red) antibodies in CA1 SR of Tg 6M mice. We found colocalization of iNOS in astrocytes. Scale bar: 25 μm. **L:** Quantitative analysis of $iNOS^+$ cells/mm^2 in CA1 SR. $iNOS^+$ cells were significantly more numerous in SR of Tg 3M and Tg 6M vs WT mice. **M**: Quantitative analysis of $iNOS^+$ cells/mm^2 in CA3 SR. $iNOS^+$ cells were significantly more numerous in SR of Tg 3M vs WT mice. **N-N2:** Double staining immunohistochemistry with anti IL1β (green) and anti GFAP (red) antibodies in CA1 SR of Tg 6M mice. We found colocalization of IL1β in astrocytes. Scale bar: 25 μm. **O:** Quantitative analysis of IL1β+ cells/mm^2 in CA1 SR. IL1β+ cells were significantly more numerous in SR of Tg 6M vs WT mice. **P:** Quantitative analysis of IL1β+ cells/mm^2 in CA3 SR. IL1β+ cells were significantly more numerous in SR of Tg 6M vs WT mice.

Double labelling confocal microscopy with anti iNOS (Figure 41K2) and anti GFAP (Figure 41K1) demonstrated that in CA1 SR of Tg 6M iNOS was expressed GFAP-positive astrocytes, as evidenced by the yellow-orange colour in Figure 41K (arrows). Double labelling confocal microscopy with anti iNOS and anti GFAP demonstrated that in CA3 SR of Tg 6M iNOS was expressed in GFAP+ astrocytes (not shown).

We found a significant increase of iNOS expression in cells in CA1 SR of Tg 3M (+51%) and of Tg 6M (+66%) in comparison to WT. The statistical analysis was performed on the density of iNOS+ cells in CA1 SR (One-way ANOVA: $F(2,13)=5.12$, $P=0.0268$; Newman-Keuls post-test: *$P<0.05$ Tg 3M and, *$P<0.05$ Tg 6M vs WT; WT: n=5; Tg 3M: n=4; Tg 6M: n=5; Figure 41L).

We found a significant increase of iNOS expression in cells of CA3 SR of Tg 3M (+58%), while in Tg 6M iNOS expression in cell was not different from control values (+1%) in comparison to WT mice. The statistical analysis was performed on the density of iNOS+ cells in CA3 SR (One-way ANOVA: $F(2,11)=8.762$, $P=0.0077$; Newman-Keuls post-test: *$P<0.05$ Tg 3M vs Tg 6M and WT; WT: n=4; Tg 3M: n=4; Tg 6M: n=4; Figure 41M). Both in CA1 SR and CA3 SR iNOS was also expressed in neurons, but the effect was not different from WT mice (data not shown).

We compared the results obtained in CA1 to those obtained in CA3 by two-way ANOVA with ROIs and experimental groups as the two variables.

The statistical analysis on the density of iNOS+ cells revealed that in WT and Tg 3M animals there was no significant difference between CA1 and CA3 SR while a significant increase was found in CA1 SR of Tg 6M. We found a significant main effect for ROIs ($F(1,20)=25.23$, $P<0.001$), experimental groups ($F(2,20)=6.513$, $P<0.01$), and

for Interaction ($F(2,20)=3.540$, $P<0.05$). Bonferroni post test showed that the density of iNOS+ cells in CA1 SR of Tg 6M was significantly higher than in CA3 SR ($P<0.001$).
Immunofluorescence staining with anti IL1β antibody (Figure 41N, N2, green) was performed on hippocampal sections of TgCRND8 (Tg 3M, Tg 6M) and control mice (WT). Astrocytes were counterstained with anti GFAP antibody (Figure 41N, N1, red) and microglia with anti CD68 antibody (not shown).
Images of fluorescent immunostaining were taken in CA1 (Figure 41N-N2) and CA3 hippocampal regions (not shown) with confocal microscopy and the quantitative analysis of the density of + cells were performed in CA1 and CA3 SR, separately. Double labelling confocal microscopy with anti IL1β (Figure 41N2) and anti GFAP (Figure 41N1) demonstrated that in CA1 SR of Tg 6M, IL1β was expressed in GFAP+ astrocytes, as evidenced by the yellow-orange colour in Figure 41N (arrows). Double labelling confocal microscopy with anti IL1β and anti GFAP demonstrated that in CA3 SR of Tg 6M, IL1β was expressed in GFAP+ astrocytes (not shown).
We found a slight increase of IL1β expression in cells in CA1 SR of Tg 3M (+25%, not significant) and a significant increase in CA1 SR of Tg 6M (+83%) in comparison to WT mice. The statistical analysis was performed on the density of IL1β+ cells in CA1 SR (One-way ANOVA: $F(2,11)=5.733$, $P=0.0248$; Newman-Keuls post-test: *$P<0.05$ Tg 6M vs WT; WT: n=4; Tg 3M: n=3; Tg 6M: n=5; Figure 41O).
We found a slight significant increase of IL1β expression in cells of CA3 SR of Tg 3M (+28%, not significant), while in Tg 6M IL1β expression in cells was significantly higher than in WT (+122%). The statistical analysis was performed on the density of IL1β+ cells in CA3 SR (One-way ANOVA: $F(2,11)=4.730$, $P=0.0394$; Newman-Keuls post-test: *$P<0.05$ Tg 6M vs WT; WT: n=4; Tg 3M: n=3; Tg 6M: n=5; Figure 41P).
Two-way ANOVA analysis demonstrated that IL1β expression in cells was not significantly different in CA1 SR in comparison to CA3 SR of all groups examined.
Both in CA1 SR and CA3 SR IL1β was also expressed in microglia, but the effect was not different from WT mice (data not shown).

4.14 Characterization of neurons in CA1 and CA3 pyramidal layers in TgCRND8 mice

We evaluated the time-course of the extent of damage of CA1 and CA3 pyramidal neurons in Tg mice using the immunohistochemical staining of neurons with anti NeuN antibody (red) on hippocampal sections of TgCRND8 mice at 3 (Tg 3M) and 6 months

of age (Tg 6M) and of WT control mice. Images of fluorescent immunostaining were taken in CA1 (Figure 42A-C) and CA3 hippocampal regions (Figure 42H-J) with confocal microscopy and the quantitative analyses of the density (Figure 42D) and the volume of pyramidal neurons (Figure 42F), and of thickness of the pyramidal layer (Figure 42E) were performed.

The graphs in Figure 42D-F show the results of the quantitative analyses in CA1. The density of neurons was significantly lower in CA1 SP of Tg mice at 3 (-15% vs WT) and 6 months (-28% vs WT) of age than in CA1 of WT mice (Figure 42D). (One-way ANOVA: $F(2,12)=9.552$, $P=0.0033$; Newman-Keuls post-test: **$P<0.01$ Tg 6M vs WT, *$P<0.05$ Tg 3M vs WT, $^{\#}P<0.05$ Tg 6M vs Tg 3M; WT: n=5; Tg 3M: n=6; Tg 6M: n=4). Consistently, we found a reduction of CA1 SP thickness in 3 (-12%) and 6 months (-40%) aged Tg mice in comparison to WT mice (Figure 42E). The effect was statistically significant at 6 months of age only (One-way ANOVA: $F(2,10)=4.658$, $P=0.0372$; Newman-Keuls post-test: *$P<0.05$ Tg 6M vs WT; WT: n=4; Tg 3M: n=5; Tg 6M: n=4). Also, we found a statistically significant reduction of the average volume of CA1 pyramidal neurons both at 3 (-36% vs WT) and 6 months (-42% vs WT) of age in comparison to WT mice (Figure 42F). (One-way ANOVA: $F(2,12)=23.50$, $P<0.0001$; Newman-Keuls post-test: ***$P<0.001$ Tg 3M vs WT, Tg 6M vs WT; WT: n=5; Tg 3M: n=6; Tg 6M: n=4).

Correlation analysis between the number of CA1 Pyramidal neurons and the thickness of CA1 Pyramidal layer is shown in the graph in Figure 42G. We found a highly significant correlation between the two parameters (**$P=0.01$, $R^2=0.5763$; WT: n=5; Tg 3M: n=6; Tg 6M: n=4).

We analysed the density of CA3 pyramidal neurons, their volume and the thickness of CA3 SP. Surprisingly, the density of CA3 pyramidal neurons in SP of Tg 3M and Tg 6M (-8% vs WT, Figure 42K) (One-way ANOVA: $F(2,12)=2.933$, $P=0.0918$, n.s.; WT: n=5; Tg 3M: n=6; Tg 6M: n=4) and the thickness of the pyramidal layer (+19% vs WT, Figure 42L) (One-way ANOVA: $F(2,12)=1.897$, $P=0.1923$, n.s.; WT: n=5; Tg 3M: n=6; Tg 6M: n=4) were not significantly different from WT mice.

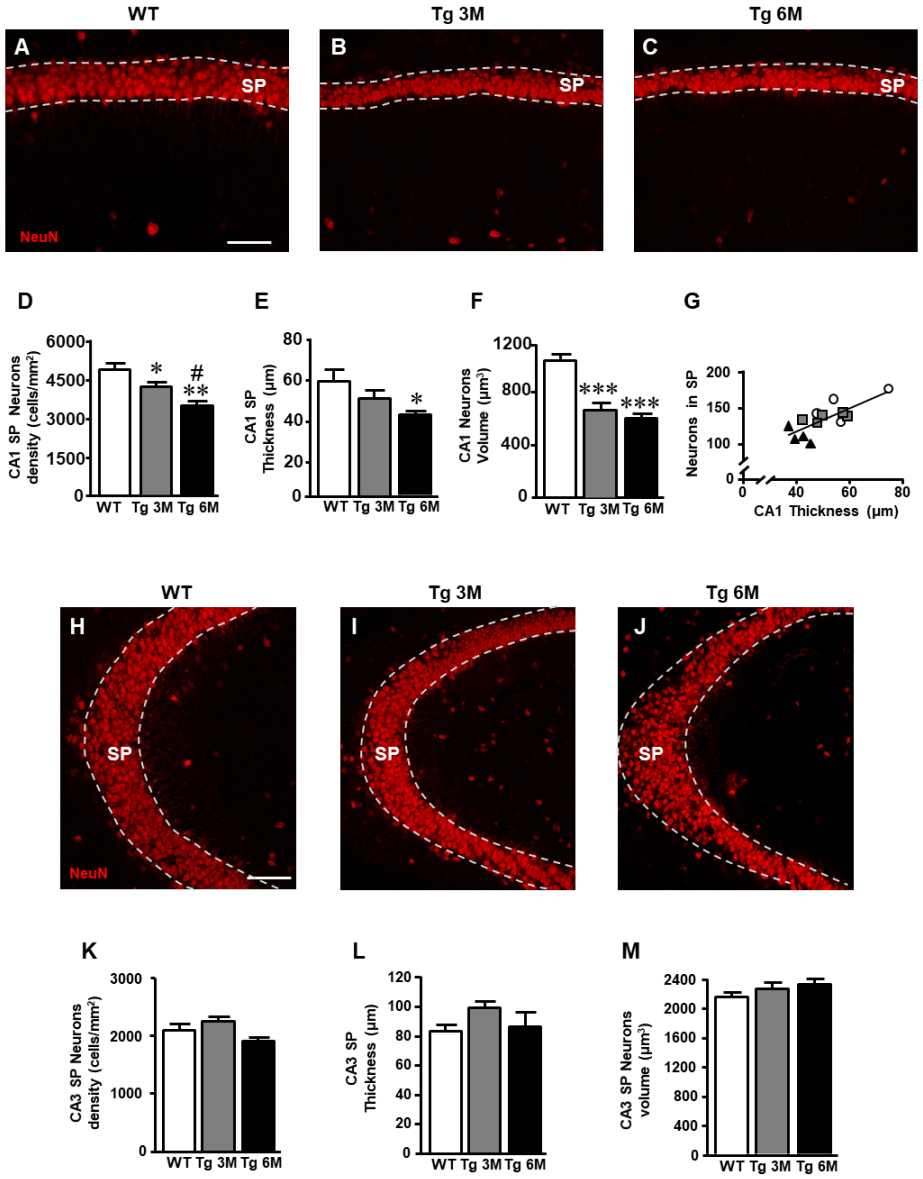

Figure 42. Analysis of neurons in CA1 and CA3 of WT, Tg 3M and Tg 6M. **A-C:** Representative confocal photomicrographs of NeuN immunostaining of neurons (red) in CA1 of a WT (A), a Tg 3M (B) and a Tg 6M (C). Scale bar: 60 µm. **D:** Quantitative analysis of neurons/mm^2 in CA1 SP (D) of WT, Tg 3M and Tg 6M. Neurons were significantly less numerous in SP of Tg 6M and Tg 3M vs WT mice. **E:** Measure of thickness of CA1 SP (E) of WT, Tg 3M and Tg 6M. Thickness of CA1 SP was significantly reduced in Tg 6M vs WT. **F:** Measure of neurons volume in CA1 SP (F) of WT, Tg 3M and Tg 6M. Neurons volume was significantly reduced in Tg 6M and Tg 3M vs WT. **G:** Correlation analysis between number of CA1 SP neurons and CA1 SP thickness. There is a highly significative correlation. **H-J:** Representative confocal photomicrographs of NeuN immunostaining of neurons (red) in CA3 of a WT (H), a Tg 3M (I) and a Tg 6M (J). Scale bar: 60 µm. **K:** Quantitative analysis of neurons/mm^2 in CA3 SP (K) of WT, Tg 3M and Tg 6M. There are no significant differences in SP of Tg 6M and Tg 3M vs WT mice. **L:** Measure of thickness of CA3 SP (L) of WT, Tg 3M and Tg 6M. There are no significant differences in thickness of CA3 SP of Tg 6M and Tg 3M vs WT. **M:** Measure of neurons volume in CA3 SP (M) of WT, Tg 3M and Tg 6M. There are no significant differences in neurons volume in CA3 SP of Tg 6M and Tg 3M vs WT. Data reported in all graph bars are expressed as mean±SEM.

Also, the average volume of CA3 pyramidal neurons of transgenic mice at 3 and 6 months of age was not significantly different from WT mice (Figure 42M) (One-way ANOVA: F(2,12)=1.268, P=0.3165, n.s.; WT: n=5; Tg 3M: n=6; Tg 6M: n=4), as shown by the statistical analysis , as shown by the statistical analysis.

4.15 Quantitative analysis of apoptotic neurons in CA1 and CA3 hippocampus of TgCRND8 mice

We performed a double staining immunohistochemistry with anti CytC (red) and anti NeuN (green) antibodies on hippocampal sections of TgCRND8 at 3 (Tg 3M) and 6 months of age (Tg 6M) and of WT control mice.-Images of fluorescent immunostaining were taken in CA1 (Figure 43A-C, A1-C1) and CA3 hippocampal regions (Figure 43F-H, F1-H1) with epifluorescence microscopy. Figure 43D-D2 shows a CytC+ neuron (arrow) in CA1 SP at a higher magnification, acquired with laser confocal microscopy.

We performed the quantitative analyses of apoptotic neurons in CA1 and CA3 SP. We found a statistically significant increase of density of apoptotic neurons in CA1 of Tg mice at 3 (+129%) and 6 months (+82%) of age in comparison to WT mice (Figure 43E). (One-way ANOVA: F(2,13)=9.956, P=0.0024; Newman-Keuls post-test: **P<0.01 Tg 3M vs WT, *P<0.05 Tg 6M vs WT; WT: n=4; Tg 3M: n=6; Tg 6M: n=6).

The analysis of CytC+ neurons performed in CA3 SP showed a slight, not statistically significant increase at 6 months of age (+36%) in comparison to WT mice, as shown by qualitative (Figure 43F-H1) and quantitative analyses (Figure 43I) (One-way ANOVA: F(2,12)=0.890, P=0.4362, n.s.; WT: n=4; Tg 3M: n=6; Tg 6M: n=5).

We compared the results obtained in CA1 to those obtained in CA3 by two-way ANOVA with ROIs and experimental groups as the two variables.

Two-way ANOVA analysis demonstrated that apoptotic neurons were not significantly different in CA1 SP in comparison to CA3 SP of all groups examined (WT, Tg 3M and Tg 6M). Nevertheless, the percent increase of apoptotic neurons in CA1 SP of Tg 3M and Tg 6M was significantly higher than in CA3 SP (see Table 8).

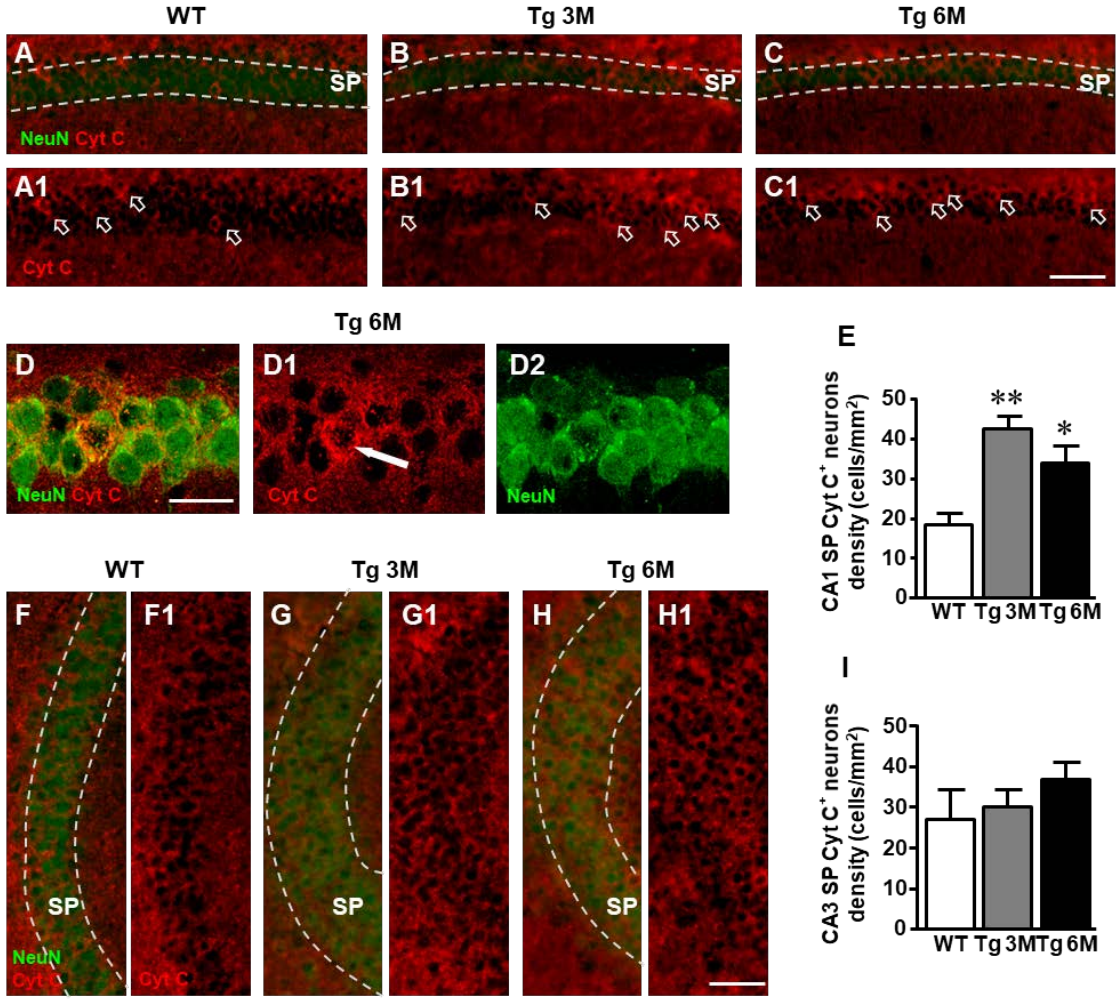

Figure 43. Analysis of apoptotic neurons in CA1 and CA3 of WT, Tg 3M and Tg 6M. **A-C1:** Representative epifluorescence photomicrographs of Cyt C immunostaining of apoptotic neurons (red) and NeuN immunostaining of neurons (green) in CA1 SP of WT (A-A1), a Tg 3M (B-B1) and a Tg 6M (C-C1). The arrows in A1, B1 and C1 point to apoptotic neurons in CA1 SP. Scale bar: 100 µm. **D-D2:** Confocal magnification of apoptotic neurons in CA1 SP of a Tg 6M. Scale bar: 30 µm. **E:** Quantitative analysis of apoptotic neurons/mm^2 in CA1 SP of WT, Tg 3M and Tg 6M. Apoptotic pyramidal neurons were significantly more numerous in SP of Tg 3M and Tg 6M vs WT mice. **F-H1:** Representative epifluorescence photomicrographs of Cyt C immunostaining of apoptotic neurons (red) and NeuN immunostaining of neurons (green) in CA3 SP of WT (F-F1), a Tg 3M (G-G1) and a Tg 6M (H-H1). The arrows in F1, G1 and H1 point to apoptotic neurons in CA3 SP. Scale bar: 100 µm. **I:** Quantitative analysis of apoptotic neurons/mm^2 in CA3 SP of WT, Tg 3M and Tg 6M. There are no significant differences in SP of Tg 6M and Tg 3M vs WT mice. Data reported in all graph bars are expressed as mean±SEM

4.16 Analysis of neuron-astrocytes-microglia triad in CA1 and CA3 hippocampus of TgCRND8 mice

To evaluate the presence of neuron-astrocytes-microglia triads in CA1 and CA3 SR, we performed triple staining immunohistochemistry with anti NeuN, anti GFAP and anti IBA1 antibodies on hippocampal sections of TgCRND8 (Tg 3M, Tg 6M) and control mice (WT). Images of fluorescent immunostaining were taken in CA1 (Figure 44A-C)

and CA3 (Figure 44D-F) hippocampal regions with confocal microscopy and the quantitative analysis of the density of the triads was performed in CA1 and CA3 SR.

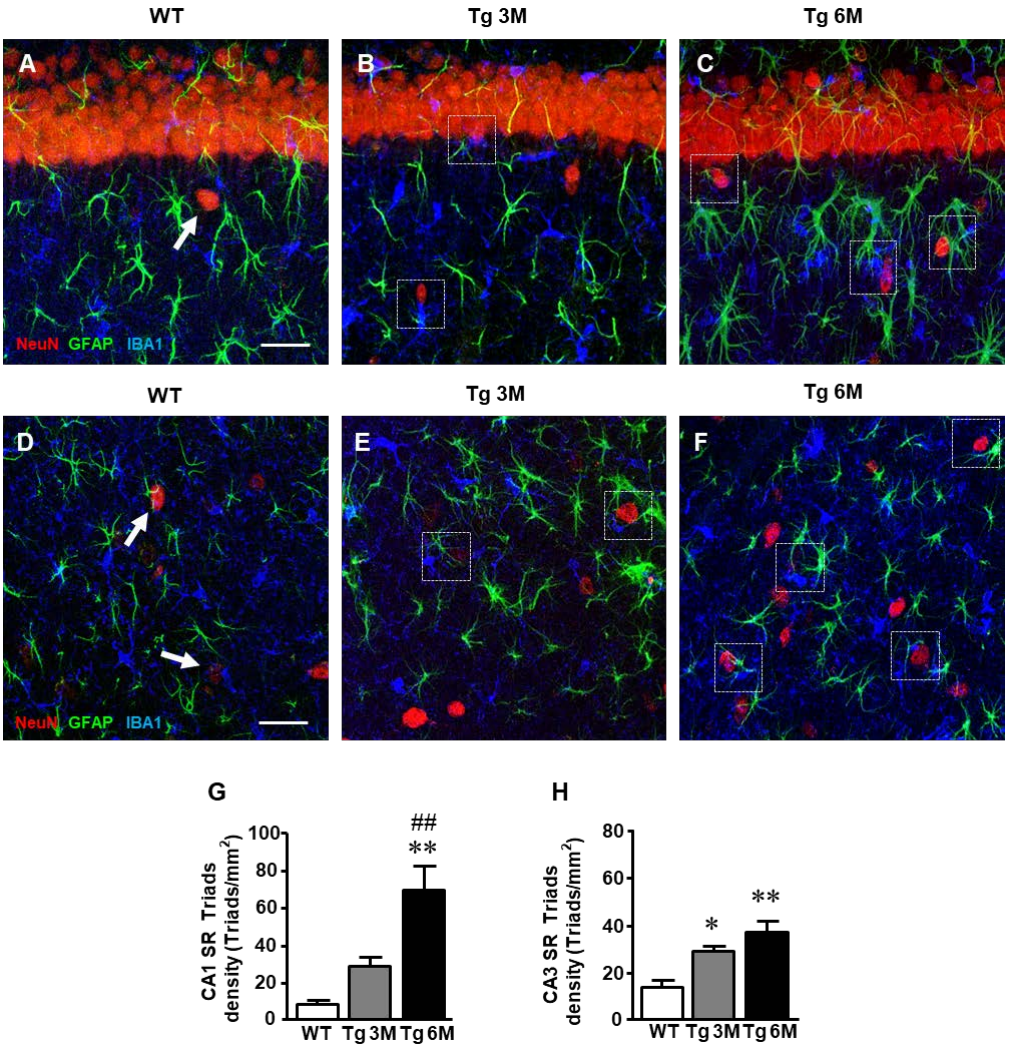

Figure 44. Characterization and quantification of the neuron-astrocyte-microglia triads in CA1 and CA3 SR of WT, TG 3M and TG 6M mice. **A-C:** Representative confocal photomicrographs of triple immunostaining of neurons (NeuN, red), astrocytes (GFAP, green) and microglia (IBA1, blue) in the CA1 SR of a WT(A), a TG 3M (B), and of a TG 6M mouse (C). Scale bar: 40 µm. **D-F:** Representative confocal photomicrographs of triple immunostaining of neurons (NeuN, red), astrocytes (GFAP, green) and microglia (IBA1, blue) in the CA3 SR of a WT(D), a TG 3M (E), and of a TG 6M mouse (F). Scale bar: 40 µm. Examples of triads in Tg 3M and Tg 6M are shown in the framed areas (B-C, E-F). In WT mice (A-D) groups of neuron-astrocyte-microglia not considered as triads are pointed by arrows. **G-H:** Quantitative analysis of neuron-astrocyte-microglia triads/mm^2 in CA1 (G) and CA3 (H) SR. Triads are significantly more numerous in CA1 SR of Tg 6M vs WT mice. In CA3 SR, triads are significantly more numerous in Tg 3M and Tg 6M than in WT mice. Data reported in all graph bars are expressed as mean±SEM.

The presence of triads in CA1 and CA3 SR is shown qualitatively in Fig 8A-C and 8 D-E, respectively. The Quantitative analysis of triads in CA1 SR is shown in the graph in Figure 44G. We found a statistically significant increase of triads density in CA1 SR of

Tg 6M (+ 674%) in comparison with WT mice (One-way ANOVA: $F(2,8)=12.66$, $P=0.0033$; Newman-Keuls post-test: **P<0.01 Tg 6M vs WT, ##P<0.01 Tg 6M vs Tg 3M; WT: n=3; Tg 3M: n=4; Tg 6M: n=4).

In CA3 SR, we found a statistically significant increase of triads density both in Tg 3M (+111%) and Tg 6M (+170%) in comparison to WT mice (Figure 44H). (One-way ANOVA: $F(2,9)=11.55$, $P=0.0033$; Newman-Keuls post-test: *P<0.05 Tg 3M vs WT, **P<0.01 Tg 6M vs WT; WT: n=4; Tg 3M: n=4; Tg 6M: n=4).

We compared the results obtained in CA1 to those obtained in CA3 by two-way ANOVA with ROIs and experimental groups as the two variables.

The statistical analysis on the density of triads revealed that in WT and Tg 3M animals there was no significant difference between CA1 and CA3 SR while a significant increase was found in CA1 SR of Tg 6M. Indeed, we found a significant main effect for experimental groups ($F(2,17)=21.97$, $P<0.001$), and for Interaction ($F(2,17)=5.134$, $P<0.05$), but not for ROIs ($F(1,17)=3.148$; n.s.). Bonferroni post test showed that the density of triads in CA1 SR of Tg 6M was significantly higher than in CA3 SR ($P<0.01$).

4.17 Comparisons between CA1 and CA3

The most salient differences between CA1 and CA3 are reported in Table 8. Each column represents the percent variation, normalized to the control values found in WT mice, of each parameter investigated in transgenic mice at 3 and 6 months of age. The differences between the parameters investigated in CA1 and CA3 at 3 or 6 months of age, were then evaluated using the Student's t test. It is evident from the data in the table that astrogliosis was higher in CA1, both in terms of density of astrocytes and of length of astrocyte-branches. The number of IBA1+ microglia did not vary significantly between the two areas, while CD68+ microglia was more pronounced in both SP and SR of CA3. TNFα showed a very peculiar characteristic: it was expressed by astrocytes in CA1 SR, while in CA3 it was present not only in astrocytes, but also in other structures. The percent variation of iNOS was higher in CA1 SR at 3 months of age, while that of IL1β varied similarly in CA1 and CA3 SR at 3 and 6 months of age. CA1 pyramidal neurons of transgenic mice were significantly smaller and less numerous than those of WT mice, causing significant shrinkage of CA1 SP. On the contrary, CA3 pyramidal neurons of transgenic mice did not change significantly, in terms of both number and volume and did not show significant increase of apoptosis, even at 6

months of age. The decrease of CA1 pyramidal neurons possibly was caused, at least in part, by increase of apoptotic mechanisms, which indeed were significantly more pronounced in CA1 than in CA3 SP. Interestingly, neuron-astrocytes-microglia triads were more numerous in CA1 SR than in CA3 SR. Astrocytes and microglia, forming triads with neurons, help clearing apoptotic and degenerating neurons at higher degree in CA1, in comparison to CA3.

Table 8. Differences between CA1 and CA3 in all parameters investigated.

	Tg 3M		**Tg 6M**	
	CA1	**CA3**	**CA1**	**CA3**
Density of astrocytes in SP	+43	+8	+65**	+5
Intensity of GFAP in SR	+33	+13	+32	+8
Length of astrocyte branches in SR	+17**	-3	+32**	-5
Density of IBA1+ microglia in SP	+7	+2	+35	+46
Density of IBA1+ microglia in SR	+1	-2	+72	+48
Density of CD68+ microglia in SP	+82	+252	+347*	+1,448
Density of CD68+ microglia in SR	+36	+940	+902*	+3,395
Volume of CD68+ microglia in SR	+ 487*	+170	+626	+434
Density of triads in SR	+219	+111	+674**	+170
Density of TNF-α+ cells in SR	+187	+254	+410	+1646
iNOS	+50.75	+58.86	+65.87*	+1.342
IL1β	+25.11	+28.38	+83.55	+122.5
Density of Cyt C+ neurons in SP	+129***	+10	+82	+36
Density of neurons in SP	-15**	+7	-28**	-8
Volume of neurons in SP	-36***	+5	-42***	+8
Thickness of SP	-12**	+19	-40*	+3

All data represent percent differences from WT, taken as 100%. *P<0.05; **P<0.01; ***P<0.001 in comparison to CA3 (Student's t test).

IN VIVO AND *IN VITRO* MODELS OF BRAIN ISCHEMIA

Part IV – In vivo model of ischemia

4.18 Analysis of neurons and neuronal debris in CA3 Stratum Pyramidale, Stratum Lucidum and Stratum Radiatum of sham, 2VO-vehicle, and 2VO-dipyridamole treated rats

In order to evaluate whether chronic ischemia may cause loss of neurons in area CA3 of the hippocampus, we performed an analysis of neurons immunolabelled with anti NeuN antibody in SP, SL and SR of CA3 of sham (SHAM), 2VO-vehicle, and 2VO-dipyridamole treated rats (Figure 45A-C).

Our results demonstrated that there was no significant decrease of CA3 pyramidal neurons in the hippocampus of 2VO-vehicle in comparison to controls (One-way Anova: $F_{(2,14)}$=0.9879, ns, Figure 45D).

It has been reported that SL of area CA3 is mainly a-neuronal (Amaral and Lavenex, 2007). Nevertheless, immunostaining of neurons using the anti NeuN antibody revealed the presence of numerous neurons, that we defined "*ectopic*", scattered throughout the SL of 2VO-vehicle and 2VO-dipyridamole treated rats. Quantitative analysis in Figure 45F (plain columns) showed that ectopic neurons were significantly more numerous in the SL of 2VO-vehicle rats (+78%) and of 2VO-dipyridamole treated rats (+140%) in comparison to sham rats (One-way ANOVA: $F_{(2,13)}$=15.14, P<0.001; Newman-Keuls post test: *P<0.05 2VO-vehicle vs sham, ***P<0.001 2VO-dipyridamole treated rats vs Sham).

Ectopic neurons were significantly more numerous in SR of 2VO-vehicle (+103%) and of 2VO-dipyridamole treated rats (+98%) in comparison to sham rats (One-way ANOVA, $F_{(2,14)}$=29.65, P<0.001, Newman-Keuls post test, ***P<0.001 2VO-dipyridamole treated rats vs Sham, 2VO-vehicle vs Sham). In both SL and SR, we found no significant differences in the number of ectopic neurons between 2VO-vehicle and 2VO-dipyridamole treated rats.

It has been described that interneurons in the CA3 SL are calretinin+ and are known to be sensitive to ischemia (Freund and Magloczky, 1993; Hsu and Buszaki, 1993). We thus performed calretinin immunostaining of CA3 interneurons (Molgaard et al., 2014). The anti calretinin antibody revealed the presence of many interneurons, mainly located

in SL CA3, as shown in Figure 45E-E3. Quantitative analysis in Figure 45F (hatched columns) showed that the density of calretinin+ interneurons was not different in 2VO-vehicle rats or in 2VO-dipyridamole treated rats in comparison to sham rats in both SL and SR. On the other hand, statistical analysis showed that calretinin+ interneurons were significantly less numerous than ectopic neurons in SL of 2VO-vehicle rats or in 2VO-dipyridamole treated rats and in SR of sham and 2VO-vehicle rats or in 2VO-dipyridamole treated rats ($^{\#}$ $P < 0.05$ and $^{\#\#}$ $P < 0.01$ vs ectopic neurons, two-tailed Student's t test, Figure 45F). These latter results indicated that the increased ectopic neurons in 2VO-vehicle rats or in 2VO-dipyridamole treated rats were not calretinin+ interneurons. From the graph in Figure 45F it is also evident that calretinin+ interneurons were significantly more numerous in SL than in SR of all experimental groups.

As already demonstrated (Cerbai et al., 2012; Lana et al., 2014), astrocytes branches infiltrating the neuronal cell body seem to be fragmenting ectopic neurons to form neuronal debris, thus cooperating with the microglia in phagocytic events (see below). NeuN staining revealed the presence of neuronal debris (Figure 46A and see Methodological considerations) scattered throughout the CA3 SL and SR of sham, 2VO-vehicle and 2VO-dipyridamole rats. Figure 46A shows a magnification of the framed area in Figure 46B. The dotted circles evidence the dimensions of neuronal debris in comparison to a neuron (open arrow). In the GFAP and NeuN double stained slice shown in Figure 46B, which represents a sub-slice obtained stacking 15 consecutive confocal z scans (0.3 µm each, total thickness 4.5 µm) starting at a depth of 3 µm into the slice, it is clearly visible a neuronal debris closely apposed to GFAP+ astrocyte branches (dotted circle). In the Figures 46 A-B it is also possible to appreciate the size difference between the debris and a healthy neuronal cell body (open arrow). Quantitative analysis showed that neuronal debris were significantly more numerous in CA3 SL of 2VO-vehicle rats (+103%) than in sham rats (Figure 46C) and this effect was reverted in 2VO-dipyridamole rats (+29%), as shown by statistical analysis (one way ANOVA $F_{(2,11)}=8.654$; $P=0.0055$; $^{*}P<0.05$ vs the two other groups, Newman-Keuls Multiple Comparison Test). Quantitative analysis in SR showed that neuronal debris were significantly more numerous in CA3 SR of 2VO-vehicle rats (+82%) than in sham rats and this effect was reverted in 2VO-dipyridamole rats (+33%), as shown by statistical analysis (one way ANOVA $F_{(2,12)}=8.133$; $P<0.0059$; * $P<0.001$ vs the two other groups, Newman-Keuls Multiple Comparison Test) (Figure 46C). From the graph

in Figure 46C it is also evident that neuronal debris were significantly more numerous in SL than in SR of all experimental groups.

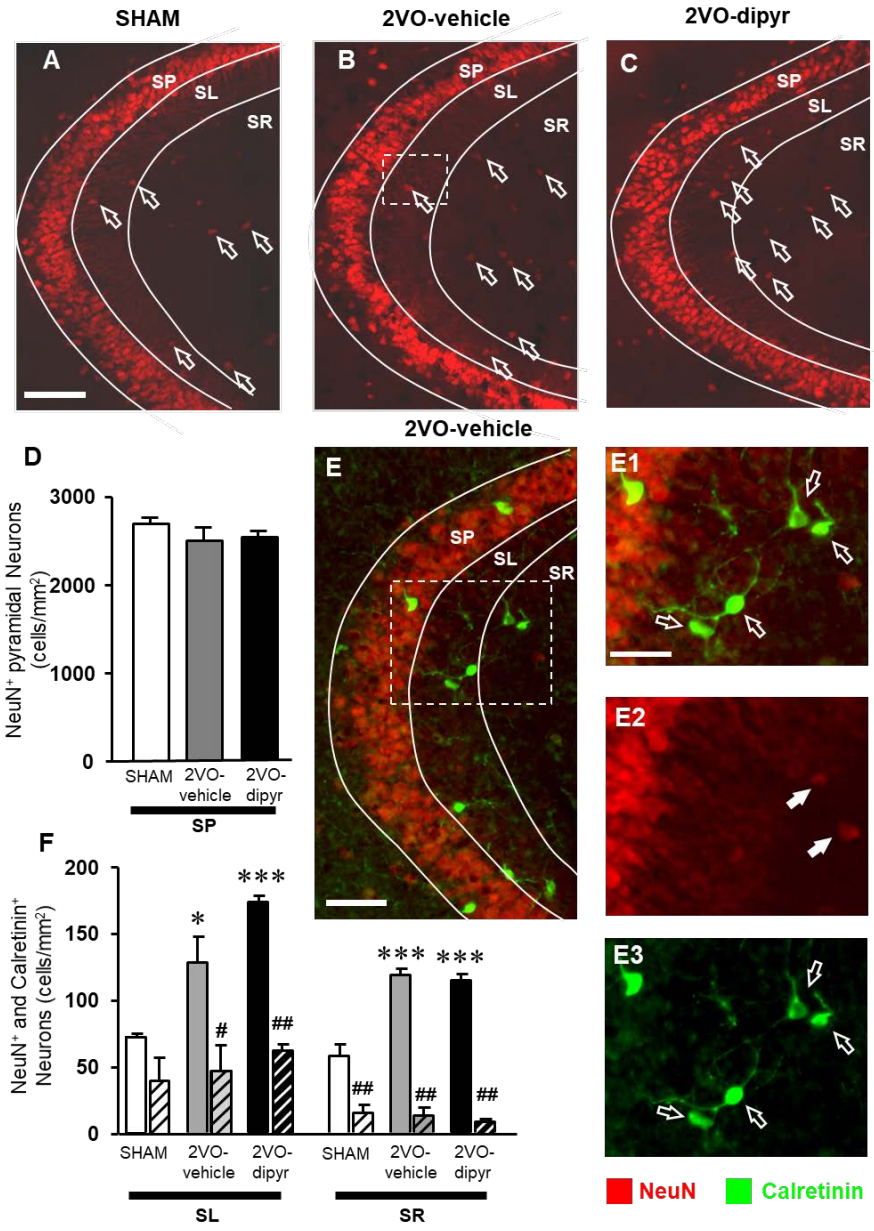

Figure 45. Immunohistochemical analysis of neurons with anti NeuN antibody in SP, SL and SR of CA3 of sham, 2VO-vehicle and 2VO-dipyridamole rats. **A-C:** Representative photomicrographs of NeuN immunostaining (red) of neurons in CA3 of sham (A), 2VO-vehicle (B), and 2VO-dipyridamole rats (C). The white lines indicate the borders of CA3 subregions SP, SL and SR. Scale bar: 80 µm. **D:** Quantitative analysis of NeuN+ pyramidal neurons (cells/mm2) in CA3 SP of sham (white columns), 2VO-vehicle (grey columns) and 2VO-dipyridamole rats (black columns). Data in graph bars are mean±SEM. SP: sham, n=5; 2VO-vehicle, n=5; 2VO-dipyridamole, n=5. **E-E3:** Representative photomicrographs of double immunostaining for neurons (red) and interneurons with anti calbinding antibody (green, open arrows) in CA3 SP, SL and SR of a 2VO-vehicle rat. Scale bar: 60 µm. **E1-E3:** Magnification of the framed area in panel E showing the calretinin interneurons (open arrows, E1) and ectopic neurons (E2, white arrows. Scale bar: 30 µm. **F:** Quantitative analysis of NeuN+ ectopic

neurons (cells/mm^2) and calretinin+ interneurons in CA3 SL and SR of sham (white columns), 2VO-vehicle (grey columns) and 2VO-dipyridamole rats (black columns). Data in graph bars are mean±SEM. SL: sham, n=4; 2VO-vehicle, n=5; 2VO-dipyridamole, n=5. SR: sham, n=5; 2VO-vehicle, n=5; 2VO-dipyridamole, n=5. Ectopic neurons: plain columns; Calretinin+ interneurons: hatched columns. Please note the different range of the Y-axis between panels D and F.

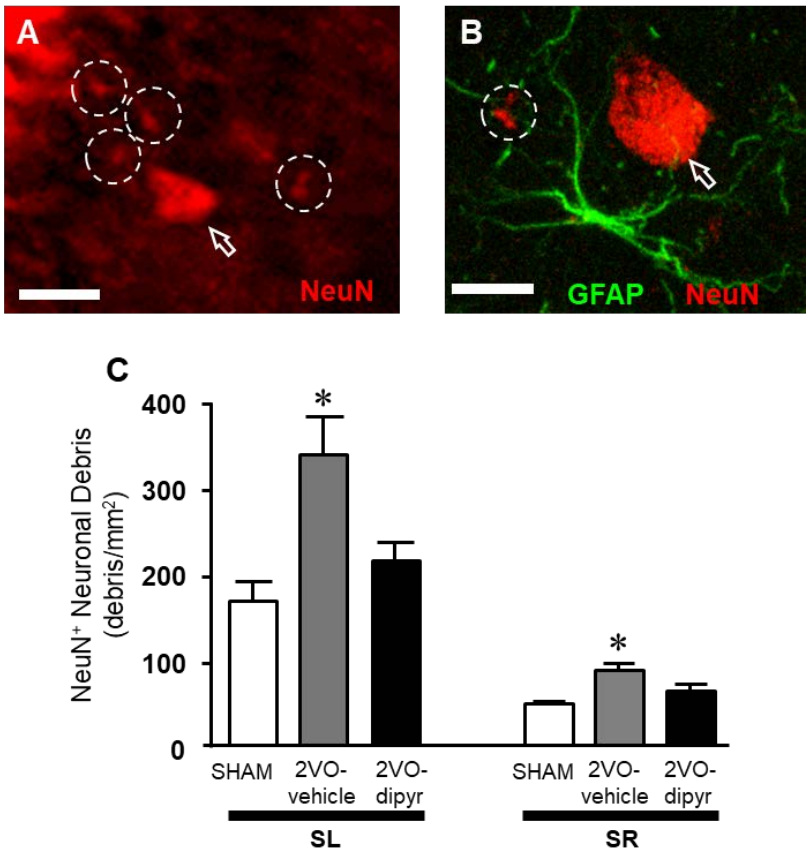

Figure 46. Examples of neuronal debris. **A:** magnification of the framed image in Figure 2B showing the size difference between a neuron (open arrow) and neuronal debris (circles). Scale bar: 15 µm. **B:** double immunofluorescent staining of astrocytes (GFAP, green) and neurons (NeuN, red) that shows a neuronal debris (circle) closely apposed to astrocyte branches. Scale bar: 10 µm. **C:** Quantitative analysis of NeuN+ neuronal debris (debris/mm^2) in CA3 SL and SR of sham (white columns), 2VO-vehicle (grey columns) and 2VO-dipyridamole rats (black columns). Data in graph bars are mean±SEM. SL: sham, n=5; 2VO-vehicle, n=4; 2VO-dipyridamole, n=5. SR: sham, n=5; 2VO-vehicle, n=5; 2VO-dipyridamole, n=5.

4.19 Analysis of apoptotic neurons in CA3 stratum pyramidale of sham, 2VO-vehicle, and 2VO-dipyridamole treated rats

It was previously demonstrated, in a similar animal model of chronic hypoperfusion, that CA1 pyramidal neurons undergo apoptotic death between 2 and 25 weeks after the onset of 2VO (Bennett et al., 1998; Lana et al., 2014). Therefore, in order to verify in our model whether CA3 pyramidal neurons were also undergoing apoptsis, hippocampal sections from sham, 2VO-vehicle, and 2VO-dipyridamole rats were triple

immunostained with anti NeuN for neurons (green), with anti CytC for apoptosis (red), and with anti IBA1 for microglia (blue) (Figure 47). The presence of a diffuse CytC immunostaining in the cytoplasm is highly visible in some pyramidal neurons of CA3 SP (open arrows in Figure 47A-C, that show the merged immunostaining of NeuN and CytC). Figure 47D represents the magnification of the framed area in Figure 47B showing the diffuse CytC immunostaining in the cytoplasm of two apoptotic neurons. All CytC+ cells in SP were neurons since they were also NeuN+. CytC+ neurons in SP were counted

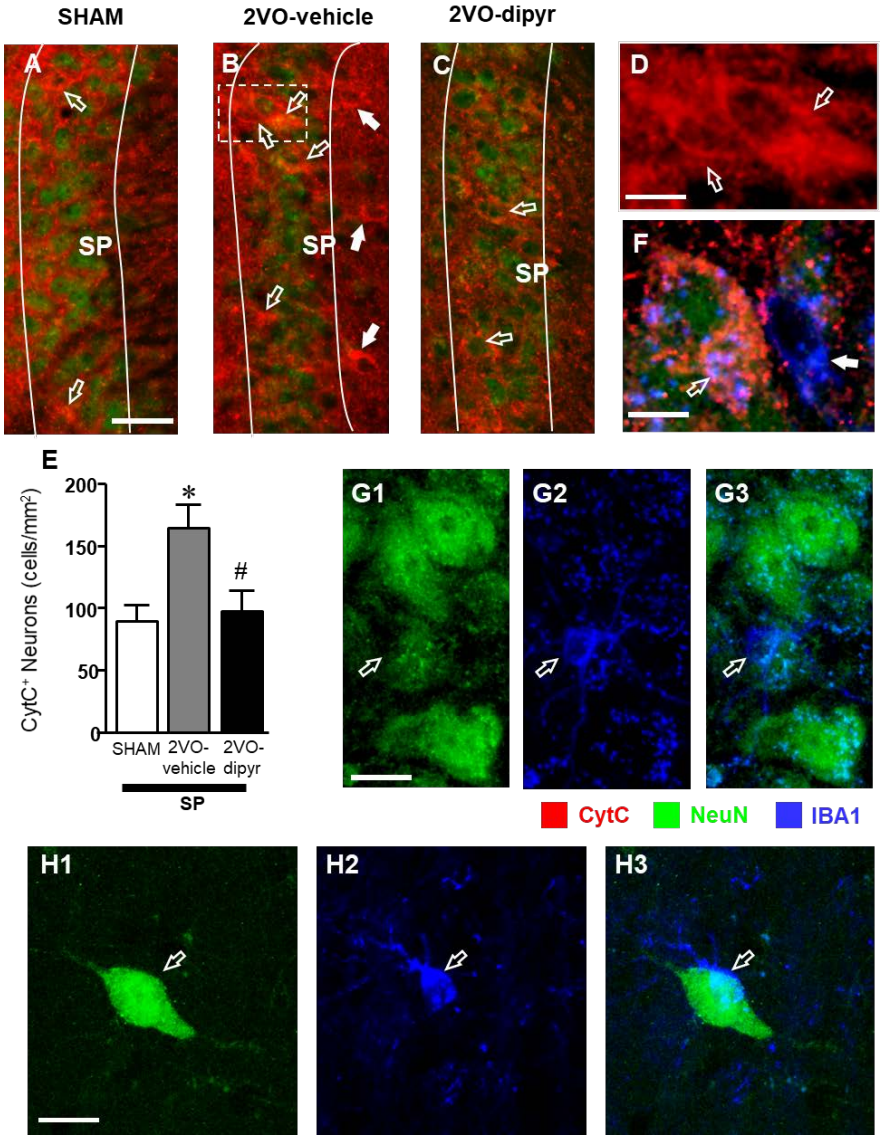

Figure 47. Analysis of apoptotic pyramidal neurons in CA3 SP of sham, 2VO-vehicle and 2VO-dipyridamole rats. **A-C:** Representative photomicrographs of double immunostaining for neurons (green) and cytochrome C (red) in CA3 SP of sham (A), 2VO-vehicle (B), and 2VO-dipyridamole rats (C). The white lines indicate the borders of the CA3 subregion SP. Open arrows point to apoptotic neurons in CA3 SP. The white arrow in panel B shows a CytC+ ectopic neuron. Scale bar: 80 µm. **D:** Magnification of the framed area in panel B showing the

CytC immunostaining of two apoptotic neurons. Scale bar: 10 μm. **E:** Quantitative analysis of CytC+ NeuN+ apoptotic neurons (cells/mm^2) in CA3 SP of sham (white columns), 2VO-vehicle (grey columns) and 2VO-dipyridamole rats (black columns). Data in graph bars are mean±SEM. SP: sham, n=4; 2VO-vehicle, n=5; 2VO-dipyridamole, n=5. **F:** Representative confocal immunostaining of neurons (NeuN, green), CytC (red), and microglia (IBA1, blue) in CA3 SP of 2VO-dipyridamole rats. The panels show a neuron "sub-slice" of 10 consecutive confocal z scans, total thickness 3 μm, acquired starting at 1.8 μm depth into the neuron. The white arrow shows a microglia cell (blue) that approaches an apoptotic neuron, sending its branches to phagocytose the it (open arrow). Scale bar: 5 μm. **G1-G3:** Representative confocal immunostaining of neurons (NeuN, green) and microglia (IBA1, blue) in CA3 SP of 2VO-dipyridamole rat. The panels show a neuron "sub-slice" of 33 consecutive confocal z scans, total thickness 9.9 μm, acquired starting at 3 μm depth into the neuron. sub-slice of 33 consecutive confocal z scans of NeuN (green, G1) and IBA1 (blue, G2) immunostaining and the merge of the two previous images (G3). The empty arrow shows a microglia that actively phagocytoses a CA3 pyramidal neuron. Scale bar: 7.5 μm. **H1-H):** sub-slice of 8 consecutive confocal z scans of NeuN (green, H1) and IBA1 (blue, H2) immunostaining and the merge of the two previous images (H3). The open arrow shows a microglia that actively phagocytoses a neuron in CA3 Str. Radiatum. Scale bar: 10 μm.

Quantitative analysis shown in Figure 47E demonstrates that CytC+ neurons were significantly more numerous in 2VO-vehicle rats (+82%) than in sham rats and dipyridamole significantly reverted this effect (2VO-dipyridamole +9% vs sham, n.s.), as shown by statistical analysis (One-way ANOVA: $F_{(2,11)}=5.697$, *P=0.02; Newman-Keuls post test: *P<0.05 2VO-vehicle vs sham, $^{\#}$P<0.05 2VO-dipyridamole vs 2VO-vehicle rats). The white arrows in panel 47B show CytC+ ectopic neurons (red).

In order to verify whether CytC+ neurons, undergoing apoptosis, were phagocytosed by microglia, sections were triple immunostained with anti NeuN for neurons (green), anti CytC (red), and with anti IBA1 for microglia (blue) (Figure 47F). The image 47F shows a sub-slice of a neuron, obtained from 10 consecutive confocal z scans (total thickness 3 μm) acquired starting at a depth of 1.8 μm into the neuron, showing the internal part of the cell. The presence of a diffuse CytC immunostaining in the cytoplasm indicates that the cell is undergoing apoptosis. The merge of the three confocal scans shows that the apoptotic CytC+ neuron was in contact with a microglial cell (blue, white arrow). The image is a clear example of a microglial cell projecting its branches to surround and to infiltrate the neuronal cell body.

The images in Figure 47G1-G3 show immunostaining with anti NeuN for neurons (green), and with anti IBA1 for microglia (blue) of CA3 SP of 2VO-dipyridamole rat. The image is a sub-slice obtained from 33 consecutive confocal z scans (thickness 9.9 μm) acquired starting at a depth of 3.0 μm into the neuron indicated by the open arrow (Figure 47G1), showing the internal part of the cell. The merge of the two images shows that a microglial cell is in the act of phagocytosing the pyramidal neuron (open arrows,

Figure 47G3). The image is again a clear example of a microglial cell projecting its branches to surround and to infiltrate the neuronal cell body. The neuron shows signs of degeneration.

The images in Figure 47H1-H3 show immunostaining with anti NeuN for neurons (green), and with anti IBA1 for microglia (blue) of CA3 SR of 2VO rat. The image is a sub-slice obtained from 8 consecutive confocal z scans (thickness 2.4 μm) acquired starting at a depth of 6.0 μm into the neuron, indicated by the open arrow, showing the internal part of the cell. The merge of the two images shows that a microglial cell is in the act of phagocytosing the ectopic neuron (open arrows, Figure 47H3). The image is an example of a microglial cell projecting its branches to surround and to infiltrate the neuron which does not appear to have any sign of degeneration.

4.20 Analysis of astrocytes in CA3 Stratum Pyramidale, Stratum Lucidum and stratum radiatum of sham, 2VO-vehicle, and 2VO-dipyridamole treated rats

Astrocytes were immunolabelled with anti GFAP antibody (Figures 48A-C) and quantified in CA3 SP, SL e SR of sham, 2VO-vehicle, and 2VO-dipyridamole rats.

We found a statistically significant increase of astrocytes in SP of 2VO-vehicle (+15%) and 2VO-dipyridamole rats (+45%) compared to sham rats, as shown in Figure 48D by statistical analysis (One-way ANOVA: $F_{(2,12)}$=17.58, P=0.0003, Newman-Keuls post test: ***P<0.001 2VO-dipyridamole rats vs sham, **P<0.01 2VO-vehicle vs sham and 2VO-dipyridamole rats). The number of astrocytes did not change significantly in SL of 2VO-vehicle rats (-10%). We found a significant increase of astrocytes in SL of 2VO-dipyridamole rats (+19%) in comparison to sham rats, as shown by statistical analysis (One-way ANOVA: $F_{(2,12)}$=9.504, P=0.0034; Newman-Keuls post test: *P<0.05 2VO-dipyridamole vs sham rats). In CA3 SR a significant increase of astrocytes was found both in 2VO-vehicle (+18%) and 2VO-dipyridamole rats (+18%), as demonstrated by statistical analysis (One-way ANOVA: $F_{(2,12)}$=10.18, P=0.0026; Newman-Keuls post test: **P<0.01 2VO-dipyridamole and 2VO-vehicle rats vs sham).

The length of astrocytes branches was measured, as reported in the Methods section, separately in SP, SL and SR of sham, 2VO-vehicle, and 2VO-dipyridamole rats. The results, shown in Figure 48E demonstrated that no significant differences were found either among the CA3 subregions or among the three experimental groups.

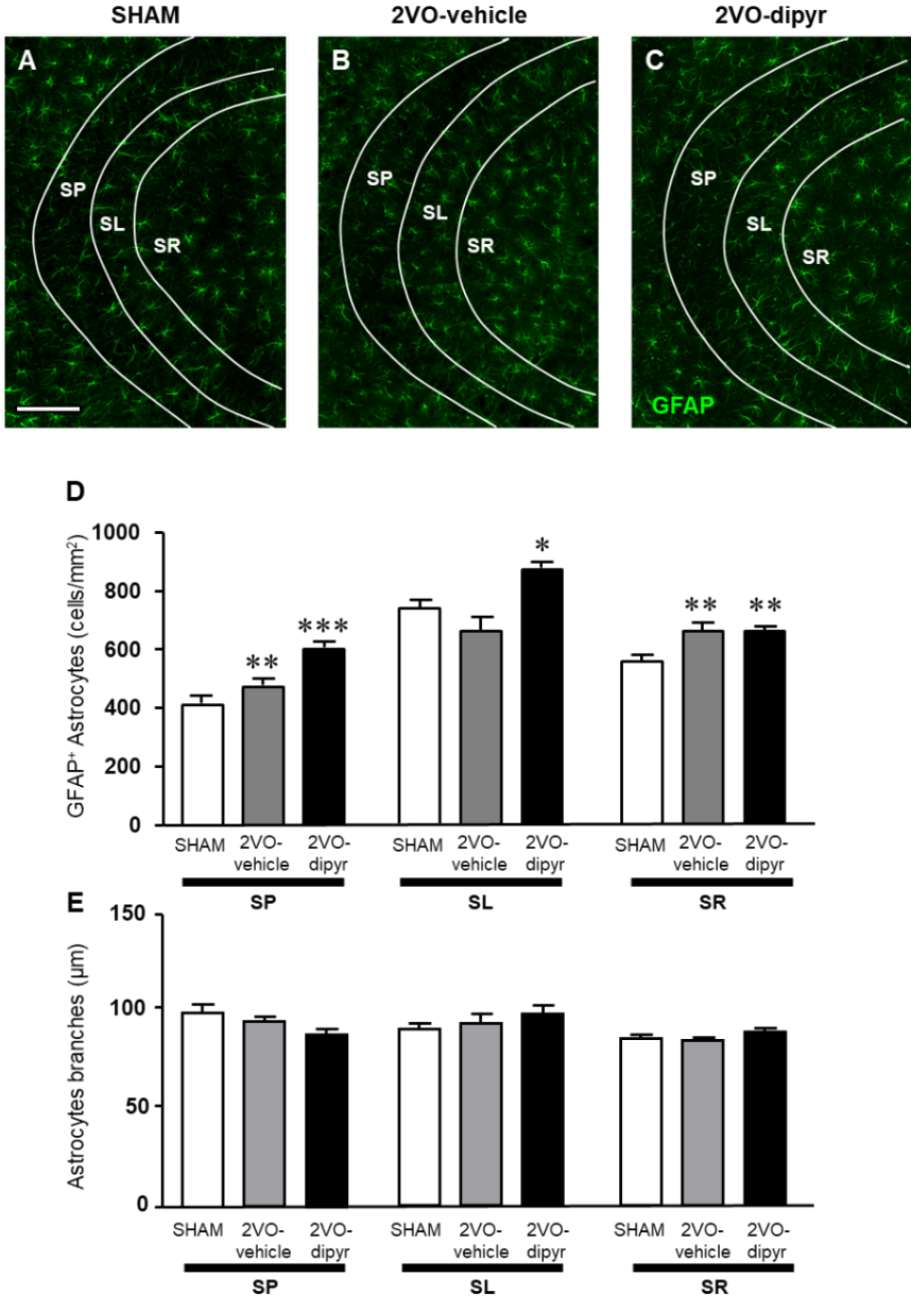

Figure 48. Analysis of astrocytes in CA3 SP, SL and SR of sham, 2VO-vehicle and 2VO-dipyridamole rats. **A-C:** Representative photomicrographs of GFAP immunostaining (green) of astrocytes in CA3 of sham (A), 2VO-vehicle (B), and 2VO-dipyridamole rats (C). The white lines indicate the subdivision of the CA3 subregions: SP, SL and SR. Scale bar: 80 µm. **D:** Quantitative analysis of GFAP+ astrocytes (cells/mm^2) in CA3 SP, SL and SR of sham (white columns), 2VO-vehicle (grey columns) and 2VO-dipyridamole rats (black columns). Data in graph bars are mean±SEM. SP: sham, n=5; 2VO-vehicle, n=5; 2VO-dipyridamole, n=5. SL: sham, n=5; 2VO-vehicle, n=5; 2VO-dipyridamole, n=5. SR: sham, n=5; 2VO-vehicle, n=5; 2VO-dipyridamole, n=5. **E:** Quantitative analysis of the length of principal astrocyte branches (µm) in CA3 SP, SL and SR of sham (white columns), 2VO-vehicle (grey columns) and 2VO-dipyridamole rats (black columns). Data in graph bars are mean±SEM. SP: sham, n=5; 2VO-vehicle, n=5; 2VO-dipyridamole, n=5. SL: sham, n=5; 2VO-vehicle, n=5; 2VO-dipyridamole, n=5. SR: sham, n=5; 2VO-vehicle, n=5; 2VO-dipyridamole, n=5.

4.21 TNFα expression in CA3 Stratum Pyramidale, Stratum Lucidum and stratum radiatum of sham, 2VO-vehicle, and 2VO-dipyridamole treated rats

We analyzed whether the levels of TNFα were modified in CA3 of 2VO rats. As shown in Figure 49A-B, we found a significant increase of TNFα+ cells in SR of 2VO-vehicle rats (+89% vs sham rats), and dipyridamole completely blocked this effect (-6% vs sham rats, n.s.).

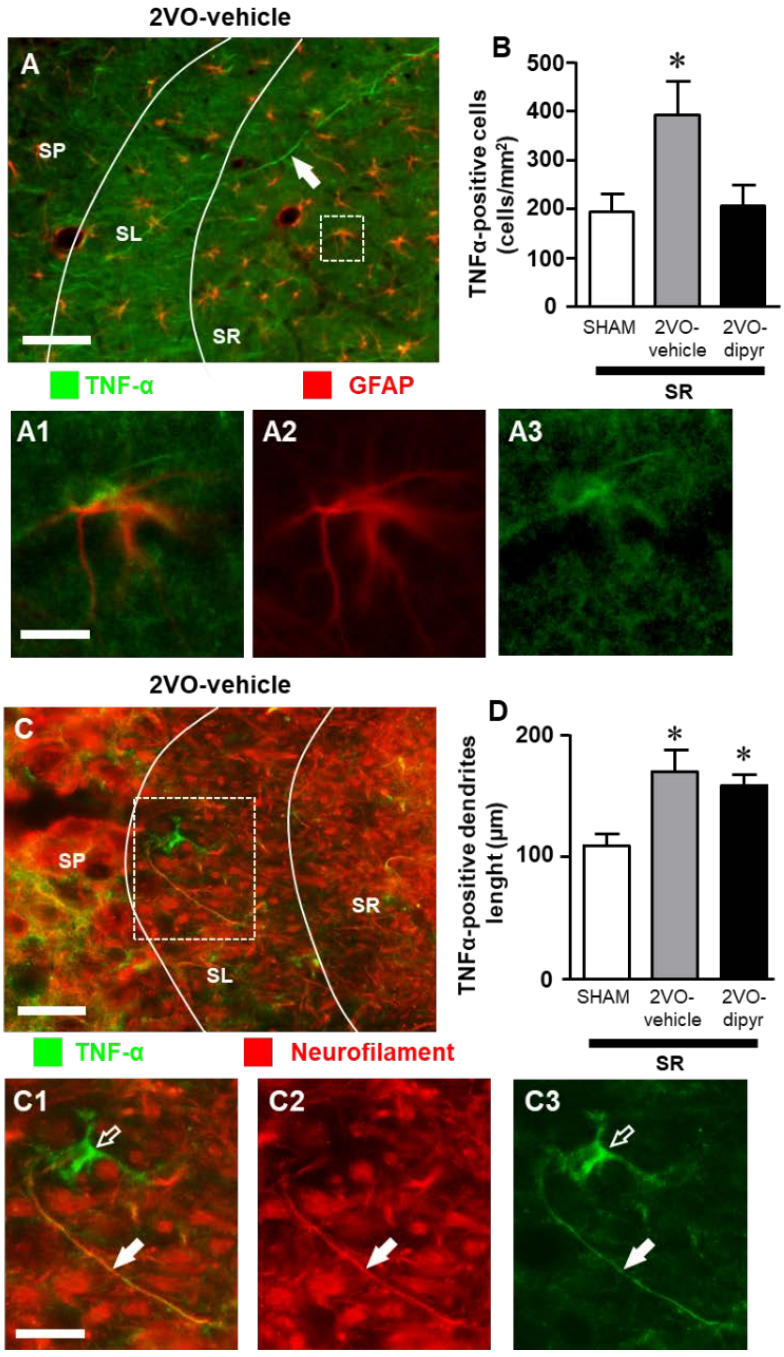

Figure 49. Analysis of TNFα expression in CA3 SP, SL and SR of sham, 2VO-vehicle and 2VO-dipyridamole rats. **A-A3:** Representative photomicrographs of TNFα (green) and GFAP

(red) immunostaining of astrocytes in CA3 of a 2VO-vehicle rat. The white lines indicate the subdivision of the CA3 subregions: SP, SL and SR. Scale bar: 100 µm. **A1-A3:** Magnification of the framed area in panel A showing a TNFα+ astrocyte. Scale bar: 25 µm. **B:** Quantitative analysis of TNFα+ cells (cells/mm^2) in CA3 SR of sham (white columns), 2VO-vehicle (grey columns) and 2VO-dipyridamole rats (black columns). Data in graph bars are mean±SEM; sham, n=4; 2VO-vehicle, n=4; 2VO-dipyridamole, n=4. **C-C3:** Representative photomicrographs of TNFα (green) and neurofilament (red) immunostaining in CA3 of a 2VO-vehicle rat. The white lines indicate the subdivision of the CA3 subregions: SP, SL and SR. Scale bar: 50 µm. **C1-C3:** Magnification of the framed area in panel C showing a TNFα+, and neurofilament positive dendrite. Scale bar: 25 µm. **D:** Quantitative analysis of TNFα+ dendrites (µm) in CA3 SR of sham (white columns), 2VO-vehicle (grey columns) and 2VO-dipyridamole rats (black columns). Data in graph bars are mean±SEM.; sham, n=4; 2VO-vehicle, n=4; 2VO-dipyridamole, n=4.

As shown in Figure 49B statistical analysis performed by one way ANOVA followed by Newman Keuls multiple comparison test demonstrated that this effect was statistically significant (One-way ANOVA: $F_{(2,11)}$=4.966, P<0.05; Newman-Keuls post test: *P<0.05 2VO-vehicle vs sham and vs 2VO-dipyridamole).

Double labelling immunofluorescent microscopy using antibodies for TNFα and GFAP demonstrated that TNFα+ cells were astrocytes (Figure 49A1-A3, magnification of the framed area in Figure 49A). Furthermore, in CA3 SL and SR we found an increase of TNFα expression in neuronal dendrites (Figure 49A, arrow). Indeed, double labelled immunofluorescence with antibodies for TNFα and neurofilament (Figure 49C-C3) demonstrated colocalization of TNFα in many, but not all, neurofilament-positive dendrites, both in SL and SR of 2VO rats (Figure 49C1-C3, magnification of the framed areas in Figure 49C).

Quantitative analysis of the length of TNFα+ dendrites in SR (Figure 49D) demonstrated a significant increase in 2VO-vehicle rats (+56% vs sham), but dipyridamole only partially reversed this effect (+46% vs sham) (One-way ANOVA: $F_{(2,11)}$=6.607, P<0.05; Newman-Keuls post test: *P<0.05 2VO-vehicle and 2VO-dipyridamole vs sham). Figures 49C1-C3 clearly show a TNFα+ cell (open arrow) negative for neurofilament, possibly representing an astrocyte. We never found any colocalization of TNFα with microglia markers (data not shown).

4.22 Analysis of microglia in CA3 Stratum Pyramidale, Stratum Lucidum and stratum radiatum of sham, 2VO-vehicle, and 2VO-dipyridamole treated rats

Total microglia (resting plus activated microglia) was labelled using anti IBA1 antibody (Figure 50A-C) in area CA3 SP, SL and SR of sham, 2VO-vehicle and 2VO-

dipyridamole rats. IBA1+ microglia cells were quantified in the ROI of SR (Figure 50D).

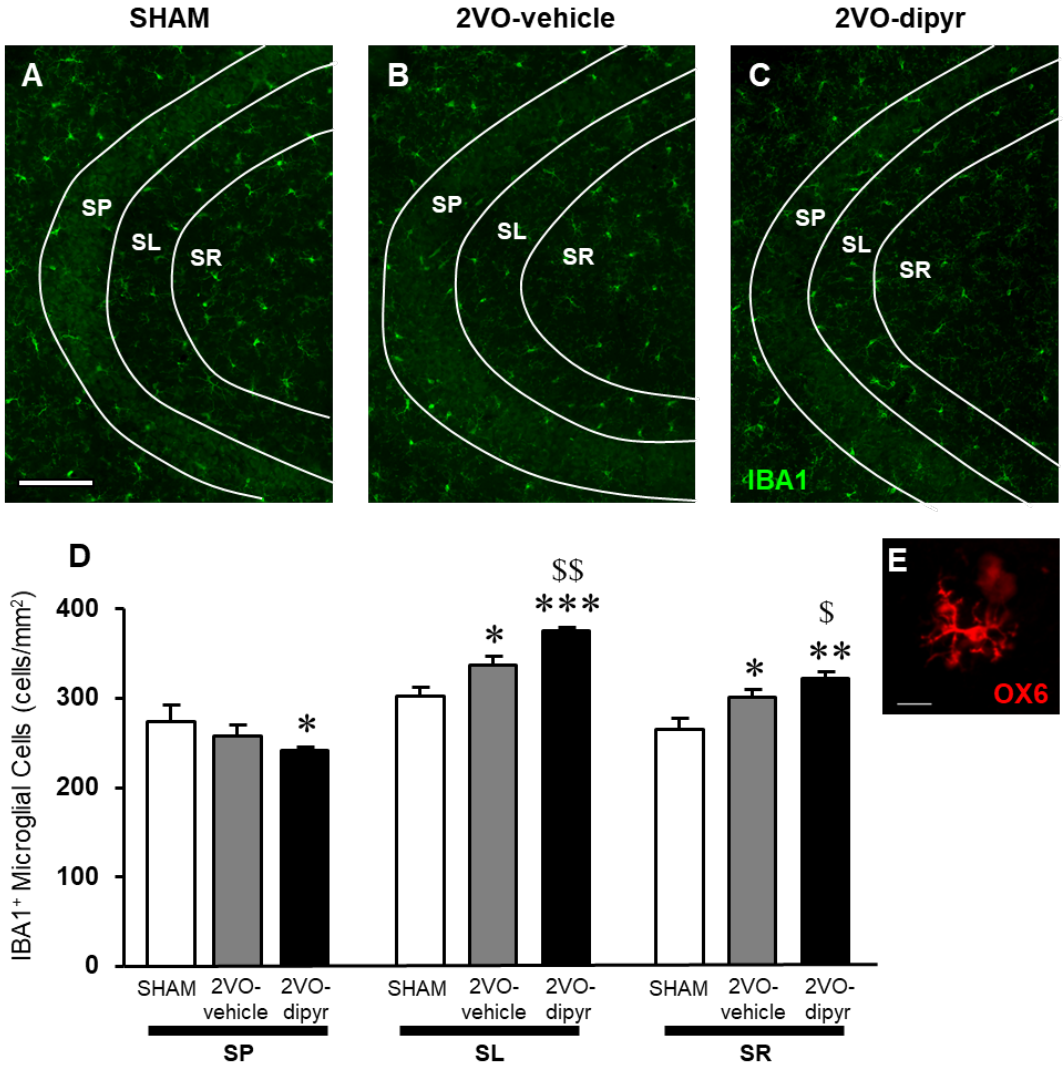

Figure 50. Analysis of microglia in CA3 SP, SL and SR of sham, 2VO-vehicle and 2VO-dipyridamole rats. **A-C:** Representative photomicrographs of IBA1 immunostaining (green) of microglial cells in CA3 of sham (A), 2VO-vehicle (B), and 2VO-dipyridamole rats (C). The white lines indicate the borders of the CA3 subregions: SP, SL and SR. Scale bar: 80 µm. **D:** Quantitative analysis of IBA1+ microglial cells (cells/mm^2) in CA3 SP, SL and SR of sham (white columns), 2VO-vehicle (grey columns) and 2VO-dipyridamole rats (black columns). Data in graph bars are mean±SEM. SP: sham, n=5; 2VO-vehicle, n=5; 2VO-dipyridamole, n=5. SL: sham, n=5; 2VO-vehicle, n=5; 2VO-dipyridamole, n=5. SR: sham, n=5; 2VO-vehicle, n=5; 2VO-dipyridamole, n=5. **E:** representative image of an OX6-positive microglia. Scale bar: 10 µm.

A significant decrease of microglia was found in SP of 2VO-dipyridamole rats (-12%), as demonstrated by statistical analysis (One-way ANOVA: $F_{(2,12)}$=1.554; Newman-Keuls post test: *P<0.05 2VO-dipyridamole vs sham). A significant increase of microglia was found in SL of 2VO-vehicle (+12%) and 2VO-dipyridamole (+24%) rats in comparison to sham rats (One-way ANOVA: $F_{(2,12)}$=17.56, P=0.0003; Newman-

Keuls post test: *P<0.05 2VO-vehicle vs sham, ***P<0.001 2VO-dipyridamole vs sham, $$P<0.01 2VO-dipyridamole vs 2VO-vehicle). A significant increase of microglia was also found in SR of 2VO-vehicle (+14%) and 2VO-dipyridamole (+22%) rats in comparison to sham rats (One-way ANOVA: $F_{(2,12)}$=7.865, P<0.01; Newman-Keuls post test: **P<0.01 2VO-dipyridamole vs sham, *P<0.05 2VO-vehicle vs sham, $P<0.05 2VO-dipyridamole vs 2VO-vehicle).

We then utilized the OX6 antibody (anti MHC-II) to visualize activated microglia. Very sparse OX6+ microglia cells were found in SP, SL and SR of the three experimental groups (see image in Figure 50E). Quantitative analysis of OX6-positive activated microglia did not give any significant difference in any area among the three experimental groups (not shown).

4.23 Characterization and quantification of neuron-astrocytes-microglia triads in CA3 stratum lucidum and stratum radiatum of sham, 2VO-vehicle, and 2VO-dipyridamole treated rats

In order to verify the hypothesis that astrocytes and microglia might actively collaborate in the triad formation around apoptotic neurons and neuronal debris in the CA3 region of the hippocampus of 2VO rats as demonstrated in CA1 (Cerbai et al., 2012; Lana et al., 2016), we studied the interplay among neurons and microglia in CA3 SL and SR of sham, 2VO-vehicle and 2VO-dipyridamole rats using the triple immunostaining of neurons, astrocytes, and microglia.

Neurons, astrocytes, and microglia were triple immunostained in the CA3 of sham, 2VO-vehicle, and 2VO-dipyridamole rats. Triple immunostaining of astrocytes with anti GFAP antibody (green), neurons with anti NeuN antibody (red) and microglia with anti IBA1 antibody (blue) in the CA3 SR of a 2VO-vehicle rat clearly shows the presence of neuron-astrocytes- microglia triads in CA3 SL and SR of all experimental groups (Figure 51A-C). Figures 51B-B1 show an example of neuron-astrocyte-microglia triad in CA3 SR of a 2VO-vehicle rat: the neuron (red) is tightly embraced by astrocyte branches (green), the microglial cell (blue) is in a phagocytic state, the three cells are in direct contact with each other. The open arrow indicates a neuron fragment engulfed in the cytoplasm of phagocytic microglia.

Figure 51B shows a “top-down view” while 8B1 a “bottom-up view” of the 3D rendering of one triad located in the SR of a 2VO-vehicle rat. It is possible to see that an ectopic neuron is tightly surrounded by astrocyte branches that form a micro scar

around it. To complete the triad, a microglia cell (IBA1+, blue) is in close contact with the neuronal cell body, possibly phagocytosing the neuron. Indeed, it is clearly visible in panel 51B that portion of the neuronal cytoplasm is engulfed by the microglia cell (arrow).

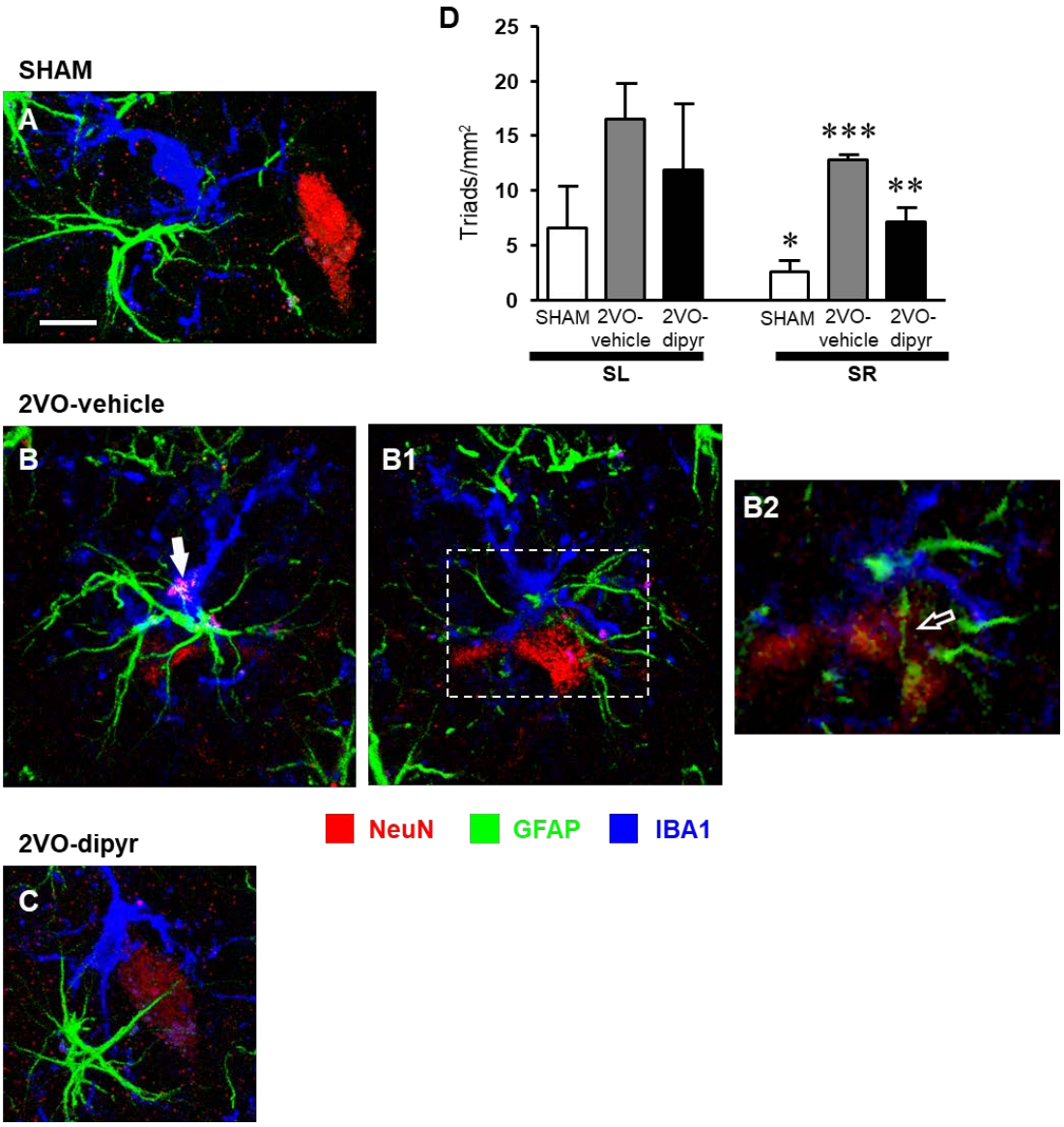

Figure 51. Analysis of the neuron-astrocyte-microglia triads in CA3 SL and SR of sham, 2VO-vehicle and 2VO-dipyridamole rats. **(A-C)**: Confocal microscopy 3D renderings of triple immunostaining of neurons (NeuN, red), astrocytes (GFAP, green) and microglia (IBA1, blue) in CA3 SL and SR of sham (A), 2VO-vehicle (B), and 2VO-dipyridamole rats (C). Scale bar: 10 µm. (B-B1): B shows a "top-down view" while B1 a "bottom-up view" of the 3D rendering of one triad located in the SR of a 2VO-vehicle rat. The open arrow (pink colour) indicates a neuron fragment engulfed in the cytoplasm of phagocytic microglia. (B2): Image obtained by a digital subslicing of the neuron-astrocyte-microglia triad shown in panel B, obtained stacking 3 consecutive z scans (total thickness 0.9 µm) starting at a depth of 7.4 µm into the neuron. The open arrow in B2 indicate the presence of astrocytes branches infiltrating the neuronal cell body. Scale bar: 5 µm. **(D)**: Quantitative analysis of neuron-astrocyte-microglia triads (n of triads/mm^2) in CA3 SL and SR of sham (white columns), 2VO-vehicle (grey columns) and

2VO-dipyridamole rats (black columns). Data in graph bars are mean±SEM. SL: Sham, n=4; 2VO-vehicle, n=4; 2VO-dipyridamole, n=5. SR: Sham, n=4; 2VO-vehicle, n=4; 2VO-dipyridamole, n=5.

This image clearly shows that astrocyte branches (open arrow), not visible in the top-down and bottom up 3D renderings, are located inside the neuronal cell body. These morphological features are consistent with the hypothesis that astrocyte branches are bisecting this ectopic neuron to form neuronal debris. Quantitative analysis of the neuron-astrocytes-microglia triads (as defined in Methodological considerations) was performed in CA3 SL and SR of shams, 2VO-vehicle and 2VO-dipyridamole rats. Results in Figure 51D show that in SL of 2VO-vehicle and 2VO-dypiridamole rats the number of triads, although increased, was not statistically different from sham rats (One-way ANOVA $F_{(2,10)}$=0.947, n.s.). However, the number of triads significantly increased in SR of 2VO-vehicle rats (+392%). Dipyridamole partially but significantly prevented this effect (+169%), as shown by statistical analysis (One-way ANOVA $F_{(2,10)}$=19.69; P=0.0003; *** P < 0.001 vs shams; $^{\#\#}$P<0.01 vs 2VO-vehicle; *P<0.05 vs 2VO-dipyridamole; Newman-Keuls Multiple Comparison Test).

Part V - In vitro models of brain ischemia

4.24 Electrophysiological experiments

It has been established that 7 min OGD episodes bring about irreversible depression of neurotransmission and the appearance of a severe neuronal depolarization or AD (Pugliese et al., 2006, 2007, 2009), a critical event that has been demonstrated both *in vivo* (Somjen, 2001) and *in vitro* (Pugliese et al., 2006, 2007, 2009). Therefore, we studied the effects of two selective adenosine A_{2B} receptor antagonists, MRS-1704 and PSB603, on AD development in the CA1 region of acute rat hippocampal slices under severe OGD episodes by extracellular recording of fEPSPs on 133 hippocampal slices taken from 42 rats.

4.25 The selective adenosine A_{2B} receptor antagonism prevents or delays AD development and protects from synaptic failure induced by severe OGD in CA1 hippocampus

In agreement with our previous results (Pugliese et al., 2006, 2007, 2009), in untreated OGD slices the d.c. shift presented a mean latency of 6.04 ± 0.2 min (calculated from the beginning of OGD) and a mean peak amplitude of -6.7±0.4 mV (*n* = 24) (Figure

52A). Seven min OGD exposure induced a rapid and irreversible depression of fEPSPs amplitude evoked by Schaffer-collateral stimulation, since synaptic potentials did not recover their amplitude after return to oxygenated aCSF (Figure 52D, *n* = 24, 2.5±2.7% of pre-OGD level, calculated 50 min from the end of OGD). Control slices, followed for up to 3 h in oxygenated aCSF, maintained stable fEPSPs for the entire experimental time recording and never developed the d.c. shift (data not shown). OGD was then applied in the presence of the selective adenosine A_{2B} receptor antagonists MRS1754 or PSB603, administered 15 min before, during and 5 min after OGD. The two A_{2B} receptor antagonists did not modify basal synaptic transmission measured before OGD. Indeed, MRS1754 (500 nM, *n*=17) did not modify fEPSPs amplitude under normoxic conditions (from 1.05±0.06 mV immediately before to 1.01±0.08 mV after 15 min drug application, *n*=17). In addition, PSB603 did not change the amplitude of synaptic potentials under normoxic conditions (from 1.32±0.12 mV before to 1.35±0.14 mV after 15 min drug application, *n*=15). These data indicate that the blockade of A_{2B} receptors does not modify low-frequency-induced CA1 synaptic transmission under normoxic conditions, in agreement with results reported in mouse hippocampal slices (Gonçalves et al., 2015). Nevertheless, the two A_{2B} receptor antagonists were able to prevent or delay the appearance of AD and to modify synaptic responses after OGD. During 7 min OGD, MRS1754 prevented the appearance of AD in 13 out of 17 slices tested (Figure 52B). In these 13 slices a complete recovery of fEPSPs was recorded (111.9±7.4%, calculated 50 min from the end of OGD, Figure 52D). In the remaining 4 slices, AD developed, although at later times (Figure 52F, mean AD latency: 7.37±0.41 min; mean peak amplitude: -5.8±1.1 mV, *n*=4), and, unexpectedly, was followed by a consistent fEPSP recovery (85.2±15.3%, *n*=4, Figure 52D). During 7 min OGD, PSB603 prevented the appearance of AD in 11 out of 15 slices tested (Figure 52C). In these 11 slices a complete recovery of fEPSPs was found (110.4±10.2 %, *n*=11, Figure 52E). In the remaining 4 slices in which AD appeared, a delay in AD latency was recorded (Figure 52F, mean AD latency: 7.33±0.08 min; mean peak amplitude: -6.8±1.9 mV, *n*=4). Moreover, in these 4 PSB603-treated slices, a significant recovery of fEPSP (36.2±19.7%, *n*=4, Figure 52E) was found. In the slices in which AD appeared in the presence of MRS1754 or PSB603, we compared the time of AD appearance in the absence and in the presence of drugs. As illustrated in Figure 52F, during 7 min OGD, AD appeared in OGD slices with a mean latency of 6.04±0.2 min (left panel) and a mean peak amplitude of 6.7±0.4 mV (*n*=24, right panel). When 7 min OGD was applied

in the presence of 500 nM MRS1754 or 50 nM PSB603 the d.c. shifts were always delayed (Figure 52F, left panel), while AD amplitude values were not significantly modified in comparison to OGD slices (Figure 52F, right panel). In an experimental group of slices which never developed AD in the presence of PSB603 (50 nM; *n*=6) and MRS1754 (500 nM; *n* = 6), we followed the evolution of the synaptic response for 3 hours after the end of the 7 min ischemic like insult in comparison to untreated OGD slices (*n*=6). As reported in the representative electrophysiological traces shown in Figure 52G, PSB603 (50 nM) and MRS1754 (500 nM) allowed the recovery of synaptic potentials for at least 3 h after 7 min OGD.

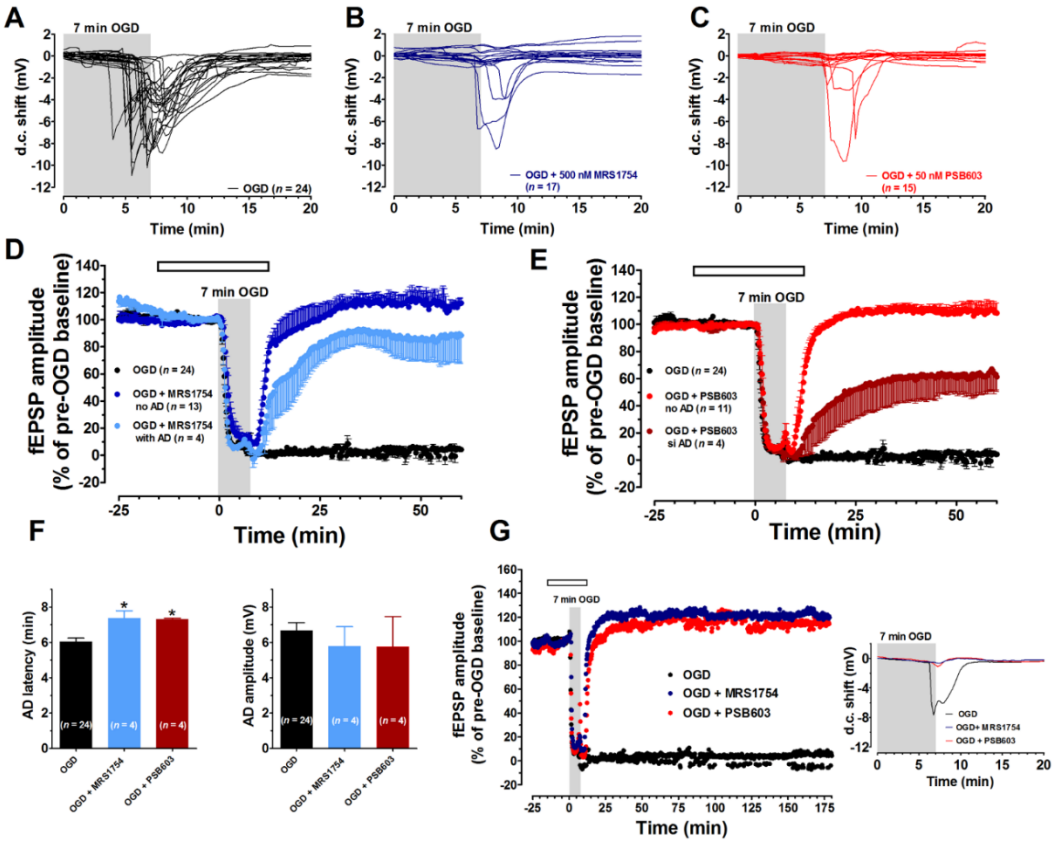

Figure 52. The selective adenosine A2B receptor antagonists MRS1754 or PSB603 significantly reduced the synaptic failure induced by 7 min OGD in the CA1 region of rat hippocampal slices. **A-C:** AD was recorded as a negative d.c. shift in response to 7 min OGD in untreated OGD slices (A), in 500 nM MRS1754-treated slices (B) or 50 nM PSB603-treated slices **C:** Note that MRS1754 prevented the appearance of AD in 13 out of 17 slices, while PSB603 in 11 out of 15 slices. **D:** The graph shows the time-course of the effect of 7 min OGD on fEPSP amplitude, expressed as percentage of pre-OGD baseline in the CA1 hippocampal region in the absence (n=24) or in the presence of 500 nM MRS1754 (n=17). Note that, in untreated slices, the ischemic-like insult caused gradual reduction, up to disappearance, of fEPSPs amplitude that did not recover after washing in oxygenated aCSF. On the contrary, after reperfusion in oxygenated standard solution, a recovery of fEPSP in all MRS1754 treated OGD slices was found, even in those in which AD developed. **E:** The graph shows the time course of the effect of 7 min OGD on fEPSP amplitude in 50 nM PSB603 treated OGD slices. Note that,

after reperfusion in normal oxygenated standard solution, a recovery of fEPSP was found in all OGD-treated PSB603 slices, even those in which AD occurred. **F:** Left panel: each column represents the mean±SEM of AD latency recorded in the CA1 region during 7 min OGD in the absence or in the presence of MRS1754 (500 nM) or PSB603 (50 nM). AD latency was measured from the beginning of OGD insult. Note that when OGD was applied in the presence of MRS1754 or PSB603 the appearance of AD was significantly delayed in comparison to OGD untreated slices. *P<0.05 vs OGD, One-way ANOVA followed by Newman-Keuls Multiple comparison test. Right panel: each column represents the mean±SEM of AD amplitude recorded in the CA1 during 7 min OGD. The number of slices is reported in the columns. **G:** The graph shows the time course of the effect of 7 min OGD on fEPSP amplitude in OGD-untreated slices and in 500 nM MRS1754- or 50 nM PSB603-treated slices. The selective antagonism of adenosine A_{2B} receptors counteracted the CA1 synaptic damage induced by severe OGD up to 3 hours from the end of the insult. Inset: 7 min OGD induced AD was recorded untreated OGD slices, but not in the presence of 500 nM MRS1754 or 50 nM PSB603. Grey bar: OGD time duration. Open bar: time of drug application. Amplitude of fEPSPs (mean±SEM) is expressed as percentage of pre-OGD baseline.

4.26 Analysis of neuronal damage in CA1 stratum pyramidale 1 h and 3 h after the end of 7 min OGD

The extent of neuronal damage caused by 7 min OGD in SP of hippocampal CA1 was assessed by immunohistochemistry using the anti NeuN antibody in control slices, in slices after 7 min OGD, and after 7 min OGD in the presence of 500 nM MRS1754 or 50 nM PSB603, both at 1 h and 3 h after the end of OGD. Representative images of NeuN immunostaining in CA1 of slices collected 1 h after the end of OGD are shown in Figure 53A-D. Figure 53E and F show the quantitative analyses of the area of NeuN+ immunofluorescence in CA1, which represents an index of the number of pyramidal neurons, 1 h and 3 h after the end of OGD, respectively. The data demonstrate that NeuN+ CA1 pyramidal neurons significantly decreased both 1 h (Figure 53E) and 3 h (Figure 53F) after the end of 7 min OGD. Statistical analysis showed that 7 min OGD caused a statistically significant reduction of NeuN+ area at 1 h (-29.6%, *P<0.05 vs control slices) and at 3 h (-41%, *P<0.05 vs control slices). The time-course of the effect, indicating that the decrease of NeuN+ area was more pronounced at 3 h than at 1 h after the end of OGD, demonstrates that neuronal degeneration is an ongoing process at least at these time points. The decrease of NeuN+ area in CA1 SP was completely antagonized by treatment with 50 nM PSB603 (-1% at 1 h and -14% at 3 h, n.s. vs control slices). This effect was statistically significant vs 7 min OGD slices both at 1 h and 3 h after the end of OGD ($^{\$}$P<0.05 vs respective OGD). Treatment with 500 nM MRS1754 completely blocked the decrease of NeuN+ area in CA1 SP 3 h after the end of OGD (-7% vs control slices, n.s.; $^{\#}$P<0.05 vs OGD). MRS1754 had no effect 1 h after the end of OGD (-31.5% vs control slices; n.s. vs OGD). Therefore, antagonism of A_{2B}

receptors blocked the neuronal damage induced by 7 min OGD up to 3 hours after the end of the simil ischemic insult. In the OGD slices treated either with MRS1754 or PSB603 that developed AD we found a partial reduction of neuronal damage at 1 h after the end of OGD (data not shown). Closer examination of CA1 SP with confocal microscopy indicated the presence of many damaged neurons both 1 h and 3 h after the end of 7 min OGD. The representative confocal z stacks in Figure 54B and B, each obtained stacking 37 consecutive confocal z scans (0.3 µm each, total thickness 11.1 µm) through the thickness of CA1, show that 3 h after the end of OGD the layout and morphology of CA1 pyramidal neurons was significantly different from that of the control slice (Figure 54A). Panels 54A1 and B1 are magnification of the framed areas in panels 54A and B, and show stacks of 2 consecutive z scans, 0.3 µm each, total thickness 0.6 µm, taken at 2.1 µm depth inside the neurons. It appears evident from panel 54B1 the altered morphology of pyramidal neurons after OGD, in comparison to those of the control slice shown in panel 54A1.

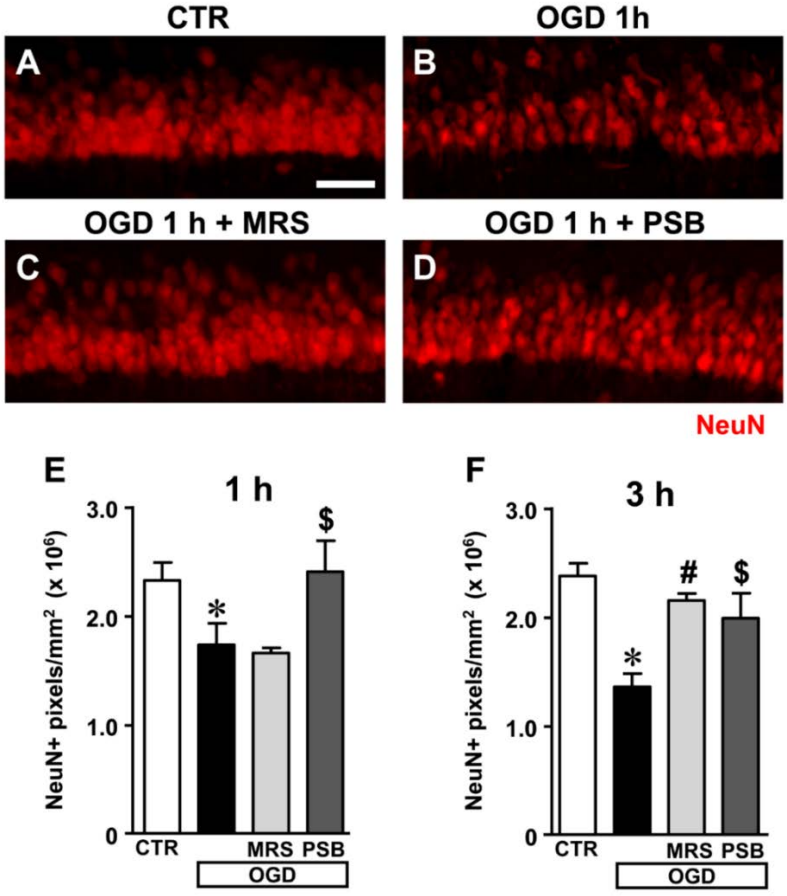

Figure 53. Analysis of NeuN+ immunofluorescence in CA1 SP after the simil-ischemic insult. **A-D:** Representative images of NeuN+ immunofluorescence in the ROI of CA1 of a control slice (CTR, A), a slice collected 1 h after 7 min OGD (OGD, B), a slice treated with 500 nM MRS1754 (OGD+MRS, C), and a slice treated with 50 nM PSB603 (OGD+PSB, D), all

harvested 1 h after the end of 7 min OGD. Scale bar: 75 µm. **E-F:** Quantitative analyses of NeuN+ immunofluorescence in the four experimental groups 1 h (E) and 3 h (F) after the end of 7 min OGD. Each column represents the area, expressed in pixels (x 10^6) above a threshaged, maintained constant for all slices investigated. **E:** Statistical analysis: One-way ANOVA: $F_{(3;13)}$=6.296, P<0.01, Newman-Keuls multiple comparison test: *P<0.05, OGD vs CTR; $^{\$}$P<0.05, OGD+PSB vs OGD. CTR, n=6; OGD, n=5; OGD+PSB, n=3; OGD+MRS, n=3. **F:** Statistical analysis: One-way ANOVA: $F_{(3,16)}$=4.924, P<0.02; Newman-Keuls multiple comparison test: *P<0.05 OGD vs CTR, $^{\#}$P<0.05 OGD+MRS vs OGD, $^{\$}$P<0.05 OGD+PSB vs OGD. CTR, n=6; OGD, n=3; OGD+PSB, n=4; OGD+MRS n=4. All data in the graphs are expressed as mean±S.E.M.

Indeed, in CA1 SP of OGD slices, both at 1 h and 3 h after the end of OGD, we observed the presence of many neurons with nuclei that exhibit a highly condensed NeuN+ nucleus and very faint NeuN cytoplasmic labelling (Figure 54B-B1, open arrows). We defined these neurons as High Density Nucleus neurons, “HDN neurons”. Furthermore, we observed many NeuN+ neurons that have lost the NeuN+ nuclear immunofluorescence, an index of damaged nuclei, while NeuN+ immunofluorescence persists in the cytoplasm (Figure 54B-B1, white arrows). We defined these neurons as Low Density Nucleus neurons, “LDN neurons”. In order to better characterize this phenomenon, we performed the quantitative analysis of HDN and LDN neurons in control, 7 min OGD, 7 min OGD plus MRS1754 and 7 min OGD plus PSB603 slices at 1 h and 3 h after the end of OGD. The results, presented in Figure 54C-D, show that HDN neurons increased significantly in 7 min OGD slices both at 1 h (+603% vs control slices, **P<0.01) and 3 h (+794% vs control slices, ***P<0.001) after the end of OGD. The increase of damaged, HDN neurons in the CA1 area caused by the simil-ischemic insult was significantly blocked by treatment with 50 nM PSB603 at 1 h and 3 h after the end of OGD (-97% at 1 h, and -77% at 3 h vs 7 min OGD slices, both $^{\$\$\$}$P<0.001; n.s. vs controls). Conversely, treatment with 500 nM MRS1754 significantly blocked the increase of HDN neurons only 3 h after the end of OGD (-70% vs 7 min OGD slices, $^{\#\#\#}$P<0.001; n.s. vs control slices), but not 1 h after the end of OGD (+12% vs OGD slices, n.s.; $^{\#\#}$ P<0.01 vs control slices). In addition, as shown by the representative images in Figure 54B-B1, we found many LDN neurons in SP 1 h and 3 h after the end of 7 min OGD. As demonstrated by quantitative analysis (Figure 54E-F) LDN neurons in SP were significantly increased both 1 h and 3 h after OGD, in comparison to control slices. The increase of LDN neurons, in comparison to control slices, was 1489% at 1 h (***P<0.01 vs control slices) and 1033% at 3 h after the end of 7 min OGD (***P<0.01 vs control slices). The increase of damaged, LDN neurons brought about by the simil-ischemic insult was significantly blocked by treatment with

50 nM PSB603 both at 1 and 3 h after the end of OGD (-98% at 1 h, and -62% at 3 h vs OGD, both $^{\$\$\$}$P<0.001). Treatment with 500 nM MRS1754 significantly blocked the increase of LDN neurons only 3 h after the end of OGD (-52% vs 7 min OGD, $^{\#\#\#}$P<0.001), but not 1 h after the end of OGD (-17% vs 7 min OGD, n.s.; $^{\#\#}$P<0.01 vs controls). These data further confirm the efficacy of the two A_{2B} receptor antagonists, and particularly of PSB603, in reducing not only the electrophysiological effects but also the morphological modifications that OGD caused on CA1 pyramidal neurons, up to 3 h after the end of the ischemic-like insult.

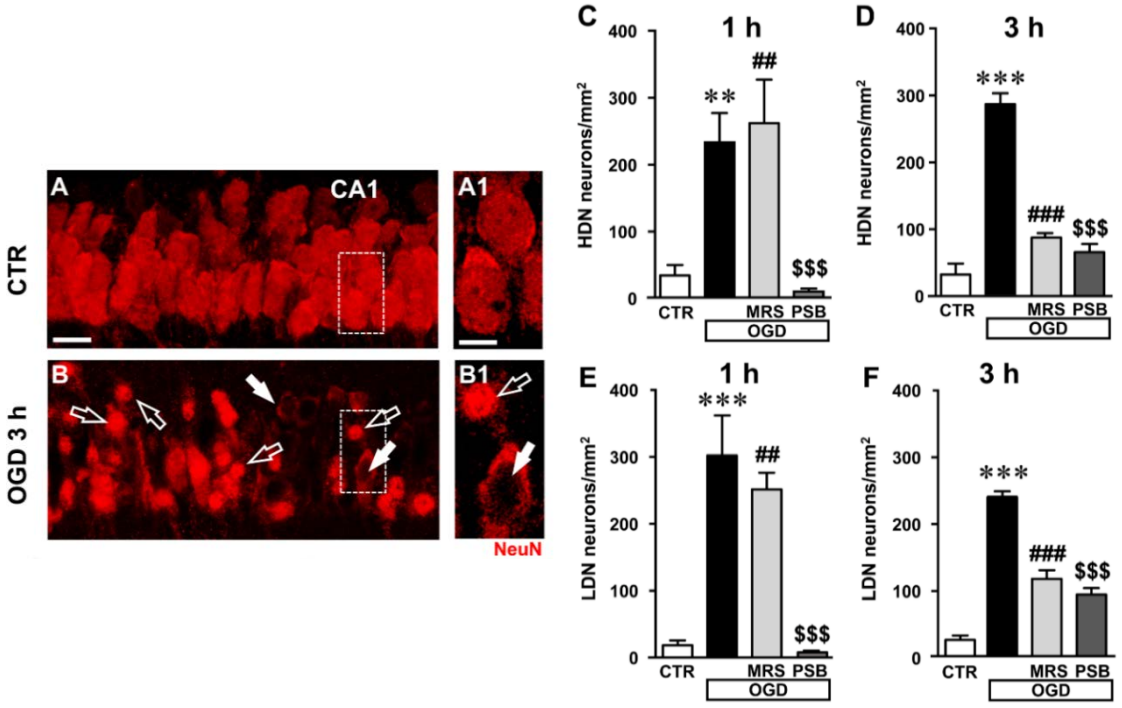

Figure 54. Analysis of damaged neurons in CA1 SP after the simil-ischemic insult. **A-B1:** Representative images of NeuN+ immunofluorescence in the CA1 area of a control slice (CTR, A,A1), and of a slice harvested 3 h after the end of 7 min OGD (OGD, B,B1). **A1-B1:** magnification of digital subslices of the framed areas in A,B (stacks of 2 consecutive z scans taken at 2.1 µm depth inside the neurons, total thickness 0.6 µm). Note the presence of many HDN neurons (open arrows) and LDN neurons (white arrows) in CA1 SP after OGD (B, B1). Scale bars: A, B: 25 µm; A1, B1: 10 µm. **C-D:** Quantitative analyses of NeuN+ HDN neurons in CA1 SP 1 h (C) and 3 h (D) after the end of OGD. **C:** One-way ANOVA: $F_{(3;12)}$=11.32, P<0.001. Newman-Keuls multiple comparison test: **P<0.01, OGD vs CTR; $^{\#\#}$P<0.01, OGD+MRS vs CTR; $^{\$\$\$}$P<0.001 OGD+PSB vs OGD. CTR, n=5; OGD, n=5; OGD+PSB, n=3; OGD+MRS, n=3. **D:** One-way ANOVA: $F_{(3;12)}$=64.33, P<0.001. Newman-Keuls multiple comparison test: ***P<0.001, OGD vs CTR; $^{\#\#\#}$P<0.001, OGD+MRS vs OGD; $^{\$\$\$}$P<0.001 OGD+PSB vs OGD. CTR, n=5; OGD, n=3; OGD+PSB, n=4; OGD+MRS, n=4. **E-F:** Quantitative analysis of NeuN+ LDN neurons in CA1 SP 1 h (E) and 3 h (F) after the end of OGD. **E:** One-way ANOVA: $F_{(3;14)}$=13.80, P<0.001. Newman-Keuls multiple comparison test: ***P<0.01, OGD vs CTR; $^{\#\#}$P<0.01, OGD+MRS vs CTR; $^{\$\$\$}$P<0.001 OGD+PSB vs OGD. CTR, n=6; OGD, n=6; OGD+PSB, n=3; OGD+MRS, n=3. **F:** One-way ANOVA: $F_{(3;12)}$=69.77, P<0.001. Newman-Keuls multiple comparison test: ***P<0.001, OGD vs CTR; $^{\#\#\#}$P<0.001,

OGD+MRS vs OGD; $^{\$\$\$}$P<0.001 OGD+PSB vs OGD. CTR, n=5; OGD, n=3; OGD+PSB, n=4; OGD+MRS, n=4. All data in the graphs are expressed as mean±S.E.M.

4.27 Analysis of apoptotic neurons in stratum pyramidale of CA1 1h and 3 h after 7 min OGD

These data demonstrate that 7 min OGD can induce neuronal damage in CA1 SP, as evidenced by immunohistochemical analyses that highlight conformational modifications of pyramidal neurons that may subtend cell death. Therefore, we studied whether all the above-described effects and the decrease of neurons in CA1 SP might be caused by apoptosis. To this end, as an apoptosis marker we used CytC, a protein which, in physiological conditions, is found in mitochondria but in the most advanced stages of apoptosis is intensely and diffusely released in the cytoplasm, where it activates caspases (Yang et al., 1997; Kluck et al., 1997; Jiang and Wang, 2004; Suen et al., 2008) and can be used as a marker of apoptosis using immunohistochemical analysis (Martínez-Fábregas et al., 2014). Using a selective antibody, CytC can be visualized in apoptotic cells as an intense and diffuse cytoplasmic immunostaining, as shown by the white arrows in the representative confocal images of an OGD slice 1 h after the end of OGD (Figure 55A-A2). As shown in the confocal subslice of the framed area of Figure 55A2, obtained stacking 17 consecutive confocal z scans through the CytC+ neuron (0.3 µm each, total thickness 5.1 µm), it is evident that the CytC+ neuron is a LDN neuron (Figure 55B1 open arrow), thus demonstrating that LDN neurons are apoptotic.

From the quantitative analysis of CytC+ neurons in CA1 SP, we demonstrated that both 1 h and 3 h after the end of 7 min OGD many CA1 pyramidal neurons were apoptotic (Figure 55C-D). The increase was statistically significant in comparison to control slices both at 1 h (+277% vs control slices, ***P<0.001) and at 3 h (+107% vs control slices, **P<0.01) after OGD. These data indicate that in CA1 area, already after 1 h from the end of OGD, neurons had clear signs of apoptotic processes.

In the presence of MRS1754 or PSB603, there was a significant reduction of CytC immunostaining, both at 1 h and 3 h after the end of OGD, showing that antagonism of A_{2B} receptors significantly reduced neuronal death by apoptosis at both times investigated. Indeed, treatment with MRS1754 decreased apoptotic neurons by 61% at 1 h ($^{\#\#\#}$P<0.001 vs 7 min OGD; n.s. vs control slices) and by 33% at 3 h ($^{\#}$P<0.05 vs 7 min OGD; n.s. vs control slices), in comparison to OGD slices.

Treatment with PSB603 decreased apoptotic neurons by 63% ($^{\$\$\$}$P<0.001 vs 7 min

OGD; n.s. vs control slices) and by 46% ($^{\$\$}$P<0.001 vs 7 min OGD; n.s. vs control slices) in comparison to OGD slices. In the OGD slices treated either with MRS1754 or PSB603 that developed AD the number of HDN and LDN neurons were partially decreased in comparison to OGD slices (data not shown). These data indicate that in the CA1 area already 1 h after the end of OGD, when there was still no recovery of neurotransmission, neurons showed obvious signs of apoptosis. These data demonstrate that antagonism of A_{2B} receptors brought about significant protection against neuron degeneration.

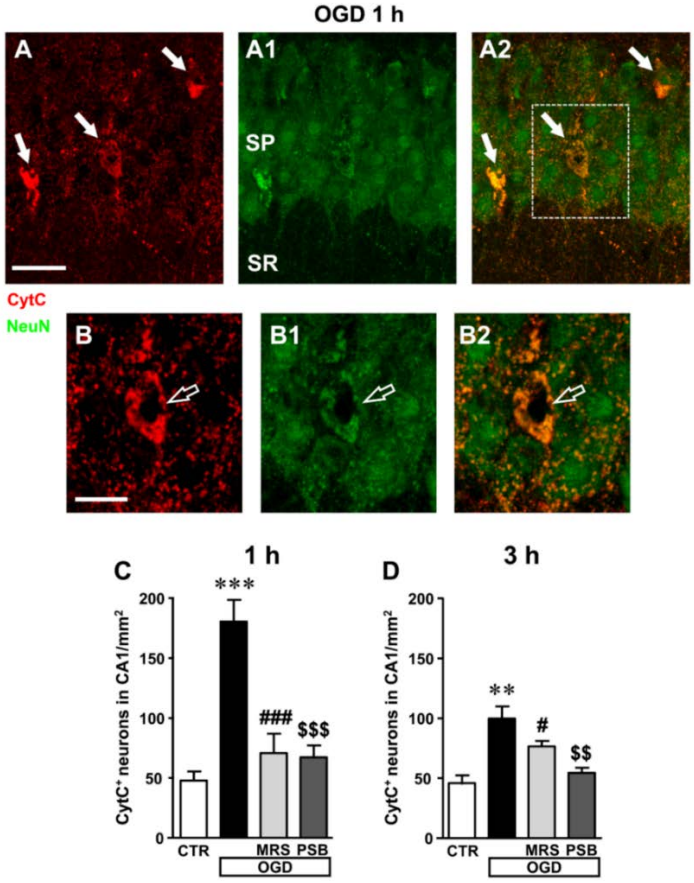

Figure 55: Analysis of CytocromeC+ (CytC+) neurons in CA1 SP after the simil-ischemic insult. **A-A2:** Representative microphotographs, taken at the laser scanning confocal microscope, of apoptotic neurons labelled with anti CytC antibody (A, red), of pyramidal neurons labelled with anti NeuN antibody (A1, green) and the merge of the two previous images (A2). NeuN+ and CytC+ apoptotic neurons in CA1 SP are indicated by the arrows (yellow-orange color in A2). Scale bar: 25 µm. **B-B2:** Subslice of the framed area in A2, obtained stacking 17 consecutive confocal z-scans (5.1 µm total thickness), shown at higher magnification (2x). The open arrow shows an LDN apoptotic pyramidal neuron. Scale bar: 10 µm. **C-D:** Quantitative analysis of NeuN+ and CytC+ neurons in CA1 SP at 1 h (C) and 3 h (D) after the end of 7 min OGD. Note the significant increase of CytC+ neurons both 1 h and 3h after the end of OGD. **C:** Statistical analysis: One-way ANOVA: $F_{(3;11)}$=18.40, P<0.001, Newman-Keuls multiple comparison test: ***P<0.001, OGD vs CTR; $^{\#\#\#}$P<0.001, OGD+MRS vs OGD; $^{\$\$\$}$P<0.001, OGD+PSB vs OGD. CTR, n=4; OGD, n=3; OGD+PSB, n=4; OGD+MRS, n=4. **D:** Statistical analysis: One-way ANOVA:

$F_{(3;11)}$=11.41, P<0.02, Newman-Keuls multiple comparison test: **P<0.01, OGD vs CTR; $^{\#}$P<0.05, OGD+MRS vs OGD; $^{\$\$}$P<0.01, OGD+PSB vs OGD. CTR, n=4; OGD, n=3; OGD+PSB, n=4; OGD+MRS, n=4. All data in the graphs are expressed as mean±S.E.M.

4.28 Analysis of phospho-mTOR in area CA1 of the hippocampus 1 h and 3 h after 7 min OGD

We used a selective antibody for phospho-(Ser244)-mTOR, the activated form of mTOR, to investigate whether mTOR activation might be modified in our experimental conditions. Representative qualitative images of mTOR activation in cell bodies and dendrites of CA1 pyramidal neurons in a control slice are shown in Figure 56A1 (green). Neurons were also immunolabelled with anti NeuN antibody (red).

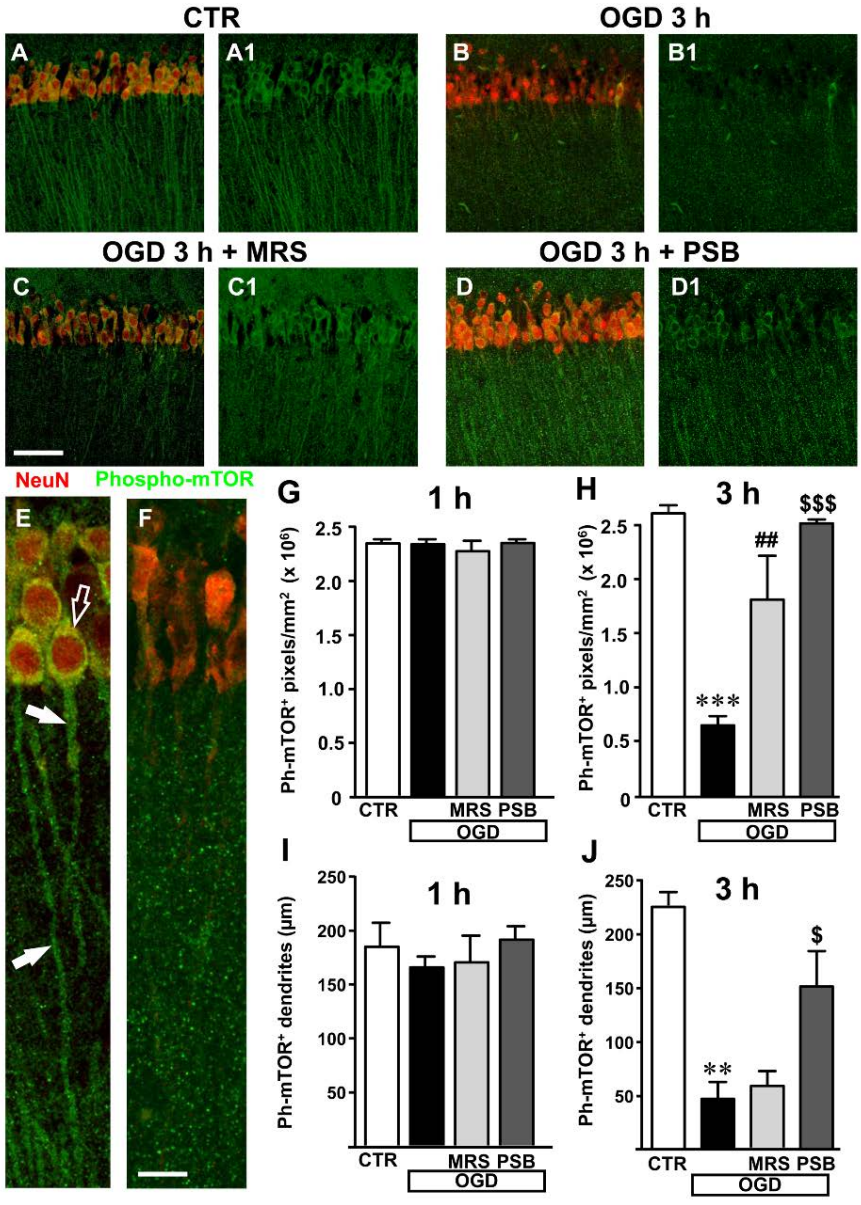

Figure 56. mTOR activation in CA1 SP and SR after the simil ischemic insult. Representative microphotographs, taken at the laser scanning confocal microscope, showing immunolabelling

with anti NeuN antibody (red) and anti phospho-mTOR antibody (green) of a control slice (**A-A1**), a slice harvested 3 h after 7 min OGD (**B-B1**), a slice treated with MRS and harvested 3 h after 7 min OGD (**C-C1**), and a slice treated with PSB and harvested 3 h after 7 min OGD (**D-D1**). Scale bar: 75 µm. **E-F:** Digital subslices of a control slice (E) and a slice collected 3 h after 7 min OGD (F) immunostained for phospho-mTOR (green) and NeuN (red). The open arrow shows the presence of activated mTOR in the cell body and arrows in the dendrites of pyramidal neurons in the control slice (E). **G-H:** Quantitative analysis of activated mTOR in CA1 SP in the different experimental conditions. Each column represents the $mTOR^+$ immunofluorescent area calculated using the ImageJ program (number of pixels above a reference, fixed threshaged). **G:** No difference among the four experimental groups, was found 1 h after the end of 7 min OGD. Statistical analysis: One-way ANOVA: $F_{(3;11)}=0.4563$, $P>0.05$, ns. **H:** Slices harvested 3 h after the end of 7 min OGD. Note the significant decrease of activated mTOR in CA1 pyramidal neurons 3 h after the end of OGD. Both MRS and PSB significantly blocked this effect. Statistical analysis: One-way ANOVA: $F_{(3;10)}=26.99$, $P<0.001$, Newman-Keuls multiple comparison test: ***$P<0.001$, OGD vs CTR; $^{\#\#}P<0.01$, OGD+MRS vs OGD; $^{\$\$\$}P<0.001$, OGD +PSB vs OGD. CTR, n=4; OGD, n=3; OGD+PSB, n=3; OGD+MRS, n=4. All data are expressed as mean±S.E.M. **I-J:** Quantitative analysis of phospho-$mTOR^+$ dendrites in CA1 SR in the different experimental conditions. **I**: Length of phospho-$mTOR^+$ dendrites in CA1 SR 1 h after the end of 7 min OGD. No difference among the four experimental groups, was observed. Statistical analysis: One-way ANOVA: $F_{(3;11)}=0.7143$, $P>0.05$, n.s.. **J:** Length of $mTOR^+$ dendrites in CA1 SR 3 h after the end of 7 min OGD. Note the significant decrease of activated mTOR in dendrites 3 h after the end of OGD. PSB significantly blocked this effect. Statistical analysis: One-way ANOVA: $F_{(3;9)}=12.38$, $P<0.02$, Newman-Keuls multiple comparison test: **$P<0.01$, OGD vs CTR; $^{\$}P<0.05$, OGD+PSB vs OGD. CTR, n=3; OGD, n=3; OGD+PSB, n=3; OGD+MRS, n=4. All data in the graphs are expressed as mean±S.E.M.

The merge of the immunofluorescence (yellow-orange) in a control slice is shown in Figure 56A. It is evident from the images that in basal conditions activated mTOR is present in CA1 pyamidal neurons where it is localized both in the cell body and in neuronal apical dendritic tree spanning throughout the SR. The simil ischemic condition caused a significant decrease of mTOR activation 3 h after the end of OGD, as shown in the representative image of Figure 56B-B1. This effect is more evident in Figure 56E-F, that represent digital subslices obtained stacking 9 consecutive confocal z-scans throughout the neuronal cell bodies (0.3 µm each, total thickness 2.7 µm) of control and OGD slices. The images clearly show that in control conditions phospho-mTOR was present both in the cell body (Figure 56E, open arrow) and in the dendrites (Figure 56E, white arrows), while 3 h after 7 min OGD activation of mTOR decreased both in cell body and dendrites (Figure 56F). Quantitative analysis showed that in slices harvested 1 h after the end of 7 min OGD, no significant modification of activated mTOR immunostaining was present in the neuronal cell body (Figure 56G) or in the apical dendrites of CA1 pyramidal neurons in any of the groups investigated (Figure 56I). On the contrary, in slices harvested 3 h after the end of 7 min OGD, we found highly significant decrease of activated mTOR immunostaining in the cytoplasm and dendrites of CA1 pyramidal neurons (Figure 56H, J).

Indeed, statistical analysis, shown in Figure 56H, demonstrates that 3 hours after the end of 7 min OGD there was a statistically significant reduction of activated mTOR immunostaining in the cytoplasm of CA1 pyramidal neurons (-74.8%, ***P<0.001 vs control slices, Figure 56H) in comparison to control slices. As shown in Figure 56H, treatment with 50 nM PSB603 blocked this effect (-4% vs control slices, n.s., $^{\$\$\$}$P<0.001 vs 7 min OGD), while treatment with 500 nM MRS1754 partially, but still significantly attenuatedd this effect (-31% vs controls, n.s., $^{\#\#}$P<0.01 vs 7 min OGD). We used, as a determinant of mTOR activation in the dendrites, the analysis of the length of phospho-mTOR+ dendrites, as reported in the methods. The results shown in Figure 56I reveal that mTOR activation was not statistically significant among the four experimental groups 1 h after the end of 7 min OGD. However, in the slices collected 3 h after the end of 7 min OGD we found a significant decrease of mTOR+ dendrites in the SR of the CA1 area (Figure 56J).

From the statistical analysis we found a significant decrease of mTOR immunopositive dendrites in CA1 SR of 7 min OGD slices 3 h after the end of OGD (-80% vs controls, **P<0.01, Figure 56J). The selective antagonist MRS1754, did not significantly modify this effect, while treatment with PSB603 partially, but significantly, reversed this effect (+226% vs 7 min OGD, $^{\$}$P<0.05). These data demonstrate that OGD significantly decreased mTOR activation and that the selective antagonism of A_{2B} receptors significantly reduced this impairment, a further indication of prevention of neuronal degeneration by blockade of this receptor.

4.29 Analysis of astrocytes in CA1 Stratum Radiatum after 7 min OGD

Astrocytes were labelled with the anti GFAP antibody and quantified in the SR of CA1 hippocampus in the four experimental conditions: in control slices, in slices after 7 min OGD alone, and after 7 min OGD in the presence of 500 nM MRS1754 or 50 nM PSB603, both at 1 h and 3 h after the end of OGD, as shown in the representative microphotographs in Figure 57A-D, taken at 3 h after the end of OGD. In the SR of slices harvested 1 h after the end of 7 min OGD we found a slight, not significant increase of astrocytes (Figure 57E, +19%, n.s. vs controls), which became significant at 3 h after the end of 7 min OGD (Figure 57F, +43% vs control slices, **P<0.01). Both A_{2B} receptor antagonists, partially but significantly, reduced the increase of astrocytes caused by the simil ischemic conditions. MRS1754 decreased the number of astrocytes by 10% (n.s. vs OGD), while PSB603 by 13% ($^{\$}$P<0.05 vs OGD). Quantitative analysis

of total microglia did not reveal statistically significant modifications in the different experimental conditions both at 1 h and 3 h after the end of 7 min OGD (data not shown).

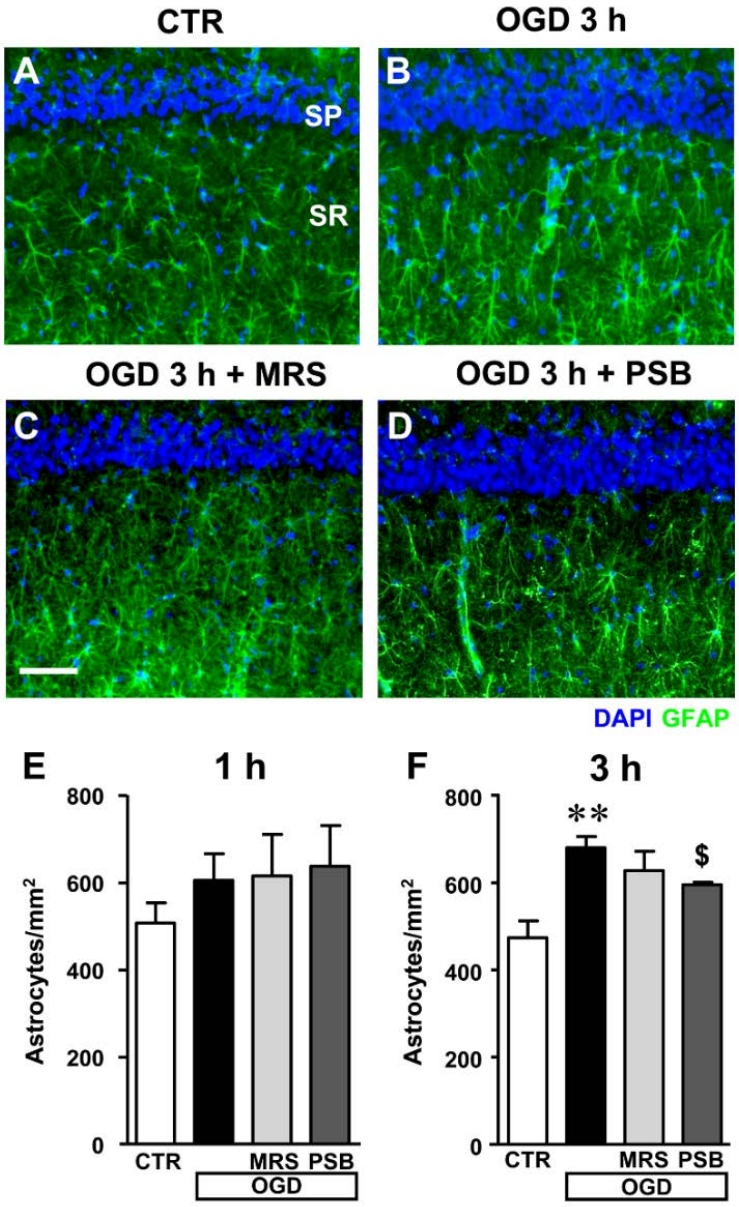

Figure 57. Quantitative analysis of astrocytes in the CA1 area in the different experimental conditions after the simil ischemic insult. **A-D:** Representative microphotographs, taken at the epifluorescence microscope, of astrocytes immunolabelled with anti GFAP antibodies in the SR (green) of a control (A), OGD (B), OGD plus MRS1754 (C), and OGD plus PSB603 (D) slice. Scale bar: 50 μm. **E-F:** Quantitative analysis of astrocytes in the SR of CA1 in control, OGD, OGD plus MRS1754 and OGD plus PSB603 slices at 1 h (E) and 3 h (F) after 7 min OGD. **E:** No significant differences among the four experimental groups analyzed was found. Statistical analysis: One-way ANOVA: $F_{(3;18)}$=0.877, P>0.05, ns. CTR, n=8; OGD, n=7; OGD+PSB, n=3; OGD+MRS, n=4. **F:** Statistical analysis: One-way ANOVA: $F_{(3;15)}$=6.734, P<0.01, Newman-Keuls multiple comparison test: **P<0.01, OGD vs CTR; $^{\$}$P<0.05, OGD+PSB vs OGD. CTR, n=7; OGD, n=4; OGD+PSB, n=4; OGD+MRS, n=4. All data in the graphs are expressed as mean ± S.E.M.

4.30 Neurodegeneration of CA1 pyramidal neurons induced by glutamate was not prevented by adenosine A_{2B} receptor antagonists

In order to have an insight into the mechanism of A_{2B} receptor antagonism-induced neuroprotection, we verified whether MRS1754 and PSB603 might protect CA1 pyramidal neurons from the well-known neurodegenerative effects caused by glutamate exposure. We incubated the hippocampal slices *in vitro* with 100 µM glutamate for 10 min and verified the effect of MRS1754 and PSB603 on glutamate-induced cell death. Administration of 100 µM glutamate for 10 min caused significant amage to pyramidal neurons at 3 h after the end of incubation, evidenced by the significant increase of HDN neurons in hippocampal CA1, as shown in the representative image presented in Figure 58B. Quantitative analysis (Figure 58D) demonstrated that the increase of HDN neurons was statistically significant in comparison to control slices, and that neither MRS1754 nor PSB603 protected CA1 pyramidal neurons from the excitotoxic effect of glutamate (*P<0.05 vs all other groups).

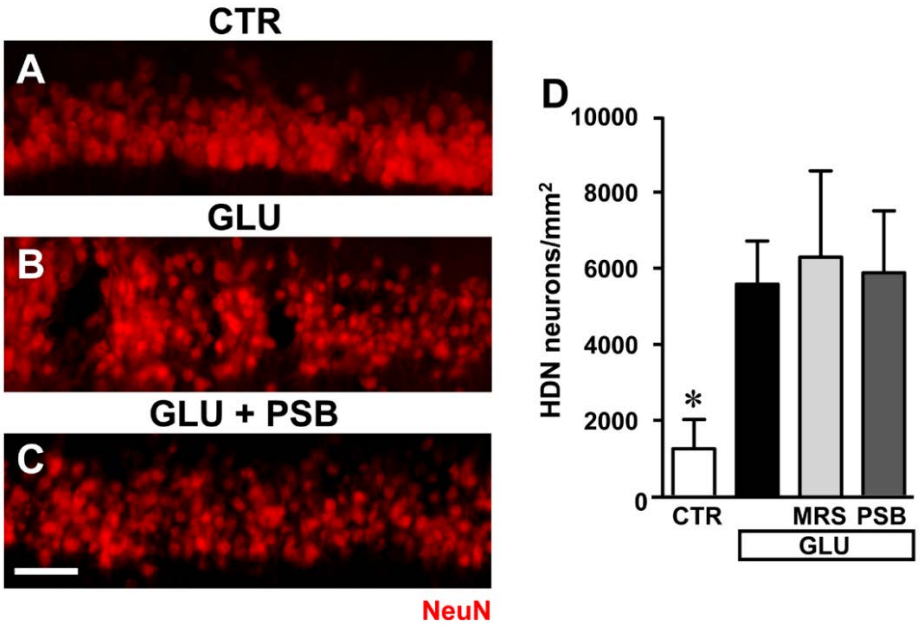

Figure 58. Evaluation of glutamate induced neurotoxicity in CA1 SP in the different experimental conditions. **A-C:** Representative microphotographs, taken at the epifluorescence microscope, of CA1 pyramidal neurons immunolabelled with anti NeuN antibodies in a control slice (A), a slice treated with glutamate (GLU, B), a slice treated with glutamate plus PSB603 (GLU+ PSB, C) slice. Scale bar: 50 µm. **D:** Quantitative analyses of NeuN+ HDN neurons in the four experimental groups 3 h after the end of drug incubation. Statistical analysis: One-way ANOVA: $F_{(3;15)}$=3.313, P<0.05, Newman-Keuls multiple comparison test: *P<0.05, vs all other groups. CTR, n=6; GLU, n=6; GLU+PSB, n=3; GLU+MRS, n=4.

Discussion

In the first part of my research, we demonstrated that the communication among neurons and astrocytes-microglia is of particular interest in physiological and pathological conditions and can provide insights into the aging process and help identify biomarkers of aging. Here we studied the changes in the intercommunication among neurons, microglia and astrocytes in the DG of the hippocampus during aging and in response to acute experimental neuroinflammation induced by treatment with LPS. Therefore, we studied two different conditions, one characterized by chronic low-grade inflammation caused by aging and the other one by a more intense, subchronic inflammatory response caused by LPS. We focussed on the DG of the hippocampus as it represents the first link of the canonical trisynaptic pathway that conveys electrophysiological inputs from the enthorinal cortex to the hippocampus proper (Amaral and Lavenex, 2007; Witter, 2007). Particularly, our study was directed to understand the modifications that might occur in the GL and PL of the DG.

The progressive modifications that occur in the aging brain, or "inflammaging," (Franceschi et al., 2007; Deleidi et al., 2015), are characterized by chronic, low-grade, upregulation of several pro-inflammatory mechanisms, and by changes in the reciprocal intercellular communication in the triads among neurons, astrocytes and microglia (Cerbai et al., 2012; Lana et al., 2014, 2016, 2017) that cause neuroinflammation. Here we demonstrated that in the GL and PL of aged and LPS-treated rats astrocytes were less numerous than in adult rats. Nevertheless, in the GL of LPS-treated rats the GFAP+ astrocytes acquired the morphology of reactive astrocytes, with principal branches longer than astrocytes of adult rats. Total and activated microglia increased in aged rats and in rats treated with LPS. Mainly in the GL of aged but also, to a lesser extent, in the GL of LPS-treated rats many neurons showed signs of apoptosis. Consistent with these results, the number of granular neurons decreased significantly in GL and PL of aged rats. This effect was not evident in GL and PL of LPS-treated rats, suggesting that the subchronic neuroinflammation was insufficient to reproduce a similar degree of granular cell loss. We found that in PL of aged and LPS-treated rats many damaged neurons were embraced by microglia and were infiltrated by astrocyte branches, which appeared to be bisecting the neuron to form cellular debris which were phagocytosed by reactive microglia. Triads were significantly more numerous in PL of aged and LPS-treated rats. This effect was consistent with microglia scavenging dying neurons. The levels of the chemokine CX3CL1 increased, and in the PL of aged and LPS-treated rats

CX3CL1 immunoreactivity was colocalized both in the branches and in the cell body of activated microglia.

The networks of communication among different cells change during aging or disease, and this aspect is particularly true and can have great consequences in the brain. It is not clear whether age-related changes of intercommunication and interplay among different cell types are simply adaptations to aging, or actively contribute to aging or disease mechanisms *per se*. Consequently, the interplay among different cell types may modulate or even control aging or may be unbalanced in particular diseases (De Keyser et al., 2008; Sofroniew, 2009). For a long time neurons have been considered the basic functional units of the central nervous system, and glia only trophic and supportive elements. However, recently it is becoming evident that for the functional organization of the brain proper intercommunication among cells that form the neuron-astrocyte-microglia ‘‘triad’’ is fundamental (Barres, 2008; Allen & Barres 2009). We and others (Cerbai et al., 2012; Lana et al., 2016; Re et al., 2014) demonstrated that in stress conditions, astrocytes fragment degenerating neurons and cooperate with microglia in the disposal of neuronal debris.

In line with our previous data (Cerbai et al., 2012; Lana et al., 2016), here we found that many neurons in the granular layer of aged rat hippocampus underwent apoptosis, which caused cellular degeneration and death. The decrease of neurons in DG of aged rats, possibly made more significant by reduction of neurogenesis during aging (Kuhn et al., 1996), may contribute to age-related memory impairments, as demonstrated in previous experiments with similar rat models (Lana et al., 2016). In the aged rat DG, not only neurons showed signs of degeneration, but also astrocytes were less numerous and had morphological features of clasmatodendrosis (Hulse et al., 2001; Mercatelli et al., 2016). In a less neuron-centric view of neurodegeneration during aging, the loss of astrocytes and their functions such as brain homeostasis maintenance, extracellular glutamate and ion buffering, as well as energy and nutrient supply to neurons, may contribute to spread of neural damage and degeneration (Miller et al., 2017). It has been demonstrated (Bernal & Peterson, 2011) that the decrease of astrocytes in DG of aged rats is accompanied by decreased astrocyte-dependent VEGF expression during aging, further supporting our findings. Nevertheless, the findings in this regards are still controversial (for rev. see Rodrìguez-Arellano, 2016).

The current investigation did not find significant decrease of neurons in DG of LPS-treated rats. Since LPS is detrimental for neurogenesis (Ekdahl et al., 2003; Littlefield et

al., 2015), other mechanisms must be taken into consideration to explain this apparent discrepancy. First, apoptotic neurons in GL of LPS-treated rats, although more numerous than in adult rats, were significantly less numerous than in aged rats, and the consequent the neuronal death may be less relevant. Furthermore, although in LPS-treated rats, as in aged rats, astrocytes were less numerous than in adult rats, in LPS-treated rats astrocytes were in a reactive state. Indeed, astrocyte branches were longer, and were able to pass through the entire depth of the granular layer, a finding indicative of a better trophic support exerted by astrocytes towards granular cells in LPS-treated rats. This phenomenon, contrary to that observed in CA1 (Lana et al., 2014), can be considered a protective effect of astrocytes towards neurons.

Taken together with our previous reports (Cerbai et al., 2012; Lana et al., 2014, 2016) our findings confirm that reactive astrogliosis is not a single, uniform process, and not always a negative phenomenon. In moderate astrogliosis, astrocytes have hypertrophic bodies and processes (Wilhelmsson et al., 2006), are distributed in contiguous, non-overlapping domains (Bushong, et al., 2002), their proliferation is limited and do not form scars. In line with these findings, it has it been shown that adaptive astrogliosis is beneficial for neurons, while suppression of astroglia reactivity may increase neuronal vulnerability, exacerbating the pathological progression and altering regeneration (Sofroniew, 2009; Burda and Sofroniew, 2014; Pekny et al., 2014). Supporting our findings, other data demonstrated that hypertrophy of astrocytes may reflect astrocytes adaptive plasticity, as demonstrated in aged rodents increasing morphological complexity by an enriched environment (Rodrìguez et al., 2013; Sampedro-Piquero et al., 2014).

Here we showed that many neurons that form triads with astrocytes and microglia in the PL of the DG were granular cells, located very close to the GL, although clearly detached from it. These results are in agreement with the current knowledge that during the first steps of apoptosis caspases break the cell cytoskeleton, allowing the apoptotic cell to detach from the surrounding, healthy cells (Böhm, 2003). This mechanism may explain how apoptotic, damaged neurons migrate from the GL to the PL to form triads in which phagocytosis may take place. Active and controlled cell death may serve a homeostatic function in regulating the number of cell population in healthy and pathological conditions (Becker and Bonni, 2004; Kerr et al., 1972). Thus, triad formation seems a specific mechanism for disposal of degenerating neurons, not only through phagocytosis, but also through the mechanism of phagoptosis (Brown and

Neher, 2012). Phagoptosis is triggered by cell stress which is too mild to cause cell death, too serious to allow adaptation of the neuron to the damage but sufficient to recruit astrocytes and microglia for phagocytosis (Kao et al., 2011).

Microglia activation has been long considered detrimental for neuron survival, more recently it appears that this is not always the case (Solito and Sastre, 2012; Zhu et al., 2016). Furthermore, given the increased number of total and activated microglia cells in the DG of rats treated with LPS, we can hypothesize that the scavenging processes were more effective in DG of LPS-treated rats than in aged rats. These data are in agreement with results that showed that during aging, although microglia increased, the cells had morphological modifications that caused less neuroprotective and defensive capabilities of microglia (Tremblay et al., 2011; Streit and Xue, 2013; Streit et al., 2009).

In the current study, we confirmed that hippocampal levels of CX3CL1 (Cerbai et al., 2012) increased significantly both in aged and LPS-treated rats. At the morphological level, we found that CX3CL1 was never colocalized with neurons or astrocytes, but only with activated microglia. This is an interesting, unexpected finding since, as reported by Luo et al. (2016), although CX3CL1 is considered to be principally expressed by neurons, while its receptor by microglia (Cardona et al., 2006; Harrison et al., 1998; Lauro et al., 2008), it is still debatable whether other cell types also express CX3CL1. We had previously demonstrated that CX3CL1 immunostaining in CA1 was localized on neurons phagocytized by microglia (Cerbai et al., 2012). Nevertheless, in the periphery CX3CL1 is expressed in different inflammatory conditions by monocytes, macrophages, and other cells types such as fibroblasts, endothelial cells, and dendritic cells (Jones et al., 2010). Therefore, as the resident macrophage cells of the brain, it is possible that in particular areas and in certain stress conditions such as inflammation, microglia will express CX3CL1. Consistent with these data we also found a highly significant increase not only of total but also of activated microglia in PL of LPS-treated rats. On the other hand, microglia express the only receptor for CX3CL1, whose role in the CX3CL1-associated activation of microglia is well known (Jung et al., 2000). Therefore, it is also plausible that immunofluorescence of CX3CL1 that we detected on microglia might depend upon the binding of CX3CL1 to its receptor. Indeed, although it has been shown that CX3CL1 maintains microglia in a quiescent state (Lyons et al., 2009; Bachstetter et al., 2011), it has also been demonstrated that soluble CX3CL1 increases and is released in cerebral ischemia (Denes et al., 2008), in response to apoptosis (Fuller and Van Eldik, 2008) and to glutamate excitotoxicity (Chapman et al.,

2000). Nevertheless, CX3CL1 role as a neuroprotective or neurotoxic molecule remains unresolved (Lauro et al., 2015). It has been shown that CX3CL1 is neuroprotective in cultured rat hippocampal neurons (Limatola et al., 2005; Cipriani et al., 2011) and *Cx3cr1*$^{-/-}$ mice show reduced damage after cerebral ischemia; this protection may be due to the anti-inflammatory state of local microglia (Tang et al., 2014). CX3CL1 may also be or deleterious (Liu et al., 2015) in different models of neurodegenerative diseases, indicating that the effects of CX3CL1 may be different, according upon different degenerative stimuli (Lauro et al., 2008).

Comparison of the results obtained in studies of the DG, CA1 and CA3

It is generally believed that neuroinflammation is characterized by astroglia activation, which can be typified by morphological changes, accompanied by low to moderate levels of inflammatory mediators in the parenchyma. Although it is commonly agreed that astroglia is activated and reacts similarly in different conditions (Ransohoff, 2016) and brain areas, our data demonstrate the responses of astrocytes and microglia to aging and LPS-induced inflammation to the same stressful stimuli are different not only among different subregions but also within the same hippocampal subregion. The differential reactivity of astrocytes and microglia is reported in Table 2, which is built from results taken from our present data and from previous published papers (Cerbai et al., 2012; Lana et al., 2016), all obtained in the same rat models of aging and brain inflammation. From the data reported in Table 2 it is interesting to note that in all hippocampal subregions of aged rats, astrocytes decreased significantly, while total microglia decreased in CA1 only, and increased in CA3 and DG. In LPS-treated rats both total and activated microglia increased in all three regions, while astrocytes did not vary in CA1 SR (SR), increased in CA3 SR and decreased in DG PL. Of note is also the much lower density of activated microglia in CA1 in comparison to CA3 and DG, in the three experimental models. Thus, taken together with the results from our previous investigations of the hippocampus under identical conditions, we conclude that in DG PL, and in CA1 and CA3 SR (Cerbai et al., 2012; Lana et al., 2016), all subregions of rat hippocampus that are contiguous and interconnected, astrocytes and microglia show very different reactivity in the three experimental groups. These data demonstrate that astrocytes and microglial responses to the same insult are not uniform but vary significantly from area to area and in different stress conditions. It will be of great interest to confirm whether these differences of glial reactivity may explain the differential susceptibility of the hippocampal areas to aging or to different inflammatory

insults (Masgrau et al., 2017). It was previously demonstrated that activated microglia are seen diffusely scattered throughout the brain after two days of LPS infusion (Wenk et. al, 2000). During the next weeks, the number of activated microglia gradually decreases in all cerebral regions and after four weeks, the greatest inflammatory response is concentrated within the hippocampus (Wenk et. al, 2000). These findings suggest that LPS initiates a cascade of biochemical processes that show time-dependent, regional and cell specific changes that are maximal after four weeks of LPS infusion (Wenk, 2000; Hauss-Wegrzyniak, 1998).

In the second part of my research we demostrated that on the one hand, glial cells play a main defensive role against exogenous pathogens and endogenous noxious molecules in the CNS. On the other hand, they can exert deleterious effects in a sustained pro-inflammatory response. Rapid neuroprotective effect of microglia is facilitated by its regular distribution, which minimizes the distance from possible pro-inflammatory triggers, such as amyloid deposits, cell debris and entire damaged neurons. Astrocytes constantly contact neuron surfaces, interact with neuron debris (Reemst et al. 2016), thus the continuous meshwork of their projections may be the first glial structure contacting possible targets of microglia phagocytosis. We demonstrated the hypothesis that a direct cell-cell interaction exists between astrocytes and microglia in rat hippocampus, influencing and mediating microglial branching and, in turn, addressing branch tree extension towards pro-inflammatory triggers. We also demonstrated that the astrocyte meshwork disruption occurring in aged hippocampus, could be related to dysregulation of microglial defensive activity.

Analyses on microglia morphology, disclosed by IBA1 staining, revealed that branch volume in LPS-treated rats was higher than in control rats. According to previous findings, extension of microglial projections during inflammation can be considered a chemotactic process sensing the localization of phagocytosis targets in an inflammatory milieu (Hanisch & Kettenmann, 2007). This process is known to depend on ECM components (Honda et al., 2001) and soluble chemoattractants (Fan et al., 2017; Hall, 1998; Ohsawa et al., 2000). Confocal imaging of IBA1 immunostaining showed remarkable branch sprout along microglial projections in LPS-rats, suggesting that microglial branch sprouting might be triggered by neuroinflammation. IBA1 is a microglial marker known to promote actin rearrangement in migration and phagocytosis processes (Damani et al., 2011). Measurements here reported on immunofluorescence intensity showed that a correspondence exists between IBA1 expression in microglial projections

and their volume, being both higher in LPS than in control rats. Therefore, it can be suggested that an increase of IBA1-mediated cytoskeletal rearrangement may play a key-role in the initial steps of microglial activation and migration in an inflammatory milieu, such as in the hippocampus of LPS rats. In aged rats, our analyses reported lower branching and smaller volume of their projections in comparison to the other animal groups. These data are consistent with previous findings (Wong, 2013; von Bernhardi et al., 2015) and suggest that aged microglia cells are characterized by low efficient cytoskeletal remodeling in their projections and, consequently, impairment of microglial migration and phagocytic activity.

Confocal microscopy analysis of IBA1+ microglia and GFAP+ astrocytes in aged CA1 hippocampus first correlated the extent of microglial branching with integrity of the astrocyte meshwork. In a previous paper of our group, the remarkable disruption of the astrocyte meshwork in aged rats is ascribable to clasmatodendrosis: a fragmentation of astrocytes projections. These data support the existence of astroglia-microglia crosstalk in the rat hippocampus, involved in microglia distribution and branching. The analyses of microglial expression of integrin-β1, a known mechanosensor (Fan et al., 2017), suggested the involvement of mechanotransduction in these interactions: in control and LPS rats, microglial integrin-β1 was significantly concentrated at contact sites between microglia cells projections and astrocytes projections. In the current work, we have postulated a link between integrin-β1 localization at microglia cells and astrocytes projections contacts and the dynamic remodeling of microglial branch tree, which is present in normal CNS and may be intensified during inflammation (Hanisch & Kettenmann, 2007). Quantitative analyses in aged rats revealed a parallel decrease of microglia cells and astrocytes projections contact extent and integrin-β1 expression. Morphological analyses revealed a dichotomous situation: microglia processes appeared ramified and showed high accumulation of integrin-β1 at contact sites within the intact astrocyte meshwork, whereas they appeared unbranched, enlarged and with scanty integrin-β1 accumulation in the disrupted astrocyte meshwork. These data suggest that a scattered impairment of astroglia-microglia direct interaction might hamper microglial branching and migration in aged rats.

The same pattern of contact distribution was observed also in LPS rats. These data suggest that local increase of astroglia-microglia interactions may address microglia branching towards damaged neurons in the “find me” step of neurophagocytic activity. In aged rats, a direct correlation was found between integrity of the astrocyte meshwork,

microglia-astrocyte interactions and patterns of neurophagocytic activity. In aged rats, impairment of microglia-astrocyte interaction due to clasmatodendrosis may reduce the efficiency of microglial neurophagocytic activity, thus contributing to the increase of pro-inflammatory cell debris in the nervous tissue.

In summary, our findings suggest that in rat hippocampus a direct astrocytes-microglia interaction exists, affecting microglial branching and distribution. Such interaction is dynamic, involves accumulation of integrin-β1 at microglia-astrocyte contacts and may address microglia branching towards targets of phagocytosis. We hypothesize that the impairment of this interaction in aged rats hampers the migration of microglia causing inefficient phagocytosis of injured neurons. A detrimental loop could be triggered in the aged rat hippocampus where accumulation of toxic debris might hamper microglia clearance activity by inducing disruption of the astrocyte meshwork. The data reported in the present study contribute to expand the wealthy panel of interactions occurring among the different cell populations of the nervous tissue and add plausibility to the idea that such interactions give rise to a network of morphological and functional reciprocal reliance and dependency. To comprehend peculiar aspects of the onset and progression of neuroinflammation, it is necessary to cosidered that any tissue, and first of all the nervous tissue, is not composed by a collection of single elements but rather by interacting and interdependent cell populations that cooperate to maintain homeostasis and functionality of an organ. Different kind of alterations affecting one population reasonably will reverberate to the others either favoring or dysregulating their activities.

The third part of my study was to investigate and compare the quantitative, temporal, and spatial modifications of the interplay between astrocytes, microglia and neurons in CA1 and CA3 hippocampus of TgCRND8 mice, a mouse model of Aβ deposition, at 3 and 6 months of age. The comparison between these two hippocampal areas is fundamental and can help explaining the more pronounced sensitivity of CA1 pyramidal neurons to neurodegenerative insults, both in experimental animals and in humans (Bartsch et al., 2015; Mueller et al., 2010; Small et al., 2011). It is also important because of the critical, although different, role of these areas in memory processing and because of their significant functional, structural, and morphological alterations in AD (Bartsch and Wulff, 2015). Therefore, in this work, we studied the different patterns of neuron degeneration and apoptosis, glia activation/modification, as well as different expression of proinflammatory mediators, at different stages of plaque deposition,

subdividing the hippocampus in the two main regions of interest CA1 and CA3. The principal findings of this study were that the two contiguous and interconnected hippocampal regions of transgenic mice display remarkably different cellular modifications and neuronal vulnerability to the deposition of Aβ plaques. Interestingly, while total Aβ load in CA1 was not significantly different from that of CA3, both at 3 and 6 months of age, in CA1 SR of Tg 6M mice the Medium and Large plaques were significantly more numerous than in CA3 SR. As expected, we found many hypertrophic astrocytes surrounding and infiltrating Aβ plaques, both in CA1 and CA3. Nevertheless, astrogliosis was also evident not only close to the plaques, but also in the SR parenchyma far from and devoid of plaques. Astrogliosis, evidenced by increased recruitment of astrocytes, increased expression of GFAP and elongation of astrocyte branches, significantly increased in the entire CA1 of transgenic mice, mainly at 6 months of age, while in CA3 it was significantly lower than in CA1. Healthy astrocytes are indispensable for synaptogenesis, synaptic maintenance and maturation (Pfrieger, 2009; Heneka et al., 2010), significantly contributing to memory-associated processes (Verkhratsky et al., 2011), but they are also involved in AD, as first suggested by Alois Alzheimer (Alzheimer, 1910). The involvement of astrocytes in AD progression is variegated, depending upon the brain area interested and the gravity of the disease. Indeed, in the hippocampus, progression of AD has been associated with an early atrophy of astrocytes, defined clasmatodendrosis (Hulse et al., 2001; Penfield, 1928) that, at later stages of the disease, coexists with reactive astrocytes around plaques (Olabarria et al. 2010; Yeh et al. 2011). We never found clasmatodendrotic astrocytes in CA1 and CA3 parenchyma of transgenic mice at both 3 and 6 months of age.

Dissecting the hippocampus in the two main regions CA1 and CA3 we observed significant differences in most of the parameters investigated, at different stages of plaque deposition. In CA1 SR of 6 months aged transgenic mice, we found significantly higher levels of the expression of the cytokines TNFα, IL1β, as well as iNOS in astrocytes, confirming our and others' results in TgCNRD8 mice (Luccarini et al., 2012) and other models of neurodegenerative diseases (Deng et al., 2014; Lana et al., 2017). It has been demonstrated that the inflammatory cytokine TNFα is usually expressed in the brain by activated microglia, and, to a lesser extent, by activated astrocytes and neurons (Perry et al., 2002). Nevertheless, many studies have shown that the gradual deposition of Aβ peptide and overproduction of inflammatory mediators activate astrocytes, further inducing expression and release of cytokines, interleukins, NO and other

proinflammatory mediators (Heneka et al., 2015; Choi et al., 2014) that in turn increase pro-apoptotic cascades in the surrounding brain areas (Luccarini et al., 2012), and exacerbate AD pathology (Tan et al., 2007). Furthermore, it has been demonstrated that TNFα induces apoptosis primarily through the activation of cell-surface TNFα type I receptors that contain death domains (Park et al., 2007). In line with these data, our results demonstrate that in CA1 SP, both at 3 and 6 months of age, a significant number of pyramidal neurons underwent apoptosis, possibly targeted by increased TNFα expression and release by astrocytes. In addition, stimulation of iNOS by cytokines in astrocytes may cause increased concentrations of NO that can be toxic to neurons. Indeed, iNOS is upregulated AD patients' brain (Vodovoz et al., 1996) and Knock Out of iNOS is protective in mouse models of AD (Nathan et al., 2005). These mechanisms may be the cause of the significant loss of CA1 pyramidal neurons and shrinkage of CA1 stratum pyramidale, evidenced in CA1 but not in CA3.

It is known that Aß plaques induce production and release of pro-inflammatory cytokines by neurons and astrocytes (Hickman et al. 2008, Daria et al. 2017) which, in turn, promote a shift in microglia activity, from surveillance/maintenance mode, to execution of immune tasks. Microglia can assume two different phenotypic forms, M1 and M2 (Loane & Kumar, 2016). While M1 microglia can express and release proinflammatory cytokines (de Bilbao et al., 2009; Protti, et al., 2013), M2 microglia is more active in the surveillance/maintenance of tissue homeostasis, phagocytosing apoptotic or degenerating neurons, preventing secondary inflammatory mechanisms and promoting tissue regeneration (Hu et al., 2012; Suenaga et al., 2015). In both CA1 and CA3 of transgenic mice, we found an increase of total microglia, and of reactive microglia, corresponding to the M1 phenotype, which significantly increased in CA1 SP and SR at 3 and 6 months of age. These data indicate that the inflammatory milieu triggered by plaque deposition caused increased recruitment of microglia cells, and significantly increased its reactivity. Furthermore, in agreement with data obtained by Bolmont et al. (2008) in the cortex of APPPS1 transgenic mice, we found significant spatial orientation of microglia towards Large plaques, both in CA1 and CA3 SR of Tg 6M mice.

The reactivity state of microglia in CA1 SR, together with increased astrogliosis, caused increased formation of neuron-astrocytes-microglia triads. The concerted actions of astrocytes and microglia in the formation of triads with neurons can recognize "danger signals", including cellular debris produced from apoptotic or necrotic cells (Milligan &

Watkins, 2009), and can clear the damaged neurons or neuronal debris by phagocytosis (Cerbai et al., 2012; Lana et al., 2014). Indeed, we found several reactive microglia cells that cooperated with astrocytes in the phagocytosis of degenerated neurons, mainly in SR of transgenic mice. Under physiological conditions, the effects of astrocytes and microglia are protective, removing entire neurons by phagoptosis (Lana et al., 2017), clearing dysfunctional synapses and controlling inflammation and the diffusion of cellular damage to neighboring tissue. Also, activated microglia contribute to Aß-clearance and removal of cytotoxic debris from the nervous tissue. However, phagocytosis of living healthy neurons by microglial in inflamed CNS has also been reported (Neher et al. 2012; Vilalta & Brown 2017). Furthermore, uninterrupted microglia activation may exacerbate inflammation, increase Aß-deposition and intensify neurodegeneration (Michaud et al. 2015). Indeed, in AD, as for astrocytes, pro-inflammatory and detrimental, or antiinflammatory and even protective properties have been attributed to microglia (Heneka et al., 2015; Heppner et al., 2015; Mandrekar & Landreth, 2010). All these different findings may suggest that microglia may acquire heterogeneous activation states, or, as in our results, microglia can be protective or detrimental, depending on the region where it is located and other concauses.

Here we have demonstrated that not only the proximity to plaques determines the development of a specific reactive phenotype of microglia (Plescher et al., 2018) and astrocytes (Olabarria et al., 2010), but also the different plaque size and distribution within different brain areas. In CA1 and CA3 hippocampus, although Aβ load was similar, plaque organization in terms of dimensions was different, and glia and neurons responded with differential patterns of activation and neurodegeneration. The sensitivity of the subregional pyramidal neurons to neurodegeneration was very different, at both 3 and 6 months of age. Our paper is in line with recent evidence showing hippocampal subregional-specific patterns of neurodegeneration at different stages of Aß deposition (Mahar et al., 2017; Albuquerque et al., 2015).

Significant progress has been made in understanding the relationships of amyloid pathology to hippocampal dysfunctions, however complete understanding of this process across hippocampal anatomical areas remains incomplete. Although the hippocampus is often described as a unitary structure, this is hardly the case. The unique molecular and synaptic milieu of its spatial domains allow asking how AD pathophysiology can arise in one region versus the other one. Memory impairment, particularly episodic and spatial memory, is the most important symptom of AD, often

related to the dysfunction of pyramidal neurons in CA1 and entorhinal cortex (Hyman et al., 1984; Kerchner et al., 2010; Scheff et al., 2007; West et al., 2000). Studies have shown that lesions centering on CA1 are sufficient for memory impairment (Zola-Morgan et al., 1986). Indeed, our data lend support to the idea that Aβ load exerts greater effects on CA1 than on CA3. Many authors found that the CA1 is the most vulnerable region of the hippocampus to neuronal loss both in animal models of AD and in AD patients (Corbett et al., 2013; Stepanichev et al., 2006; West et al., 2000; Price et al., 2001; Rossler et al., 2002). Among AD patients, variable degree of atrophy between CA1 and CA3 is often found, CA3 being the least damaged area (Hyman et al., 1984). On the other hand, in different transgenic mouse models of AD it has also been found (Gruart et al., 2008) that learning and memory deficits are not directly correlated to Aβ load. Therefore, other factors, besides Aβ deposition may be involved in memory deficits.

The loss of CA1 pyramidal neurons, which underwent neuronal death by apoptosis, caused shrinkage of the CA1 pyramidal cell layer. All these modifications may be at the basis of memory loss, which was repeatedly demonstrated in this transgenic mouse model of Aß deposition, even at early stages (Chishti et al., 2001; Hamm et al., 2017). Interestingly however, it has been shown that increased physical activity improves behavioural and cognitive deficits in murine models of AD (García-Mesa et al., 2011) and reduces the risk of AD in humans (Buchman et al., 2012). The precise mechanism of action underlying the positive effects of physical activity are still not known, but may involve astrocytes (Latimer et al., 2011), indicating that astrogliosis may become a therapeutic target for AD (Colangelo et al., 2014).

In the fourth part of this research, we used the model of brain chronic hypoperfusion with the permanent bilateral common carotid artery occlusion or two vessel occlusion (2VO) in the rat (Sarti et al, 2002a,b; Farkas et al., 2007; Lana et al., 2014), which is a suitable animal species for this purpose since the circle of Willis affords reduced blood flow to the brain (Otori et al., 2003). As outlined by Farkas and coworkers (2007) the rat 2VO model is useful to investigate the long-term effects of chronic cerebral hypoperfusion (Farkas et al., 2007) since hypoperfusion is global although mild, and represents a model of cerebrovascular stenosis in aging humans. Furthermore, the damage to the nervous tissue, although chronic, is less dramatic than in focal ischemic models (Farkas et al., 2007). In a recent paper, we studied the quantitative and

qualitative changes induced by 2VO on neurons, astrocytes, microglia, in hippocampal CA1 (Lana et a.l, 2014). Here we studied the effect of 2VO on hippocampal area CA3 and the comparison between the results obtained in CA1 and CA3 will be useful to understand the different reactivity of the two areas after the hypoxic insult, and more specifically to understand if and why CA3 pyramidal neurons show better adaptation to an ischemic insult and to degeneration in comparison to CA1 pyramidal neurons. In our study, dipyridamole was tested in the 2VO model to evaluate its protective role against the physiopathological mechanisms that the ischemic insult exerts in the CA3 region of the hippocampus.

Brain chronic hypoperfusion, caused by partial carotid occlusion during aging, represents a chronic, dynamic process that causes multiple progressive alterations, and eventually leads to neurodegeneration (Ozacmak et al., 2007; Farkas et al., 2007) and vascular dementia (Chmayssani et al., 2007). The CA1 region of the hippocampus results particularly vulnerable to decreased blood flow and glucose supply caused by 2VO occlusion, that cause failure of neuronal signaling, and impairments in hippocampally-based forms of memory (De Jong et al., 1999; Liu et al., 2005; Farkas et al., 2006; Melani et al., 2010; Lana et al., 2013). It is well known that CA3 and CA1 hippocampal areas, although well interconnected, respond differently to ischemic/hypoxic insults (Kirino et al., 2000). As demonstrated in animal models (Schmidt-Kastner & Freund 1991), CA1 neurons of patients with cerebral hypoxia are the most vulnerable in the brain (Zola-Morgan et al., 1986; Petito et al., 1987). At early stages after an ischemic insult, the pyramidal neurons from CA1 and CA3 are exposed to similar triggering events such as the increase of extracellular glutamate (Mitani et al., 1992). Energy deprivation reduces intracellular ATP modifying the ionic gradients and inverting glutamate transport both in pyramidal CA1 (Rossi et al., 2000) and CA3 neurons (Jabaudon et al., 2000). At later times, NMDA-mediated responses increase in CA1 pyramidal neurons, which become more sensitive, while are transiently depressed in CA3 pyramidal neurons, that become more resistant. It has also been demonstrated that the balance kinase/phosphatase is different between CA1 and CA3. In CA1, the balance kinase/phosphatase is in favour of kinase activity, while in CA3 it is in favour of phosphatase activity (Gee et al., 2006). Nevertheless, the question that remains to be answered to is how and why these two contiguous, interconnected regions of the hippocampus respond differently to an ischemic event.

Here we exploited the 2VO hypoperfusion paradigm to verify whether and how the interaction between glia and neurons in CA3 may change after hypoperfusion. Immunohistochemistry and confocal microscopy analysis revealed the presence of significantly more numerous "ectopic" pyramidal neurons in the CA1 Str. Radiatum of 2VO rats, localized both in SL and SR layers. Since the SL subregion is paradigmatically defined as “a-neuronal” (Amaral et al., 2007), the ectopic neurons are likely deriving from CA3 SP. Our results demonstrate that the CA3 of hypoperfused rats undergoes a process of low-grade inflammation and programmed cell death, and astrocytes and microglia form triads with degenerating neurons and cooperate in the phagocytosis and clearance of ectopic neurons and neuronal debris. This phenomenon may represent a sign of alteration and damage of the hippocampal CA3 pyramidal neurons. The cells we defined as ectopic neurons had a pyramidal shape, typical of pyramidal neurons and were located both in SL and in SR. Using immunostaining for CytC, a marker for apoptosis, we demonstrated that in SP and SL of CA3 of 2VO-vehicle rats many neurons were apoptotic, significantly more numerous in SP of hypoperfused rats. We also demonstrated the presence of a significantly higher number of neuronal debris, possibly deriving from apoptotic neurons, both in SL and SR of 2VO-vehicle rats, but not in SL and SR of 2VO-dypiridamole treated rats. This latter finding may explain the protective effect of dypiridamole, as explained in more details below.

Despite the increase of apoptotic neurons, of ectopic neurons and of neuronal debris in hippocampal SL and SR of 2VO-vehicle rats, we did not find significant decrease of CA3 pyramidal neurons in comparison to sham rats. This effect could depend upon increased neurogenesis during the restitution phase of brain chronic ischemia, as shown *in vivo* (Dirnagl, 2012; Farkas et al., 2007) and *in vitro* (Maraula et al., 2013) in models of chronic ischemia. Newborn neurons may then migrate from the subgranular zone (SGZ) of the DG to integrate the apoptotic neurons in the CA3 pyramidal layer.

During chronic cerebral hypoperfusion, astrogliosis is generally considered a late-emerging event (Farkas et al., 2007; Farkas et al., 2004, 2006; Pappas et al., 1996; Schmidt-Kastner et al., 2005) in the hippocampus. Consistently, we found significant increase of astrocytes in SP and SR of 2VO-vehicle rats and in SP, SL and SR of 2VO-dypiridamole treated rats. The length of astrocyte branches were not different among groups and regions investigated, indicating that the astrocytes were not hypertrophic or hyperactivated. We hypothesize that the increased number of astrocytes might be the

consequence of higher demand of oxygen and nutrients by neurons that are in a hypoxic/hypoglycemic milieu given by the hypoperfusion state. The reduced trophic support to CA3 neurons could be balanced by increased number of astrocytes. This phenomenon, contrary to that observed in CA1 in the same model of chronic cerebral hypoxia (Lana et al., 2014) can be considered a protective effect of astrocytes towards neurons. The idea that an increased number of astrocytes is always a negative phenomenon is rapidly changing, thanks to new data and to new concepts that suggest a more complex and more variegated role of astrocytes in physiological mechanisms and in different neuropathological disorders (Sofroniew et al., 2009; Verkhratsky et al., 2013; Burda et al., 2014). It is becoming more and more evident that dysfunctions in the process of astrogliosis contribute to or are the primary cause of damaging mechanisms in the central nervous system, both through loss of normal functions and through increase of damaging effects (Sofroniew, 2009). As reported by Sofroniew (Sofroniew, 2009; Sofroniew and Vinters, 2010), and demonstrated in other papers from our laboratory (Lana et al., 2012, 2014, 2016) astrogliosis is not a single uniform process, nor always synonymous with scar formation. In moderate reactive astrogliosis, such as the one we found in CA3 SL and SR, astrocyte proliferation is scarce, and astrocytes do not form scars but occupy non-overlapping domains (Bushong et al., 2002). Astrocytes infiltrate their branches inside the body of ectopic pyramidal neurons to trigger or help their disgregation, as previously found (Cerbai et al 2012, Re et al. 2014, Lana et al., 2014, 2016). Indeed, with the triple immunostaining of neurons, astrocytes and microglia we demonstrated that in in SL and SR of the three experimental groups many ectopic neurons were surrounded by astrocyte branches and by microglia forming the so-called triads. Triads were significantly more numerous in the SR of 2VO-vehicle rats than in the two other groups. Dypiridamole reduced this effect, although not completely. The phenomenon of neuron infiltration, and fragmentation by astrocytes branches, first demonstrated in our laboratory (Cerbai et al., 2012), was later confirmed by Re and coworkers in a model of ALS (Re et al., 2014) and in other papers from our group (Lana et al., 2014, 2016). As we demonstrated, astrocyte branches intermingled and penetrated the neuronal cytoplasm, fragmenting the neuronal cell body to give rise to cellular debris. The fragmentation of ectopic neurons may be the consequence of the apoptotic process, which these neurons were undertaking because of the hypoxic state of the tissue after 2VO. As demonstrated in other models of neurodegeneration (Cerbai et al., 2012; Huizinga et al., 2012; Polazzi and Monti, 2010), fragmentation of apoptotic

neurons may be triggered or accelerated by astrocyte branches that infiltrate the neuronal cell body, forming smaller debris ready for phagocytosis by microglia. Thus, we hypothesize that it may represent a mechanism common to many neurodegenerative processes.

We found an increase of IBA1+ microglia in SL and SR of 2VO-vehicle and 2VO-dypiridamole treated rats, an indication that the low grade of local inflammation could recruit microglia in these regions, while in SP of 2VO-dipyridamole rats IBA1+ microglia decreased. Microglia recruitment and activation has long been considered a negative mechanism that leads to accumulation of neurotoxic phagocytes, but more recently, it is considered a reversible multistep process which leads to neuroprotective effects (Hanisch & Kettenmann, 2007; Kettenmann et al., 2013; Ransohoff & Perry, 2009). We found that many microglial cells cooperated with astrocytes forming triads to remove, through phagocytosis, degenerating, apoptotic neurons, both in SR of 2VO-vehicle and 2VO-dypiridamole treated rats. In SL and SR of 2VO-dypiridamole treated rats we found the presence of a significantly lower number of neuronal debris. Several authors have indicated that microglial activation following neuronal injury represents mainly a protective mechanism that limits further neurodegeneration (Minghetti & Levi, 1998; Streit et al., 1999; Polazzi and Contestabile, 2002). Indeed, it has been shown that phagocytosis of apoptotic cells by microglia decreases the production of pro-inflammatory cytokines, such as TNFα and IL-12, without affecting the secretion of anti-inflammatory and potentially neuroprotective molecules, such as IL-10 and TGF-ßl (Magnus et al., 2001). It has also been demonstrated that microglia releases molecules able to rescue neurons from apoptotic death and, in turn, diffusible signals from apoptotic neurons enhance the neuroprotective properties of microglia (Polazzi et al., 2001). This effect may also be responsible for the recently described phenomenon of phagoptosis (Zhang et al., 2015) through which microglia is able to phagocyte whole neurons damaged by the ischemic insult that do not show any sign of neurodegeneration. The heterogeneous distribution of microglia, which is more densely present in SL in comparison to SP, may thus be functional for the protective role that microglia may have in these conditions (Morsch et al., 2015), and particularly in this CA3 subregion where we also demonstrated a higher number of ectopic neurons and triads. It was also found that CA1 pyramidal cell death, 1 day after OGD, was significantly increased in microglia-depleted organotypic cultures, again suggesting a neuroprotective role of the normal content of microglia (Montero et al., 2009). Since it

is well known that the CA3 area of the hippocampus is more resistant than the CA1 to hypoxic insults, the increase of microglia cells that occurs in concert with the removal of dead cells (Nathan and Ding, 2010) may have both anti-inflammatory effects and consequently neuroprotective properties (Liesz et al., 2009). Indeed, the increase of microglia in CA3 and its decrease in CA1 (Lana et al., 2014) may explain the higher sensitivity of CA1 pyramidal cells to an ischemic insult. Our results may be interpreted as follows: the increase of total microglia in CA3 SL and SR of 2VO-vehicle rats, during the restitution phase of brain chronic hypoperfusion, may depend on the release of anti-inflammatory cytokines that boosts an anti-inflammatory milieu (Spite and Serhan, 2010). Though very sparse OX-positive, activated, microglia cells were found in SP, SL and SR of the three experimental groups, many IBA1+, reactive microglia cells (Beynon and Walker, 2012) phagocytosed ectopic pyramidal neurons or neuronal debris in CA3 SR of 2VO-vehicle rats. The high motility of microglia that effectively monitor the status of the local surroundings may explain the decrease of microglia in CA3 SP and the increase in CA3 SL and SR where it endocytoses small cellular debris derived from apoptotic cells. Therefore, post-ischemic production of cytokines and recruitment of microglia to the damaged tissue (Farkas et al., 2002) can facilitate tissue repair by increasing phagocytosis or phagoptosis, promoting the resolution of inflammation and exerting direct cytoprotective effects on surviving cells in the ischemic area. It would be of interest to investigate the modification of the number of microglia in the acute phase of brain chronic hypoperfusion, taking hippocampal slices at earlier times after 2VO-vehicle and make a comparison between CA3 and CA1 areas.

As reported (Iadecola and Anrather, 2011), the post-ischemic insult is a self-limiting process subsiding during the so-called restitution phase (Dirnagl, 2012; Farkas et al., 2007) and preparing the terrain for the structural and functional reorganization of the injured brain. The restitution phase is thought to be orchestrated by the interplay of numerous cells, processes and mediators (Spite and Serhan, 2010), including development of an anti-inflammatory milieu, removal of dying/apoptotic cells, and neurogenesis (Nathan and Ding, 2010; Spite and Serhan, 2010). We used hippocampal slices from animals 90 days after 2VO, a sufficient time for the tissue to undergo the restitution phase after brain chronic hypoxia (Dirnagl, 2012; Farkas et al., 2007).

Dipyridamole, introduced in therapy in 1959 as an antianginal drug (Picano, 1989), is a potent inhibitor of platelet activation (Heptinstall et al., 1986), reduces thrombi formation *in vivo* (Elkeles et al., 1968), and has beneficial effects in therapy for

secondary stroke prevention (Halkes et al., 2006). Experimentally we have demonstrated that dipyridamole significantly restores hippocampally based spatial memory (Melani et al., 2010) and has a protective effect on hippocampal CA1 pyramidal neurons (Lana et al., 2014) 90 days after 2VO. The increases of extracellular adenosine (Figueredo et al., 1999), together with increased VEGF production (Ernens et al., 2010), and the potentiation of the NO system (Aktas et al., 2003; Venkatesh et al., 2010) help explaining the protecting effect of dipyridamole in this rat model of hypoperfusion. Dipyridamole has a positive effect on blood flow and angiogenesis through the nitrite/NO endocrine system (Venkatesh et al., 2010), increases NO levels and decreases superoxide formation both in ischemic and non-ischemic animals (Pattillo et al., 2011), and has pleiotropic pharmacological effects, such as antioxidant and anti-inflammatory proprieties (Blake, 2004; Eisert, 2002; Hsieh et al., 2010; Riksen et al., 2005). Dipyridamole decreases the production of proinflammatory cytokines (Al Bahrani et al., 2007), chemokines (Weyrich et al., 2005), inhibits matrix metalloprotease-9 (Weyrich et al., 2005), COX-2 activity (Chen et al., 2006), and the neutrophil adhesion to endothelium (Chello et al., 1999).

We demonstrated that apoptosis in CA3 SP decreased significantly in 2VO-dipyridamole rats in comparison to 2VO-vehicle rats. An interesting result was the reduction of neuronal death associated with the formation of the triads in CA3 SR in 2VO-dipyridamole rats in comparison with 2VO-vehicle rats. These data show clearly the beneficial effect of dipyridamole against the physiopathological mechanisms of the ischemic insult. The conspicuous number of ectopic neurons and the increase of microglial cells in 2VO-vehicle and 2VO-dipyridamole rats in comparison to sham rats might be due not only to phagocytosis by microglia, but also to the newly defined mechanism of neuronal death called phagoptosis (Zhang et al., 2015). In this mechanism microglial cells engulf and digest whole neurons that appear damaged but still not fragmented. According to our data we show that microglial cells engulf some ectopic neurons, particularly in SL of 2VO-vehicle and 2VO-dipyridamole rats.

We hypothesize that the administration of dipyridamole during the acute phase of brain chronic hypoperfusion is responsible for the smart opposition towards the progression of the pathophysiological mechanisms of the ischemic insult. This hypothesis is sustained by the reversion of many of the effects observed in 2VO-vehicle rats by dipyridamole, such as the further increase of microglia in CA3 SL and SR that mirrors the decrease of neuronal debris in the same regions. We had previously demonstrated

that dypiridamole restores the number of microglia in CA1 (Lana et al., 2014). Further experiments are needed to fully understand the mechanisms of dipyridamole in rescuing the CA1 hippocampal region from the damages induced by chronic hypoperfusion

Taken together, our results demonstrate the presence of neuronal damage and alteration in the interplay between neurons and glia in CA3 of 2VO-vehicle rats. The effect of dipyridamole to revert or slow the progression of the pathophysiological mechanisms of brain chronic hypoperfusion seem to depend in this region upon its role as an anti-inflammatory drug increasing the phagocytic/phagoptotic activity of microglia. Astrocytes and microglial cells actions might contribute to the neuronal damage in a pathological condition but also represent a protective mechanism to control the inflammatory process and the ensuing diffusion of the cellular damage in the neighbouring tissues.

Finally, in the last part of my research we investigated the putative protective role of adenosine A_{2B} receptors in cerebral ischemia in the CA1 region of hippocampal slices under oxygen-glucose deprivation, an experimental condition that mimics, albeit with the limits of *in vitro* methodology, the most common causes of cerebral ischemia, such as vessel occlusion. *In vitro* slices give a partial view of the physiology of the brain because of the absence of an intact vascular system and the altered tridimensional microenvironment. These alterations involve not only neurons but also glia, and more generally the physiology of the neurovascular unit formed by astrocytes, pericytes, microglia, neurons and the extracellular matrix (Holloway and Gavins, 2015). Nevertheless, the *in vitro* systems have many benefits such as the opportunity to obtain highly valuable information in terms of the time-course of the electrophysiological events, changes in membrane potential (AD), changes in synaptic transmission and morphological and biochemical changes in neurons and glia. Our results confirm that in the CA1 region of rat hippocampus, the application of a 7 min OGD induced the appearance of AD, followed by irreversible synaptic damage and neurodegeneration of CA1 pyramidal neurons (Coppi et al., 2007; Pugliese et al., 2006, 2009; Traini et al., 2011). We now demonstrate that these events are accompanied by neurodegeneration of CA1 pyramidal neurons, with reduction of neuronal density and significant increase of apoptotic neurons. For the first time we demonstrated here that antagonism of A_{2B} receptors using the selective ligands MRS1754 or PSB603, applied before, during and after OGD, prevented or delayed the appearance of AD, and prevented the irreversible loss of neurotransmission induced by 7 min OGD. Adenosine A_{2B} receptor antagonism

also counteracted the reduction of neuronal density in CA1 SP and decreased apoptosis at least up to 3 hours after the end of the insult. Both A_{2B} receptor antagonists did not protect CA1 neurons from neurodegeneration induced by glutamate application, indicating that the antagonistic effect is upstream of glutamate release.

The hippocampus, and particularly CA1 SP, is one of the most vulnerable brain regions to ischemic damage. We used the acute preparation of rat hippocampal slice, which allows measurements of synaptic transmission with good spatial and temporal resolution. In the early phases, hypoxia/ischemia is known to induce a massive increase of extracellular glutamate levels which trigger hyperactivation of glutamate receptors, production of reactive oxygen species, pathological increase of intracellular Ca^{2+}, rapid decrease in ATP reserves and activation of various proteolytic enzymes (Karadottir et al., 2005; Al Majed et al., 2006; Kovacs et al., 2006). In hippocampal slices, a severe OGD insult as that applied in the present experiments elicits the appearance of AD within the OGD period and is invariably followed by irreversible loss of neurotransmission (Pugliese et al., 2007, 2009; Frenguelli et al., 2007), an index of cell suffering, damage to neurons and to the surrounding tissue (Somjen, 2001). AD is caused by the sudden increase of extracellular K^+ and by the contemporary explosive rise in glutamate extracellular concentration (Somjen, 2001). Contemporarily to the extracellular increase of glutamate, the extracellular concentration of adenosine significantly increases, as demonstrated both in *in vivo* and *in vitro* experiments (Latini and Pedata, 2001). After 5 min OGD, adenosine reaches an extracellular concentration of 30 μM in hippocampal slices (Latini et al., 1999; Pearson et al., 2006). At such high concentration, adenosine can stimulate all its receptor subtypes, including the A_{2B} receptor, which exhibits affinity for adenosine with an EC50 in the range of 5-20 μM, lower than all other subtypes (Fredholm et al., 2011). For this reason, it is possible that activation of A2B receptors occurs mainly during pathological conditions, such as inflammation, hypoxia, trauma, and ischemia (Fredholm et al., 2001).

Our data show that A_{2B} receptor antagonists, by preventing or delaying the onset of AD, prevent the irreversible loss of neurotransmission induced by 7 min OGD allowing complete recovery of synaptic potentials. We showed for the first time that a partial recovery of neurotransmission was also observed in a group of hippocampal slices, treated with A2B receptor antagonists, that developed AD immediately after reoxygenation. This delay of AD appearance might account for the partial recovery of neurotransmission observed in these slices. The occurrence of AD after the end of OGD

period is a peculiar characteristic that we observed in our hippocampal preparation. We envisage that when the AD appears during the reoxygenation period, similarly to the phenomenon of spreading depression (Somjen, 2001), neurons are less damaged, and they can partially recover their electrical activity. Thus, even in those slices treated with the A_{2B} receptor antagonists in which AD takes place, this event is less harmful to neuronal viability. This is a substantial difference from A_{2A} receptor antagonist-mediated neuroprotection during a 7 min OGD insult. Indeed, fEPSP recovery was never observed in those few slices undergoing AD in the presence of the A_{2A} receptor blocker ZM241385, as previously published (Pugliese et al., 2009).

As to the mechanism by which A_{2B} receptor antagonists protect from hypoxia/ischemia, recent studies by Gonçalves et al. (2015) have demonstrated that in mouse hippocampus A_{2B} receptors are expressed on glutamatergic terminals, anatomically comparable to those from which our recordings were performed. Their selective stimulation counteracts the predominant A_1 receptor-mediated inhibition of synaptic transmission. In accordance to data reported by Canals et al. (2008) in a model of chemical penumbra produced by a mitochondrial gliotoxin in the hippocampus *in vitro*, we would have expected conservation of synaptic transmission during the first min of OGD and acceleration of AD appearance. In our conditions, a similar response was observed only in a limited number of slices during 7 min OGD. Furthermore, when overstimulated such as during ischemia, A_1 receptors undergo desensitization (Siniscalchi et al., 1999). This phenomenon can be further increased by A_{2B} receptors activation, triggering a vicious circle in which the beneficial effect of A_1 receptor stimulation is overcome by the noxious effect of A_{2B} receptors activation (Gonçalves et al., 2015) as already suggested for A_{2A} adenosine receptors (Pugliese et al., 2009). Further mechanistic studies suggest that the A_{2A} receptor, when stimulated, facilitates A_{2B} receptor externalization from the endoplasmic reticulum to the plasma membrane, possibly increasing the formation of the A_{2A}-A_{2B} dimer (Moriyama and Sitkovsky, 2010). All these results taken together may explain the deleterious activity of adenosine A_{2B} receptor stimulation during an ischemic insult, and the protective effect of A_{2B} receptor antagonists in this condition. Finally, observation that the A_{2B} receptor antagonists did not protect CA1 neurons from neurodegeneration induced by direct glutamate application, confirms that the mechanism underlying their protection against ischemia–induced neurodegeneration is exerted at adenosine receptors that, by the abovementioned mechanisms, regulate extracellular glutamate release. Alternatively,

since OGD is above all a problem of efficient energy recovery, the demonstration that A_{2B} receptors control astrocytic and neuronal glycogen metabolism (Magistretti et al., 1986; Allaman et al., 2003) and glucose utilization by hippocampal slices (Lemos et al., 2015) may suggest an additional effect of these receptors on metabolic activity during OGD.

Severe OGD increased apoptosis and damaged CA1 pyramidal neurons at 1 and 3 h after the end of the ischemic insult. Immunohistochemistry showed that CA1 pyramidal neurons had significant morphological changes, with increased density of nuclei (HDN neurons), karyorrhexis (LDN neurons) and possibly nuclear fragmentation, as evidenced by the significantly higher number of LDN neurons and cell death after OGD. These results are in agreement with those found by Ünal-Çevik and coworkers (2004) in the cerebral cortex of the rat after mild ischemia. Pyknosis is typical of apoptotic cells (Elmore, 2007) and may precede karyorrhexis. We demonstrated that LDN neurons, being highly positive for CytC, were undergoing apoptosis. It has been demonstrated that CytC released into the cytosol binds to apoptotic protease activating factor-1, which leads to activation of caspase-9 which is important in neuronal cell death following ischemia (Yang et al., 1997; Kluck et al., 1997; Jiang and Wang, 2004; Love, 2003; Suen et al., 2008; Martínez-Fábregas et al., 2014; Lana et al., 2014, 2016, 2017a, 2017b). In turn, caspase-9 is activated by high glutamate levels, as occurs during ischemia (Li et al., 2009). As reported in the literature, activation of mTOR, which has multiple roles in cells among which local protein synthesis at the dendritic and spine level (Frey and Morris, 1997; Thoreen et al., 2012; Tsokas et al., 2007), can be modified in ischemic conditions (Dennis et al., 2001; Laplante and Sabatini, 2012). As already reported (Maragakis and Rothstein, 2004), the decrease of mTOR activation may be secondary to the excitotoxic mechanisms evoked by massive increase of glutamate during OGD, which is known to be an important component of neuronal injury *in vitro* (Newell et al., 1995). The participation of decreased mTOR activation in OGD-induced neuronal damage is supported by our results showing decreased activation of mTOR in both the cell body and dendrites of CA1 neurons 3 h after the end of OGD.

Within the limits of the *in vitro* model and the alteration of the neurovascular unit and of neuro glia interplay, we found interesting effects on astrocytic responses. Indeed, astrocytes proliferation, possibly caused, among other stimuli, by increased release of glutamate, is one of the early events that takes place after acute focal CNS damage (Burda and Sofroniew, 2014). In accordance to our previous results (Pugliese et al.,

2009), we found evidence of significant, although limited, astrocytic proliferation in CA1 SR already 3 h after the end of OGD, possibly caused by increased glutamate release. A2B receptor antagonism significantly prevented all the above neuronal and astrocytic modifications, sparing neurons from the degenerative effects caused by the simil-ischemic conditions, and reducing astrocytes proliferation. CA1 pyramidal neurons treated with the A_{2B} receptor antagonists had a similar morphology to those of control slices, had neither increased nor decreased nuclear density, did not undergo apoptosis, and had activated mTOR levels similar to those of controls.

The similar effects obtained using two different A_{2B} receptor antagonists strengthen the hypothesis that the A_{2B} receptor is involved in the mechanisms of cerebral ischemia. Nevertheless, MRS1754 seems to have lower efficiency than PSB603 on some of the parameters investigated. It is possible that the two drugs act with a different time-course or that PSB603 is more efficacious than MRS1754 in this model.

Conclusions

In conclusion, the experimental work carried out during my doctorate demonstrates that a common scenario of derangement of the interplay between neurons and glia is at the basis of many neurodegenerative processes in the hippocampus. We demonstrated a variable pattern of quantitative and qualitative alterations in neurons, astrocytes and microglia cells in different animal models of neurodegeneration.

In particular, in our model of aged and LPS-treated rats, we assessed a close cooperation between astrocytes and microglia in the phagocitosis/phagoptosys of apoptotic neurons. Nevertheless, the differential expression/activation of astroglia and the alteration of their intercommunication may be responsible for the different susceptibility of the subregions of the hippocampus (CA1, CA3 and DG) to neurodegeneration during aging and LPS-induced inflammation.

Furthermore, by 3D confocal analysis we assessed microglia-astrocytes interaction in the rat hippocampus via cell-cell contacts, mediating microglial cell branching in models of inflammation. In aged rats, the impairment of such an interaction correlates with altered distribution, morphology, and inefficient clearance by microglia. These data support the idea that generally accepted functional boundaries between microglia and astrocytes should be re-evaluated to better understand how their functions overlap and interact.

In our model of Alzheimer's disease, TgCRND8 mice, we demonstrated that the responses of neurons and glia to neurodegenerative patterns induced by Aβ plaques deposition is not uniform in the different hippocampal areas: in CA1 pyramidal neurons, the higher sensitivity may be related to the different plaque distribution. All these modifications may be at the basis of memory loss, the peculiar symptom of AD, which was demonstrated in this transgenic mouse model of Aβ deposition, even at early stages.

In a similar manner to the model of normal brain aging and LPS-induced neuroinflammation, also in the model of brain ipoperfusion (bCCAo rat) we demonstrated a cooperation between microglia and astrocytes in the phagocytosis of apoptotic neurons and debris, through a new mechanism called phagoptosis. Neurons in CA3 showed a better adaptive capacity than those in CA1 to the ischemic insult, possibly due to the different behaviour of astrocytes and microglial cells.

Finally, in our *in vitro* model of brain ischemia (OGD acute hippocampal slices) we demonstrated that antagonists of adenosine A_{2B} receptors protect the CA1 area of the

hippocampus from an acute damage induced by severe hypoxic/ischemic conditions. The mechanism likely resides in the prevention from the alterations that involve not only neurons but also glia, and more generally the physiology of the neurovascular unit formed by astrocytes, pericytes, microglia, neurons, and the extracellular matrix.

It should be pointed out that every tissue, and first of all the nervous tissue, is not composed by a collection of single, separate elements but rather by interacting and interdependent cell populations that cooperate to maintain homeostasis and functionality of the organ. Different types of alterations that affect one population reasonably reverberate to the other ones, either favoring or dysregulating their activities.

References

Abbracchio MP, Brambilla R, Ceruti S, Kim HO, von Lubitz DK, Jacobson KA, Cattabeni F. G protein-dependent activation of phospholipase C by adenosine A3 receptors in rat brain. Mol Pharmacol. 1995 Dec;48(6):1038-45.

Adair TH. Growth regulation of the vascular system: an emerging role for adenosine. Am J Physiol Regul Integr Comp Physiol. 2005 Aug;289(2):R283-R296.

Adams HP Jr, Bendixen BH, Kappelle LJ, Biller J, Love BB, Gordon DL, Marsh EE 3rd. Classification of subtype of acute ischemic stroke. Definitions for use in a multicenter clinical trial. TOAST. Trial of Org 10172 in Acute Stroke Treatment. Stroke. 1993 Jan;24(1):35-41.

Adams HP Jr, del Zoppo G, Alberts MJ, Bhatt DL, Brass L, Furlan A, Grubb RL, Higashida RT, Jauch EC, Kidwell C, Lyden PD, Morgenstern LB, Qureshi AI, Rosenwasser RH, Scott PA, Wijdicks EF; American Heart Association/American Stroke Association Stroke Council; American Heart Association/American Stroke Association Clinical Cardiology Council; American Heart Association/American Stroke Association Cardiovascular Radiology and Intervention Council; Atherosclerotic Peripheral Vascular Disease Working Group; Quality of Care Outcomes in Research Interdisciplinary Working Group. Guidelines for the early management of adults with ischemic stroke: a guideline from the American Heart Association/American Stroke Association Stroke Council, Clinical Cardiology Council, Cardiovascular Radiology and Intervention Council, and the Atherosclerotic Peripheral Vascular Disease and Quality of Care Outcomes in Research Interdisciplinary Working Groups: The American Academy of Neurology affirms the value of this guideline as an educational tool for neurologists. Circulation. 2007 May 22;115(20): e478-534. Erratum in: Circulation. 2007 Oct 30;116(18):e515.

Adogu POU, Ubajaka CF, Emelumadu OF, Alutu COC. Epidemiologic Transition of Diseases and Health-Related Events in Developing Countries: A Review. Am J Med Sci. 2015; 5:150-7.

Aktas B, Utz A, Hoenig-Liedl P, Walter U, Geiger J. Dipyridamole enhances NO/cGMP-mediated vasodilator-stimulated phosphoprotein phosphorylation and signaling in human platelets: in vitro and in vivo/ex vivo studies. Stroke. 2003 Mar;34(3):764-9.

Al-Bahrani A, Taha S, Shaath H, Bakhiet M. TNF-alpha and IL-8 in acute stroke and the modulation of these cytokines by antiplatelet agents. Curr Neurovasc Res. 2007 Feb;4(1):31-7.

Albuquerque MS, Mahar I, Davoli MA, Chabot JG, Mechawar N, Quirion R, Krantic S. Regional and sub-regional differences in hippocampal GABAergic neuronal vulnerability in the TgCRND8 mouse model of Alzheimer's disease. Front Aging Neurosci. 2015 Mar 24;7:30.

Allaman I, Lengacher S, Magistretti PJ, Pellerin L. A2B receptor activation promotes glycogen synthesis in astrocytes through modulation of gene expression. Am J Physiol Cell Physiol. 2003 Mar;284(3):C696-704.

Al-Majed AA, Sayed-Ahmed MM, Al-Omar FA, Al-Yahya AA, Aleisa AM, Al-Shabanah OA. Carnitine esters prevent oxidative stress damage and energy depletion following transient forebrain ischaemia in the rat hippocampus. Clin Exp Pharmacol Physiol. 2006 Aug;33(8):725-33.

Auffret A, Gautheron V, Repici M, Kraftsik R, Mount HT, Mariani J, Rovira C. Age-dependent impairment of spine morphology and synaptic plasticity in hippocampal CA1 neurons of a

presenilin 1 transgenic mouse model of Alzheimer's disease. J Neurosci. 2009 Aug 12;29(32):10144-52.

Ajami B, Bennett JL, Krieger C, Tetzlaff W, Rossi FM. Local self-renewal can sustain CNS microglia maintenance and function throughout adult life. Nat Neurosci. 2007 Dec;10(12):1538-43.

Ala TA, Beh GO, Frey WH 2nd. Pure hippocampal sclerosis: a rare cause of dementia mimicking Alzheimer's disease. Neurology. 2000 Feb 22;54(4):843-8.

Allard D, Turcotte M, Stagg J. Targeting A2 adenosine receptors in cancer. Immunol Cell Biol. 2017 Apr;95(4):333-339. doi: 10.1038/icb.2017.8. Epub 2017 Feb 8.

Allen NJ, Barres BA. Neuroscience: Glia - more than just brain glue. Nature. 2009 Feb 5;457(7230):675-7. doi: 10.1038/457675a.

Ali MM, Ghouri RG, Ans AH, Akbar A, Toheed A. Recommendations for Anti-inflammatory Treatments in Alzheimer's Disease: A Comprehensive Review of the Literature. Cureus. 2019 May 8;11(5): e4620.

Alzheimer A. “Beitra¨ge zur Kenntnis der pathologischen Neuroglia und ihrer Beziehungen zu den Abbauvorga¨ngen im Nervengewebe”. In: Histologische und histopathologische Arbeiten u ber die Grosshirnrinde mit besonderer Beru cksichtigung der pathologischen Anatomie der Geisteskrankheiten, 1910, Nissl F, Alzheimer A, Eds, Gustav Fischer, Jena, Germany, pp. 401-562.

Alzheimer A, Stelzmann RA, Schnitzlein HN, Murtagh FR. An English translation of Alzheimer's 1907 paper, "Uber eine eigenartige Erkankung der Hirnrinde". Clin Anat. 1995;8(6):429-31.

Amaral DG. A Golgi study of cell types in the hilar region of the hippocampus in the rat. J Comp Neurol. 1978 Dec 15;182(4 Pt 2):851-914.

Amaral DG, Lavenex P. Hippocampal neuroanatomy. In: Andersen P, Morris R, Amaral DG, O’Keefe J, editors. The Hippocampus Book. New York: Oxford University Press; 2007. p.37-114.

Amaral DG, Witter MP. The three-dimensional organization of the hippocampal formation: a review of anatomical data. Neuroscience. 1989;31(3):571-91.

Amisten S, Braun OO, Bengtsson A, Erlinge D. Gene expression profiling for the identification of G-protein coupled receptors in human platelets. Thromb Res. 2008;122(1):47-57.

Amuna P, Zotor FB. Epidemiological and nutrition transition in developing countries: impact on human health and development. Proc Nutr Soc. 2008 Feb;67(1):82-90.

Anderson P, Morris R, Amaral D, Bliss T, O'Keefe J. The hippocampus book (first ed.). New York: Oxford University Press; 2007. p. 3.

Andiné P. Involvement of adenosine in ischemic and postischemic calcium regulation. Mol Chem Neuropathol. 1993 Jan-Feb;18(1-2):35-49.

Andreyev AY, Kushnareva YE, Starkov AA. Mitochondrial metabolism of reactive oxygen species. Biochemistry (Mosc). 2005;70:200-14.

Araque A, Parpura V, Sanzgiri RP, Haydon PG. Tripartite synapses: glia, the unacknowledged partner. Trends Neurosci. 1999 May;22(5):208-15.

Arnold SE, Franz BR, Gur RC, Gur RE, Shapiro RM, Moberg PJ, Trojanowski JQ. Smaller neuron size in schizophrenia in hippocampal subfields that mediate cortical-hippocampal interactions. Am J Psychiatry. 1995 May;152(5):738-48.

Astrup T. Regulation of haemostasis and tissue repair in various organs by procoagulants and fibrinolytic agents. Rinsho Ketsueki. 1981 Sep;22(9):1377-93.

Bachstetter AD, Morganti JM, Jernberg J, Schlunk A, Mitchell SH, Brewster KW, Hudson CE, Cole MJ, Harrison JK, Bickford PC, Gemma C. Fractalkine and CX 3 CR1 regulate hippocampal neurogenesis in adult and aged rats. Neurobiol Aging. 2011 Nov;32(11):2030-44.

Badaut J, Lasbennes F, Magistretti PJ, Regli L. Aquaporins in brain: distribution, physiology, and pathophysiology. J Cereb Blood Flow Metab. 2002 Apr;22(4):367-78.

Bamford J, Sandercock P, Dennis M, Burn J, Warlow C. Classification and natural history of clinically identifiable subtypes of cerebral infarction. Lancet. 1991 Jun 22;337(8756):1521-6

Banati RB, Gehrmann J, Czech C, Mönning U, Jones LL, König G, Beyreuther K, Kreutzberg GW. Early and rapid de novo synthesis of Alzheimer beta A4-amyloid precursor protein (APP) in activated microglia. Glia. 1993 Nov;9(3):199-210.

Barcia C, Ros CM, Annese V, Carrillo-de Sauvage MA, Ros-Bernal F, Gómez A, Yuste JE, Campuzano CM, de Pablos V, Fernandez-Villalba E, Herrero MT. ROCK/Cdc42-mediated microglial motility and gliapse formation lead to phagocytosis of degenerating dopaminergic neurons in vivo. Sci Rep. 2012;2:809.

Barres BA. The mystery and magic of glia: a perspective on their roles in health and disease. Neuron. 2008 Nov 6;60(3):430-40. doi: 10.1016/j.neuron.2008.10.013.

Bartsch T, Döhring J, Reuter S, Finke C, Rohr A, Brauer H, Deuschl G, Jansen O. Selective neuronal vulnerability of human hippocampal CA1 neurons: lesion evolution, temporal course, and pattern of hippocampal damage in diffusion-weighted MR imaging. J Cereb Blood Flow Metab. 2015 Nov;35(11):1836-45.

Bartsch T, Wulff P. The hippocampus in aging and disease: From plasticity to vulnerability. Neuroscience. 2015 Nov 19;309:1-16.

Becker EB, Bonni A. Cell cycle regulation of neuronal apoptosis in development and disease. Prog Neurobiol. 2004 Jan;72(1):1-25.

Buxbaum JD, Oishi M, Chen HI, Pinkas-Kramarski R, Jaffe EA, Gandy SE, Greengard P. Cholinergic agonists and interleukin 1 regulate processing and secretion of the Alzheimer beta/A4 amyloid protein precursor. Proc Natl Acad Sci U S A. 1992 Nov 1;89(21):10075-8.

Baylis D, Bartlett DB, Patel HP, Roberts HC. Understanding how we age: insights into inflammaging. Longev Healthspan. 2013 May 2;2(1):8.

Beckman JS, Koppenol WH. Nitric oxide, superoxide, and peroxynitrite: the good, the bad, and ugly. Am J Physiol. 1996 Nov;271(5 Pt 1):C1424-37.

Bellucci A, Luccarini I, Scali C, Prosperi C, Giovannini MG, Pepeu G, Casamenti F. Cholinergic dysfunction, neuronal damage and axonal loss in TgCRND8 mice. Neurobiol Dis. 2006 Aug;23(2):260-72.

Benes FM, Kwok EW, Vincent SL, Todtenkopf MS. A reduction of nonpyramidal cells in sector CA2 of schizophrenics and manic depressives. Biol Psychiatry. 1998 Jul 15;44(2):88-97.

Bennett SA, Tenniswood M, Chen JH, Davidson CM, Keyes MT, Fortin T, Pappas BA. Chronic cerebral hypoperfusion elicits neuronal apoptosis and behavioral impairment. Neuroreport. 1998 Jan 5;9(1):161-6.

Bernal GM, Peterson DA. Phenotypic and gene expression modification with normal brain aging in GFAP-positive astrocytes and neural stem cells. Aging Cell. 2011 Jun;10(3):466-82.

Beukers MW, den Dulk H, van Tilburg EW, Brouwer J, Ijzerman AP. Why are A(2B) receptors low-affinity adenosine receptors? Mutation of Asn273 to Tyr increases affinity of human A(2B) receptor for 2-(1-Hexynyl) adenosine. Mol Pharmacol. 2000 Dec;58(6):1349-56

Beynon SB, Walker FR. Microglial activation in the injured and healthy brain: what are we really talking about? Practical and theoretical issues associated with the measurement of changes in microglial morphology. Neuroscience. 2012 Dec 6;225:162-71.

Blake AD. Dipyridamole is neuroprotective for cultured rat embryonic cortical neurons. Biochem Biophys Res Commun. 2004 Feb 6;314(2):501-4.

Blasko I, Marx F, Steiner E, Hartmann T, Grubeck-Loebenstein B. TNFalpha plus IFNgamma induce the production of Alzheimer beta-amyloid peptides and decrease the secretion of APPs. FASEB J. 1999 Jan;13(1):63-8.

Böhm I. Disruption of the cytoskeleton after apoptosis induction with autoantibodies. Autoimmunity. 2003 May;36(3):183-9.

Boissard CG, Lindner MD, Gribkoff VK. Hypoxia produces cell death in the rat hippocampus in the presence of an A1 adenosine receptor antagonist: an anatomical and behavioral study. Neuroscience. 1992 Jun;48(4):807-12.

Bolmont T, Haiss F, Eicke D, Radde R, Mathis CA, Klunk WE, Kohsaka S, Jucker M, Calhoun ME. Dynamics of the microglial/amyloid interaction indicate a role in plaque maintenance. J Neurosci. 2008 Apr 16;28(16):4283-92.

Borchelt DR, Thinakaran G, Eckman CB, Lee MK, Davenport F, Ratovitsky T, Prada CM, Kim G, Seekins S, Yager D, Slunt HH, Wang R, Seeger M, Levey AI, Gandy SE, Copeland NG, Jenkins NA, Price DL, Younkin SG, Sisodia SS. Familial Alzheimer's disease-linked presenilin 1 variants elevate Abeta1-42/1-40 ratio in vitro and in vivo. Neuron. 1996 Nov;17(5):1005-13.

Boroujerdi A, Kim HK, Lyu YS, Kim DS, Figueroa KW, Chung JM, Luo ZD. Injury discharges regulate calcium channel alpha-2-delta-1 subunit upregulation in the dorsal horn that contributes to initiation of neuropathic pain. Pain. 2008 Oct 15;139(2):358-66. doi: 10.1016/j.pain.2008.05.004.

Bradley W, Daroff R, Fenichel G, Marsden C. Neurology in Clinical Practice. 1991 Butterworth-Heinemann, Stoneham, MA, USA

Brady NR, Elmore SP, van Beek JJ, Krab K, Courtoy PJ, Hue L, Westerhoff HV. Coordinated behavior of mitochondria in both space and time: a reactive oxygen species-activated wave of mitochondrial depolarization. Biophys J. 2004 Sep;87(3):2022-34.

Brewer GJ. Effects of acidosis on the distribution of processing of the beta-amyloid precursor protein in cultured hippocampal neurons. Mol Chem Neuropathol. 1997 Jun;31(2):171-86.

Brodie C, Blumberg PM, Jacobson KA. Activation of the A2A adenosine receptor inhibits nitric oxide production in glial cells. FEBS Lett. 1998 Jun 12;429(2):139-42.

Brown AM, Baltan Tekkök S, Ransom BR. Energy transfer from astrocytes to axons: the role of CNS glycogen. Neurochem Int. 2004 Sep;45(4):529-36.

Brown GC, Neher JJ. Eaten alive! Cell death by primary phagocytosis: 'phagoptosis'. Trends Biochem Sci. 2012 Aug;37(8):325-32.

Buchman AS, Boyle PA, Yu L, Shah RC, Wilson RS, Bennett DA. Total daily physical activity and the risk of AD and cognitive decline in older adults. Neurology. 2012 Apr 24;78(17):1323-9.

Buckmaster PS, Schwartzkroin PA. Hippocampal mossy cell function: a speculative view. Hippocampus. 1994 Aug;4(4):393-402.

Burda JE, Sofroniew MV. Reactive gliosis and the multicellular response to CNS damage and disease. Neuron. 2014 Jan 22;81(2):229-48.

Bushong EA, Martone ME, Ellisman MH. Maturation of astrocyte morphology and the establishment of astrocyte domains during postnatal hippocampal development. Int J Dev Neurosci. 2004 Apr;22(2):73-86.

Bushong EA, Martone ME, Jones YZ, Ellisman MH. Protoplasmic astrocytes in CA1 stratum radiatum occupy separate anatomical domains. J Neurosci. 2002 Jan 1;22(1):183-92.

Burke SP, Nadler JV. Regulation of glutamate and aspartate release from slices of the hippocampal CA1 area: effects of adenosine and baclofen. J Neurochem. 1988 Nov;51(5):1541-51.

Burnstock G. A basis for distinguishing two types of purinergic receptor. In: Cell Membrane Receptors for Drugs and Hormones: A Multidisciplinary Approach, 1978, Straub RW, Bolis L, Eds, Raven Press, New York, NY, USA, pp. 107-18.

Calabresi P, Centonze D, Bernardi G. Cellular factors controlling neuronal vulnerability in the brain: a lesson from the striatum. Neurology. 2000 Nov 14;55(9):1249-55.

Cao XH, Zhao SS, Liu DY, Wang Z, Niu LL, Hou LH, Wang CL. ROS-Ca(2+) is associated with mitochondria permeability transition pore involved in surfactin-induced MCF-7 cells apoptosis. Chem Biol Interact. 2011 Mar 15;190(1):16-27.

Canals S, Larrosa B, Pintor J, Mena MA, Herreras O. Metabolic challenge to glia activates an adenosine-mediated safety mechanism that promotes neuronal survival by delaying the onset of spreading depression waves. J Cereb Blood Flow Metab. 2008 Nov;28(11):1835-44.

Caplan LR. Do transient ischemic attacks have a neuroprotective effect? Neurology. 2000 Nov 28;55(10):1596.

Cardona AE, Pioro EP, Sasse ME, Kostenko V, Cardona SM, Dijkstra IM, Huang D, Kidd G, Dombrowski S, Dutta R, Lee JC, Cook DN, Jung S, Lira SA, Littman DR, Ransohoff RM. Control of microglial neurotoxicity by the fractalkine receptor. Nat Neurosci. 2006 Jul;9(7):917-24.

Carlsson J, Yoo L, Gao ZG, Irwin JJ, Shoichet BK, Jacobson KA. Structure-based discovery of

A2A adenosine receptor ligands. J Med Chem. 2010 May 13;53(9):3748-55.

Cerbai F, Lana D, Nosi D, Petkova-Kirova P, Zecchi S, Brothers HM, Wenk GL, Giovannini MG. The neuron-astrocyte-microglia triad in normal brain ageing and in a model of neuroinflammation in the rat hippocampus. PLoS One. 2012;7(9):e45250. doi: 10.1371/journal.pone.0045250.

Ceruti S, Cattabeni F, Abbracchio M. Trasmissione Purinergica. In: Farmacologia generale e molecolare, 2004, Clementi F, Fumagalli G, Eds, Utet, Torino, Italy, p.569.

Chandrasekera PC, McIntosh VJ, Cao FX, Lasley RD. Differential effects of adenosine A2a and A2b receptors on cardiac contractility. Am J Physiol Heart Circ Physiol. 2010 Dec;299(6):H2082-9. doi: 10.1152/ajpheart.00511.2010. Epub 2010 Oct 8.

Chapman GA, Moores K, Harrison D, Campbell CA, Stewart BR, Strijbos PJ. Fractalkine cleavage from neuronal membranes represents an acute event in the inflammatory response to excitotoxic brain damage. J Neurosci. 2000 Aug 1;20(15):RC87.

Chao TI, Rickman M, Wolff JR. The synapse-astrocyte boundary: an anatomical basis for an integrative role of glia in synaptic transmission. In: Volterra A, Magistretti P, Philip GH, editors. The Tripartite Synapse: Glia in Synaptic transmission. New York: Oxford University Press; 2002. p3-23.

Chello M, Mastroroberto P, Malta E, Cirillo F, Celi V. Inhibition by dipyridamole of neutrophil adhesion to vascular endothelium during coronary bypass surgery. Ann Thorac Surg. 1999 May;67(5):1277-82.

Chen G, Chen KS, Knox J, Inglis J, Bernard A, Martin SJ, Justice A, McConlogue L, Games D, Freedman SB, Morris RG. A learning deficit related to age and beta-amyloid plaques in a mouse model of Alzheimer's disease. Nature. 2000 Dec 21-28;408(6815):975-9.

Chen JF, Eltzschig HK, Fredholm BB. Adenosine receptors as drug targets—what are the challenges? Nat Rev Drug Discov. 2013 Apr;12(4):265-86.

Chen Y, Ju L, Rushdi M, Ge C, Zhu C. Receptor-mediated cell mechanosensing. Mol Biol Cell. 2017 Nov 7;28(23):3134-3155.

Chen TH, Kao YC, Chen BC, Chen CH, Chan P, Lee HM. Dipyridamole activation of mitogen-activated protein kinase phosphatase-1 mediates inhibition of lipopolysaccharide-induced cyclooxygenase-2 expression in RAW 264.7 cells. Eur J Pharmacol. 2006 Jul 17;541(3):138-46.

Chen JF, Sonsalla PK, Pedata F, Melani A, Domenici MR, Popoli P, Geiger J, Lopes LV, de Mendonça A. Adenosine A2A receptors and brain injury: broad spectrum of neuroprotection, multifaceted actions and "fine tuning" modulation. Prog Neurobiol. 2007 Dec;83(5):310-31.

Cheong SL, Federico S, Venkatesan G, Mandel AL, Shao YM, Moro S, Spalluto G, Pastorin G. The A3 adenosine receptor as multifaceted therapeutic target: pharmacology, medicinal chemistry, and in silico approaches. Med Res Rev. 2013 Mar;33(2):235-335.

Chevallier NL, Soriano S, Kang DE, Masliah E, Hu G, Koo EH. Perturbed neurogenesis in the adult hippocampus associated with presenilin-1 A246E mutation. Am J Pathol. 2005 Jul;167(1):151-9.

Chishti MA, Yang DS, Janus C, Phinney AL, Horne P, Pearson J, Strome R, Zuker N, Loukides J, French J, Turner S, Lozza G, Grilli M, Kunicki S, Morissette C, Paquette J,

Gervais F, Bergeron C, Fraser PE, Carlson GA, George-Hyslop PS, Westaway D. Early-onset amyloid deposition and cognitive deficits in transgenic

mice expressing a double mutant form of amyloid precursor protein 695. J Biol Chem. 2001 Jun 15;276(24):21562-70.

Chmayssani M, Festa JR, Marshall RS. Chronic ischemia and neurocognition. Neuroimaging Clin N Am. 2007 Aug;17(3):313-24, viii.

Choi DW. Methods for antagonizing glutamate neurotoxicity. Cerebrovasc Brain Metab Rev. 1990 Summer;2(2):105-47.

Choi SS, Lee HJ, Lim I, Satoh J, Kim SU. Human astrocytes: secretome profiles of cytokines and chemokines. PLoS One. 2014 Apr 1;9(4):e92325.

Chui DH, Tanahashi H, Ozawa K, Ikeda S, Checler F, Ueda O, Suzuki H, Araki W, Inoue H, Shirotani K, Takahashi K, Gallyas F, Tabira T. Transgenic mice with Alzheimer presenilin 1 mutations show accelerated neurodegeneration without amyloid plaque formation. Nat Med. 1999 May;5(5):560-4.

Cipriani R, Villa P, Chece G, Lauro C, Paladini A, Micotti E, Perego C, De Simoni MG, Fredholm BB, Eusebi F, Limatola C. CX3CL1 is neuroprotective in permanent focal cerebral ischemia in rodents. J Neurosci. 2011 Nov 9;31(45):16327-35.

Citron M, Westaway D, Xia W, Carlson G, Diehl T, Levesque G, Johnson-Wood K, Lee M, Seubert P, Davis A, Kholodenko D, Motter R, Sherrington R, Perry B, Yao H, Strome R, Lieberburg I, Rommens J, Kim S, Schenk D, Fraser P, St George Hyslop P, Selkoe DJ. Mutant presenilins of Alzheimer's disease increase production of 42-residue amyloid beta-protein in both transfected cells and transgenic mice. Nat Med. 1997 Jan;3(1):67-72.

Claiborne BJ, Amaral DG, Cowan WM. Quantitative, three-dimensional analysis of granule cell dendrites in the rat dentate gyrus. J Comp Neurol. 1990 Dec 8;302(2):206-19.

Cleveland DW, Hwo SY, Kirschner MW. Purification of tau, a microtubule-associated protein that induces assembly of microtubules from purified tubulin. J Mol Biol. 1977 Oct 25;116(2):207-25.

Colangelo AM, Alberghina L, Papa M. Astrogliosis as a therapeutic target for neurodegenerative diseases. Neurosci Lett. 2014 Apr 17;565:59-64.

Coco S, Verderio C, Trotti D, Rothstein JD, Volterra A, Matteoli M. Non-synaptic localization of the glutamate transporter EAAC1 in cultured hippocampal neurons. Eur J Neurosci. 1997 Sep;9(9):1902-10.

Codita A, Winblad B, Mohammed AH. Of mice and men: more neurobiology in dementia. Curr Opin Psychiatry. 2006 Nov;19(6):555-63.

Comery TA, Martone RL, Aschmies S, Atchison KP, Diamantidis G, Gong X, Zhou H, Kreft AF, Pangalos MN, Sonnenberg-Reines J, Jacobsen JS, Marquis KL. Acute gamma-secretase inhibition improves contextual fear conditioning in the Tg2576 mouse model of Alzheimer's disease. J Neurosci. 2005 Sep 28;25(39):8898-902.

Coney AM, Marshall JM. Role of adenosine and its receptors in the vasodilatation induced in the cerebral cortex of the rat by systemic hypoxia. J Physiol. 1998 Jun 1;509 (Pt 2):507-18.

Coppi E, Cellai L, Maraula G, Pugliese AM, Pedata F. Adenosine A_{2A} receptors inhibit delayed rectifier potassium currents and cell differentiation in primary purified oligodendrocyte cultures. Neuropharmacology. 2013 Oct;73:301-10.

Corbett NJ, Gabbott PL, Klementiev B, Davies HA, Colyer FM, Novikova T, Stewart MG. Amyloid-beta induced CA1 pyramidal cell loss in young adult rats is alleviated by systemic treatment with FGL, a neural cell adhesion molecule-derived mimetic peptide. PLoS One. 2013 Aug 9;8(8):e71479.

Corradetti R, Lo Conte G, Moroni F, Passani MB, Pepeu G. Adenosine decreases aspartate and glutamate release from rat hippocampal slices. Eur J Pharmacol. 1984 Sep 3;104(1-2):19-26.

Corsellis JA, Goldberg GJ, Norton AR. "Limbic encephalitis" and its association with carcinoma. Brain. 1968 Sep;91(3):481-96.

Cotrina ML, Lin JH, Alves-Rodrigues A, Liu S, Li J, Azmi-Ghadimi H, Kang J, Naus CC, Nedergaard M. Connexins regulate calcium signaling by controlling ATP release. Proc Natl Acad Sci U S A. 1998 Dec 22;95(26):15735-40.

Cotter D, Wilson S, Roberts E, Kerwin R, Everall IP. Increased dendritic MAP2 expression in the hippocampus in schizophrenia. Schizophr Res. 2000 Jan 21;41(2):313-23.

Crespo S, Bridges M, Nakhleh R, McPhail A, Pungpapong S, Keaveny AP. Non-invasive assessment of liver fibrosis using magnetic resonance elastography in liver transplant recipients with hepatitis C. Clin Transplant. 2013 Sep-Oct;27(5):652-8.

Cristalli G, Lambertucci C, Marucci G, Volpini R, Dal Ben D. A2A adenosine receptor and its modulators: overview on a druggable GPCR and on structure-activity relationship analysis and binding requirements of agonists and antagonists.

Csóka B, Németh ZH, Selmeczy Z, Koscsó B, Pacher P, Vizi ES, Deitch EA, Haskó G. Role of A(2A) adenosine receptors in regulation of opsonized E. coli-induced macrophage function. Purinergic Signal. 2007 Sep;3(4):447-52.

Cunha RA. Neuroprotection by adenosine in the brain: From A(1) receptor activation to A (2A) receptor blockade. Purinergic Signal. 2005 Jun;1(2):111-34.

Cunha RA. Adenosine as a neuromodulator and as a homeostatic regulator in the nervous system: different roles, different sources and different receptors. Neurochem Int. 2001 Feb;38(2):107-25.

Cunha RA, Constantino MC, Sebastião AM, Ribeiro JA. Modification of A1 and A2a adenosine receptor binding in aged striatum, hippocampus and cortex of the rat. Neuroreport. 1995 Jul 31;6(11):1583-8.

Cunha RA, Ribeiro JA, Sebastião AM. Purinergic modulation of the evoked release of [3H]acetylcholine from the hippocampus and cerebral cortex of the rat: role of the ectonucleotidases. Eur J Neurosci. 1994 Jan 1;6(1):33-42.

Daly JW, Butts-Lamb P, Padgett W. Subclasses of adenosine receptors in the central nervous system: interaction with caffeine and related methylxanthines. Cell Mol Neurobiol. 1983 Mar;3(1):69-80.

Daly JW, Padgett WL. Agonist activity of 2- and 5'-substituted adenosine analogs and their N6-cycloalkyl derivatives at A1- and A2-adenosine receptors coupled to adenylate cyclase. Biochem Pharmacol. 1992 Mar 3;43(5):1089-93.

Daly RJ. Identification of receptor tyrosine kinase (RTK) substrates by the cloning of receptor targets (CORT) strategy. Methods Mol Biol. 2001;124:239-49.

Damani MR, Zhao L, Fontainhas AM, Amaral J, Fariss RN, Wong WT. Age-related alterations in the dynamic behavior of microglia. Aging Cell. 2011 Apr;10(2):263-76.

Darashchonak N, Koepsell B, Bogdanova N, von Versen-Höynck F. Adenosine A2B receptors induce proliferation, invasion and activation of cAMP response element binding protein (CREB) in trophoblast cells. BMC Pregnancy Childbirth. 2014 Jan 3;14:2.

Daria A, Colombo A, Llovera G, Hampel H, Willem M, Liesz A, Haass C, Tahirovic S. Young microglia restore amyloid plaque clearance of aged microglia. EMBO J. 2017 Mar 1;36(5):583-603. doi: 10.15252/embj.201694591

Daval JL, Nicolas F. Opposite effects of cyclohexyladenosine and theophylline on hypoxic damage in cultured neurons. Neurosci Lett. 1994 Jul 4;175(1-2):114-6.

Daval JL, Von Lubitz DK, Deckert J, Redmond DJ, Marangos PJ. Protective effect of cyclohexyladenosine on adenosine A1-receptors, guanine nucleotide and forskolin binding sites following transient brain ischemia: a quantitative autoradiographic study. Brain Res. 1989 Jul 10;491(2):212-26.

De Bilbao F, Arsenijevic D, Moll T, Garcia-Gabay I, Vallet P, Langhans W, Giannakopoulos P. In vivo over-expression of interleukin-10 increases resistance to focal brain ischemia in mice. J Neurochem. 2009 Jul;110(1):12-22. doi:10.1111/j.1471-4159.2009.06098.

De Jong GI, Farkas E, Stienstra CM, Plass JR, Keijser JN, de la Torre JC, Luiten PG. Cerebral hypoperfusion yields capillary damage in the hippocampal CA1 area that correlates with spatial memory impairment. Neuroscience. 1999;91(1):203-10.

De Keyser J, Mostert JP, Koch MW. Dysfunctional astrocytes as key players in the pathogenesis of central nervous system disorders. J Neurol Sci. 2008 Apr 15;267(1-2):3-16.

Dehnes Y, Chaudhry FA, Ullensvang K, Lehre KP, Storm-Mathisen J, Danbolt NC. The glutamate transporter EAAT4 in rat cerebellar Purkinje cells: a glutamate-gated chloride channel concentrated near the synapse in parts of the dendritic membrane facing astroglia. J Neurosci. 1998 May 15;18(10):3606-19.

Del Rio-Hortega P. Are the glia with very few processes homologous with Schwann cells? by Pío del Río-Hortega. 1922. Clin Neuropathol. 2012 Nov-Dec;31(6):460-2.

del Zoppo GJ, Schmid-Schönbein GW, Mori E, Copeland BR, Chang CM. Polymorphonuclear leukocytes occlude capillaries following middle cerebral artery occlusion and reperfusion in baboons. Stroke. 1991 Oct;22(10):1276-83.

Deleidi M, Jäggle M, Rubino G. Immune aging, dysmetabolism, and inflammation in neurological diseases. Front Neurosci. 2015 Jun 3;9:172.

Dénes A, Ferenczi S, Halász J, Környei Z, Kovács KJ. Role of CX3CR1 (fractalkine receptor) in brain damage and inflammation induced by focal cerebral ischemia in mouse. J Cereb Blood Flow Metab. 2008 Oct;28(10):1707-21.

Deng W, Aimone JB, Gage FH. New neurons and new memories: how does adult hippocampal neurogenesis affect learning and memory? Nat Rev Neurosci. 2010May;11(5):339-50. doi: 10.1038/nrn2822.

Deng Y, Xie D, Fang M, Zhu G, Chen C, Zeng H, Lu J, Charanjit K. Astrocyte-derived proinflammatory cytokines induce hypomyelination in the periventricular white matter in the hypoxic neonatal brain. PLoS One. 2014 Jan 31;9(1):e87420.

Dennis PB, Jaeschke A, Saitoh M, Fowler B, Kozma SC, Thomas G. Mammalian TOR: a homeostatic ATP sensor. Science. 2001 Nov 2;294(5544):1102-5

Desmond NL, Levy WB. Granule cell dendritic spine density in the rat hippocampus varies with spine shape and location. Neurosci Lett. 1985 Mar 15;54(2-3):219-24.

DeWitt DA, Perry G, Cohen M, Doller C, Silver J. Astrocytes regulate microglial phagocytosis of senile plaque cores of Alzheimer's disease. Exp Neurol. 1998 Feb;149(2):329-40.

Dickson DW, Davies P, Bevona C, Van Hoeven KH, Factor SM, Grober E, Aronson MK, Crystal HA. Hippocampal sclerosis: a common pathological feature of dementia in very old (> or = 80 years of age) humans. Acta Neuropathol. 1994;88(3):212-21.

Di Giorgio FP, Carrasco MA, Siao MC, Maniatis T, Eggan K. Non-cell autonomous effect of glia on motor neurons in an embryonic stem cell-based ALS model. Nat Neurosci. 2007 May;10(5):608-14.

Di Iorio P, Kleywegt S, Ciccarelli R, Traversa U, Andrew CM, Crocker CE, Werstiuk ES, Rathbone MP. Mechanisms of apoptosis induced by purine nucleosides in astrocytes. Glia. 2002 May;38(3):179-90.

Dirnagl U. Pathobiology of injury after stroke: the neurovascular unit and beyond. Ann N Y Acad Sci. 2012 Sep;1268:21-5.

Dirnagl U, Iadecola C, Moskowitz MA. Pathobiology of ischaemic stroke: an integrated view. Trends Neurosci. 1999 Sep;22(9):391-7.

Dixon AK, Gubitz AK, Sirinathsinghji DJ, Richardson PJ, Freeman TC. Tissue distribution of adenosine receptor mRNAs in the rat. Br J Pharmacol. 1996 Jul;118(6):1461-8.

Dodart JC, Mathis C, Saura J, Bales KR, Paul SM, Ungerer A. Neuroanatomical abnormalities in behaviorally characterized APP(V717F) transgenic mice. Neurobiol Dis. 2000 Apr;7(2):71-85.

Domenici MR, de Carolis AS, Sagratella S. Block by N6-L-phenylisopropyl-adenosine of the electrophysiological and morphological correlates of hippocampal ischaemic injury in the gerbil. Br J Pharmacol. 1996 Jul;118(6):1551-7.

Donoso MV, López R, Miranda R, Briones R, Huidobro-Toro JP. A2B adenosine receptor mediates human chorionic vasoconstriction and signals through arachidonic acid cascade. Am J Physiol Heart Circ Physiol. 2005 May;288(5):H2439-49.

Doyle KP, Simon RP, Stenzel-Poore MP. Mechanisms of ischemic brain damage. Neuropharmacology. 2008 Sep;55(3):310-8. doi: 10.1016/j.neuropharm.2008.01.005. Epub 2008 Jan 25.

Drubin D, Kirschner M. Purification of tau protein from brain. Methods Enzymol. 1986;134:156-60.

Duchen LW. Current status review: cerebral amyloid. Int J Exp Pathol. 1992 Aug;73(4):535-50.

Duff K, Eckman C, Zehr C, Yu X, Prada CM, Perez-tur J, Hutton M, Buee L, Harigaya Y, Yager D, Morgan D, Gordon MN, Holcomb L, Refolo L, Zenk B, Hardy J, Younkin S.

Increased amyloid-beta42(43) in brains of mice expressing mutant presenilin 1. Nature. 1996 Oct 24;383(6602):710-3.

Dunwiddie TV, Diao L. Extracellular adenosine concentrations in hippocampal brain slices and the tonic inhibitory modulation of evoked excitatory responses. J Pharmacol Exp Ther. 1994 Feb;268(2):537-45.

Dux E, Fastbom J, Ungerstedt U, Rudolphi K, Fredholm BB. Protective effect of adenosine and a novel xanthine derivative propentofylline on the cell damage after bilateral carotid occlusion in the gerbil hippocampus. Brain Res. 1990 May 21;516(2):248-56.

Dux E, Schubert P, Kreutzberg GW. Ultrastructural localization of calcium in ischemic hippocampal slices: the influence of adenosine and theophylline. J Cereb Blood Flow Metab. 1992 May;12(3):520-4.

Eastwood SL, Harrison PJ. Decreased synaptophysin in the medial temporal lobe in schizophrenia demonstrated using immunoautoradiography. Neuroscience. 1995 Nov;69(2):339-43.

Eikelenboom P, Rozemuller JM, van Muiswinkel FL. Inflammation and Alzheimer's disease: relationships between pathogenic mechanisms and clinical expression. Exp Neurol. 1998 Nov;154(1):89-98.

Eckle T, Faigle M, Grenz A, Laucher S, Thompson LF, Eltzschig HK. A2B adenosine receptor dampens hypoxia-induced vascular leak. Blood. 2008 Feb 15;111(4):2024-35. Epub 2007 Dec 4.

Eckle T, Krahn T, Grenz A, Köhler D, Mittelbronn M, Ledent C, Jacobson MA, Osswald H, Thompson LF, Unertl K, Eltzschig HK. Cardioprotection by ecto-5'-nucleotidase (CD73) and A2B adenosine receptors. Circulation. 2007 Mar 27;115(12):1581-90.

Eisert W. Dipyridamole. In: Platelets, 2002, Michelson A, Eds, Academic Press, London, UK, pp. 803-15.

Ekdahl CT, Claasen JH, Bonde S, Kokaia Z, Lindvall O. Inflammation is detrimental for neurogenesis in adult brain. Proc Natl Acad Sci U S A. 2003 Nov 11;100(23):13632-7.

Elder GA, Gama Sosa MA, De Gasperi R. Transgenic mouse models of Alzheimer's disease. Mt Sinai J Med. 2010 Jan-Feb;77(1):69-81. doi: 10.1002/msj.20159.

Elkeles RS, Hampton JR, Honour AJ, Mitchell JR, Prichard JS. Effect of a pyrimido-pyrimidine compound on platelet behaviour in vitro and in vivo. Lancet. 1968 Oct 5;2(7571):751-4.

Elmore S. Apoptosis: a review of programmed cell death. Toxicol Pathol. 2007 Jun;35(4):495-516.

Eltzschig HK, Thompson LF, Karhausen J, Cotta RJ, Ibla JC, Robson SC, Colgan SP. Endogenous adenosine produced during hypoxia attenuates neutrophil accumulation: coordination by extracellular nucleotide metabolism. Blood. 2004 Dec 15;104(13):3986-92.

Ernens I, Léonard F, Vausort M, Rolland-Turner M, Devaux Y, Wagner DR. Adenosine up-regulates vascular endothelial growth factor in human macrophages. Biochem Biophys Res Commun. 2010 Feb 12;392(3):351-6.

Fagarasan MO, Efthimiopoulos S. Mechanism of amyloid beta-peptide (1-42) toxicity in PC12 cells. Mol Psychiatry. 1996 Nov;1(5):398-403

Fan Y, Xie L, Chung CY. Signaling Pathways Controlling Microglia Chemotaxis. Mol Cells. 2017 Mar;40(3):163-168.

Fang Y, Olah ME. Cyclic AMP-dependent, protein kinase A-independent activation of extracellular signal-regulated kinase 1/2 following adenosine receptor stimulation in human umbilical vein endothelial cells: role of exchange protein activated by cAMP 1 (Epac1). J Pharmacol Exp Ther. 2007 Sep;322(3):1189-200.

Farahani R, Pina-Benabou MH, Kyrozis A, Siddiq A, Barradas PC, Chiu FC, Cavalcante LA, Lai JC, Stanton PK, Rozental R. Alterations in metabolism and gap junction expression may determine the role of astrocytes as "good samaritans" or executioners. Glia. 2005 Jun;50(4):351-61.

Farkas E, Donka G, de Vos RA, Mihály A, Bari F, Luiten PG. Experimental cerebral hypoperfusion induces white matter injury and microglial activation in the rat brain. Acta Neuropathol. 2004 Jul;108(1):57-64.

Farkas E, Institóris A, Domoki F, Mihály A, Bari F. The effect of pre- and posttreatment with diazoxide on the early phase of chronic cerebral hypoperfusion in the rat. Brain Res. 2006 May 4;1087(1):168-74.

Farkas E, Luiten PG, Bari F. Permanent, bilateral common carotid artery occlusion in the rat: a model for chronic cerebral hypoperfusion-related neurodegenerative diseases. Brain Res Rev. 2007 Apr;54(1):162-80.

Farkas E, Pratt R, Sengpiel F, Obrenovitch TP. Direct, live imaging of cortical spreading depression and anoxic depolarisation using a fluorescent, voltage-sensitive dye. J Cereb Blood Flow Metab. 2008 Feb;28(2):251-62.

Felleman DJ, Van Essen DC. Distributed hierarchical processing in the primate cerebral cortex. Cereb Cortex. 1991 Jan-Feb;1(1):1-47.

Fellin T, Pascual O, Gobbo S, Pozzan T, Haydon PG, Carmignoto G. Neuronal synchrony mediated by astrocytic glutamate through activation of extrasynaptic NMDA receptors. Neuron. 2004 Sep 2;43(5):729-43. Erratum in: Neuron. 2004 Jan 6;45(1):177.

Feoktistov I, Biaggioni I. Role of adenosine A(2B) receptors in inflammation. Adv Pharmacol. 2011;61:115-44.

Feoktistov I, Goldstein AE, Biaggioni I. Role of p38 mitogen-activated protein kinase and extracellular signal-regulated protein kinase kinase in adenosine A2B receptor-mediated interleukin-8 production in human mast cells. Mol Pharmacol. 1999 Apr;55(4):726-34.

Feoktistov I, Goldstein AE, Ryzhov S, Zeng D, Belardinelli L, Voyno-Yasenetskaya T, Biaggioni I. Differential expression of adenosine receptors cin human endothelial cells: role of A2B receptors in angiogenic factor regulation. Circ Res. 2002 Mar 22;90(5):531-8.

Feoktistov I, Ryzhov S, Zhong H, Goldstein AE, Matafonov A, Zeng D, Biaggioni I. Hypoxia modulates adenosine receptors in human endothelial and smooth muscle cells toward an A2B angiogenic phenotype. Hypertension. 2004 Nov;44(5):649-54.

Feuerstein GZ, Wang X, Barone FC. The role of cytokines in the neuropathology of stroke and neurotrauma. Neuroimmunomodulation. 1998 May-Aug;5(3-4):143-59.

Fiebich BL, Biber K, Lieb K, van Calker D, Berger M, Bauer J, Gebicke-Haerter PJ. Cyclooxygenase-2 expression in rat microglia is induced by adenosine A2a-receptors. Glia. 1996 Oct;18(2):152-60.

Figueredo VM, Diamond I, Zhou HZ, Camacho SA. Chronic dipyridamole therapy produces sustained protection against cardiac ischemia-reperfusion injury. Am J Physiol. 1999 Nov;277(5):H2091-7.

Fonarow GC, Smith EE, Saver JL, Reeves MJ, Bhatt DL, Grau-Sepulveda MV, Olson DM, Hernandez AF, Peterson ED, Schwamm LH. Timeliness of tissue-type plasminogen activator therapy in acute ischemic stroke: patient characteristics, hospital factors, and outcomes associated with door-to-needle times within 60 minutes.

Franceschi C, Capri M, Monti D, Giunta S, Olivieri F, Sevini F, Panourgia MP, Invidia L, Celani L, Scurti M, Cevenini E, Castellani GC, Salvioli S. Inflammaging and anti-inflammaging: a systemic perspective on aging and longevityemerged from studies in humans. Mech Ageing Dev. 2007 Jan;128(1):92-105.

Frank MG, Baratta MV, Sprunger DB, Watkins LR, Maier SF. Microglia serve as a neuroimmune substrate for stress-induced potentiation of CNS pro-inflammatory cytokine responses. Brain Behav Immun. 2007 Jan;21(1):47-59.

Fredholm BB, Arslan G, Halldner L, Kull B, Schulte G, Wasserman W. Structure and function of adenosine receptors and their genes. Naunyn Schmiedebergs Arch Pharmacol. 2000 Nov;362(4-5):364-74.

Fredholm BB, Chen JF, Masino SA, Vaugeois JM. Actions of adenosine at its receptors in the CNS: insights from knockouts and drugs. Annu Rev Pharmacol Toxicol. 2005;45:385-412.

Fredholm BB, Cunha RA, Svenningsson P. Pharmacology of adenosine A2A receptors and therapeutic applications. Curr Top Med Chem. 2003;3(4):413-26.

Fredholm BB, IJzerman AP, Jacobson KA, Linden J, Müller CE. International Union of Basic and Clinical Pharmacology. LXXXI. Nomenclature and classification of adenosine receptors--an update. Pharmacol Rev. 2011 Mar;63(1):1-34.

Fredholm BB, Irenius E, Kull B, Schulte G. Comparison of the potency of adenosine as an agonist at human adenosine receptors expressed in Chinese hamster ovary cells. Biochem Pharmacol. 2001 Feb 15;61(4):443-8.

Fredholm BB, Lindgren E. Protein kinase C activation increases noradrenaline release from the rat hippocampus and modifies the inhibitory effect of alpha 2-adrenoceptor and adenosine A1-receptor agonists. Naunyn Schmiedebergs Arch Pharmacol. 1988 May;337(5):477-83.

Fredholm BB, Zhang Y, van der Ploeg I. Adenosine A2A receptors mediate the inhibitory effect of adenosine on formyl-Met-Leu-Phe-stimulated respiratory burst in neutrophil leucocytes. Naunyn Schmiedebergs Arch Pharmacol. 1996 Aug-Sep;354(3):262-7.

Frenguelli BG, Wigmore G, Llaudet E, Dale N. Temporal and mechanistic dissociation of ATP and adenosine release during ischaemia in the mammalian hippocampus. J Neurochem. 2007 Jun;101(5):1400-13.

Frey U, Morris RG. Synaptic tagging and long-term potentiation. Nature. 1997 Feb 6;385(6616):533-6.

Freund TF, Maglóczky Z. Early degeneration of calretinin-containing neurons in the rat hippocampus after ischemia. Neuroscience. 1993 Oct;56(3):581-96.

Fuller AD, Van Eldik LJ. MFG-E8 regulates microglial phagocytosis of apoptotic neurons. J Neuroimmune Pharmacol. 2008 Dec;3(4):246-56.

Furukawa K, Fu W, Li Y, Witke W, Kwiatkowski DJ, Mattson MP. The actin-severing protein gelsolin modulates calcium channel and NMDA receptor activities and vulnerability to excitotoxicity in hippocampal neurons. J Neurosci. 1997 Nov 1;17(21):8178-86.

Gaarskjaer FB. Organization of the mossy fiber system of the rat studied in extended hippocampi. I. Terminal area related to number of granule and pyramidal cells. J Comp Neurol. 1978 Mar 1;178(1):49-72

Gama Sosa MA, Gasperi RD, Rocher AB, Wang AC, Janssen WG, Flores T, Perez GM, Schmeidler J, Dickstein DL, Hof PR, Elder GA. Age-related vascular pathology in transgenic mice expressing presenilin 1-associated familial Alzheimer's disease mutations. Am J Pathol. 2010 Jan;176(1):353-68.

Games D, Adams D, Alessandrini R, Barbour R, Berthelette P, Blackwell C, Car T, Clemens J, Donaldson T, Gillespie F, et al. Alzheimer-type neuropathology in transgenic mice overexpressing V717F beta-amyloid precursor protein. Nature. 1995 Feb 9;373(6514):523-7.

Gao FB, Apperly J, Raff M. Cell-intrinsic timers and thyroid hormone regulate the probability of cell-cycle withdrawal and differentiation of oligodendrocyte precursor cells. Dev Biol. 1998 May 1;197(1):54-66.

Gao Y, Phillis JW. Atropine and cerebral ischemic injury in the Mongolian gerbil. Gen Pharmacol. 1994 Jul;25(4):725-7.

Garcia AD, Doan NB, Imura T, Bush TG, Sofroniew MV. GFAP-expressing progenitors are the principal source of constitutive neurogenesis in adult mouse forebrain. Nat Neurosci. 2004 Nov;7(11):1233-41.

García-Mesa Y, López-Ramos JC, Giménez-Llort L, Revilla S, Guerra R, Gruart A, Laferla FM, Cristòfol R, Delgado-García JM, Sanfeliu C. Physical exercise protects against Alzheimer's disease in 3xTg-AD mice. J Alzheimers Dis. 2011;24(3):421-54.

Gay F. Activated microglia in primary MS lesions: defenders or aggressors? Int MS J. 2007 Sep;14(3):78-83.

Gaykema RP, van der Kuil J, Hersh LB, Luiten PG. Patterns of direct projections from the hippocampus to the medial septum-diagonal band complex: anterograde tracing with Phaseolus vulgaris leucoagglutinin combined with immunohistochemistry of choline acetyltransferase. Neuroscience. 1991;43(2-3):349-60.

Gee CE, Benquet P, Raineteau O, Rietschin L, Kirbach SW, Gerber U. NMDA receptors and the differential ischemic vulnerability of hippocampal neurons. Eur J Neurosci. 2006 May;23(10):2595-603.

Gehrmann J, Matsumoto Y, Kreutzberg GW. Microglia: intrinsic immuneffector cell of the brain. Brain Res Brain Res Rev. 1995 Mar;20(3):269-87.

Gervais FG, Xu D, Robertson GS, Vaillancourt JP, Zhu Y, Huang J, LeBlanc A, Smith D, Rigby M, Shearman MS, Clarke EE, Zheng H, Van Der Ploeg LH, Ruffolo SC, Thornberry NA, Xanthoudakis S, Zamboni RJ, Roy S, Nicholson DW. Involvement of caspases in

proteolytic cleavage of Alzheimer's amyloid-beta precursor protein and amyloidogenic A beta peptide formation. Cell. 1999 Apr 30;97(3):395-406.

Gessi S, Borea PA. Farmacologia cellulare e molecolare, sistemi di trasmissione. Trasmissione purinergica. In: Farmacologia-Principi Di Base e Applicazioni Terapeutiche, 2011, Rossi F, Cuomo V, Riccardi C, Eds, Minerva Medica, Torino, Italy, pp. 165-76.

Gessi S, Varani K, Merighi S, Cattabriga E, Pancaldi C, Szabadkai Y, Rizzuto R, Klotz KN, Leung E, Mac Lennan S, Baraldi PG, Borea PA. Expression, pharmacological profile, and functional coupling of A2B receptors in a recombinant system and in peripheral blood cells using a novel selective antagonist radioligand, [3H]MRE 2029-F20. Mol Pharmacol. 2005 Jun;67(6):2137-47.

Gibson CL. Cerebral ischemic stroke: is gender important? J Cereb Blood Flow Metab. 2013 Sep;33(9):1355-61. doi: 10.1038/jcbfm.2013.102. Epub 2013 Jun 12.

Ginhoux F, Lim S, Hoeffel G, Low D, Huber T. Origin and differentiation of microglia. Front Cell Neurosci. 2013 Apr 17;7:45. doi: 10.3389/fncel.2013.00045.

Ginsberg MD. Adventures in the pathophysiology of brain ischemia: penumbra, gene expression, neuroprotection: the 2002 Thomas Willis Lecture. Stroke. 2003 Jan;34(1):214-23.

Giovannini MG, Scali C, Prosperi C, Bellucci A, Vannucchi MG, Rosi S, Pepeu G, Casamenti F. Beta-amyloid-induced inflammation and cholinergic hypofunction in the rat brain in vivo: involvement of the p38MAPK pathway. Neurobiol Dis. 2002 Nov;11(2):257-74.

Giovannini MG, Mutolo D, Bianchi L, Michelassi A, Pepeu G. NMDA receptor antagonists decrease GABA outflow from the septum and increase acetylcholine outflow from the hippocampus: a microdialysis study. J Neurosci. 1994 Mar;14(3 Pt 1):1358-65.

Giunta B, Fernandez F, Nikolic WV, Obregon D, Rrapo E, Town T, Tan J. Inflammaging as a prodrome to Alzheimer's disease. J Neuroinflammation. 2008 Nov 11;5:51. doi: 10.1186/1742-2094-5-51.

Golgi C. Contribuzione alla fine anatomia degli organi centrali del sistema nervoso. Rivista Clinica di Bologna (1871).

Gonçalves FQ, Pires J, Pliassova A, Beleza R, Lemos C, Marques JM, Rodrigues RJ, Canas PM, Köfalvi A, Cunha RA, Rial D. Adenosine A2b receptors control A1 receptor-mediated inhibition of synaptic transmission in the mouse hippocampus. Eur J Neurosci. 2015 Apr;41(7):878-88.

González-Fernández E, Sánchez-Gómez MV, Pérez-Samartín A, Arellano RO, Matute C. A3 Adenosine receptors mediate oligodendrocyte death and ischemic damage to optic nerve. Glia. 2014 Feb;62(2):199-216.

Gordon GR, Choi HB, Rungta RL, Ellis-Davies GC, MacVicar BA. Brain metabolism dictates the polarity of astrocyte control over arterioles. Nature. 2008 Dec 11;456(7223):745-9. doi: 10.1038/nature07525.

Graham SH, Chen J, Lan JQ, Simon RP. A dose-response study of neuroprotection using the AMPA antagonist NBQX in rat focal cerebral ischemia. J Pharmacol Exp Ther. 1996 Jan;276(1):1-4.

Grass D, Pawlowski PG, Hirrlinger J, Papadopoulos N, Richter DW, Kirchhoff F, Hülsmann S. Diversity of functional astroglial properties in the respiratory network. J Neurosci. 2004 Feb 11;24(6):1358-65.

Grant MB, Davis MI, Caballero S, Feoktistov I, Biaggioni I, Belardinelli L. Proliferation, migration, and ERK activation in human retinal endothelial cells through A(2B) adenosine receptor stimulation

Grilli M, Diodato E, Lozza G, Brusa R, Casarini M, Uberti D, Rozmahel R, Westaway D, St George-Hyslop P, Memo M, Ongini E. Presenilin-1 regulates the neuronal threshold to excitotoxicity both physiologically and pathologically. Proc Natl Acad Sci U S A. 2000 Nov 7;97(23):12822-7.

Grossberg S. The imbalanced brain: from normal behavior to schizophrenia. Biol Psychiatry. 2000 Jul 15;48(2):81-98. Review.

Gruart A, López-Ramos JC, Muñoz MD, Delgado-García JM. Aged wild-type and APP, PS1, and APP + PS1 mice present similar deficits in associative learning and synaptic plasticity independent of amyloid load. Neurobiol Dis. 2008 Jun;30(3):439-50

Gu L, Huang B, Shen W, Gao L, Ding Z, Wu H, Guo J. Early activation of nSMase2/ceramide pathway in astrocytes is involved in ischemia-associated neuronal damage via inflammation in rat hippocampi. J Neuroinflammation. 2013 Sep 3;10:109.

Gultekin SH, Rosenfeld MR, Voltz R, Eichen J, Posner JB, Dalmau J. Paraneoplastic limbic encephalitis: neurological symptoms, immunological findings and tumour association in 50 patients. Brain. 2000 Jul;123 (Pt 7):1481-94.

Guo Q, Sebastian L, Sopher BL, Miller MW, Ware CB, Martin GM, Mattson MP. Increased vulnerability of hippocampal neurons from presenilin-1 mutant knock-in mice to amyloid beta-peptide toxicity: central roles of superoxide production and caspase activation. J Neurochem. 1999 Mar;72(3):1019-29.

Haass C, Hung AY, Schlossmacher MG, Oltersdorf T, Teplow DB, Selkoe DJ. Normal cellular processing of the beta-amyloid precursor protein results in the secretion of the amyloid beta peptide and related molecules. Ann N Y Acad Sci. 1993 Sep 24;695:109-16.

Haass C, Selkoe DJ. Cellular processing of beta-amyloid precursor protein and the genesis of amyloid beta-peptide. Cell. 1993 Dec 17;75(6):1039-42.

Hagberg H, Andersson P, Lacarewicz J, Jacobson I, Butcher S, Sandberg M. Extracellular adenosine, inosine, hypoxanthine, and xanthine in relation to tissue nucleotides and purines in rat striatum during transient ischemia. J Neurochem. 1987 Jul;49(1):227-31.

Halkes PH, van Gijn J, Kappelle LJ, Koudstaal PJ, Algra A. Aspirin plus dipyridamole versus aspirin alone after cerebral ischaemia of arterial origin (ESPRIT): randomised controlled trial. Lancet. 2006 May 20;367(9523):1665-73.

Hall A. Rho GTPases and the actin cytoskeleton. Science. 1998 Jan 23;279(5350):509-14.

Halliday GM, Shepherd CE, McCann H, Reid WG, Grayson DA, Broe GA, Kril JJ. Effect of anti-inflammatory medications on neuropathological findings in Alzheimer disease. Arch Neurol. 2000 Jun;57(6):831-6.

Hama H, Hara C, Yamaguchi K, Miyawaki A. PKC signaling mediates global enhancement of excitatory synaptogenesis in neurons triggered by local contact with astrocytes. Neuron. 2004 Feb 5;41(3):405-15.

Hamm V, Héraud C, Bott JB, Herbeaux K, Strittmatter C, Mathis C, Goutagny R. Differential contribution of APP metabolites to early cognitive deficits in a TgCRND8 mouse model of Alzheimer's disease. Sci Adv. 2017 Feb 24;3(2):e1601068.

Hanger DP, Brion JP, Gallo JM, Cairns NJ, Luthert PJ, Anderton BH. Tau in Alzheimer's disease and Down's syndrome is insoluble and abnormally phosphorylated. Biochem J. 1991 Apr 1;275 (Pt 1):99-104.

Hanisch UK. Functional diversity of microglia how heterogeneous are they to begin with? Front Cell Neurosci. 2013 May 14;7:65. doi: 10.3389/fncel.2013.00065.

Hanisch UK, Kettenmann H. Microglia: active sensor and versatile effector cells in the normal and pathologic brain. Nat Neurosci. 2007 Nov;10(11):1387-94.

Hardy J, Allsop D. Amyloid deposition as the central event in the aetiology of Alzheimer's disease. Trends Pharmacol Sci. 1991 Oct;12(10):383-8.

Harrington CR, Louwagie J, Rossau R, Vanmechelen E, Perry RH, Perry EK, Xuereb JH, Roth M, Wischik CM. Influence of apolipoprotein E genotype on senile dementia of the Alzheimer and Lewy body types. Significance for etiological theories of Alzheimer's disease. Am J Pathol. 1994 Dec;145(6):1472-84.

Harrison GP, Miele G, Hunter E, Lever AM. Functional analysis of the core human immunodeficiency virus type 1 packaging signal in a permissive cell line. J Virol. 1998 Jul;72(7):5886-96.

Hart ML, Jacobi B, Schittenhelm J, Henn M, Eltzschig HK. Cutting Edge: A2B Adenosine receptor signaling provides potent protection during intestinal ischemia/reperfusion injury. J Immunol. 2009 Apr 1;182(7):3965-8.

Haskó G, Csóka B, Németh ZH, Vizi ES, Pacher P. A(2B) adenosine receptors in immunity and inflammation. Trends Immunol. 2009 Jun;30(6):263-70.

Haskó G, Pacher P, Deitch EA, Vizi ES. Shaping of monocyte and macrophage function by adenosine receptors. Pharmacol Ther. 2007 Feb;113(2):264-75.

Hata R, Maeda K, Hermann D, Mies G, Hossmann KA. Evolution of brain infarction after transient focal cerebral ischemia in mice. J Cereb Blood Flow Metab. 2000 Jun;20(6):937-46.

Hauss-Wegrzyniak B, Lukovic L, Bigaud M, Stoeckel ME. Brain inflammatory response induced by intracerebroventricular infusion of lipopolysaccharide: an immunohistochemical study. Brain Res. 1998 Jun 1;794(2):211-24.

Heneka MT, Rodríguez JJ, Verkhratsky A. Neuroglia in neurodegeneration. Brain Res Rev. 2010 May;63(1-2):189-211. doi: 10.1016/j.brainresrev.2009.11.004.

Heneka MT, Carson MJ, El Khoury J, Landreth GE, Brosseron F, Feinstein DL, Jacobs AH, Wyss-Coray T, Vitorica J, Ransohoff RM, Herrup K, Frautschy SA, Finsen B, Brown GC, Verkhratsky A, Yamanaka K, Koistinaho J, Latz E, Halle A, Petzold GC, Town T, Morgan D, Shinohara ML, Perry VH, Holmes C, Bazan NG, Brooks DJ, Hunot S, Joseph B, Deigendesch N, Garaschuk O, Boddeke E, Dinarello CA, Breitner JC, Cole GM, Golenbock DT, Kummer MP. Neuroinflammation in Alzheimer's disease. Lancet Neurol. 2015 Apr;14(4):388-405.

Heppner FL, Ransohoff RM, Becher B. Immune attack: the role of inflammation in Alzheimer disease. Nat Rev Neurosci. 2015 Jun;16(6):358-72.

Heptinstall S, Fox S, Crawford J, Hawkins M. Inhibition of platelet aggregation in whole blood by dipyridamole and aspirin. Thromb Res. 1986 Apr 15;42(2):215-23.

Herreras O, Somjen GG. Effects of prolonged elevation of potassium on hippocampus of anesthetized rats. Brain Res. 1993 Jul 23;617(2):194-204.

Hettinger BD, Lee A, Linden J, Rosin DL. Ultrastructural localization of adenosine A2A receptors suggests multiple cellular sites for modulation of GABAergic neurons in rat striatum. J Comp Neurol. 2001 Mar 12;431(3):331-46.

Hickman SE, Allison EK, El Khoury J. Microglial dysfunction and defective beta-amyloid clearance pathways in aging Alzheimer's disease mice. J Neurosci. 2008 Aug 13;28(33):8354-60.

Hinz JM. Impact of abasic site orientation within nucleosomes on human APE1 endonuclease activity. Mutat Res. 2014 Aug-Sep;766-767:19-24.

Hirase H. A multi-photon window onto neuronal-glial-vascular communication. Trends Neurosci. 2005 May;28(5):217-9.

Ho L, Purohit D, Haroutunian V, Luterman JD, Willis F, Naslund J, Buxbaum JD, Mohs RC, Aisen PS, Pasinetti GM. Neuronal cyclooxygenase 2 expression in the hippocampal formation as a function of the clinical progression of Alzheimer disease. Arch Neurol. 2001 Mar;58(3):487-92.

Hoek RM, Ruuls SR, Murphy CA, Wright GJ, Goddard R, Zurawski SM, Blom B, Homola ME, Streit WJ, Brown MH, Barclay AN, Sedgwick JD. Down-regulation of the macrophage lineage through interaction with OX2 (CD200). Science. 2000 Dec 1;290(5497):1768-71.

Holcomb L, Gordon MN, McGowan E, Yu X, Benkovic S, Jantzen P, Wright K, Saad I, Mueller R, Morgan D, Sanders S, Zehr C, O'Campo K, Hardy J, Prada CM, Eckman C, Younkin S, Hsiao K, Duff K. Accelerated Alzheimer-type phenotype in transgenic mice carrying both mutant amyloid precursor protein and presenilin 1 transgenes. Nat Med. 1998 Jan;4(1):97-100.

Holloway PM, Gavins FN. Modeling Ischemic Stroke In Vitro: Status Quo and Future Perspectives. Stroke. 2016 Feb;47(2):561-9.

Honda S, Sasaki Y, Ohsawa K, Imai Y, Nakamura Y, Inoue K, Kohsaka S. Extracellular ATP or ADP induce chemotaxis of cultured microglia through Gi/o-coupled P2Y receptors. J Neurosci. 2001 Mar 15;21(6):1975-82.

Hossmann KA. Viability thresholds and the penumbra of focal ischemia. Ann Neurol. 1994 Oct;36(4):557-65.

Hossmann KA. Periinfarct depolarizations. Cerebrovasc Brain Metab Rev. 1996 Fall;8(3):195-208.

Hossmann KA. Experimental models for the investigation of brain ischemia. Cardiovasc Res. 1998 Jul;39(1):106-20.

Hsiao K, Chapman P, Nilsen S, Eckman C, Harigaya Y, Younkin S, Yang F, Cole G. Correlative memory deficits, Abeta elevation, and amyloid plaques in transgenic mice. Science. 1996 Oct 4;274(5284):99-102.

Hsieh MS, Zhong WB, Yu SC, Lin JY, Chi WM, Lee HM. Dipyridamole suppresses high glucose-induced osteopontin secretion and mRNA expression in rat aortic smooth muscle cells. Circ J. 2010 Jun;74(6):1242-50.

Hsu M, Buzsáki G. Vulnerability of mossy fiber targets in the rat hippocampus to forebrain ischemia. J Neurosci. 1993 Sep;13(9):3964-79.

Hu X, Li P, Guo Y, Wang H, Leak RK, Chen S, Gao Y, Chen J. Microglia/macrophage polarization dynamics reveal novel mechanism of injury expansion after focal cerebral ischemia. Stroke. 2012 Nov;43(11):3063-70.

Huizinga R, van der Star BJ, Kipp M, Jong R, Gerritsen W, Clarner T, Puentes F, Dijkstra CD, van der Valk P, Amor S. Phagocytosis of neuronal debris by microglia is associated with neuronal damage in multiple sclerosis. Glia. 2012 Mar;60(3):422-31.

Hulse RE, Winterfield J, Kunkler PE, Kraig RP. Astrocytic clasmatodendrosis in hippocampal organ culture. Glia. 2001 Feb;33(2):169-79.

Hyman BT, Van Hoesen GW, Damasio AR, Barnes CL. Alzheimer's disease: cell-specific pathology isolates the hippocampal formation. Science. 1984 Sep 14;225(4667):1168-70.

Iadecola C. Bright and dark sides of nitric oxide in ischemic brain injury. Trends Neurosci. 1997 Mar;20(3):132-9

Iadecola C, Anrather J. The immunology of stroke: from mechanisms to translation. Nat Med. 2011 Jul 7;17(7):796-808.

Ishizuka N, Cowan WM, Amaral DG. A quantitative analysis of the dendritic organization of pyramidal cells in the rat hippocampus. J Comp Neurol. 1995 Nov 6;362(1):17-45

Jacobson KA, Gao ZG. Adenosine receptors as therapeutic targets. Nat Rev Drug Discov. 2006 Mar;5(3):247-64.

Jankowsky JL, Younkin LH, Gonzales V, Fadale DJ, Slunt HH, Lester HA, Younkin SG, Borchelt DR. Rodent A beta modulates the solubility and distribution of amyloid deposits in transgenic mice. J Biol Chem. 2007 Aug 3;282(31):22707-20

Ji XD, Gallo-Rodriguez C, Jacobson KA. A selective agonist affinity label for A_3 adenosine receptors. Biochem Biophys Res Commun. 1994 Aug 30;203(1):570-6.

Jiang X, Wang X. Cytochrome C-mediated apoptosis. Annu Rev Biochem. 2004;73:87-106.

Jiménez AI, Castro E, Mirabet M, Franco R, Delicado EG, Miras-Portugal MT. Potentiation of ATP calcium responses by A2B receptor stimulation and other signals coupled to Gs proteins in type-1 cerebellar astrocytes. Glia. 1999 Apr;26(2):119-28.

Johansson B, Fredholm BB. Further characterization of the binding of the adenosine receptor agonist [3H]CGS 21680 to rat brain using autoradiography. Neuropharmacology. 1995 Apr;34(4):393-403.

Johnston SC, Mendis S, Mathers CD. Global variation in stroke burden and mortality: estimates from monitoring, surveillance, and modelling. Lancet Neurol. 2009 Apr;8(4):345-54.

Jones BA, Beamer M, Ahmed S. Fractalkine/CX3CL1: a potential new target for inflammatory diseases. Mol Interv. 2010 Oct;10(5):263-70.

Jourdain P, Bergersen LH, Bhaukaurally K, Bezzi P, Santello M, Domercq M, Matute C, Tonello F, Gundersen V, Volterra A. Glutamate exocytosis from astrocytes controls synaptic strength. Nat Neurosci. 2007 Mar;10(3):331-9.

Jung S, Aliberti J, Graemmel P, Sunshine MJ, Kreutzberg GW, Sher A, Littman DR. Analysis of fractalkine receptor CX(3)CR1 function by targeted deletion and green fluorescent protein reporter gene insertion. Mol Cell Biol. 2000 Jun;20(11):4106-14.

Kandel ER. The molecular biology of memory storage: a dialogue between genes and synapses. Science. 2001 Nov 2;294(5544):1030-8. doi: 10.1126/science.1067020.

Kao AW, Eisenhut RJ, Martens LH, Nakamura A, Huang A, Bagley JA, Zhou P, de Luis A, Neukomm LJ, Cabello J, Farese RV Jr, Kenyon C. A neurodegenerative disease mutation that accelerates the clearance of apoptotic cells. Proc Natl Acad Sci U S A. 2011 Mar 15;108(11):4441-6.

Káradóttir R, Cavelier P, Bergersen LH, Attwell D. NMDA receptors are expressed in oligodendrocytes and activated in ischaemia. Nature. 2005 Dec 22;438(7071):1162-6.

Karwoski CJ, Lu HK, Newman EA. Spatial buffering of light-evoked potassium increases by retinal Müller (glial) cells. Science. 1989 May 5;244(4904):578-80.

Kassed CA, Butler TL, Navidomskis MT, Gordon MN, Morgan D, Pennypacker KR. Mice expressing human mutant presenilin-1 exhibit decreased activation of NF-kappaB p50 in hippocampal neurons after injury. Brain Res Mol Brain Res. 2003 Jan 31;110(1):152-7.

Kerchner GA, Hess CP, Hammond-Rosenbluth KE, Xu D, Rabinovici GD, Kelley DA, Vigneron DB, Nelson SJ, Miller BL. Hippocampal CA1 apical neuropil atrophy in mild Alzheimer disease visualized with 7-T MRI. Neurology. 2010 Oct 12;75(15):1381-7.

Kerr JF, Wyllie AH, Currie AR. Apoptosis: a basic biological phenomenon with wide-ranging implications in tissue kinetics. Br J Cancer. 1972 Aug;26(4):239-57.

Kesner RP, Lee I, Gilbert P. A behavioral assessment of hippocampal function based on a subregional analysis. Rev Neurosci. 2004;15(5):333-51.

Kettenmann H, Kirchhoff F, Verkhratsky A. Microglia: new roles for the synaptic stripper. Neuron. 2013 Jan 9;77(1):10-8. doi: 10.1016/j.neuron.2012.12.023.

Kim YS, Joh TH. Microglia, major player in the brain inflammation: their roles in the pathogenesis of Parkinson's disease. Exp Mol Med. 2006 Aug 31;38(4):333-47.

Kitagawa H, Mori A, Shimada J, Mitsumoto Y, Kikuchi T. Intracerebral adenosine infusion improves neurological outcome after transient focal ischemia in rats. Neurol Res. 2002 Apr;24(3):317-23.

Kluck RM, Bossy-Wetzel E, Green DR, Newmeyer DD. The release of cytochrome c from mitochondria: a primary site for Bcl-2 regulation of apoptosis. Science. 1997 Feb 21;275(5303):1132-6.

Koeppen M, Eckle T, Eltzschig HK. Interplay of hypoxia and A2B adenosine receptors in tissue protection. Adv Pharmacol. 2011;61:145-86.

Koester J, Siegelbaum SA. Propagated Signaling: The Action Potential. In: Kandel ER, Schwartz JH, Jessell TM, editors. Priciples of neural science. New York: McGraw-Hill; 2000. p. 151-71.

Kolachala V, Asamoah V, Wang L, Obertone TS, Ziegler TR, Merlin D, Sitaraman SV. TNF-alpha upregulates adenosine 2b (A2b) receptor expression and signaling in intestinal epithelial cells: a basis for A2bR overexpression in colitis. Cell Mol Life Sci. 2005 Nov;62(22):2647-57.

Kolachala V, Ruble B, Vijay-Kumar M, Wang L, Mwangi S, Figler H, Figler R, Srinivasan S, Gewirtz A, Linden J, Merlin D, Sitaraman S. Blockade of adenosine A2B receptors ameliorates murine colitis. Br J Pharmacol. 2008 Sep;155(1):127-37.

Kong T, Westerman KA, Faigle M, Eltzschig HK, Colgan SP. HIF-dependent induction of adenosine A2B receptor in hypoxia. FASEB J. 2006 Nov;20(13):2242-50.

Koscsó B, Csóka B, Selmeczy Z, Himer L, Pacher P, Virág L, Haskó G. Adenosine augments IL-10 production by microglial cells through an A2B adenosine receptor-mediated process. J Immunol. 2012 Jan 1;188(1):445-53.

Kovacs K, Toth A, Deres P, Kalai T, Hideg K, Gallyas F Jr, Sumegi B. Critical role of PI3-kinase/Akt activation in the PARP inhibitor induced heart function recovery during ischemia-reperfusion. Biochem Pharmacol. 2006 Feb 14;71(4):441-52.

Kow LM, van Harreveld A. Ion and water movements in isolated chicken retinas during spreading depression. Neurobiology. 1972;2(2):61-9.

Kraepelin E and Ross Diefendorf A. Clinical Psychiatry: A Textbook for Students and Physicians. 1910.

Kreutzberg GW. Microglia: a sensor for pathological events in the CNS. Trends Neurosci. 1996 Aug19(8):312-8.

Kushner I. The acute phase response: from Hippocrates to cytokine biology. Eur Cytokine Netw. 1991 Mar-Apr;2(2):75-80.

Lana D, Cerbai F, Di Russo J, Boscaro F, Giannetti A, Petkova-Kirova P, Pugliese AM, Giovannini MG. Hippocampal long term memory: effect of the cholinergic system on local protein synthesis. Neurobiol Learn Mem. 2013 Nov;106:246-57.

Lana D, Melani A, Pugliese AM, Cipriani S, Nosi D, Pedata F, Giovannini MG. The neuron-astrocyte-microglia triad in a rat model of chronic cerebral hypoperfusion: protective effect of dipyridamole. Front Aging Neurosci. 2014 Nov 27;6:322.

Lana D, Iovino L, Nosi D, Wenk GL, Giovannini MG. The neuron-astrocyte-microglia triad involvement in neuroinflammaging mechanisms in the CA3 hippocampus of memory-impaired aged rats. Exp Gerontol. 2016 Oct;83:71-88.

Lana D, Di Russo J, Mello T, Wenk GL, Giovannini MG. Rapamycin inhibits mTOR/p70S6K activation in CA3 region of the hippocampus of the rat and impairs long term memory. Neurobiol Learn Mem. 2017 Jan;137:15-26.

Lana D, Ugolini F, Nosi D, Wenk GL, Giovannini MG. Alterations in the Interplay between Neurons, Astrocytes and Microglia in the Rat Dentate Gyrus in Experimental Models of Neurodegeneration. Front Aging Neurosci. 2017a Sep 11;9:296.

Lana D, Ugolini F, Melani A, Nosi D, Pedata F, Giovannini MG. The neuron-astrocyte-microglia triad in CA3 after chronic cerebral hypoperfusion in the rat: Protective effect of dipyridamole. Exp Gerontol. 2017b Oct 1;96:46-62.

Laplante M, Sabatini DM. mTOR signaling in growth control and disease. Cell. 2012 Apr 13;149(2):274-93.

Latimer CS, Searcy JL, Bridges MT, Brewer LD, Popović J, Blalock EM, Landfield PW, Thibault O, Porter NM. Reversal of glial and neurovascular markers of unhealthy brain aging by exercise in middle-aged female mice. PLoS One. 2011;6(10):e26812.

Latini S, Pazzagli M, Pepeu G, Pedata F. A2 adenosine receptors: their presence and neuromodulatory role in the central nervous system. Gen Pharmacol. 1996 Sep;27(6):925-33.

Latini S, Bordoni F, Corradetti R, Pepeu G, Pedata F. Temporal correlation between adenosine outflow and synaptic potential inhibition in rat hippocampal slices during ischemia-like conditions. Brain Res. 1998 Jun 1;794(2):325-8.

Latini S, Bordoni F, Corradetti R, Pepeu G, Pedata F. Effect of A2A adenosine receptor stimulation and antagonism on synaptic depression induced by in vitro ischaemia in rat hippocampal slices. Br J Pharmacol. 1999 Nov;128(5):1035-44.

Latini S, Pedata F. Adenosine in the central nervous system: release mechanisms and extracellular concentrations. J Neurochem. 2001 Nov;79(3):463-84.

Lauro C, Di Angelantonio S, Cipriani R, Sobrero F, Antonilli L, Brusadin V, Ragozzino D, Limatola C. Activity of adenosine receptors type 1 Is required for CX3CL1-mediated neuroprotection and neuromodulation in hippocampal neurons. J Immunol. 2008 Jun 1;180(11):7590-6.

Lauro C, Catalano M, Trettel F, Limatola C. Fractalkine in the nervous system: neuroprotective or neurotoxic molecule? Ann N Y Acad Sci. 2015 Sep;1351:141-8.

Lazarov O, Peterson LD, Peterson DA, Sisodia SS. Expression of a familial Alzheimer's disease-linked presenilin-1 variant enhances perforant pathway lesion-induced neuronal loss in the entorhinal cortex. J Neurosci. 2006 Jan 11;26(2):429-34.

Leao AA. Further observations on the spreading depression of activity in the cerebral cortex. J Neurophysiol. 1947 Nov;10(6):409-14.

Ledent C, Vaugeois JM, Schiffmann SN, Pedrazzini T, El Yacoubi M, Vanderhaeghen JJ, Costentin J, Heath JK, Vassart G, Parmentier M. Aggressiveness, hypoalgesia and high blood pressure in mice lacking the adenosine A2a receptor. Nature. 1997 Aug 14;388(6643):674-8.

Lee JM, Zipfel GJ, Choi DW. The changing landscape of ischaemic brain injury mechanisms. Nature. 1999 Jun 24;399(6738 Suppl):A7-14.

Lemos C, Pinheiro BS, Beleza RO, Marques JM, Rodrigues RJ, Cunha RA, Rial D, Köfalvi A. Adenosine A2B receptor activation stimulates glucose uptake in the mouse forebrain. Purinergic Signal. 2015 Dec;11(4):561-9.

Li Q, Han X, Lan X, Hong X, Li Q, Gao Y, Luo T, Yang Q, Koehler RC, Zhai Y, Zhou J, Wang J. Inhibition of tPA-induced hemorrhagic transformation involves adenosine A2b receptor activation after cerebral ischemia. Neurobiol Dis. 2017 Dec;108:173-182.

Li XG, Somogyi P, Ylinen A, Buzsáki G. The hippocampal CA3 network: an in vivo intracellular labeling study. J Comp Neurol. 1994 Jan 8;339(2):181-208.

Li XX, Nomura T, Aihara H, Nishizaki T. Adenosine enhances glial glutamate efflux via A2a adenosine receptors. Life Sci. 2001 Feb 9;68(12):1343-50.

Liauw J, Hoang S, Choi M, Eroglu C, Choi M, Sun GH, Percy M, Wildman-Tobriner B, Bliss T, Guzman RG, Barres BA, Steinberg GK. Thrombospondins 1 and 2 are necessary for synaptic plasticity and functional recovery after stroke. J Cereb Blood Flow Metab. 2008 Oct;28(10):1722-32.

Liesz A, Suri-Payer E, Veltkamp C, Doerr H, Sommer C, Rivest S, Giese T, Veltkamp R. Regulatory T cells are key cerebroprotective immunomodulators in acute experimental stroke. Nat Med. 2009 Feb;15(2):192-9.

Lim GP, Yang F, Chu T, Chen P, Beech W, Teter B, Tran T, Ubeda O, Ashe KH, Frautschy SA, Cole GM. Ibuprofen suppresses plaque pathology and inflammation in a mouse model for Alzheimer's disease. J Neurosci. 2000 Aug 1;20(15):5709-14.

Limatola C, Lauro C, Catalano M, Ciotti MT, Bertollini C, Di Angelantonio S, Ragozzino D, Eusebi F. Chemokine CX3CL1 protects rat hippocampal neurons against glutamate-mediated excitotoxicity. J Neuroimmunol. 2005 Sep;166(1-2):19-28.

Linden J, Thai T, Figler H, Jin X, Robeva AS. Characterization of human A(2B) adenosine receptors: radioligand binding, western blotting, and coupling to G(q) in human embryonic kidney 293 cells and HMC-1 mast cells. Mol Pharmacol. 1999 Oct;56(4):705-13.

Lindsberg PJ, Carpén O, Paetau A, Karjalainen-Lindsberg ML, Kaste M. Endothelial ICAM-1 expression associated with inflammatory cell response in human ischemic stroke. Circulation. 1996 Sep 1;94(5):939-45.

Ling P, Yao Z, Meyer CF, Wang XS, Oehrl W, Feller SM, Tan TH. Interaction of hematopoietic progenitor kinase 1 with adapter proteins Crk and CrkL leads to synergistic activation of c-Jun N-terminal kinase. Mol Cell Biol. 1999 Feb;19(2):1359-68.

Littlefield AM, Setti SE, Priester C, Kohman RA. Voluntary exercise attenuates LPS-induced reductions in neurogenesis and increases microglia expression of a proneurogenic phenotype in aged mice. J Neuroinflammation. 2015 Jul 30;12:138.

Liu HX, Zhang JJ, Zheng P, Zhang Y. Altered expression of MAP-2, GAP-43, and synaptophysin in the hippocampus of rats with chronic cerebral hypoperfusion correlates with cognitive impairment. Brain Res Mol Brain Res. 2005 Sep 13;139(1):169-77.

Liu Y, Wu XM, Luo QQ, Huang S, Yang QW, Wang FX, Ke Y, Qian ZM. CX3CL1/CX3CR1-mediated microglia activation plays a detrimental role in ischemic mice brain via p38MAPK/PKC pathway. J Cereb Blood Flow Metab. 2015 Oct;35(10):1623-31.

Livingston M, Heaney LG, Ennis M. Adenosine, inflammation and asthma a review. Inflamm Res. 2004 May;53(5):171-8.

Loane DJ, Kumar A. Microglia in the TBI brain: The good, the bad, and the dysregulated. Exp Neurol. 2016 Jan;275 Pt 3:316-327. doi: 10.1016/j.expneurol.2015.08.018.

Lobsiger CS, Cleveland DW. Glial cells as intrinsic components of non-cell-autonomous neurodegenerative disease. Nat Neurosci. 2007 Nov;10(11):1355-60.

Logan M, Sweeney MI. Adenosine A1 receptor activation preferentially protects cultured cerebellar neurons versus astrocytes against hypoxia-induced death. Mol Chem Neuropathol. 1997 Jun;31(2):119-33.

Lopez AD, Mathers CD, Ezzati M, Jamison DT, Murray CJ. Global and regional burden of disease and risk factors, 2001: systematic analysis of population health data. Lancet. 2006 May 27;367(9524):1747-57.

Lopes LV, Halldner L, Rebola N, Johansson B, Ledent C, Chen JF, Fredholm BB, Cunha RA. Binding of the prototypical adenosine A(2A) receptor agonist CGS 21680 to the cerebral cortex of adenosine A(1) and A(2A) receptor knockout mice. Br J Pharmacol. 2004

Mar;141(6):1006-14.

Lorente de Nó R. Studies on the structure of the cerebral cortex. II. Continuation of the study of the ammonic system. J Psychol Neurol. 1934; 46:113-77.

Love S. Apoptosis and brain ischaemia. Prog Neuropsychopharmacol Biol Psychiatry. 2003 Apr;27(2):267-82.

Luccarini I, Grossi C, Traini C, Fiorentini A, Ed Dami T, Casamenti F. Aβ plaque-associated glial reaction as a determinant of apoptotic neuronal death and cortical gliogenesis: a study in APP mutant mice. Neurosci Lett. 2012 Jan 6;506(1):94-9.

Lue LF, Walker DG, Rogers J. Modeling microglial activation in Alzheimer's disease with human postmortem microglial cultures. Neurobiol Aging. 2001 Nov-Dec;22(6):945-56.

Luo C, Ikegaya Y, Koyama R. Microglia and neurogenesis in the epileptic dentate gyrus. Neurogenesis (Austin). 2016 Sep 26;3(1):e1235525.

Lupica CR, Bell JA, Hoffman AF, Watson PL. Contribution of the hyperpolarization-activated current (I(h)) to membrane potential and GABA release in hippocampal interneurons. J Neurophysiol. 2001 Jul;86(1):261-8.

Lyons A, Downer EJ, Crotty S, Nolan YM, Mills KH, Lynch MA. CD200 ligand receptor interaction modulates microglial activation in vivo and in vitro: a role for IL-4. J Neurosci. 2007 Aug 1;27(31):8309-13.

Lyons A, Lynch AM, Downer EJ, Hanley R, O'Sullivan JB, Smith A, Lynch MA. Fractalkine-induced activation of the phosphatidylinositol-3 kinase pathway attentuates microglial activation in vivo and in vitro. J Neurochem. 2009 Sep;110(5):1547-56.

Lynge J, Schulte G, Nordsborg N, Fredholm BB, Hellsten Y. Adenosine A 2B receptors modulate cAMP levels and induce CREB but not ERK1/2 and p38 phosphorylation in rat skeletal muscle cells. Biochem Biophys Res Commun. 2003 Jul 18;307(1):180-7.

Ma J, Yee A, Brewer HB Jr, Das S, Potter H. Amyloid-associated proteins alpha 1-antichymotrypsin and apolipoprotein E promote assembly of Alzheimer beta-protein into filaments. Nature. 1994 Nov 3;372(6501):92-4.

Magistretti PJ, Hof PR, Martin JL. Adenosine stimulates glycogenolysis in mouse cerebral cortex: a possible coupling mechanism between neuronal activity and energy metabolism. J Neurosci. 1986 Sep;6(9):2558-62.

Magnus T, Chan A, Grauer O, Toyka KV, Gold R. Microglial phagocytosis of apoptotic inflammatory T cells leads to down-regulation of microglial immune activation. J Immunol. 2001 Nov 1;167(9):5004-10.

Mahar I, Albuquerque MS, Mondragon-Rodriguez S, Cavanagh C, Davoli MA, Chabot JG, Williams S, Mechawar N, Quirion R, Krantic S. Phenotypic Alterations in Hippocampal NPY- and PV-Expressing Interneurons in a Presymptomatic Transgenic Mouse Model of Alzheimer's Disease. Front Aging Neurosci. 2017 Jan 19;8:327.

Mandrekar-Colucci S, Landreth GE. Microglia and inflammation in Alzheimer's disease. CNS Neurol Disord Drug Targets. 2010 Apr;9(2):156-67.

Maragakis NJ, Rothstein JD. Glutamate transporters: animal models to neurologic disease. Neurobiol Dis. 2004 Apr;15(3):461-73.

Maraula G, Traini C, Mello T, Coppi E, Galli A, Pedata F, Pugliese AM. Effects of oxygen and glucose deprivation on synaptic transmission in rat dentate gyrus: role of A2A adenosine receptors. Neuropharmacology. 2013 Apr;67:511-20.

Marr D. Simple memory: a theory for archicortex. Philos Trans R Soc Lond B Biol Sci. 1971 Jul 1;262(841):23-81.

Martin, JH. Lymbic system and cerebral circuits for emotions, learning and memory. In: Martin, JH editor. Neuroanatomy: text and atlas. New York: McGraw-Hill; 2003. p.382.

Martínez-Fábregas J, Díaz-Moreno I, González-Arzola K, Janocha S, Navarro JA, Hervás M, Bernhardt R, Velázquez-Campoy A, Díaz-Quintana A, De la Rosa MA. Structural and functional analysis of novel human cytochrome C targets in apoptosis. Mol Cell Proteomics. 2014 Jun;13(6):1439-56.

Masgrau R, Guaza C, Ransohoff RM, Galea E. Should We Stop Saying 'Glia' and 'Neuroinflammation'? Trends Mol Med. 2017 Jun;23(6):486-500.

Masurkar AV. Towards a circuit-level understanding of hippocampal CA1 dysfunction in Alzheimer's disease across anatomical axes. J Alzheimers Dis Parkinsonism. 2018;8(1). pii: 412.

Matsumoto K, Graf R, Rosner G, Shimada N, Heiss WD. Flow thresholds for extracellular purine catabolite elevation in cat focal ischemia. Brain Res. 1992 May 8;579(2):309-14.

Matsumoto H, Kumon Y, Watanabe H, Ohnishi T, Takahashi H, Imai Y, Tanaka J. Expression of CD200 by macrophage-like cells in ischemic core of rat brain after transient middle cerebral artery occlusion. Neurosci Lett. 2007 May 11;418(1):44-8.

Matthias K, Kirchhoff F, Seifert G, Hüttmann K, Matyash M, Kettenmann H, Steinhäuser C. Segregated expression of AMPA-type glutamate receptors and glutamate transporters defines distinct astrocyte populations in the mouse hippocampus. J Neurosci. 2003 Mar 1;23(5):1750-8.

Mauch DH, Nägler K, Schumacher S, Göritz C, Müller EC, Otto A, Pfrieger FW. CNS synaptogenesis promoted by glia-derived cholesterol. Science. 2001 Nov 9;294(5545):1354-7.

McGeer PL, McGeer EG. Glial cell reactions in neurodegenerative diseases: pathophysiology and therapeutic interventions. Alzheimer Dis Assoc Disord. 1998;12 Suppl 2:S1-6.

McGeer PL, McGeer EG. The inflammatory response system of brain: implications for therapy of Alzheimer and other neurodegenerative diseases. Brain Res Brain Res Rev. 1995 Sep;21(2):195-218.

McGeer PL, Schulzer M, McGeer EG. Arthritis and anti-inflammatory agents as possible protective factors for Alzheimer's disease: a review of 17 epidemiologic studies. Neurology. 1996 Aug;47(2):425-32.

McGowan E, Eriksen J, Hutton M. A decade of modeling Alzheimer's disease in transgenic mice. Trends Genet. 2006 May;22(5):281-9.

Medina-Pulido L, Molina-Arcas M, Justicia C, Soriano E, Burgaya F, Planas AM, Pastor-Anglada M. Hypoxia and P1 receptor activation regulate the high-affinity concentrative adenosine transporter CNT2 in differentiated neuronal PC12 cells. Biochem J. 2013 Sep 15;454(3):437-45.

Melani A, Cipriani S, Vannucchi MG, Nosi D, Donati C, Bruni P, Giovannini MG, Pedata F. Selective adenosine A2a receptor antagonism reduces JNK activation in oligodendrocytes after cerebral ischaemia. Brain. 2009 Jun;132(Pt 6):1480-95.

Melani A, Corti F, Cellai L, Vannucchi MG, Pedata F. Low doses of the selective adenosine A2A receptor agonist CGS21680 are protective in a rat model of transient cerebral ischemia. Brain Res. 2014 Mar 10;1551:59-72.

Melani A, Corti F, Stephan H, Müller CE, Donati C, Bruni P, Vannucchi MG, Pedata F. Ecto-ATPase inhibition: ATP and adenosine release under physiological and ischemic in vivo conditions in the rat striatum. Exp Neurol. 2012 Jan;233(1):193-204.

Melani A, Gianfriddo M, Vannucchi MG, Cipriani S, Baraldi PG, Giovannini MG, Pedata F. The selective A2A receptor antagonist SCH 58261 protects from neurological deficit, brain damage and activation of p38 MAPK in rat focal cerebral ischemia.

Melani A, Pantoni L, Bordoni F, Gianfriddo M, Bianchi L, Vannucchi MG, Bertorelli R, Monopoli A, Pedata F. The selective A2A receptor antagonist SCH 58261 reduces striatal transmitter outflow, turning behavior and ischemic brain damage induced by permanent focal ischemia in the rat. Brain Res. 2003 Jan 10;959(2):243-50.

Melani A, Pantoni L, Corsi C, Bianchi L, Monopoli A, Bertorelli R, Pepeu G, Pedata F. Striatal outflow of adenosine, excitatory amino acids, gamma-aminobutyric acid, and taurine in awake freely moving rats after middle cerebral artery occlusion: correlations with neurological deficit and histopathological damage. Stroke. 1999 Nov;30(11):2448-54; discussion 2455.

Mercatelli R, Lana D, Bucciantini M, Giovannini MG, Cerbai F, Quercioli F, Zecchi-Orlandini S, Delfino G, Wenk GL, Nosi D. Clasmatodendrosis and β-amyloidosis in aging hippocampus. FASEB J. 2016 Apr;30(4):1480-91.

Merighi S, Borea PA, Gessi S. Adenosine receptors and diabetes: Focus on the A(2B) adenosine receptor subtype. Pharmacol Res. 2015 Sep;99:229-36.

Merrill JE. Effects of interleukin-1 and tumor necrosis factor-alpha on astrocytes, microglia, oligodendrocytes, and glial precursors in vitro. Dev Neurosci. 1991;13(3):130-7.

Michaud JP, Rivest S. Anti-inflammatory signaling in microglia exacerbates Alzheimer's disease-related pathology. Neuron. 2015 Feb 4;85(3):450-2.

Miller AP, Shah AS, Aperi BV, Kurpad SN, Stemper BD, Glavaski-Joksimovic A. Acute death of astrocytes in blast-exposed rat organotypic hippocampal slice cultures. PLoS One. 2017 Mar 6;12(3):e0173167.

Milligan ED, Watkins LR. Pathological and protective roles of glia in chronic pain. Nat Rev Neurosci. 2009 Jan;10(1):23-36.

Milton SL, Nayak G, Kesaraju S, Kara L, Prentice HM. Suppression of reactive oxygen species production enhances neuronal survival in vitro and in vivo in the anoxia-tolerant turtle Trachemys scripta. J Neurochem. 2007 May;101(4):993-1001.

Minghetti L, Levi G. Microglia as effector cells in brain damage and repair: focus on prostanoids and nitric oxide. Prog Neurobiol. 1998 Jan;54(1):99-125.

Mirabet M, Mallol J, Lluis C, Franco R. Calcium mobilization in Jurkat cells via A2b adenosine receptors. Br J Pharmacol. 1997 Nov;122(6):1075-82.

Mishiro K, Ishiguro M, Suzuki Y, Tsuruma K, Shimazawa M, Hara H. A broad-spectrum matrix metalloproteinase inhibitor prevents hemorrhagic complications induced by tissue plasminogen activator in mice. Neuroscience. 2012 Mar 15;205:39-48.

Mitani A, Andou Y, Kataoka K. Selective vulnerability of hippocampal CA1 neurons cannot be explained in terms of an increase in glutamate concentration during ischemia in the gerbil: brain microdialysis study. Neuroscience. 1992;48(2):307-13.

Mohmmad Abdul H, Wenk GL, Gramling M, Hauss-Wegrzyniak B, Butterfield DA. APP and PS-1 mutations induce brain oxidative stress independent of dietary cholesterol: implications for Alzheimer's disease. Neurosci Lett. 2004 Sep 23;368(2):148-50.

Molgaard S, Ulrichsen M, Boggild S, Holm ML, Vaegter C, Nyengaard J, Glerup S. Immunofluorescent visualization of mouse interneuron subtypes. Version 2. F1000Res. 2014 Oct 13 [revised 2014 Jan 1];3:242.

Montero M, González B, Zimmer J. Immunotoxic depletion of microglia in mouse hippocampal slice cultures enhances ischemia-like neurodegeneration. Brain Res. 2009 Sep 29;1291:140-52.

Moran A, Forouzanfar M, Sampson U, Chugh S, Feigin V, Mensah G. The epidemiology of cardiovascular diseases in sub-Saharan Africa: the Global Burden of Diseases, Injuries and Risk Factors 2010 Study. Prog Cardiovasc Dis. 2013 Nov-Dec;56(3):234-9. doi: 10.1016/j.pcad.2013.09.019.

Mori M, Nishizaki T, Okada Y. Protective effect of adenosine on the anoxic damage of hippocampal slice. Neuroscience. 1992;46(2):301-7.

Moriyama K, Sitkovsky MV. Adenosine A2A receptor is involved in cell surface expression of A2B receptor. J Biol Chem. 2010 Dec 10;285(50):39271-88.

Morsch M, Radford R, Lee A, Don EK, Badrock AP, Hall TE, Cole NJ, Chung R. In vivo characterization of microglial engulfment of dying neurons in the zebrafish spinal cord. Front Cell Neurosci. 2015 Aug 31;9:321. doi: 10.3389/fncel.2015.00321.

Mrak RE, Griffinbc WS. The role of activated astrocytes and of the neurotrophic cytokine S100B in the pathogenesis of Alzheimer's disease. Neurobiol Aging. 2001 Nov-Dec;22(6):915-22.

Mueller SG, Schuff N, Yaffe K, Madison C, Miller B, Weiner MW. Hippocampal atrophy patterns in mild cognitive impairment and Alzheimer's disease. Hum Brain Mapp. 2010 Sep;31(9):1339-47.

Mulakayala N, Rao P, Iqbal J, Bandichhor R, Oruganti S. Synthesis of novel therapeutic agents for the treatment of multiple sclerosis: a brief overview. Eur J Med Chem. 2013 Feb;60:170-86.

Mullan M, Houlden H, Windelspecht M, Fidani L, Lombardi C, Diaz P, Rossor M, Crook R, Hardy J, Duff K, et al. A locus for familial early-onset Alzheimer's disease on the long arm of chromosome 14, proximal to the alpha 1-antichymotrypsin gene. Nat Genet. 1992 Dec;2(4):340-2.

Müller CE, Jacobson KA. Recent developments in adenosine receptor ligands and their potential as novel drugs. Biochim Biophys Acta. 2011 May;1808(5):1290-308.

Murakami S, Terakura M, Kamatani T, Hashikawa T, Saho T, Shimabukuro Y, Okada H. Adenosine regulates the production of interleukin-6 by human gingival fibroblasts via cyclic AMP/protein kinase A pathway. J Periodontal Res. 2000 Apr;35(2):93-101.

Nagai M, Re DB, Nagata T, Chalazonitis A, Jessell TM, Wichterle H, Przedborski S. Astrocytes expressing ALS-linked mutated SOD1 release factors selectively toxic to motor neurons. Nat Neurosci. 2007 May;10(5):615-22. Epub 2007 Apr 15.

Nakano Y, Kondoh G, Kudo T, Imaizumi K, Kato M, Miyazaki JI, Tohyama M, Takeda J, Takeda M. Accumulation of murine amyloidbeta42 in a gene-dosage-dependent manner in PS1 'knock-in' mice. Eur J Neurosci. 1999 Jul;11(7):2577-81.

Nakka VP, Gusain A, Mehta SL, Raghubir R. Molecular mechanisms of apoptosis in cerebral ischemia: multiple neuroprotective opportunities. Mol Neurobiol. 2008Feb;37(1):7-38.

Nathan C, Calingasan N, Nezezon J, Ding A, Lucia MS, La Perle K, Fuortes M, Lin M, Ehrt S, Kwon NS, Chen J, Vodovotz Y, Kipiani K, Beal MF. Protection from Alzheimer's-like disease in the mouse by genetic ablation of inducible nitric oxide synthase. J Exp Med. 2005 Nov 7;202(9):1163-9.

Nathan C, Ding A. SnapShot: Reactive Oxygen Intermediates (ROI). Cell. 2010 Mar 19;140(6):951-951.e2.

Nedergaard M. Direct signaling from astrocytes to neurons in cultures of mammalian brain cells. Science. 1994 Mar 25;263(5154):1768-71.

Nedergaard M, Cooper AJ, Goldman SA. Gap junctions are required for the propagation of spreading depression. J Neurobiol. 1995 Dec;28(4):433-44.

Nedergaard M, Ransom B, Goldman SA. New roles for astrocytes: redefining the functional architecture of the brain. Trends Neurosci. 2003 Oct;26(10):523-30.

Neher JJ, Neniskyte U, Brown GC. Primary phagocytosis of neurons by inflamed microglia: potential roles in neurodegeneration. Front Pharmacol. 2012 Feb 28;3:27.

Newell DW, Barth A, Papermaster V, Malouf AT. Glutamate and non-glutamate receptor mediated toxicity caused by oxygen and glucose deprivation in organotypic hippocampal cultures. J Neurosci. 1995 Nov;15(11):7702-11.

Newman GC, Hospod FE, Trowbridge SD, Motwani S, Liu Y. Restoring adenine nucleotides in a brain slice model of cerebral reperfusion. J Cereb Blood Flow Metab. 1998 Jun;18(6):675-85.

Ngai AC, Coyne EF, Meno JR, West GA, Winn HR. Receptor subtypes mediating adenosine-induced dilation of cerebral arterioles. Am J Physiol Heart Circ Physiol. 2001 May;280(5):H2329-35.

Nishizaki T, Nagai K, Nomura T, Tada H, Kanno T, Tozaki H, Li XX, Kondoh T, Kodama N, Takahashi E, Sakai N, Tanaka K, Saito N. A new neuromodulatory pathway with a glial contribution mediated via A(2a) adenosine receptors. Glia. 2002 Aug;39(2):133-47.

Obrenovitch TP. The ischaemic penumbra: twenty years on. Cerebrovasc Brain Metab Rev. 1995 Winter;7(4):297-323.

O'Donnell MJ, Xavier D, Liu L, Zhang H, Chin SL, Rao-Melacini P, Rangarajan S, Islam S, Pais P, McQueen MJ, Mondo C, Damasceno A, Lopez-Jaramillo P, Hankey GJ, Dans AL, Yusoff K, Truelsen T, Diener HC, Sacco RL, Ryglewicz D, Czlonkowska A, Weimar C,

Wang X, Yusuf S; INTERSTROKE investigators. Risk factors for ischaemic and intracerebral haemorrhagic stroke in 22 countries (the INTERSTROKE study): a case-control study. Lancet. 2010 Jul 10;376(9735):112-23.

Ohsawa K, Irino Y, Sanagi T, Nakamura Y, Suzuki E, Inoue K, Kohsaka S. P2Y12 receptor-mediated integrin-beta1 activation regulates microglial process extension induced by ATP. Glia. 2010 May;58(7):790-801.

O'Kane EM, Stone TW. Interaction between adenosine A1 and A2 receptor-mediated responses in the rat hippocampus in vitro. Eur J Pharmacol. 1998 Nov 27;362(1):17-25.

Olabarria M, Noristani HN, Verkhratsky A, Rodríguez JJ. Concomitant astroglial atrophy and astrogliosis in a triple transgenic animal model of Alzheimer's disease. Glia. 2010 May;58(7):831-8.

Ongini E, Adami M, Ferri C, Bertorelli R. Adenosine A2A receptors and neuroprotection. Ann N Y Acad Sci. 1997 Oct 15;825:30-48.

Ortore G, Martinelli A. A2B receptor ligands: past, present and future trends. Curr Top Med Chem. 2010;10(9):923-40.

Otori T, Katsumata T, Muramatsu H, Kashiwagi F, Katayama Y, Terashi A. Long-term measurement of cerebral blood flow and metabolism in a rat chronic hypoperfusion model. Clin Exp Pharmacol Physiol. 2003 Apr;30(4):266-72.

Ozacmak VH, Sayan H, Cetin A, Akyildiz-Igdem A. AT1 receptor blocker candesartan-induced attenuation of brain injury of rats subjected to chronic cerebral hypoperfusion. Neurochem Res. 2007 Aug;32(8):1314-21.

Panjehpour M, Castro M, Klotz KN. Human breast cancer cell line MDA-MB-231 expresses endogenous A2B adenosine receptors mediating a Ca2+ signal. Br J Pharmacol. 2005 May;145(2):211-8.

Pappas BA, de la Torre JC, Davidson CM, Keyes MT, Fortin T. Chronic reduction of cerebral blood flow in the adult rat: late-emerging CA1 cell loss and memory dysfunction. Brain Res. 1996 Feb 5;708(1-2):50-8.

Park KJ, Lee SH, Kim TI, Lee HW, Lee CH, Kim EH, Jang JY, Choi KS, Kwon MH, Kim YS. A human scFv antibody against TRAIL receptor 2 induces autophagic cell death in both TRAIL-sensitive and TRAIL-resistant cancer cells. Cancer Res. 2007 Aug 1;67(15):7327-34.

Pasinetti GM, Aisen PS. Cyclooxygenase-2 expression is increased in frontal cortex of Alzheimer's disease brain. Neuroscience. 1998 Nov;87(2):319-24.

Patterson D, Gardiner K, Kao FT, Tanzi R, Watkins P, Gusella JF. Mapping of the gene encoding the beta amyloid precursor protein and its relationship to the Down syndrome region of chromosome 21. Proc Natl Acad Sci U S A. 1988 Nov;85(21):8266-70.

Pattillo CB, Bir SC, Branch BG, Greber E, Shen X, Pardue S, Patel RP, Kevil CG. Dipyridamole reverses peripheral ischemia and induces angiogenesis in theDb/Db diabetic mouse hind-limb model by decreasing oxidative stress. Free Radic Biol Med. 2011 Jan 15;50(2):262-9.

Pająk B, Kania E, Orzechowski A. Killing Me Softly: Connotations to Unfolded Protein Response and Oxidative Stress in Alzheimer's Disease. Oxid Med Cell Longev. 2016; 2016:1805304. doi: 10.1155/2016/1805304.

Payen JF, Fauvage B, Falcon D, Lavagne P. [Brain oedema following blood-brain barrier disruption: mechanisms and diagnosis]. Ann Fr Anesth Reanim. 2003 Mar;22(3):220-5.

Pearson T, Damian K, Lynas RE, Frenguelli BG. Sustained elevation of extracellular adenosine and activation of A1 receptors underlie the post-ischaemic inhibition of neuronal function in rat hippocampus in vitro. J Neurochem. 2006 Jun;97(5):1357-68.

Pedata F, Dettori I, Coppi E, Melani A, Fusco I, Corradetti R, Pugliese AM. Purinergic signalling in brain ischemia. Neuropharmacology. 2016 May;104:105-30.

Pedata F, Gianfriddo M, Turchi D, Melani A. The protective effect of adenosine A2A receptor antagonism in cerebral ischemia. Neurol Res. 2005 Mar;27(2):169-74.

Pedata F, Latini S, Pugliese AM, Pepeu G. Investigations into the adenosine outflow from hippocampal slices evoked by ischemia-like conditions. J Neurochem. 1993 Jul;61(1):284-9.

Pedata F, Melani A, Pugliese AM, Coppi E, Cipriani S, Traini C. The role of ATP and adenosine in the brain under normoxic and ischemic conditions. Purinergic Signal. 2007 Sep;3(4):299-310. doi: 10.1007/s11302-007-9085-8.

Pedata F, Pepeu G, Spignoli G. Biphasic effect of methylxanthines on acetylcholine release from electrically-stimulated brain slices. Br J Pharmacol. 1984 Sep;83(1):69-73.

Pedata F, Pugliese AM, Coppi E, Dettori I, Maraula G, Cellai L, Melani A. Adenosine A2A receptors modulate acute injury and neuroinflammation in brain ischemia. Mediators Inflamm. 2014; 2014:805198.

Pekny M, Wilhelmsson U, Pekna M. The dual role of astrocyte activation and reactive gliosis. Neurosci Lett. 2014 Apr 17;565:30-8.

Penfield W. Neuroglia and microglia - the interstitial tissue of the central nervous system. In: Special cytology: the form and functions of the cell in health and disease, 1928, Cowdry EV, Eds, Hoeber, New York, NY, USA, pp. 1033-68.

Perez-Buira S, Barrachina M, Rodriguez A, Albasanz JL, Martín M, Ferrer I. Expression levels of adenosine receptors in hippocampus and frontal cortex in argyrophilic grain disease. Neurosci Lett. 2007 Aug 23;423(3):194-9.

Petito CK, Kraig RP, Pulsinelli WA. Light and electron microscopic evaluation of hydrogen ion-induced brain necrosis. J Cereb Blood Flow Metab. 1987 Oct;7(5):625-32.

Pfrieger FW. Roles of glial cells in synapse development. Cell Mol Life Sci. 2009 Jul;66(13):2037-47.

Phillis JW. The effects of selective A1 and A2a adenosine receptor antagonists on cerebral ischemic injury in the gerbil. Brain Res. 1995 Dec 24;705(1-2):79-84.

Phillis JW, Goshgarian HG. Adenosine and neurotrauma: therapeutic perspectives. Neurol Res. 2001 Mar-Apr;23(2-3):183-9.

Phillis JW, Smith-Barbour M, O'Regan MH. Changes in extracellular amino acid neurotransmitters and purines during and following ischemias of different durations in the rat cerebral cortex. Neurochem Int. 1996 Aug;29(2):115-20.

Phillis JW, Smith-Barbour M, O'Regan MH, Perkins LM. Amino acid and purine release in rat brain following temporary middle cerebral artery occlusion. Neurochem Res. 1994 Sep;19(9):1125-30.

Picano E. Dipyridamole-echocardiography test: historical background and physiologic basis. Eur Heart J. 1989 Apr;10(4):365-76.

Pierce KD, Furlong TJ, Selbie LA, Shine J. Molecular cloning and expression of an adenosine A2b receptor from human brain. Biochem Biophys Res Commun. 1992 Aug 31;187(1):86-93.

Plescher M, Seifert G, Hansen JN, Bedner P, Steinhäuser C, Halle A. Plaque-dependent morphological and electrophysiological heterogeneity of microglia in an Alzheimer's disease mouse model. Glia. 2018 Jul;66(7):1464-1480.

Polazzi E, Contestabile A. Reciprocal interactions between microglia and neurons: from survival to neuropathology. Rev Neurosci. 2002;13(3):221-42.

Polazzi E, Gianni T, Contestabile A. Microglial cells protect cerebellar granule neurons from apoptosis: evidence for reciprocal signaling. Glia. 2001 Dec;36(3):271-80.

Polazzi E, Monti B. Microglia and neuroprotection: from in vitro studies to therapeutic applications. Prog Neurobiol. 2010 Nov;92(3):293-315.

Pont-Lezica L, Béchade C, Belarif-Cantaut Y, Pascual O, Bessis A. Physiological roles of microglia during development. J Neurochem. 2011 Dec;119(5):901-8. doi: 10.1111/j.1471-4159.2011.07504.x.

Potter H, Ma J, Das S, Kayyali U. The involvement of amyloid associated proteins in the formation of beta protein filaments in Alzheimer's disease. Prog Clin Biol Res. 1994;390:57-71.

Price JL, Ko AI, Wade MJ, Tsou SK, McKeel DW, Morris JC. Neuron number in the entorhinal cortex and CA1 in preclinical Alzheimer disease. Arch Neurol. 2001 Sep;58(9):1395-402.

Protti GG, Gagliardi RJ, Forte WC, Sprovieri SR. Interleukin-10 may protect against progressing injury during the acute phase of ischemic stroke. Arq Neuropsiquiatr. 2013 Nov;71(11):846-51.

Puffinbarger NK, Hansen KR, Resta R, Laurent AB, Knudsen TB, Madara JL, Thompson LF. Production and characterization of multiple antigenic peptide antibodies to the adenosine A2b receptor. Mol Pharmacol. 1995 Jun;47(6):1126-32.

Pugliese AM, Coppi E, Spalluto G, Corradetti R, Pedata F. A3 adenosine receptor antagonists delay irreversible synaptic failure caused by oxygen and glucose deprivation in the rat CA1 hippocampus in vitro. Br J Pharmacol. 2006 Mar;147(5):524-32.

Pugliese AM, Coppi E, Volpini R, Cristalli G, Corradetti R, Jeong LS, Jacobson KA, Pedata F. Role of adenosine A3 receptors on CA1 hippocampal neurotransmission during oxygen-glucose deprivation episodes of different duration. Biochem Pharmacol. 2007 Sep 1;74(5):768-79.

Pugliese AM, Traini C, Cipriani S, Gianfriddo M, Mello T, Giovannini MG, Galli A, Pedata F. The adenosine A2A receptor antagonist ZM241385 enhances neuronal survival after oxygen-glucose deprivation in rat CA1 hippocampal slices. Br J Pharmacol. 2009 Jul;157(5):818-30.

Pyapali GK, Sik A, Penttonen M, Buzsaki G, Turner DA. Dendritic properties of hippocampal CA1 pyramidal neurons in the rat: intracellular staining in vivo and in vitro. J Comp Neurol. 1998 Feb 16;391(3):335-52.

Ramírez G, Rey S, von Bernhardi R. Proinflammatory stimuli are needed for induction of microglial cell-mediated AbetaPP_{244-C} and Abeta-neurotoxicity in hippocampal cultures. J Alzheimers Dis. 2008 Sep;15(1):45-59.

Ramón y Cajal S. Estructura del asta de Ammon y fascia dentata. Ann Soc Esp Hist Nat. 1893. 22.

Ransohoff RM. How neuroinflammation contributes to neurodegeneration. Science. 2016 Aug 19;353(6301):777-83.

Ransohoff RM, Perry VH. Microglial physiology: unique stimuli, specialized responses. Annu Rev Immunol. 2009;27:119-45.

Ransom B, Behar T, Nedergaard M. New roles for astrocytes (stars at last). Trends Neurosci. 2003 Oct;26(10):520-2.

Rapp PR, Gallagher M. Preserved neuron number in the hippocampus of aged rats with spatial learning deficits. Proc Natl Acad Sci U S A. 1996 Sep3;93(18):9926-30.

Re DB, Le Verche V, Yu C, Amoroso MW, Politi KA, Phani S, Ikiz B, Hoffmann L, Koolen M, Nagata T, Papadimitriou D, Nagy P, Mitsumoto H, Kariya S, Wichterle H, Henderson CE, Przedborski S. Necroptosis drives motor neuron death in models of both sporadic and familial ALS. Neuron. 2014 Mar 5;81(5):1001-1008.

Rebeck GW, Perls TT, West HL, Sodhi P, Lipsitz LA, Hyman BT. Reduced apolipoprotein epsilon 4 allele frequency in the oldest old Alzheimer's patients and cognitively normal individuals. Neurology. 1994 Aug;44(8):1513-6. Erratum in: Neurology. 1995 Mar;45(3 Pt 1):598

Rebola N, Canas PM, Oliveira CR, Cunha RA. Different synaptic and subsynaptic localization of adenosine A2A receptors in the hippocampus and striatum of the rat. Neuroscience. 2005;132(4):893-903.

Rebola N, Oliveira CR, Cunha RA. Transducing system operated by adenosine A(2A) receptors to facilitate acetylcholine release in the rat hippocampus. Eur J Pharmacol. 2002 Nov 1;454(1):31-8.

Rebola N, Pinheiro PC, Oliveira CR, Malva JO, Cunha RA. Subcellular localization of adenosine A(1) receptors in nerve terminals and synapses of the rat hippocampus. Brain Res. 2003 Oct 10;987(1):49-58.

Reemst K, Noctor SC, Lucassen PJ, Hol EM. The Indispensable Roles of Microglia and Astrocytes during Brain Development. Front Hum Neurosci. 2016 Nov 8;10:566.

Reilly JF, Games D, Rydel RE, Freedman S, Schenk D, Young WG, Morrison JH, Bloom FE. Amyloid deposition in the hippocampus and entorhinal cortex: quantitative analysis of a transgenic mouse model. Proc Natl Acad Sci U S A. 2003 Apr 15;100(8):4837-42.

Ribak CE, Seress L. Five types of basket cell in the hippocampal dentategyrus: a combined Golgi and electron microscopic study. J Neurocytol. 1983Aug;12(4):577-97.

Ribak CE, Vaughn JE, Saito K. Immunocytochemical localization of glutamic acid decarboxylase in neuronal somata following colchicine inhibition of axonal transport. Brain

Res. 1978 Jan 27;140(2):315-32.

Ribeiro JA, Sebastião AM, de Mendonça A. Adenosine receptors in the nervous system: pathophysiological implications. Prog Neurobiol. 2002 Dec;68(6):377-92.

Riksen NP, Oyen WJ, Ramakers BP, Van den Broek PH, Engbersen R, Boerman OC, Smits P, Rongen GA. Oral therapy with dipyridamole limits ischemia-reperfusion injury in humans. Clin Pharmacol Ther. 2005 Jul;78(1):52-9.

Risold PY, Swanson LW. Chemoarchitecture of the rat lateral septal nucleus. Brain Res Brain Res Rev. 1997 Sep 19;24(2-3):91-113.

Rivkees SA, Reppert SM. RFL9 encodes an A2b-adenosine receptor. Mol Endocrinol. 1992 Oct;6(10):1598-604.

Rock RB, Gekker G, Hu S, Sheng WS, Cheeran M, Lokensgard JR, Peterson PK. Role of microglia in central nervous system infections. Clin Microbiol Rev. 2004 Oct;17(4):942-64, table of contents.

Rodríguez-Arellano JJ, Parpura V, Zorec R, Verkhratsky A. Astrocytes in physiological aging and Alzheimer's disease. Neuroscience. 2016 May 26;323:170-82.

Rodríguez JJ, Terzieva S, Olabarria M, Lanza RG, Verkhratsky A. Enriched environment and physical activity reverse astrogliodegeneration in the hippocampus of AD transgenic mice. Cell Death Dis. 2013 Jun 20;4:e678.

Rogers J, Lue LF. Microglial chemotaxis, activation, and phagocytosis of amyloid beta-peptide as linked phenomena in Alzheimer's disease. Neurochem Int. 2001 Nov-Dec;39(5-6):333-40.

Rogers J, Strohmeyer R, Kovelowski CJ, Li R. Microglia and inflammatory mechanisms in the clearance of amyloid beta peptide. Glia. 2002 Nov;40(2):260-9.

Rolls ET, Kesner RP. A computational theory of hippocampal function, and empirical tests of the theory. Prog Neurobiol. 2006 May;79(1):1-48.

Rosenblueth A, García Ramos J. Some phenomena usually associated with spreading depression. Acta Physiol Lat Am. 1966;16(2):141-79.

Rosin DL, Robeva A, Woodard RL, Guyenet PG, Linden J. Immunohistochemical localization of adenosine A2A receptors in the rat central nervous system. J Comp Neurol. 1998 Nov 16;401(2):163-86.

Ross JM, Öberg J, Brené S, Coppotelli G, Terzioglu M, Pernold K, Goiny M, Sitnikov R, Kehr J, Trifunovic A, Larsson NG, Hoffer BJ, Olson L. High brain lactate is a hallmark of aging and caused by a shift in the lactate dehydrogenase A/B ratio. Proc Natl Acad Sci U S A. 2010 Nov 16;107(46):20087-92.

Rossi DJ, Oshima T, Attwell D. Glutamate release in severe brain ischaemia is mainly by reversed uptake. Nature. 2000 Jan 20;403(6767):316-21

Rössler M, Zarski R, Bohl J, Ohm TG. Stage-dependent and sector-specific neuronal loss in hippocampus during Alzheimer's disease. Acta Neuropathol. 2002 Apr;103(4):363-9.

Rudolphi KA, Keil M, Hinze HJ. Effect of theophylline on ischemically induced hippocampal damage in Mongolian gerbils: a behavioral and histopathological study. J Cereb Blood Flow Metab. 1987 Feb;7(1):74-81.

Rudolphi KA, Schubert P, Parkinson FE, Fredholm BB. Adenosine and brain ischemia. Cerebrovasc Brain Metab Rev. 1992 Winter;4(4):346-69.

Ruitenberg A, Kalmijn S, de Ridder MA, Redekop WK, van Harskamp F, Hofman A, Launer LJ, Breteler MM. Prognosis of Alzheimer's disease: the Rotterdam Study. Neuroepidemiology. 2001 Aug;20(3):188-95.

Rutecki PA. Neuronal excitability: voltage-dependent currents and synaptic transmission. J Clin Neurophysiol. 1992 Apr;9(2):195-211.

Sahlas DJ, Bilbao JM, Swartz RH, Black SE. Clasmatodendrosis correlating with periventricular hyperintensity in mixed dementia. Ann Neurol. 2002 Sep;52(3):378-81.

Saijo K, Glass CK. Microglial cell origin and phenotypes in health and disease. Nat Rev Immunol. 2011 Oct 25;11(11):775-87.

Salminen A, Kaarniranta K, Kauppinen A. Inflammaging: disturbed interplay between autophagy and inflammasomes. Aging (Albany NY). 2012 Mar;4(3):166-75.

Salvemini D, Misko TP, Masferrer JL, Seibert K, Currie MG, Needleman P. Nitric oxide activates cyclooxygenase enzymes. Proc Natl Acad Sci U S A. 1993 Aug 1;90(15):7240-4.

Salvioli S, Monti D, Lanzarini C, Conte M, Pirazzini C, Bacalini MG, Garagnani P, Giuliani C, Fontanesi E, Ostan R, Bucci L, Sevini F, Yani SL, Barbieri A, Lomartire L, Borelli V, Vianello D, Bellavista E, Martucci M, Cevenini E, Pini E, Scurti M, Biondi F, Santoro A, Capri M, Franceschi C. Immune system, cell senescence, aging and longevity--inflamm-aging reappraised. Curr Pharm Des.2013;19(9):1675-9.

Sampedro-Piquero P, De Bartolo P, Petrosini L, Zancada-Menendez C, Arias JL, Begega A. Astrocytic plasticity as a possible mediator of the cognitive improvements after environmental enrichment in aged rats. Neurobiol Learn Mem. 2014 Oct;114:16-25.

Sanai N, Tramontin AD, Quiñones-Hinojosa A, Barbaro NM, Gupta N, Kunwar S, Lawton MT, McDermott MW, Parsa AT, Manuel-García Verdugo J, Berger MS, Alvarez-Buylla A. Unique astrocyte ribbon in adult human brain contains neural stem cells but lacks chain migration. Nature. 2004 Feb 19;427(6976):740-4

Sachdeva S, Gupta M. Adenosine and its receptors as therapeutic targets: An overview. Saudi Pharm J. 2013 Jul;21(3):245-53.

Sánchez-Abarca LI, Tabernero A, Medina JM. Oligodendrocytes use lactate as a source of energy and as a precursor of lipids. Glia. 2001 Dec;36(3):321-9.

Santello M, Volterra A. Synaptic modulation by astrocytes via Ca2+-dependent glutamate release. Neuroscience. 2009 Jan 12;158(1):253-9.

Sapirstein A, Bonventre JV. Phospholipases A2 in ischemic and toxic brain injury. Neurochem Res. 2000 May;25(5):745-53.

Sarti C, Pantoni L, Bartolini L, Inzitari D. Cognitive impairment and chronic cerebral hypoperfusion: what can be learned from experimental models. J Neurol Sci. 2002 Nov 15;203-204:263-6.

Sarti C, Pantoni L, Bartolini L, Inzitari D. Persistent impairment of gait performances and working memory after bilateral common carotid artery occlusion in the adult Wistar rat. Behav Brain Res. 2002 Oct 17;136(1):13-20.

Sastre M, Dewachter I, Landreth GE, Willson TM, Klockgether T, van Leuven F, Heneka MT. Nonsteroidal anti-inflammatory drugs and peroxisome proliferator-activated receptor-gamma agonists modulate immunostimulated processing of amyloid precursor protein through regulation of beta-secretase. J Neurosci. 2003 Oct 29;23(30):9796-804.

Scali C, Prosperi C, Giovannelli L, Bianchi L, Pepeu G, Casamenti F. Beta (1-40) amyloid peptide injection into the nucleus basalis of rats induces microglia reaction and enhances cortical gamma-aminobutyric acid release in vivo. Brain Res. 1999 Jun 12;831(1-2):319-21.

Scemes E, Giaume C. Astrocyte calcium waves: what they are and what they do. Glia. 2006 Nov 15;54(7):716-25.

Scharfman HE. The CA3 "backprojection" to the dentate gyrus. Prog Brain Res. 2007;163:627-37.

Scheff SW, Price DA, Schmitt FA, DeKosky ST, Mufson EJ. Synaptic alterations in CA1 in mild Alzheimer disease and mild cognitive impairment. Neurology. 2007 May 1;68(18):1501-8.

Schenk D, Barbour R, Dunn W, Gordon G, Grajeda H, Guido T, Hu K, Huang J, Johnson-Wood K, Khan K, Kholodenko D, Lee M, Liao Z, Lieberburg I, Motter R, Mutter L, Soriano F, Shopp G, Vasquez N, Vandevert C, Walker S, Wogulis M, Yednock T, Games D, Seubert P. Immunization with amyloid-beta attenuates Alzheimer-disease-like pathology in the PDAPP mouse. Nature. 1999 Jul 8;400(6740):173-7.

Schipke CG, Kettenmann H. Astrocyte responses to neuronal activity. Glia. 2004 Aug 15;47(3):226-32.

Seress L, Pokorny J. Structure of the granular layer of the rat dentate gyrus. A light microscopic and Golgi study. J Anat. 1981 Sep;133(Pt 2):181-95.

Schmidt-Kastner R, Aguirre-Chen C, Saul I, Yick L, Hamasaki D, Busto R, Ginsberg MD. Astrocytes react to oligemia in the forebrain induced by chronic bilateral common carotid artery occlusion in rats. Brain Res. 2005 Aug 2;1052(1):28-39.

Schmidt-Kastner R, Freund TF. Selective vulnerability of the hippocampus in brain ischemia. Neuroscience. 1991;40(3):599-636.

Schneider I, Reverse D, Dewachter I, Ris L, Caluwaerts N, Kuiperi C, Gilis M, Geerts H, Kretzschmar H, Godaux E, Moechars D, Van Leuven F, Herms J. Mutant presenilins disturb neuronal calcium homeostasis in the brain of transgenic mice, decreasing the threshold for excitotoxicity and facilitating long-term potentiation. J Biol Chem. 2001 Apr 13;276(15):11539-44.

Schuessel K, Frey C, Jourdan C, Keil U, Weber CC, Müller-Spahn F, Müller WE, Eckert A. Aging sensitizes toward ROS formation and lipid peroxidation in PS1M146L transgenic mice. Free Radic Biol Med. 2006 Mar 1;40(5):850-62.

Schulte G, Fredholm BB. The G(s)-coupled adenosine A(2B) receptor recruits divergent pathways to regulate ERK1/2 and p38. Exp Cell Res. 2003 Oct 15;290(1):168-76.

Schwartz-Bloom RD, Sah R. gamma-Aminobutyric acid(A) neurotransmission and cerebral ischemia. J Neurochem. 2001 Apr;77(2):353-71.

Schwarzschild MA, Chen JF, Ascherio A. Caffeinated clues and the promise of adenosine A(2A) antagonists in PD. Neurology. 2002 Apr 23;58(8):1154-60.

Sciotti VM, Roche FM, Grabb MC, Van Wylen DG. Adenosine receptor blockade augments interstitial fluid levels of excitatory amino acids during cerebral ischemia. J Cereb Blood Flow Metab. 1992 Jul;12(4):646-55.

Sebastião AM, Ribeiro JA. Adenosine A2 receptor-mediated excitatory actions on the nervous system. Prog Neurobiol. 1996 Feb;48(3):167-89.

Selkoe DJ. Translating cell biology into therapeutic advances in Alzheimer's disease. Nature. 1999 Jun 24;399(6738 Suppl): A23-31.

Selkoe DJ. Amyloid beta-protein precursor: new clues to the genesis of Alzheimer's disease. Curr Opin Neurobiol. 1994 Oct;4(5):708-16.

Seifert G, Schilling K, Steinhäuser C. Astrocyte dysfunction in neurological disorders: a molecular perspective. Nat Rev Neurosci. 2006 Mar;7(3):194-206.

Selkoe DJ. Translating cell biology into therapeutic advances in Alzheimer's disease. Nature. 1999 Jun 24;399(6738 Suppl): A23-31.

Selkoe DJ. Amyloid beta-protein precursor: new clues to the genesis of Alzheimer's disease. Curr Opin Neurobiol. 1994 Oct;4(5):708-16.

Serebruany V, Sabaeva E, Booze C, Atar OD, Eisert C, Hanley D; Aggrenox Compliance Task Force. Distribution of dipyridamole in blood components among post-stroke patients treated with extended release formulation. Thromb Haemost. 2009 Sep;102(3):538-43.

Sheng JG, Jones RA, Zhou XQ, McGinness JM, Van Eldik LJ, Mrak RE, Griffin WS. Interleukin-1 promotion of MAPK-p38 overexpression in experimental animals and in Alzheimer's disease: potential significance for tau protein phosphorylation. Neurochem Int. 2001 Nov-Dec;39(5-6):341-8.

Sheng JG, Zhu SG, Jones RA, Griffin WS, Mrak RE. Interleukin-1 promotes expression and phosphorylation of neurofilament and tau proteins in vivo. Exp Neurol. 2000 Jun;163(2):388-91.

Silver J, Miller JH. Regeneration beyond the glial scar. Nat Rev Neurosci. 2004 Feb;5(2):146-56.

Simard M, Arcuino G, Takano T, Liu QS, Nedergaard M. Signaling at the gliovascular interface. J Neurosci. 2003 Oct 8;23(27):9254-62.

Sinha S, Lieberburg I. Cellular mechanisms of beta-amyloid production and secretion. Proc Natl Acad Sci U S A. 1999 Sep 28;96(20):11049-53.

Siniscalchi A, Rodi D, Gessi S, Campi F, Borea PA. Early changes in adenosine A1 receptors in cerebral cortex slices submitted to in vitro ischemia. Neurochem Int. 1999 Jun;34(6):517-22.

Sitaraman SV, Merlin D, Wang L, Wong M, Gewirtz AT, Si-Tahar M, Madara JL. Neutrophil-epithelial crosstalk at the intestinal lumenal surface mediated by reciprocal secretion of adenosine and IL-6. J Clin Invest. 2001 Apr;107(7):861-9.

Sitkovsky MV. Use of the A(2A) adenosine receptor as a physiological immunosuppressor and to engineer inflammation in vivo. Biochem Pharmacol. 2003 Feb 15;65(4):493-501.

Small SA, Schobel SA, Buxton RB, Witter MP, Barnes CA. A pathophysiological framework of hippocampal dysfunction in ageing and disease. Nat Rev Neurosci. 2011 Sep 7;12(10):585-601.

Sofroniew MV, Vinters HV. Astrocytes: biology and pathology. Acta Neuropathol. 2010 Jan;119(1):7-35.

Sofroniew MV. Molecular dissection of reactive astrogliosis and glial scar formation. Trends Neurosci. 2009 Dec;32(12):638-47.

Solito E, Sastre M. Microglia function in Alzheimer's disease. Front Pharmacol. 2012 Feb 10;3:14.

Somjen GG. Mechanisms of spreading depression and hypoxic spreading depression-like depolarization. Physiol Rev. 2001 Jul;81(3):1065-96.

Spignoli G, Pedata F, Pepeu G. A1 and A2 adenosine receptors modulate acetylcholine release from brain slices. Eur J Pharmacol. 1984 Jan 27;97(3-4):341-2.

Spite M, Serhan CN. Novel lipid mediators promote resolution of acute inflammation: impact of aspirin and statins. Circ Res. 2010 Nov 12;107(10):1170-84.

St George-Hyslop P, Haines J, Rogaev E, Mortilla M, Vaula G, Pericak-Vance M, Foncin JF, Montesi M, Bruni A, Sorbi S, Rainero I, Pinessi L, Pollen D, Polinsky R, Nee L, Kennedy J, Macciardi F, Rogaeva E, Liang Y, Alexandrova N, Lukiw W, Schlumpf K, Tanzi R, Tsuda T, Farrer L, Cantu JM, Duara R, Amaducci L, Bergamini L, Gusella J, Roses A, Crapper McLachlan D. Genetic evidence for a novel familial Alzheimer's disease locus on chromosome 14. Nat Genet. 1992 Dec;2(4):330-4.

Steiner H. Uncovering gamma-secretase. Curr Alzheimer Res. 2004 Aug;1(3):175-81.

Steinhäuser C, Berger T, Frotscher M, Kettenmann H. Heterogeneity in the Membrane Current Pattern of Identified Glial Cells in the Hippocampal Slice. Eur J Neurosci. 1992;4(6):472-484.

Stewart WF, Kawas C, Corrada M, Metter EJ. Risk of Alzheimer's disease and duration of NSAID use. Neurology. 1997 Mar;48(3):626-32.

Stoll G, Jander S, Schroeter M. Cytokines in CNS disorders: neurotoxicity versus neuroprotection. J Neural Transm Suppl. 2000;59:81-9.

Stepanichev MY, Zdobnova IM, Zarubenko II, Lazareva NA, Gulyaeva NV. Studies of the effects of central administration of beta-amyloid peptide (25-35):pathomorphological changes in the Hippocampus and impairment of spatial memory. Neurosci Behav Physiol. 2006 Jan;36(1):101-6.

Streit WJ, Walter SA, Pennell NA. Reactive microgliosis. Prog Neurobiol. 1999 Apr;57(6):563-81.

Streit WJ, Braak H, Xue QS, Bechmann I. Dystrophic (senescent) rather than activated microglial cells are associated with tau pathology and likely precede neurodegeneration in Alzheimer's disease. Acta Neuropathol. 2009 Oct;118(4):475-85.

Streit WJ, Xue QS. Microglial senescence. CNS Neurol Disord Drug Targets. 2013 Sep;12(6):763-7.

Strle K, Zhou JH, Shen WH, Broussard SR, Johnson RW, Freund GG, Dantzer R, Kelley KW. Interleukin-10 in the brain. Crit Rev Immunol. 2001;21(5):427-49.

Suen DF, Norris KL, Youle RJ. Mitochondrial dynamics and apoptosis. Genes Dev. 2008 Jun 15;22(12):1577-90.

Suenaga M, Furuta A, Wakabayashi K, Saibara T, Matsunaga Y. Monocytic elastase-mediated apolipoprotein-E degradation: Potential involvement of microglial elastase-like proteases in apolipoprotein-E proteolysis in brains with Alzheimers disease. Biochim Biophys Acta. 2015 Aug;1854(8):1010-8.

Suh SW, Chen JW, Motamedi M, Bell B, Listiak K, Pons NF, Danscher G, Frederickson CJ. Evidence that synaptically-released zinc contributes to neuronal injury after traumatic brain injury. Brain Res. 2000 Jan 10;852(2):268-73.

Svenningsson P, Le Moine C, Fisone G, Fredholm BB. Distribution, biochemistry and function of striatal adenosine A2A receptors. Prog Neurobiol. 1999 Nov;59(4):355-96.

Tan ZS, Beiser AS, Vasan RS, Roubenoff R, Dinarello CA, Harris TB, Benjamin EJ, Au R, Kiel DP, Wolf PA, Seshadri S. Inflammatory markers and the risk of Alzheimer disease: the Framingham Study. Neurology. 2007 May 29;68(22):1902-8.

Tanemura K, Chui DH, Fukuda T, Murayama M, Park JM, Akagi T, Tatebayashi Y, Miyasaka T, Kimura T, Hashikawa T, Nakano Y, Kudo T, Takeda M, Takashima A. Formation of tau inclusions in knock-in mice with familial Alzheimer disease (FAD) mutation of presenilin 1 (PS1). J Biol Chem. 2006 Feb 24;281(8):5037-41.

Tang Z, Gan Y, Liu Q, Yin JX, Liu Q, Shi J, Shi FD. CX3CR1 deficiency suppresses activation and neurotoxicity of microglia/macrophage in experimental ischemic stroke. J Neuroinflammation. 2014 Feb 3;11:26.

Thoreen CC, Chantranupong L, Keys HR, Wang T, Gray NS, Sabatini DM. A unifying model for mTORC1-mediated regulation of mRNA translation. Nature. 2012 May 2;485(7396):109-13.

Takano T, Tian GF, Peng W, Lou N, Libionka W, Han X, Nedergaard M. Astrocyte-mediated control of cerebral blood flow. Nat Neurosci. 2006 Feb;9(2):260-7.

Takata K, Kitamura Y, Tsuchiya D, Kawasaki T, Taniguchi T, Shimohama S. High mobility group box protein-1 inhibits microglial Abeta clearance and enhances Abeta neurotoxicity. J Neurosci Res. 2004 Dec 15;78(6):880-91.

Takigawa T, Alzheimer C. Variance analysis of current fluctuations of adenosine- and baclofen-activated GIRK channels in dissociated neocortical pyramidal cells. J Neurophysiol. 1999 Sep;82(3):1647-50.

Takigawa T, Alzheimer C. Phasic and tonic attenuation of EPSPs by inward rectifier K+ channels in rat hippocampal pyramidal cells. J Physiol. 2002 Feb 15;539(Pt 1):67-75.

Thorsell A, Johnson J, Heilig M. Effect of the adenosine A2a receptor antagonist 3,7-dimethyl-propargylxanthine on anxiety-like and depression-like behavior and alcohol consumption in Wistar Rats. Alcohol Clin Exp Res. 2007 Aug;31(8):1302-7.

Tocco G, Freire-Moar J, Schreiber SS, Sakhi SH, Aisen PS, Pasinetti GM. Maturational regulation and regional induction of cyclooxygenase-2 in rat brain: implications for Alzheimer's disease. Exp Neurol. 1997 Apr;144(2):339-49.

Tomimoto H, Akiguchi I, Wakita H, Suenaga T, Nakamura S, Kimura J. Regressive changes of astroglia in white matter lesions in cerebrovascular disease and Alzheimer's disease patients. Acta Neuropathol. 1997 Aug;94(2):146-52.

Traini C, Pedata F, Cipriani S, Mello T, Galli A, Giovannini MG, Cerbai F, Volpini R, Cristalli G, Pugliese AM. P2 receptor antagonists prevent synaptic failure and extracellular signal-regulated kinase 1/2 activation induced by oxygen and glucose deprivation in rat CA1 hippocampus in vitro. Eur J Neurosci. 2011 Jun;33(12):2203-15.

Trejo J, Massamiri T, Deng T, Dewji NN, Bayney RM, Brown JH. A direct role for protein kinase C and the transcription factor Jun/AP-1 in the regulation of the Alzheimer's beta-amyloid precursor protein gene. J Biol Chem. 1994 Aug 26;269(34):21682-90.

Tremblay MÈ, Stevens B, Sierra A, Wake H, Bessis A, Nimmerjahn A. The role of microglia in the healthy brain. J Neurosci. 2011 Nov 9;31(45):16064-9. doi: 10.1523/JNEUROSCI.4158-11.2011.

Treves A, Rolls ET. Computational analysis of the role of the hippocampus in memory. Hippocampus. 1994 Jun;4(3):374-91.

Tsacopoulos M, Magistretti PJ. Metabolic coupling between glia and neurons. J Neurosci. 1996 Feb 1;16(3):877-85.

Tsokas P, Ma T, Iyengar R, Landau EM, Blitzer RD. Mitogen-activated protein kinase upregulates the dendritic translation machinery in long-term potentiation by controlling the mammalian target of rapamycin pathway. J Neurosci. 2007 May 30;27(22):5885-94.

Ulloa L, Messmer D. High-mobility group box 1 (HMGB1) protein: friend and foe. Cytokine Growth Factor Rev. 2006 Jun;17(3):189-201.

Unal-Cevik I, Kilinç M, Gürsoy-Ozdemir Y, Gurer G, Dalkara T. Loss of NeuN immunoreactivity after cerebral ischemia does not indicate neuronal cell loss: a cautionary note. Brain Res. 2004 Jul 23;1015(1-2):169-74.

Unterberg AW, Stover J, Kress B, Kiening KL. Edema and brain trauma. Neuroscience. 2004;129(4):1021-9.

Van Broeckhoven C, Backhovens H, Cruts M, De Winter G, Bruyland M, Cras P, Martin JJ. Mapping of a gene predisposing to early-onset Alzheimer's disease to chromosome 14q24.3. Nat Genet. 1992 Dec;2(4):335-9.

Van harreveld A, Mendelson M. Glutamate-induced contractions in crustacean muscle. J Cell Comp Physiol. 1959 Aug; 54:85-94.

Vassar R, Bennett BD, Babu-Khan S, Kahn S, Mendiaz EA, Denis P, Teplow DB, Ross S, Amarante P, Loeloff R, Luo Y, Fisher S, Fuller J, Edenson S, Lile J, Jarosinski MA, Biere AL, Curran E, Burgess T, Louis JC, Collins F, Treanor J, Rogers G, Citron M. Beta-secretase cleavage of Alzheimer's amyloid precursor protein by the transmembrane aspartic protease BACE. Science. 1999 Oct 22;286(5440):735-41.

Velly L, Leone M. [BIS bilateral: A simple way to detect cerebral ischemia…Yes but in a conscious patient]. Ann Fr Anesth Reanim. 2013 Oct;32(10):641-3.

Venkatesh PK, Pattillo CB, Branch B, Hood J, Thoma S, Illum S, Pardue S, Teng X, Patel RP, Kevil CG. Dipyridamole enhances ischaemia-induced arteriogenesis through an endocrine nitrite/nitric oxide-dependent pathway. Cardiovasc Res. 2010 Mar 1;85(4):661-70.

Verkhratsky A, Rodríguez JJ, Parpura V. Astroglia in neurological diseases. Future Neurol. 2013 Mar 1;8(2):149-158.

Vilalta A, Brown GC. Neurophagy, the phagocytosis of live neurons and synapses by glia,

contributes to brain development and disease. FEBS J. 2017 Nov 10.

Vodovotz Y, Lucia MS, Flanders KC, Chesler L, Xie QW, Smith TW, Weidner J, Mumford R, Webber R, Nathan C, Roberts AB, Lippa CF, Sporn MB. Inducible nitric oxide synthase in tangle-bearing neurons of patients with Alzheimer's disease. J Exp Med. 1996 Oct 1;184(4):1425-33.

Volterra A, Liaudet N, Savtchouk I. Astrocyte Ca² signalling: an unexpected complexity. Nat Rev Neurosci. 2014 May;15(5):327-35.

Volterra A, Meldolesi J. Astrocytes, from brain glue to communication elements: the revolution continues. Nat Rev Neurosci. 2005 Aug;6(8):626-40.

von Bernhardi R, Eugenín-von Bernhardi L, Eugenín J. Microglial cell dysregulation in brain aging and neurodegeneration. Front Aging Neurosci. 2015 Jul 20;7:124.

Walker DG, Kim SU, McGeer PL. Complement and cytokine gene expression in cultured microglial derived from postmortem human brains. J Neurosci Res. 1995 Mar 1;40(4):478-93.

Wan W, Sutherland GR, Geiger JD. Binding of the adenosine A2 receptor ligand [3H]CGS 21680 to human and rat brain: evidence for multiple affinity sites. J Neurochem. 1990 Nov;55(5):1763-71.

Wang DD, Bordey A. The astrocyte odyssey. Prog Neurobiol. 2008 Dec 11;86(4):342-67.

Wang G, Huang H, He Y, Ruan L, Huang J. Bumetanide protects focal cerebral ischemia-reperfusion injury in rat. Int J Clin Exp Pathol. 2014 Mar15;7(4):1487-94.

Wang J, Huxley VH. Adenosine A2A receptor modulation of juvenile female rat skeletal muscle microvessel permeability. Am J Physiol Heart Circ Physiol. 2006 Dec;291(6):H3094-105.

Watkins LR, Hutchinson MR, Ledeboer A, Wieseler-Frank J, Milligan ED, Maier SF. Norman Cousins Lecture. Glia as the "bad guys": implications for improving clinical pain control and the clinical utility of opioids. Brain Behav Immun. 2007 Feb;21(2):131-46.

Wei W, Gao Y, Wang C, Zhao L, Sun D. Excessive fluoride induces endoplasmic reticulum stress and interferes enamel proteinases secretion. Environ Toxicol. 2013 Jun;28(6):332-41.

Wen PH, Hof PR, Chen X, Gluck K, Austin G, Younkin SG, Younkin LH, DeGasperi R, Gama Sosa MA, Robakis NK, Haroutunian V, Elder GA. The presenilin-1 familial Alzheimer disease mutant P117L impairs neurogenesis in the hippocampus of adult mice. Exp Neurol. 2004 Aug;188(2):224-37.

Wenk GL, Barnes CA. Regional changes in the hippocampal density of AMPA and NMDA receptors across the lifespan of the rat. Brain Res. 2000 Dec 1;885(1):1-5.

West MJ, Slomianka L, Gundersen HJ. Unbiased stereological estimation of the total number of neurons in thesubdivisions of the rat hippocampus using the optical fractionator. Anat Rec. 1991 Dec;231(4):482-97.

Weyrich AS, Denis MM, Kuhlmann-Eyre JR, Spencer ED, Dixon DA, Marathe GK, McIntyre TM, Zimmerman GA, Prescott SM. Dipyridamole selectively inhibits inflammatory gene expression in platelet-monocyte aggregates. Circulation. 2005 Feb 8;111(5):633-42.

White PJ, Rose'Meyer RB, Hope W. Functional characterization of adenosine receptors in the nucleus tractus solitarius mediating hypotensive responses in the rat. Br J Pharmacol. 1996 Jan;117(2):305-8.

Wilhelmsson U, Bushong EA, Price DL, Smarr BL, Phung V, Terada M, Ellisman MH, Pekny M. Redefining the concept of reactive astrocytes as cells that remain within their unique domains upon reaction to injury. Proc Natl Acad Sci U S A. 2006 Nov 14;103(46):17513-8.

Witter MP. The perforant path: projections from the entorhinal cortex to the dentate gyrus. Prog Brain Res. 2007;163:43-61.

Wong WT. Microglial aging in the healthy CNS: phenotypes, drivers, and rejuvenation. Front Cell Neurosci. 2013 Mar 13;7:22.

Wu SN, Lin YT, Chen SS. Evidence of direct activation of adenosine A1 receptor by 5'-adenosine monophosphate in isolated guinea pig atrial myocytes. Jpn J Physiol. 1992;42(1):35-47.

Xaus J, Mirabet M, Lloberas J, Soler C, Lluis C, Franco R, Celada A. IFN-gamma up-regulates the A2B adenosine receptor expression in macrophages: a mechanism of macrophage deactivation. J Immunol. 1999 Mar 15;162(6):3607-14.

Xaus J, Mirabet M, Lloberas J, Soler C, Lluis C, Franco R, Celada A. IFN-gamma up-regulates the A2B adenosine receptor expression in macrophages: a mechanism of macrophage deactivation. J Immunol. 1999 Mar 15;162(6):3607-14.

Xu K, Bastia E, Schwarzschild M. Therapeutic potential of adenosine A(2A)receptor antagonists in Parkinson's disease. Pharmacol Ther. 2005 Mar;105(3):267-310. Epub 2004 Dec 21.

Yaar R, Jones MR, Chen JF, Ravid K. Animal models for the study of adenosine receptor function. J Cell Physiol. 2005 Jan;202(1):9-20.

Yamanaka K, Chun SJ, Boillee S, Fujimori-Tonou N, Yamashita H, Gutmann DH, Takahashi R, Misawa H, Cleveland DW. Astrocytes as determinants of disease progression in inherited amyotrophic lateral sclerosis. Nat Neurosci. 2008 Mar;11(3):251-3.

Yamagata K, Andreasson KI, Kaufmann WE, Barnes CA, Worley PF. Expression of a mitogen-inducible cyclooxygenase in brain neurons: regulation by synaptic activity and glucocorticoids. Neuron. 1993 Aug;11(2):371-86.

Yang D, Chen H, Koupenova M, Carroll SH, Eliades A, Freedman JE, Toselli P, Ravid K. A new role for the A2b adenosine receptor in regulating platelet function. J Thromb Haemost. 2010 Apr;8(4):817-27.

Yang D, Zhang Y, Nguyen HG, Koupenova M, Chauhan AK, Makitalo M, Jones MR, St Hilaire C, Seldin DC, Toselli P, Lamperti E, Schreiber BM, Gavras H, Wagner DD, Ravid K. The A2B adenosine receptor protects against inflammation and excessive vascular adhesion. J Clin Invest. 2006 Jul;116(7):1913-23.

Yang J, Liu X, Bhalla K, Kim CN, Ibrado AM, Cai J, Peng TI, Jones DP, Wang X. Prevention of apoptosis by Bcl-2: release of cytochrome c from mitochondria blocked. Science. 1997 Feb 21;275(5303):1129-32.

Yankner BA, Caceres A, Duffy LK. Nerve growth factor potentiates the neurotoxicity of beta amyloid. Proc Natl Acad Sci U S A. 1990 Nov;87(22):9020-3.

Yao Y, Sei Y, Abbracchio MP, Jiang JL, Kim YC, Jacobson KA. Adenosine A3 receptor agonists protect HL-60 and U-937 cells from apoptosis induced by A3 antagonists. Biochem Biophys Res Commun. 1997 Mar 17;232(2):317-22.

Yeh CY, Vadhwana B, Verkhratsky A, Rodríguez JJ. Early astrocytic atrophy in the entorhinal cortex of a triple transgenic animal model of Alzheimer's disease. ASN Neuro. 2011 Dec 19;3(5):271-9.

Yu L, Frith MC, Suzuki Y, Peterfreund RA, Gearan T, Sugano S, Schwarzschild MA, Weng Z, Fink JS, Chen JF. Characterization of genomic organization of the adenosine A2A receptor gene by molecular and bioinformatics analyses. Brain Res. 2004 Mar 12;1000(1-2):156-73.

Zetterström T, Fillenz M. Adenosine agonists can both inhibit and enhance in vivo striatal dopamine release. Eur J Pharmacol. 1990 May 3;180(1):137-43.

Zhang H, Baehrecke EH. Eaten alive: novel insights into autophagy from multicellular model systems. Trends Cell Biol. 2015 Jul;25(7):376-87.

Zhang JP, Sun GY. Free fatty acids, neutral glycerides, and phosphoglycerides in transient focal cerebral ischemia. J Neurochem. 1995 Apr;64(4):1688-95.

Zhang Z, Chopp M, Goussev A, Powers C. Cerebral vessels express interleukin 1beta after focal cerebral ischemia. Brain Res. 1998 Feb 16;784(1-2):210-7.

Zhou AM, Li WB, Li QJ, Liu HQ, Feng RF, Zhao HG. A short cerebral ischemic preconditioning up-regulates adenosine receptors in the hippocampal CA1 region of rats. Neurosci Res. 2004 Apr;48(4):397-404.

Zhou M, Kimelberg HK. Freshly isolated hippocampal CA1 astrocytes comprise two populations differing in glutamate transporter and AMPA receptor expression. J Neurosci. 2001 Oct 15;21(20):7901-8.

Zhu C, Herrmann US, Falsig J, Abakumova I, Nuvolone M, Schwarz P, Frauenknecht K, Rushing EJ, Aguzzi A. A neuroprotective role for microglia in prion diseases. J Exp Med. 2016 May 30;213(6):1047-59.

Zola-Morgan S, Squire LR, Amaral DG. Human amnesia and the medial temporal region: enduring memory impairment following a bilateral lesion limited to field CA1 of the hippocampus. J Neurosci. 1986 Oct;6(10):2950-67.